SYNTHESIS OF NOVEL BODIPY LIBRARIES AND THEIR APPLICATION IN BIOIMAGING

ZHAI DUANTING

NATIONAL UNIVERSITY OF SINGAPORE

2012

SYNTHESIS OF NOVEL BODIPY LIBRARIES AND THEIR APPLICATION IN BIOIMAGING

ZHAI DUANTING
(B. Sc., Soochow University, Suzhou, China)

A THESIS SUBMITTED

FOR THE DEGREE OF DOCTOR OF PHILOSOPHY

DEPARTMENT OF CHEMISTRY

NATIONAL UNIVERSITY OF SINGAPORE

2012

Thesis Declaration

The work in this thesis is the original work of Duanting Zhai, performed independently under the supervision of Professor Young-Tae Chang, (in the laboratory Chemical Bioimaging Lab, S9-03-03), Department of Chemistry, National University of Singapore, between 08/08/2008 and 07/08/2012.

The content of the thesis has been partly published in:

1. Zhai, D.; Lee, S. C.; Vendrell, M.; Leong, L. P.; Chang, Y. T., Synthesis of a Novel BODIPY Library and Its Application in the Discovery of a Fructose Sensor, *ACS Comb. Sci.* **2012**, *14*, 81-84.

2. Yun, S. W.; Leong, C.; Zhai, D.; Tan, Y. L.; Lim, L.; Bi, X.; Lee, J. J.; Kim, H. J.; Kang, N. Y.; Ng, S. H.; Stanton, L. W.; Chang, Y. T., Neural Stem Cell Specific Fluorescent Chemical Probe Binding to FABP7, *Proc. Natl Acad. Sci. U S A* **2012**, *109*, 10214-10217.

3. Lee, J. J; Lee, S. C.; Zhai, D.; Ahn, Y. H.; Yeo, H. Y.; Tan, Y. L.; Chang, Y. T., Bodipy-diacrylate Imaging Probes for Targeted Proteins inside Live cells, *Chem. Commun.* **2011**, *47*, 4508-4510.

Name	Signature	Date

Acknowledgements

First of all, I would like to express my deep gratitude to my supervisor, Professor Young-Tae Chang for his profound knowledge, invaluable guidance, constant support and inspiration throughout my graduate studies. The knowledge, both scientific and otherwise, that I accumulated under his supervision, will aid me greatly throughout my life.

Next, I would like to give my sincere thanks to Dr. Sung-Chan Lee and Dr. Marc Vendrell, for their warm support during my entire graduate studies. There are no sufficient words to express my gratitude to them. They did not only teach me the experiment technique, but also the research attitude.

Besides, my sincere appreciation goes to all past and present members of our lab whose participation made this journey memorable in each step of my research life. I would like to thank all the graduate students of Chang lab, Suihan, Animesh, Ghosh, Raj, Dongdong, Cheryl, Bikram, Samira, Xu Wang, Myung Won and Jun Cheng, for their cordiality and friendship. I also benefited from all other lab members, particularly but not limited to, Dr. Hyung-Ho Ha, Dr. Jae Jung Lee, Dr. Xin Li, Dr. Jun-Seok Lee, Dr. Yun-Kyung Kim, Dr. Seong Wook Yun, Dr. Hanjo Kim, Dr. Jun Young Kim, Dr. Jung Sun Yoo, Dr. Jiyeon Ock, Dr. Jinmi Kim, Dr. Sung Jin Park, Dr. Nam-Young Kang, Dr. Chai Lean Teoh, Dr. Anup Atul Kale, Dr. Gopalarao Yerragorla, Yoges, Zhi Yen, Tessa, Hui Shan, Meiling and Fronia.

I would also take the opportunity to thank all of my dear friends, whose encourage and understanding help me to finish my graduate study.

Financial and technical support from the Department of Chemistry of the National University of Singapore (NUS) is greatly acknowledged. I would like to thank all the staffs in chemistry administrative office, lab supplied for their immense support.

At last, I would like to express my greatest thanks to my parents. They teach me to be patient, sincere, brave, strong and optimistic. Without their continuous support and constant encouragement, I would not be able to complete my PhD study.

Table of Contents

Summary

Diversity-oriented fluorescent libraries (DOFL) approach, through generating large numbers of fluorescent compounds in a combinatorial way, is a powerful method to discover novel fluorescent sensors. This thesis using diversity-oriented approach introduces the successful examples of sensor development based on BODIPY structure.

We first synthesized a novel 160-member BODIPY library with an active ester motif attached (**BDD**) through Knoevenagel condensation reaction with aldehyde building blocks. BDD was then further reacted with N^1,N^1-dimethylethane-1,2-diamine and 2,2-dimethoxyethanamine to give 80-member **BDL** and 47-member **BDA** libraries, respectively. All these three libraries cover very broad spectral properties and form good chemical tool box for sensor development.

The three BODIPY libraries were then applied to high-throughput screening systems in two directions of *in vitro* screening and cell-based screening. 3 novel sensors, **Fructose Orange**, **Glutathione Green** and **Green Date**, were discovered from *in vitro* screening system. **Fructose Orange** showed up to 24-fold fluorescence increase upon recognition of fructose and an outstanding selectivity among 24 different saccharides. NMR studies confirmed the formation of five different binding interactions between the sensor and fructose. Furthermore, **Fructose Orange** was applied to the quantification of fructose in soft drinks, being the most selective fluorescent sensor for fructose reported to date. **Glutathione Green** showed ratiometric fluorescence response and outstanding selectivity over other analytes. Further experiment showed that **GSH Green** is capable of GSH quantification in cell extract, as well as responding to the GSH concentration change in cellular environment. **Green Date** showed high fluorescence response to GBL in various pH conditions and up to 10% EtOH. Furthermore, **Green Date** is able to detect the existence of GBL in different kinds of drink samples after a simple

extraction method. This discovery will help to secure the safety of drinks in public place and solve the DFSA problems. While in the cell-based screening one compound from BDD library (CDr3) was identified as a neural stem cell specific probe. This novel compound specifically detects living neural stem cells of both human and mouse origin. Furthermore, we identified its binding target by proteomic analysis as fatty acid binding protein 7 (FABP7) which is highly expressed in neural stem cells and localized in the cytoplasm. CDr3 will be a valuable chemical tool in the study and applications of neural stem cells.

In addition to sensor development, we further proved that DOFL compounds could also be more informatics and aim at specific applications. We constructed a Taming BODIPY library with very diverse physical properties. After applying to cell-based screening system, cellular localization and retention of compounds were correlated to the structures of substitutions of BODIPY dyes. Using the information, cell-permeability and background issues were overcome in developing a protein tag system based on BODIPY diacrylate structure. This novel peptide-based protein labelling system preferably changed the spectral property when it encounters a designed peptide containing two pairs of Arg-Cys. Dimeric peptide tag RC^2 and its partner compound would benefit the current protein labelling methods, especially the optical imaging of specific target protein inside living cells as demonstrated. This system would provide a promising tool for optical imaging of specific protein due to the advantages of small size, independence from other enzymes or cofactors, applicability to intracellular proteins, optical confirmation of proper conjugation from the apparent spectral change, stable binding be analyzed in SDS-PAGE, and negligible toxicity to the users.

List of Tables

List of Figures

Chapter 1

Chapter 2

Chapter 3

Chapter 4

Chapter 5

List of Charts

List of Schemes

List of Abbreviations

AcOH	Acetic acid
ACN	Acetonitrile
BSA	Bovine serum albumin
CD	Circular dichroism
$CDCl_3$	Deuterated chloroform
$CHCl_3$	Chloroform
D_2O	Deuterated oxide
DAD	Diode array detector
DCC	N,N'-Dicyclohexylcarbodiimide
DCM	Dichloromethane
DIC	N,N'-Diisopropylcarbodiimide
DIEA	Diisopropyl ethylamine
DMAP	Dimethylaminopyridine
DMF	N, N-Dimethylformamide
DMSO	Dimethyl sulfoxide
DMSO-d_6	Deuterated Dimethyl Sulfoxide
DOS	Diversity oriented synthesis
DOFL	Diversity oriented fluorescence library
DOFLA	Diversity oriented fluorescence library approach
EA	Ethyl acetate
ESI	Electrospray ionization
EtOH	Ethanol
Ex	Excitation
Em	Emission

HATU	2-(1H-7-Azabenzotriazol-1-yl)-1,1,3,3-tetramethyl uranium hexafluorophosphate methanaminium
HCl	Hydrochloric acid
HEPES	4-(2-Hydroxyethyl)-1-piperazineethanesulfonic acid
HOBt	Hydroxybenzotriazole
HPLC	High-performance liquid chromatography
HPLC-MS	High-performance liquid chromatography mass spectrometry
HTS	High throughput screening
MeOH	Methanol
MeOD	Deuterated methanol
MS	Mass spectrometry
NIR	Near infrared
NMR	Nuclear magnetic resonance
QY	Quantum yield
RBF	Round bottom flask
RT	Room temperature
TFA	Trifluoroacetic acid
THF	Tetrahydrofuran
TLC	Thin layer chromatography
TOS	Target oriented synthesis
UV	Ultraviolet

List of Publications

1. **Zhai, D.**; Lee, S. C.; Vendrell, M.; Leong, L. P.; Chang, Y. T., Synthesis of a Novel BODIPY Library and Its Application in the Discovery of a Fructose Sensor, *ACS Comb. Sci.* **2012**, *14*, 81-84.
2. Yun, S. W.; Leong, C.; **Zhai, D.**; Tan, Y. L.; Lim, L.; Bi, X.; Lee, J. J.; Kim, H. J.; Kang, N. Y.; Ng, S. H.; Stanton, L. W.; Chang, Y. T., Neural Stem Cell Specific Fluorescent Chemical Probe Binding to FABP7, *Proc. Natl. Acad. Sci. U S A* **2012**, *109*, 10214-10217.
3. Lee, J. J; Lee, S. C.; **Zhai, D.**; Ahn, Y. H.; Yeo, H. Y.; Tan, Y. L.; Chang, Y. T., Bodipy-diacrylate Imaging Probes for Targeted Proteins inside Live cells, *Chem. Commun.* **2011**, *47*, 4508-4510.
4. Vendrell, M.; Krishna, G.G.; Ghosh, K. K.; **Zhai, D.**; Lee, J. S.; Zhu, Q.; Yau, Y. H.; Shochat, S. G.; Kim, H.; Chung. J.; Olivo, M.; Chang, Y. T., Solid-phase Synthesis of BODIPY Dyes and Development of an Immunoglobulin Fluorescent Sensor, *Chem. Commun.* **2011**, *47*, 8424-8426.
5. Lee, J. J.; Kim, J. Y.; **Zhai, D.**; Yun, S. W.; Chang, Y. T., Eastern Staining: A Simple Recombinant Protein Detection Technology Using a Small Peptide Tag and Its Orthogonal Fluorescent Compound, *Interdiscip. Bio Central* **2012**, doi: 10.4051/ibc.2012.4.2.0005

Reviews

1. Vendrell, M.; **Zhai, D.**; Er, J. C.; Chang, Y. T., Combinatorial Strategies in Fluorescent Probe Development, *Chem. Rev.* **2012**, doi: 10.1021/cr200355j.

2. Das, R. K.; Samanta, A.; Ghosh, K. K.; **Zhai, D.**; Xu, W.; Su, D.; Leong, C.; Chang, Y. T., Target Identification: A Challenging Step in Forward Chemical Genetics, *Interdiscip. Bio Central* **2011**, *3*, 1-16.

Patent

1. Chang, Y. T.; Yun, S. W.; **Zhai, D.**, BODIPY Structure Fluorescence Dye for Neural Stem Cell Probe, US Provisional Appl. 61/416808, 2010.
2. Chang, Y. T.; Vendrell, M.; **Zhai, D.**; Kang, N. Y.; Chandran, Y., Alkylamino BODIPY Dyes as Selective Fluorescent Probes for Proteins and Mouse Embryonic Stem Cells, PCT Appl. PCT/SG2012/000215
3. Chang, Y. T.; **Zhai, D.**; Eng, P. S. F., BODIPY Fluorescence Sensor for Illicit Date-Rape Drug-GBL, US Provisional Appl. 61/619,591

Chapter 1

Introduction

The need for recognizing and sensing environmentally and biologically important species has led large efforts towards sensor development. Fluorescent small molecules comprise an important part among sensor families, due to their high sensitivity, fast response time, low cost and technical simplicity. During the sensing process, molecular recognition lies at the very essential part. The recognition not only refers to the binding event, but also requires selectivity between a sensor and an analyte.[1] The conventional design of fluorescent sensors was first proposed by combining well-known recognition elements with fluorophores (designed approach),[2] while the latter ones only serve as reporters. However, the limited knowledge of the recognition motif and complicated real situation restricted the successful rate. In recent years, combinatorial approach has found its way in generating and optimizing fluorescent sensors. It was first applied with designed approach to discover new sensors for defined analytes through derivatization of known recognition elements (**Target-Oriented Fluorescent Libraries, TOFL**). Combinatorial approach then broadened its scope to multi-purpose sensing by generating large numbers of diverse structures (**Diversity-Oriented Fluorescent Libraries, DOFL**). Combined with high-throughput screening, DOFL approach could discover sensors for targets which might not be accessible by rational design (e.g., cell phenotype, macrostructures).

DOFL approach has become an alternative way to sophisticated design in sensor development based on various fluorescent scaffold, including coumarin, styryl, quinoline, dapoxyl, xanthone, cyanine, BODIPY, rodamine and so on. Among them, BODIPY dyes are special not only because of their superior photophysical properties (e.g., high quantum yield, tunable fluorescence characteristics, high photostability, and

narrow emission bandwidth),[3] but also their relatively nonpolar property and electrically neutral fluorophore.[4] These properties induce minimal perturbation to functional properties of their conjugates. BODIPY dyes are therefore often preferred as sensing scaffold and labeling reagents.

The following sections will review research of the expansion of combinatorial approach on fluorescent small molecules in sensor development and recent application of BODIPY compounds.

1.1 Overview of Small Molecule Fluorophores

The process of fluorescence involves two stages: (1) a molecule at ground state absorbs a photo of suitable energy to promote to the excited state; and (2) the excited state emits another photon to return to the ground state.[4] On the other hand, the relaxation of the excited state does not always happen as fluorescence due to that energy can be lost in other ways (e.g., bond rotation or vibration, and molecular collision[5]) or through other mechanisms (e.g., photoinduced electron transfer (PeT)[6] and heavy atom effect[7]). The parameters normally used to characterize fluorophores are maximal absorption wavelength (λ_{abs}), maximal emission wavelength (λ_{em}), extinction coefficient (ε, defined by Beer-Lambert-Bouguer law), Stokes shift (difference between λ_{abs} and λ_{em}) and quantum yield (Φ, ration of photons emitted to absorbed).

The first small molecule fluorophore discovered was the naturally-occurring compound quinine, reported by Herschel in 1845.[8] However, over the years, well developed small molecule fluorophores are still restricted to a limited number of scaffolds. Although additional class of fluorophores (e.g., quantum dots and fluorescent proteins) have gained much attention recently, they are beyond the scope of this thesis and therefore not discussed here. Nevertheless, these limited fluorophores are still able

to cover full range of the spectra, from UV-visible to near-infrared. Major classes of small molecule fluorophores include pyrenes (**1**), naphthalene derivatives (e.g., dansyl chloride and naphtalimide (**2**)), coumarins (**3**), xanthone (**4**), fluorescein (**5**), NBD (**6**), rhodol (**7**), BODIPY(**8**), dapoxyl (**9**[9]), styryl (**10**[10]), rhodamine (**11**), cyanines (**12**), quinolines, indoles and imidizoles (e.g., DAPI and Hoechst), stilbene, phenanthridines, squarine, phthalocyanines and oxazines (Figure 1.1).

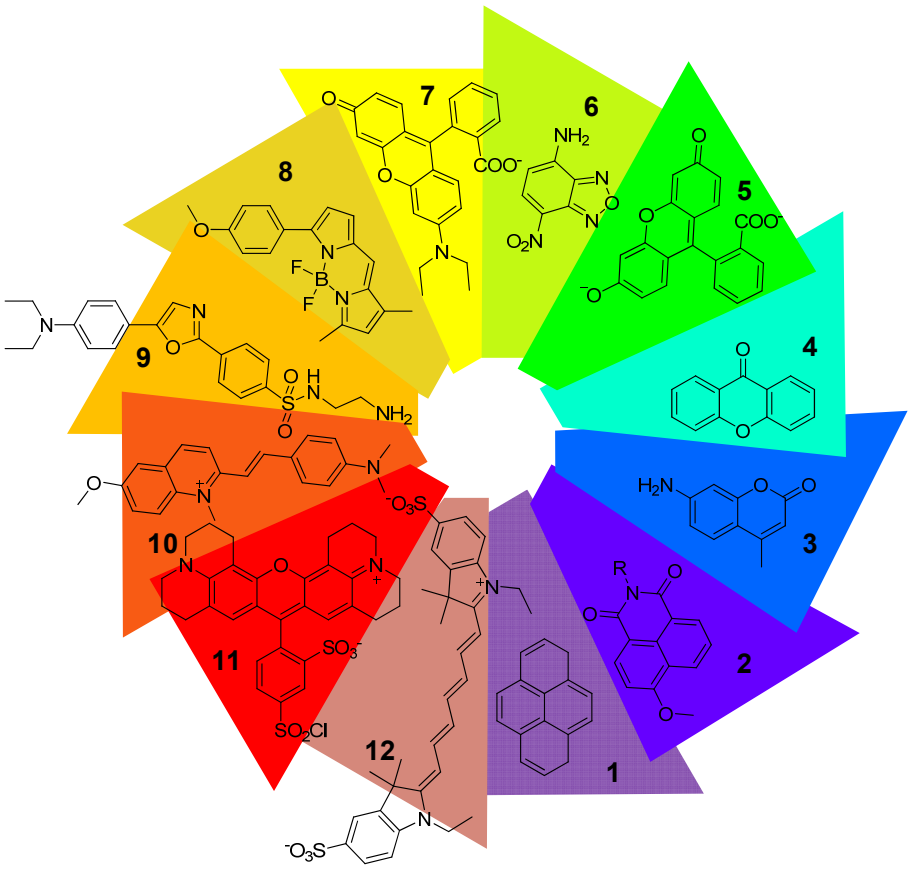

Figure 1.1 Representative structures of fluorophores with emission ranging from blue to NIR

1.2 Combinatorial Synthetic Strategies for Fluorescent Sensor Development

1.2.1 Target-Oriented Fluorescent Libraries

TOFL are created to maximize the signal response and optimize the selectivity of conventional rational design. The workflow for preparing these libraries can be summarized as: (1) searching of receptors or binding motifs based on target analytes, (2)

attaching receptors or binding motifs to reporters that can transform molecular recognition event into fluorescent signal (Figure 1.2). Due to the limited knowledge of recognition elements, the target analytes of TOFL are still restricted to several classes, such as metal ions and saccharides.

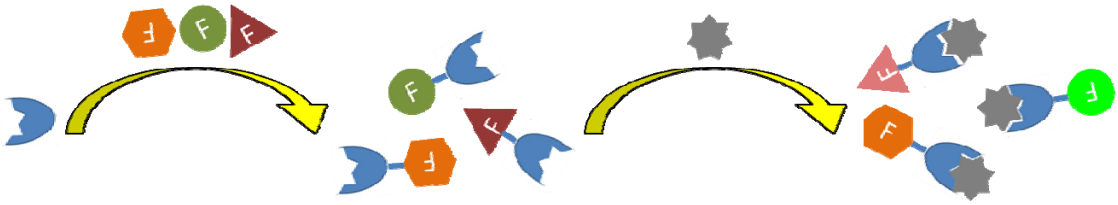

Figure 1.2 Schematic representation of TOFL for sensor development

Metal ions due to their environmental and biological importance, as well as well known binding motifs (e.g., crown ethers, polyamines, macrocyclic amines, pyridines and acetates) have become one of the most popular targets in sensor development.[11] Pioneer work by applying combinatorial approach to develop metal ion sensors was reported by Sames and co-workers, who constructed a 1470-member library of triamine ionophores for environmental copper sensing (Figure 1.3a).[12] Later researchers utilized PeT mechanism to obtain enhancing fluorescent signals to metal ions. In this case, the electron-donor property of receptor diminishes once the sensor binds to metal.[13] One example is the alkali and alkali earth metal ion sensors developed by Rivero *et al.* by derivatizing dansyl with lariat ethers and benzamides.[14] Further development on metal sensors was demonstrated by Finney and co-workers by proposing a new signalling mechanism (binding-induced restriction of fluorophore biary torsion). The discovery of Hg^{2+} and Ag^{+} sensors from biarylpyridine library successfully proved their assumption (Figure 1.3b).[15]

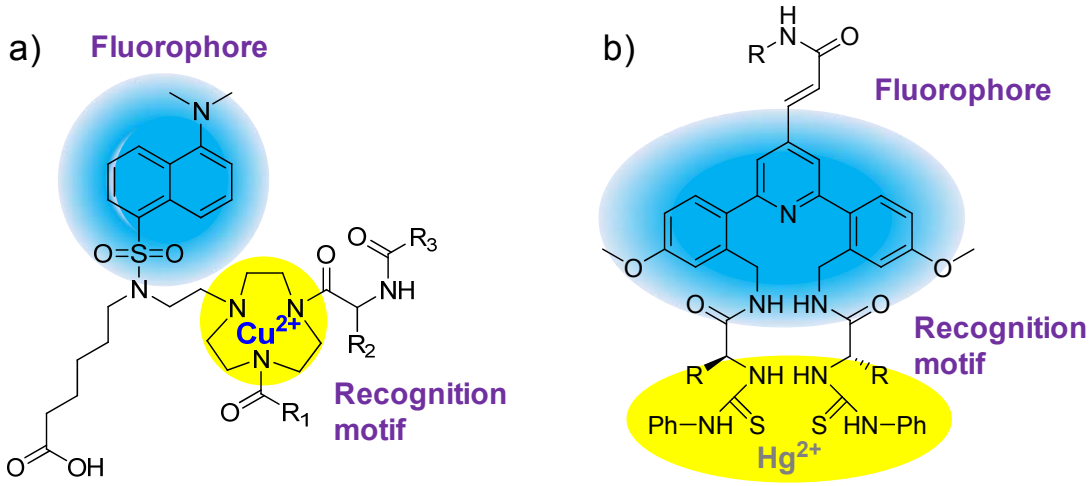

Figure 1.3 TOFL for metal ion sensing (a) Preparation of dansyl libraries through derivatization of polyamines as recognition motifs to develop fluorescent sensors for Cu^{2+}; (b) Binding-induced restriction of fluorophore biaryl torsion as a novel signaling mechanism to develop fluorescent sensors for Hg^{2+}

Saccharides are another class of analytes that have received enormous attentions for sensor development due to their biologically importance (e.g., cell signalling, immune response and cell adhesion).[16] The design of saccharides sensor was challenging (due to their restricted functional groups and conformational changing) until the landmark discovery that boronic acids could reversibly form boronic esters with sugar diols.[17] Boronic acids were then widely incorporated with different fluorophores to develop saccharides sensors.[1] However, the selectivity still remains a problem due to the structurally similarity between different saccharides.[16a] This could be improved by applying combinatorial approach. One example is the systematic work reported by Wang's lab for saccharides sensor development. They derivatized boronic acid with indole[18] and isoquinole[19] motifs to develop fluorescent saccharides sensors with high affinity. Hall and co-workers also prepared a library by combining anthracene-capped polyamines with aryl boronic acids to discover novel saccharides sensors.[20]

1.2.2 Diversity-Oriented Fluorescent Libraries

In order to accelerate fluorescent sensor development, DOFL were prepared with more diverse structure properties and screened for multi-purpose sensing. Compared with TOFL, while the fluorophores only serve as signal reporters, the fluorescent molecules in DOFL can also participate in the binding event (i.e., as both receptors and reporters). On the other hand, the analytes class of DOFL were widely expanded to those targets when even no prior knowledge of recognition is available (e.g., proteins, cells and macromolecules) (Figure 1.4).

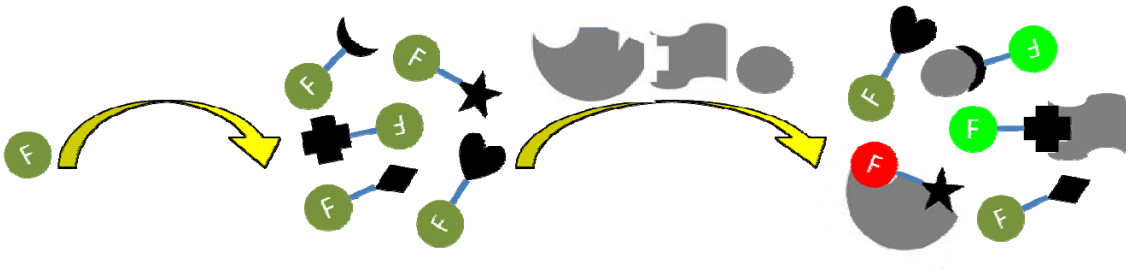

Figure 1.4 Schematic representation of DOFL for sensor development

The strategies for preparing DOFL can by summarized as two types: (1) derivatizing known fluorophores with commercial available building blocks; (2) *de novo* construction of fluorophores through multi-component, one-pot, or tandem reactions. While the first strategy usually utilizes convenient chemistry and renders relatively large library size, which is defined by availability of building blocks, the latter one faces more synthetic challenging and has relatively smaller number but with broader structural diversity.

The initial attempt on constructing DOFL was used to optimize the photophysical properties (e.g., high quantum yield and good photostability) of known fluorophores in order to develop potential candidates as sensors and imaging probes. One of the first examples explored on this purpose was coumarin dye. Bauerle and co-workers reported the first coumarin library by derivatizing eight different 3-bromocoumarins using

palladium-catalyzed coupling reactions (i.e., Suzuki, Sonogashira, and Heck cross-coupling reactions). Several structures showing relatively high quantum yield were identified after screening from this library (Figure 1.5).[21] Later, similar purpose has been shared by other researchers through derivatizing coumarin at different positions[22] and expanding to other fluorophores (e.g., rodol,[23] xanthone[24] and cyanine[25]) using different chemistries (e.g., click chemistry[22c, 24] and nucleophilic substitution[25]). DOFL were also used to study the solvent effect on derivatives of fluorophores. Dapoxyl and naphthalimide libraries reported by Yao and Heagy respectively were prepared for this purpose.[26] One successful example of DOFL constructed for sensor development was the styryl libraries reported by Chang and co-workers. These libraries, covering whole visible range of emission wavelength, were prepared from Knoevenagel condensation reactions of pyridinium salts and commercial aldehyde building blocks. New probes showing specific cellular localizations[27], as well as novel DNA[28] and RNA[10] sensors were identified from this library.

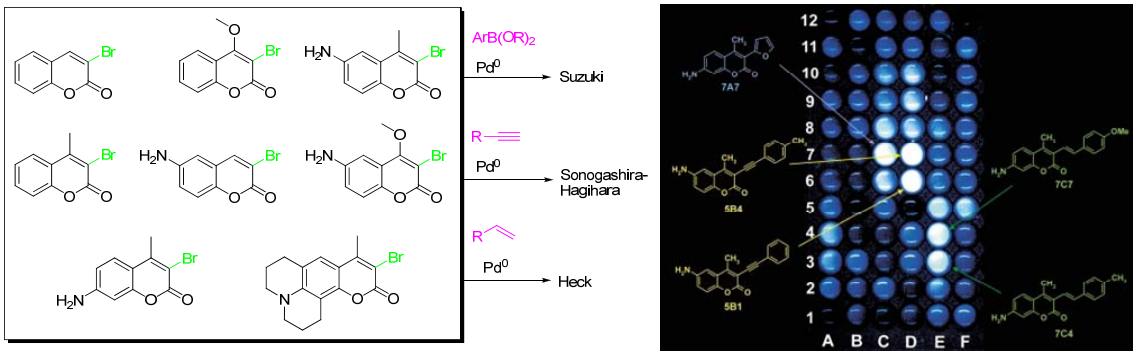

Figure 1.5 Synthesis of diversity-oriented coumarin library and identification of high quantum yield compounds after screening. This picture has been partly reproduced from ref 21 with permission. Copyright 2001 Wiley-VCH.

Preparation for DOFL also utilizes solid-phase chemistry to increase chemical diversity and facilitate purification process. With the aim of increasing chemical diversity, Lam's group designed a solid-phase approach on Rink amide resin which

enabled multi-derivatization on different points of coumarin. From this one synthetic route, different derivatives of coumarin, including imidazocoumarins, lactam coumarins, and thiomidazocoumarins, were rendered.[29] Park and co-workers also developed solid-phase synthesis of benzopyrans to prepare a 434-membered library. In their approach, five different types of reactions were allowed to happen on their fluorescent scaffold (i.e., Suzuki coupling, Stille coupling and subsequent Diels-Alder, asymmetric hydrogenation, aromatization, and click chemistry).[30] With the aim to facilitate purification process, Chang and co-workers prepared second generation of styryl libraries on chlorotrityl resin by adding amine linker using similar Knoevenagel condensation reactions, from which several sensors for β-amyloid plaques were developed (Figure 1.6a).[31] A similar approach has been applied by Chang's group to other positively charged scaffolds, which also faced difficulty in purification. A 96-membered benzimidazolium[32] and 96-member quinaldinium[33] libraries were synthesized, and GTP (Figure 1.6b) and chymotrypsin (Figure 1.6c) sensors were discovered from the two libraries, respectively. The strategy of adding amine linker to fluorophores and attaching them to chlorotrityl resin for further derivatizaiton was also expanded to other fluorophores by the same group. Libraries based on dapoxyl[9], xanthone[34] and rosamine[35] were constructed, and showed successful application in developing sensors for human serum albumin (HSA)[9], glutathione[35] (Figure 1.6d), mitochondria proteins[36] and stem cells[34, 37].

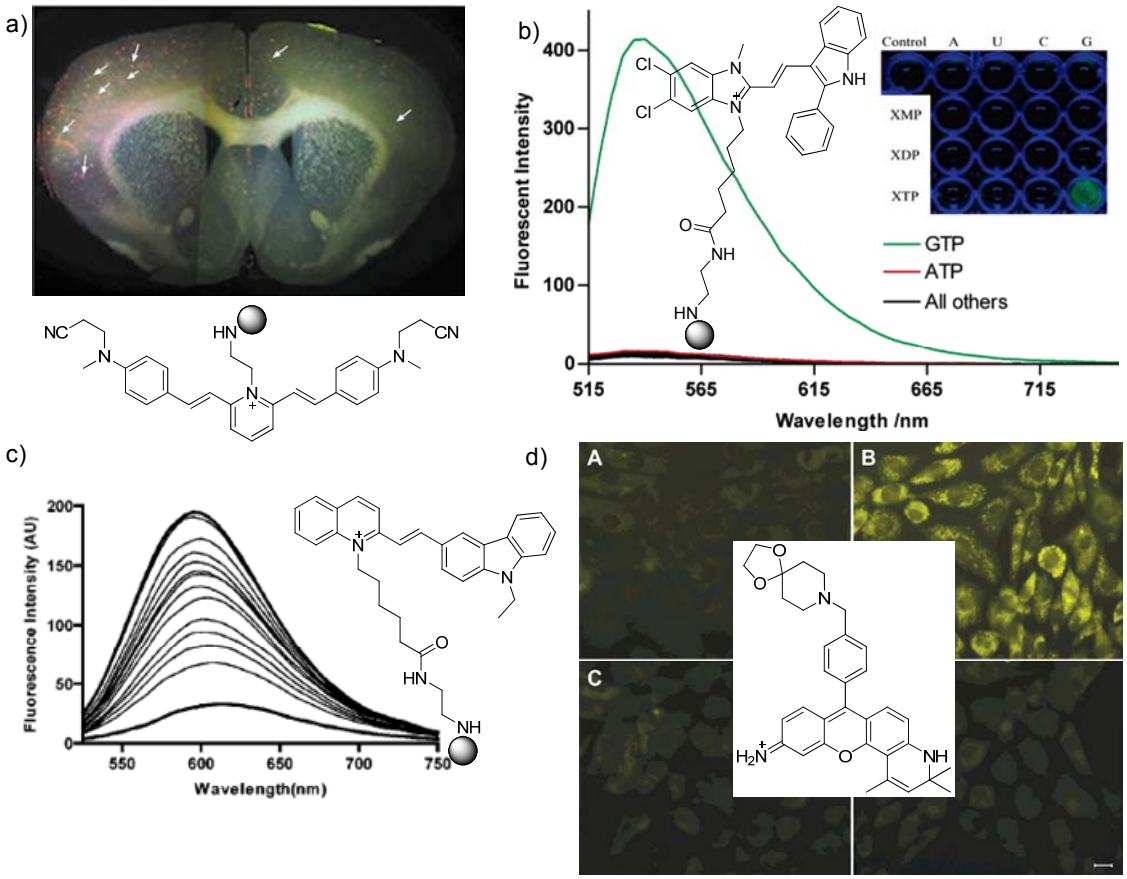

Figure 1.6 DOFL prepared from solid-phase synthesis for sensor development. (a) styryl dye and labeling of amyloid deposits in mouse brain tissue; (b) benzimidazole dye and fluorescence spectra upon incubation with GTP and other nucleotides; (c) quinaldine dye and fluorescence spectra upon incubation with chymotrypsin; (d) rosamine dye and glutathione staining in 3T3 cells. These pictures have been partly reproduced form ref 31 (a), 32 (b), 33 (c), and 35 (d) with permission. (a) Copyright 2004 Wiley-VCH. (b, c, d) Copyright 2006, 2007 and 2008 American Chemical Society.

As complement to the limited fluorescent scaffold, de novo construction was used to expand the availability of fluorophores. Park and co-workers prepared libraries based on 1,2-dihydropyrrolo[3,4-*b*]indolizin-3-one structure through condensation of α,β-unsaturated aldehydes and pyridine derivatives followed by 1,3-dipolar cycloaddition and further oxidation. One novelty of this library is the feasibility in predicting the emission wavelength from theoretical calculations of Hammett constant and energy gaps (Figure 1.7).[38] Multi-component one-pot reactions were also used for preparation

of novel fluorophores. Wang's group reported the construction of a cyanoaniline library from three-component one-pot reactions, which constitute a unique acceptor-donor-acceptor system.[39] Balakirev and co-workers reported a library through combination of 8 heterocyclic amidines, 40 aldehydes, and 5 isocyanides in droplet array platform, which facilitated the screening of this library.[40] The synthesis of new fluorophores can also be based on known motifs. Lee *et al.* prepared a 41-member benzylideneimidazolinone library based on the chromophore of the green fluorescent protein (GFP), and identified novel sensors for pH, HSA and RNA.[41]

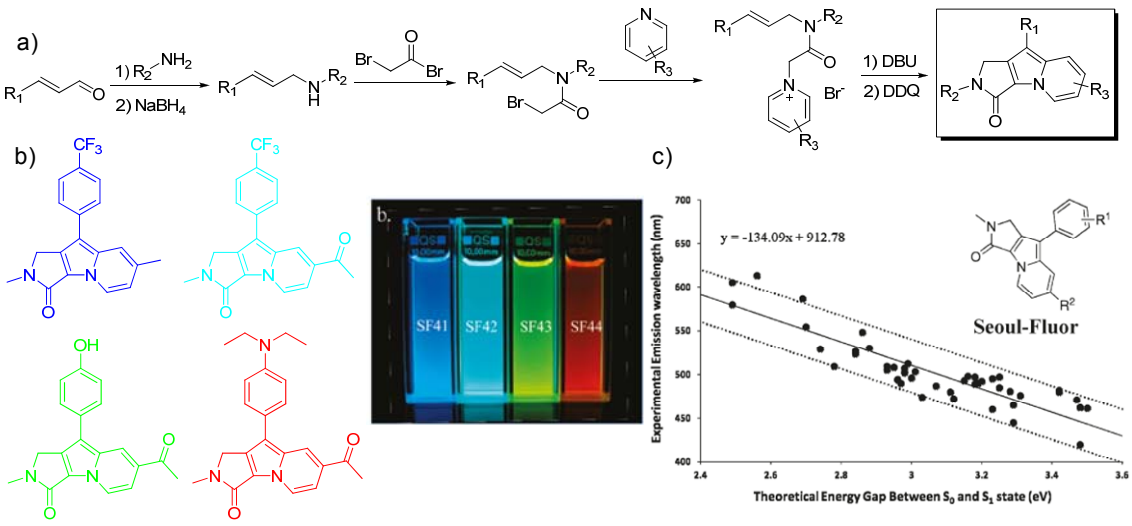

Figure 1.7 De novo construction of DOFL. (a) synthetic scheme for the preparation of 1,2-dihydropyrrolo[3,4-b]indolizin-3-ones; (b) representative chemical structures of the library and their pictures; (c) correlation of the emission wavelength and energy gap of the library compounds. These pictures have been partly reproduced form ref 38 with permission. Copyright 2011 American Chemical Society.

1.3 Screening System

Combinatorial approach accelerates sensor development not only through generation of diverse chemical toolbox, but also validation of sensors in a high-throughput manner. Various screening systems have been developed in the last decades to maximize the chance to discover "hit" compounds. According to the media used in

screening process, they can mainly be classified into *in vitro* screening and cell-based screening.

1.3.1 *In Vitro* Screening

In vitro screening is based on monitoring the fluorescence spectra change of potential sensors induced by binding with analytes. These screenings are usually technically simple, inexpensive and reproducible, and especially suitable to discover sensors for defined analytes (e.g., metal ions and sugars) or specific biomarkers (e.g., β-amyloid plaques for Alzheimer's disease[31]). When there is no prior defined target of interest, *in vitro* screening can also be performed in an unbiased manner especially for DOFL. In this case, the success rate of sensor development is enhanced as variety targets covering broad range of biological events can be included. One example is the unbiased screening of 41 benzylideneimidazolinone compounds demonstrated by Lee *et al*., from which three turn-on sensors for pH, HSA, and RNA were successfully discovered.[41]

1.3.2 Cell-Based Screening

Recent technical development of optical imaging instruments enables high-throughput screening to be performed based on cell image.[42] Compared to *in vitro* screening, cell-based screening is dealing with more complicated situation and can be affected by many unknown factors. This is also one of the major obstacles in rational design of sensors when cell-based screening was used to evaluate them. On the other hand, DOFL can benefit from this situation, especially combined with high-throughput screening, as when they are screened directly to the cells, the unique characteristics of each cell type enable the discovery of specific probes. One example is the identification of a stem cell probe (i.e., CDy1) by Chang and co-workers. 280 rosamine dyes were screened against mouse embryonic stem cells (mESC) and mouse embryonic fibroblasts

(MEF, feeder cells for mESC), and CDy1 was identified as the best hit which showed significant selectivity to mESC. CDy1 was also further characterized as an excellent tool to stain and isolate embryonic and induced pluripotent stem cells (Figure 1.8).[37]

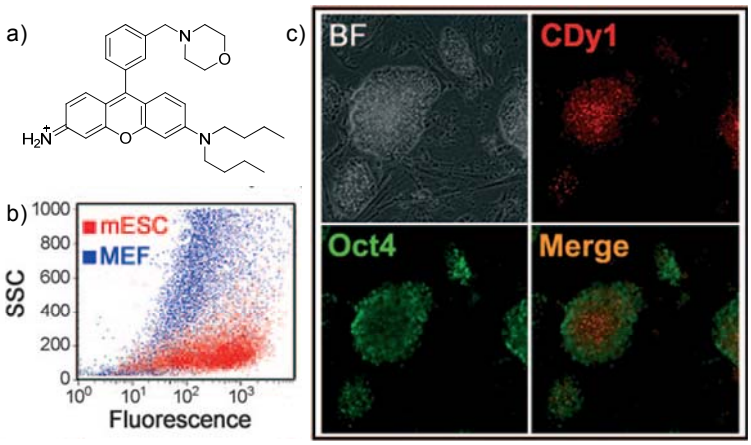

Figure 1.8 Identification of a fluorescent mESC probe (CDy1). (a) Structure of CDy1; (b) Upper panel: mESC stained with CDy1 were immunostained with anti-Oct4 antibody; lower panel: mESC treated with DMSO was used as a negative control; (c) Flow cytometry dot-plot image of mESC and MEF stained with CDy1. These pictures have been partly reproduced form ref 37 with permission. Copyright 2010 Wiley-VCH.

1.4 BODIPY Dyes

1.4.1 Overall Properties of BODIPY Dyes

BODIPY (4,4-Difluoro-4-bora-3a,4a-diaza-s-indacene) dyes were first discovered in 1968 by Treibs and Kreuzer.[43] Their unique properties among fluorophore family can be recognized from the following aspects. First is their outstanding photophysical properties, such as good photostability, high quantum yield (e.g., tetramethyl BODIPY has a quantum yield of almost 1), high extinction coefficient (ε, around 100,000 $M^{-1}cm^{-1}$), narrow emission bandwidth and environmental insensitivity.[3] Additionally, the emission wavelength of BODIPY dyes is tunable through appropriate substitution, which makes them become surrogates for some traditional dyes, such as fluorescein, tetramethylrhodamine, Texas red and many others.[4] Another important property of

BODIPY dyes is the overall lipophilicity and electrically neutral character, which allow them to be incorporated into lipophilic probes and induce minimal perturbation of functional properties of conjugates.[44] Moreover, the Stokes shift of BODIPY dyes is small (i.e., around 20 nm) making the fluorophore susceptible to self-quenching through energy transfer. This phenomenon can be used to build useful protease sensors, while the proteolysis of densely labelled proteins will lead to fluorescence increase.[45]

1.4.2 Applications of BODIPY Dyes

Over the years since first discovery of BODIPY dye, the derivatization has been made on all the possible 8 positions of its core (Figure 1.9) through different chemistries. The large chemical tool box of BODIPY dyes enables their wide applications on different purposes. In addition to the preferred fluorophores incorporated into lipophilic probes or protease sensors, which was discussed earlier, BODIPY dyes were widely used as labelling reagents for proteins and DNA, due to their superior photophysical properties.[3] Substitution on BODIPY core, especially 3- and 5-positions enlarges their conjugation area and further extended the emission wavelength. Various BODIPY derivatives covering green to NIR emission colour (Figure 1.10) have been reported and even commercialized as labelling kit for different purposes. In the mean time, BODIPY dyes were also popular fluorophores to develop novel sensors. In recent years, sensors on the basis of BODIPY scaffold have been reported to detect various analytes, including metal ions, anions, reactive oxygen species (ROS), pH, thiols, proteins and different environmental factors.

Figure 1.9 Derivatizing at different positions of BODIPY core.

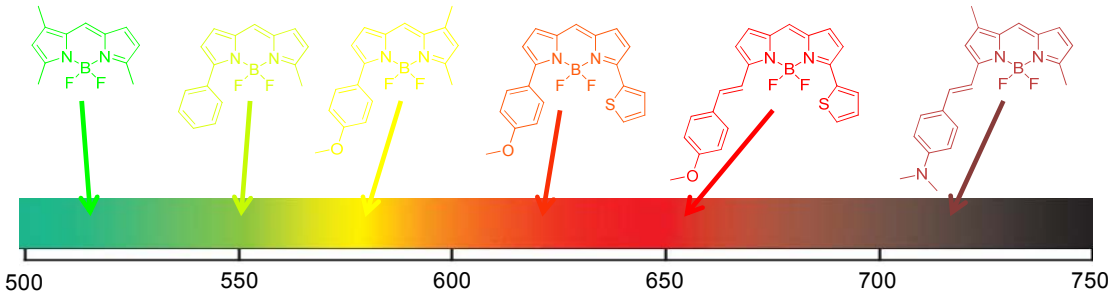

Figure 1.10 Representative structures of BODIPY derivatives covering spectra from green to NIR

Most of the BODIPY metal ions sensors were designed based on PeT mechanism, while the receptor acts as electron-donor part and quenches the fluorescence of BODIPY core. Once those sensors bind with metal ions, the electron-donning effect of receptors is diminished and the fluorescence of BODIPY will be recovered.[6] One example is the Cu^{+} sensor reported by Chang group. A well known Cu^{+} binding motif, thioether macrocycle, which can also distinguish Cu^{+} against Cu^{2+}, was conjugated with BODIPY core. This sensor (**21**, Figure 1.11) showed high fluorescence response to Cu^{+}, as well as good selectivity, and can be used as imaging tool to study Cu^{+} concentration in live cells.[46] Similar researches have also been conducted towards other metal analytes, including Ca^{2+} (**13**[47]), K^{+} (**14**[48]), Zn^{2+} (**15**[49]), Hg^{2+} (**16**[50]), Cd^{2+} (**17**[51]), Ni^{2+} (**18**[52]), Au^{3+}/Au^{+} (**19**[53]), Pb^{2+} (**20**[54]), Cu^{2+} (**22**[54]), Fe^{3+} (**23**[55]), and many others. The design for anion (e.g., F^{-}[56] and CN^{-}[57]) sensors, as well as thiol sensors[58] (e.g., cyctein) mainly utilized specific reactions. Labile groups for anions (e.g., Si substitutes for F) or thiols (e.g. 2,4-dinitrobenzenesulfonyl and maleimide) were introduced to the sensor structures and the attacking of analytes resulted in fluorescent change of sensors (**24**-**27**). Similar reaction-based approach was also used to design ROS sensors. Pioneer work was reported by Nagano group to design a highly sensitive sensor for nitric oxide (NO) (**28**). 3,4-diaminophenyl group was selected as reactive group, and after the sensor was

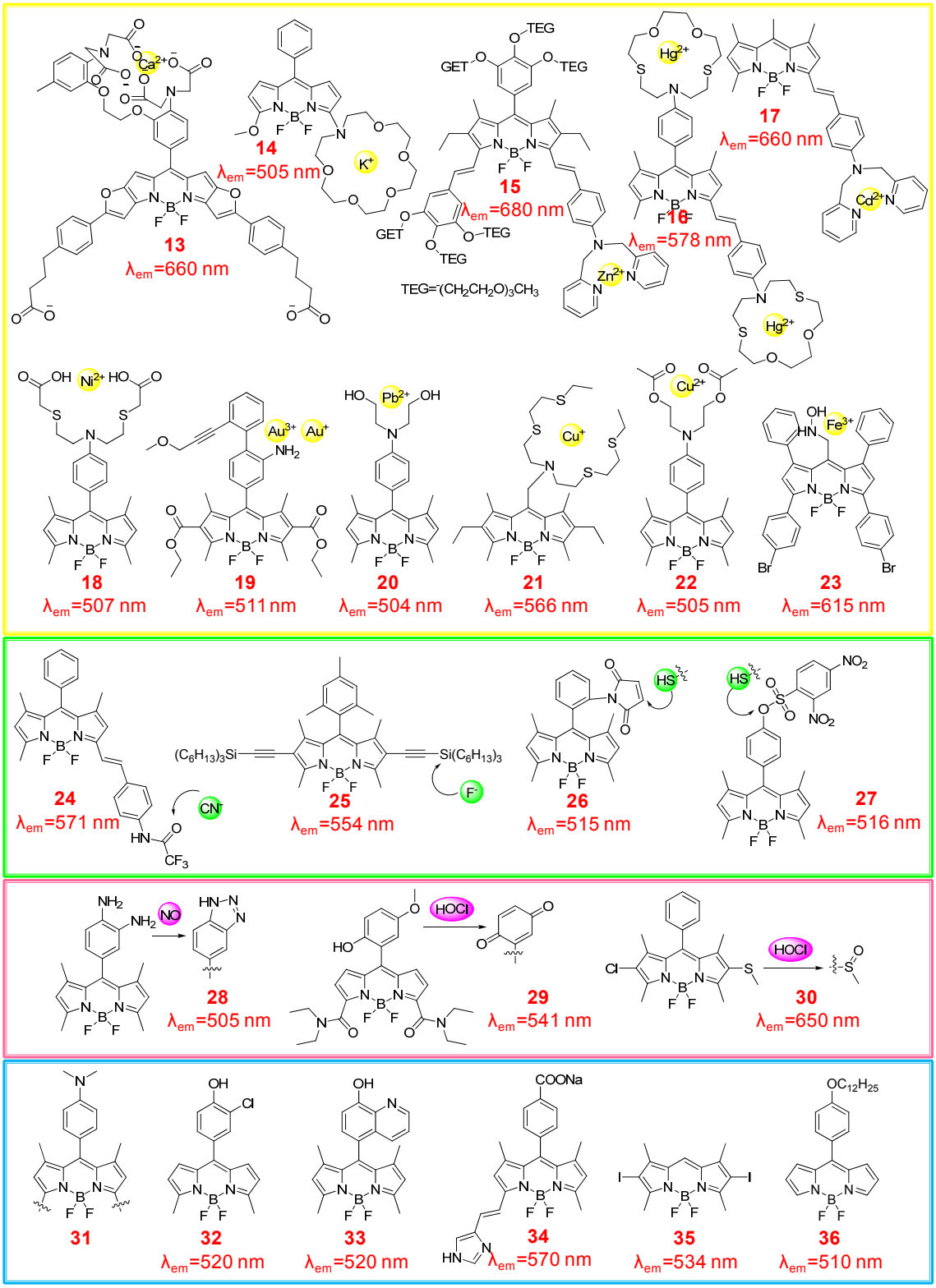

Figure 1.11 Structures of selected BODIPY sensors for metal ions, anions, thiols, ROS, and environment factors

exposed to NO, it was then oxidized to triazole to diminish the PeT effect and turn on the fluorescence.[59] Other redox labile groups were also conjugated to BODIPY to prepared sensors for different ROS (e.g., HOCl) (**29, 30**).[60] In addition, BODIPY dyes were also be designed as enzyme sensors to study enzyme's activities,[61] as well as environmental sensors to monitor changes of various factors, such as pH (**31**-**34**),[62] light (**35**),[63] viscosity (**36**),[64] and so on (Figure 1.11).

1.5 Scope and Outline

It has been discussed earlier that DOFL approach has been applied to different fluorophores and accelerated the development of fluorescent sensors by combining with high-throughput screening. It has also been highlighted that BODIPY structure is a unique fluorophore with superior spectral properties and has wide applications in fluorescent sensor and labelling reagent. Hence, we aim to design novel diversity-oriented BODIPY libraries and apply them to both *in vitro* screening and cell-based screening system in order to develop novel BODIPY-based sensors.

The aims of this thesis project are:

1) To synthesize novel diversity-oriented BODIPY libraries. In this strategy, I first introduced an active ester motif to BODIPY core and synthesized a 160-member library (**BDD**). This active ester motif can later be easily replaced by other functional groups. Hence, **BDD** was further derivatized to two other functional libraries, Lyso Tracker library (**BDL**) and Aldefluor library (**BDA**).
2) To discover novel BODIPY sensors from the three BODIPY libraries through unbiased *in vitro* screening. For this purpose, I conducted an unbiased *in vitro* screening to **BDD**, **BDL** and **BDA** against 54 different analytes. Two novel sensors

for fructose (**Fructose Orange**) and glutathione (**Glutathione Green**) was discovered and further evaluated.

3) To develop fluorescent sensors for illicit date-rape drug, gamma-butyrolactone (GBL). For this purpose, we conducted a target-oriented screening to GBL using DOFL. 5 compounds from **BDD** library were identified as GBL sensors, and one further derivative showing even better response was selected as final hit (**Green Date**). **Green Date** was also applied to detect GBL in real drink samples.
4) To develop novel fluorescent small molecule probe for neural stem cells. Cell-based screening was carried out with the three BODIPY libraries. One **BDD** compound (CDr3) showing selective staining to neural stem cell from both human and mouse origin was identified as stem cell probe. Further study showed CDr3 can bind to neural stem cell biomarker, fatty acid binding protein 7.
5) To find out the structure-cellular behaviour relationship of BODIPY dyes using DOFL approach. One BODIPY library with very diverse physical properties and different colours were synthesized and applied to cell-based screening system. Cellular localization and retention of compounds were successfully correlated to the structures of substitutions of BODIPY dyes. Using the information, a protein tag system based on BODIPY diacrylate structure was successfully developed after solving the background issue.

References

1. James, T. D.; Philips, M. D.; Shinkai, S., *Boronic Acids in Saccharide Recognition*. RSC Publishing: Cambridge, UK, 2006.

2. Lee, J. S.; Kim, Y. K.; Vendrell, M.; Chang, Y. T., Diversity-oriented fluorescence library approach for the discovery of sensors and probes. *Mol. BioSys.* **2009,** *5*, 411-421.

3. Loudet, A.; Burgess, K., BODIPY Dyes and Their Derivatives: Syntheses and Spectroscopic Properties. *Chem. Rev.* **2007,** *107*, 4891-4932.

4. Lavis, L. D.; Raines, R. T., Bright ideas for chemical biology. *ACS Chem. Biol.* **2008,** *3*, 142-155.

5. Zelent, B.; Kusba, J.; Gryczynski, I.; Johnson, M. L.; Lakowicz, J. R., Time-resolved and steady-state fluorescence quenching of N-acetyl-L-tryptophanamide by acrylamide and iodide. *Biophys. Chem.* **1998,** *73*, 53-75.

6. de Silva, A. P.; Gunaratne, H. Q.; Gunnlaugsson, T.; Huxley, A. J.; McCoy, C. P.; Rademacher, J. T.; Rice, T. E., Signaling Recognition Events with Fluorescent Sensors and Switches. *Chem. Rev.* **1997,** *97*, 1515-1566.

7. McGlynn, S. P.; Daigre, J.; Smith, F. J., External heavy atom spin-orbital coupling effect. IV. Intersystem crossing. *J. Chem. Phys.* **1963,** *39*, 675-679.

8. Herschel, J. F. W., On a case of superficial colour presented by a homogeneous liquid internally colourless. *Phil. Trans. R. Soc. London* **1845,** *135*, 143-145.

9. Min, J.; Lee, J. W.; Ahn, Y. H.; Chang, Y. T., Combinatorial dapoxyl dye library and its application to site selective probe for human serum albumin. *J. Comb. Chem.* **2007,** *9*, 1079-1083.

10. Li, Q.; Kim, Y.; Namm, J.; Kulkarni, A.; Rosania, G. R.; Ahn, Y. H.; Chang, Y. T., RNA-selective, live cell imaging probes for studying nuclear structure and function. *Chem. Biol.* **2006,** *13*, 615-623.

11. Martinez-Manez, R.; Sancenon, F., Fluorogenic and chromogenic chemosensors and reagents for anions. *Chem. Rev.* **2003,** *103*, 4419-76.

12. Singh, A.; Yao, Q.; Tong, L.; Clark Still, W.; Sames, D., Combinatorial approach to the development of fluorescent sensors for nanomolar aqueous copper. *Tetrahedron Lett.* **2000,** *41*, 9601-9605.

13. Valeur, B., *Molecular Fluorescence: Principles and Applications*. 1st ed.; Wiley-VCH: New York, 2001.

14. Rivero, I. A.; Gonzalez, T.; Pina-Luis, G.; Diaz-Garcia, M. E., Library preparation of derivatives of 1,4,10,13-tetraoxa-7,16-diaza-cyclooctadecane and their fluorescence behavior for signaling purposes. *J. Comb. Chem.* **2005,** *7*, 46-53.

15. (a) Mello, J. V.; Finney, N. S., Reversing the Discovery Paradigm: A New Approach to the Combinatorial Discovery of Fluorescent Chemosensors. *J. Am. Chem. Soc.* **2005,** *127*, 10124-10125; (b) Malashikhin, S. A.; Baldridge, K. K.; Finney, N. S., Efficient Discovery of Fluorescent Chemosensors Based on a Biarylpyridine Scaffold. *Org. Lett.* **2010,** *12*, 940-943.

16. (a) Steiner, M.-S.; Duerkop, A.; Wolfbeis, O. S., Optical methods for sensing glucose. *Chem. Soc. Rev.* **2011,** *40*, 4805-4839; (b) Gabius, H. J.; André, S.; Jiménez-Barbero, J.; Romero, A.; Solís, D., From lectin structure to functional glycomics: Principles of the sugar code. *Trends Biochem. Sci.* **2011,** *36*, 298-313.

17. (a) Wulff, G., Selective Binding to Polymers Via Covalent Bonds. The Construction of Chiral Cavities as Specific Receptor Sites. *Pure Appl. Chem.* **1982,** *54*, 2093-2102; (b) James, T. D.; Samankumara Sandanayake, K. R. A.; Shinkai, S., Saccharide sensing with molecular receptors based on boronic acid. *Angew. Chem., Int. Ed.* **1996,** *35*, 1910-1922.

18. Wang, J.; Jin, S.; Lin, N.; Wang, B., Fluorescent indolylboronic acids that are useful reporters for the synthesis of boronolectins. *Chem. Biol. Drug Des.* **2006,** *67*, 137-144.

19. Yang, W.; Yan, J.; Springsteen, G.; Deeter, S.; Wang, B., A novel type of fluorescent boronic acid that shows large fluorescence intensity changes upon binding with a carbohydrate in aqueous solution at physiological pH. *Bioorg. Med. Chem. Lett.* **2003,** *13*, 1019-1022.

20. Stones, D.; Manku, S.; Lu, X.; Hall, D. G., Modular Solid-Phase Synthetic Approach to Optimize Structural and Electronic Properties of Oligoboronic Acid Receptors and Sensors for the Aqueous Recognition of Oligosaccharides. *Chem. -Eur. J.* **2004,** *10*, 92-100.

21. Schiedel, M. S.; Briehn, C. A.; Bauerle, P., Single-compound libraries of organic materials: Parallel synthesis and screening of fluorescent dyes. *Angew. Chem., Int. Ed.* **2001,** *40*, 4677.

22. (a) Hirano, T.; Hiromoto, K.; Kagechika, H., Development of a library of 6-arylcoumarins as candidate fluorescent sensors. *Org. Lett.* **2007,** *9*, 1315-1318; (b) Roy, S.; Roy, S.; Neuenswander, B.; Hill, D.; Larock, R. C., Solution-phase synthesis of a diverse isocoumarin library. *J. Comb. Chem.* **2009,** *11*, 1128-35; (c) Sivakumar, K.; Xie, F.; Cash, B. M.; Long, S.; Barnhill, H. N.; Wang, Q., A fluorogenic 1,3-dipolar cycloaddition reaction of 3-azidocoumarins and acetylenes. *Org. Lett.* **2004,** *6*, 4603-4606.

23. Peng, T.; Yang, D., Construction of a Library of Rhodol Fluorophores for Developing New Fluorescent Probes. *Org. Lett.* **2010,** *12*, 496-499.

24. Li, J. Q.; Hu, M. Y.; Yao, S. Q., Rapid Synthesis, Screening, and Identification of Xanthone- and Xanthene-Based Fluorophores Using Click Chemistry. *Org. Lett.* **2009,** *11*, 3008-3011.

25. Samanta, A.; Vendrell, M.; Das, R.; Chang, Y.-T., Development of photostable near-infrared cyanine dyes. *Chem. Commun.* **2010,** *46*, 7406.

26. (a) Zhu, Q.; Yoon, H. S.; Parikh, P. B.; Chang, Y. T.; Yao, S. Q., Combinatorial discovery of novel fluorescent dyes based on Dapoxyl. *Tetrahedron Lett.* **2002,** *43*, 5083; (b) Cao, H.; Chang, V.; Hernandez, R.; Heagy, M. D., Matrix screening of substituted N-aryl-1,8-naphthalimides reveals new dual fluorescent dyes and unusually bright pyridine derivatives. *J. Org. Chem.* **2005,** *70*, 4929-4934.

27. Rosania, G. R.; Lee, J. W.; Ding, L.; Yoon, H. S.; Chang, Y. T., Combinatorial approach to organelle-targeted fluorescent library based on the styryl scaffold. *J. Am. Chem. Soc.* **2003,** *125*, 1130-1131.

28. Lee, J. W.; Jung, M.; Rosania, G. R.; Chang, Y. T., Development of novel cell-permeable DNA sensitive dyes using combinatorial synthesis and cell-based screening. *Chem. Commun.* **2003,** *39*, 1852-1853.

29. (a) Song, A. M.; Zhang, J. H.; Lam, K. S., Synthesis and reactions of 7-fluoro-4-methyl-6-nitro-2-oxo-2H-1-benzopyran-3-carboxylic acid: A novel scaffold for combinatorial synthesis of coumarins. *J. Comb. Chem.* **2004,** *6*, 112-120; (b) Song, A. M.; Zhang, J. H.; Lebrilla, C. B.; Lam, K. S., Solid-phase synthesis and spectral properties of 2-alkylthio-6H-pyrano 2,3-f benzimidazole-6-ones: A combinatorial approach for 2-alkylthioimidazocoumarins. *J. Comb. Chem.* **2004,** *6*, 604-610.

30. Oh, S.; Jang, H. J.; Ko, S. K.; Ko, Y.; Park, S. B., Construction of a polyheterocyclic benzopyran library with diverse core skeletons through diversity-oriented synthesis pathway. *J. Comb. Chem.* **2010,** *12*, 548-58.

31. Li, Q.; Lee, J. S.; Ha, C.; Park, C. B.; Yang, G.; Gan, W. B.; Chang, Y. T., Solid-phase synthesis of styryl dyes and their application as amyloid sensors. *Angew. Chem., Int. Ed.* **2004,** *43*, 6331-6335.

32. Wang, S. L.; Chang, Y. T., Combinatorial synthesis of benzimidazolium dyes and its diversity directed application toward GTP-selective fluorescent chemosensors. *J. Am. Chem. Soc.* **2006,** *128*, 10380-10381.

33. Wang, S. L.; Kim, Y. K.; Chang, Y. T., Diversity-oriented fluorescence library approach (DOFLA) to the discovery of chymotrypsin sensor. *J. Comb. Chem.* **2008,** *10*, 460-465.

34. Ghosh, K. K.; Ha, H. H.; Kang, N. Y.; Chandran, Y.; Chang, Y. T., Solid phase combinatorial synthesis of a xanthone library using click chemistry and its application to an embryonic stem cell probe. *Chem. Commun.* **2011,** *47*, 7488-90.

35. Ahn, Y. H.; Lee, J. S.; Chang, Y. T., Combinatorial rosamine library and application to in vivo glutathione probe. *J. Am. Chem. Soc.* **2007,** *129*, 4510-4511.

36. Kim, Y. K.; Ha, H. H.; Lee, J. S.; Bi, X.; Ahn, Y. H.; Hajar, S.; Lee, J. J.; Chang, Y. T., Control of muscle differentiation by a mitochondria-targeted fluorophore. *J. Am. Chem. Soc.* **2010,** *132*, 576-579.

37. Im, C. N.; Kang, N. Y.; Ha, H. H.; Bi, X.; Lee, J. J.; Park, S. J.; Lee, S. Y.; Vendrell, M.; Kim, Y. K.; Lee, J. S.; Li, J.; Ahn, Y. H.; Feng, B.; Ng, H. H.; Yun, S. W.; Chang, Y. T., A fluorescent rosamine compound selectively stains pluripotent stem cells. *Angew. Chem., Int. Ed.* **2010,** *49*, 7497-7500.

38. (a) Kim, E.; Koh, M.; Ryu, J.; Park, S. B., Combinatorial discovery of full-color-tunable emissive fluorescent probes using a single core skeleton, 1,2-dihydropyrrolo[3,4-beta]indolizin-3-one. *J. Am. Chem. Soc.* **2008,** *130*, 12206-12207; (b) Kim, E.; Koh, M.; Lim, B. J.; Park, S. B., Emission Wavelength Prediction of a Full-Color-Tunable Fluorescent Core Skeleton, 9-Aryl-1,2-dihydropyrrolo[3,4-b]indolizin-3-one. *J. Am. Chem. Soc.* **2011,** *133*, 6642-6649.

39. Cui, S. L.; Lin, X. F.; Wang, Y. G., Parallel synthesis of strongly fluorescent polysubstituted 2,6-dicyanoanilines via microwave-promoted multicomponent reaction. *J. Org. Chem.* **2005,** *70*, 2866-2869.

40. Burchak, O. N.; Mugherli, L.; Ostuni, M.; Lacapere, J. J.; Balakirev, M. Y., Combinatorial discovery of fluorescent pharmacophores by multicomponent reactions in droplet arrays. *J. Am. Chem. Soc.* **2011,** *133*, 10058-10061.

41. Lee, J. S.; Baldridge, A.; Feng, S.; SiQiang, Y.; Kim, Y. K.; Tolbert, L. M.; Chang, Y. T., Fluorescence response profiling for small molecule sensors utilizing the green fluorescent protein chromophore and its derivatives. *ACS Comb. Sci.* **2011,** *13*, 32-38.

42. (a) Inglese, J.; Johnson, R. L.; Simeonov, A.; Xia, M.; Zheng, W.; Austin, C. P.; Auld, D. S., High-throughput screening assays for the identification of chemical probes. *Nat. Chem. Biol.* **2007,** *3*, 466-479; (b) Carpenter, A. E., Image-based chemical screening. *Nat. Chem. Biol.* **2007,** *3*, 461-465.

43. Treibs, A.; Haberle, N., Concerning the synthesis and the electron spectrum of ms-substituted porphine. *Justus Liebigs Ann. Chem.* **1968,** *718*, 183-207.

44. Karolin, J.; Johansson, L. B. A.; Strandberg, L.; Ny, T., Fluorescence and Absorption Spectroscopic Properties of Dipyrrometheneboron Difluoride (BODIPY) Derivatives in Liquids, Lipid Membranes, and Proteins. *J. Am. Chem. Soc.* **1994,** *116*, 7801-7806.

45. Thompson, V. F.; Saldana, S.; Cong, J.; Goll, D. E., A BODIPY fluorescent microplate assay for measuring activity of calpains and other proteases. *Anal. Biochem.* **2000,** *279*, 170-178.

46. (a) Zeng, L.; Miller, E. W.; Pralle, A.; Isacoff, E. Y.; Chang, C. J., A selective turn-on fluorescent sensor for imaging copper in living cells. *J. Am. Chem. Soc.* **2006,** *128*, 10-11; (b) Domaille, D. W.; Zeng, L.; Chang, C. J., Visualizing ascorbate-triggered release of labile copper within living cells using a ratiometric fluorescent sensor. *J. Am. Chem. Soc.* **2010,** *132*, 1194-1195.

47. Matsui, A.; Umezawa, K.; Shindo, Y.; Fujii, T.; Citterio, D.; Oka, K.; Suzuki, K., A near-infrared fluorescent calcium probe: a new tool for intracellular multicolour Ca2+ imaging. *Chem. Commun.* **2011,** *47*, 10407-10409.

48. Baruah, M.; Qin, W.; Vallee, R. A.; Beljonne, D.; Rohand, T.; Dehaen, W.; Boens, N., A highly potassium-selective ratiometric fluorescent indicator based on BODIPY azacrown ether excitable with visible light. *Org. Lett.* **2005,** *7*, 4377-4380.

49. Atilgan, S.; Ozdemir, T.; Akkaya, E. U., A Sensitive and Selective Ratiometric Near IR Fluorescent Probe for Zinc Ions Based on the Distyryl-Bodipy Fluorophore. *Org. Lett.* **2008,** *10*, 4065-4067.

50. Yuan, M.; Li, Y.; Li, J.; Li, C.; Liu, X.; Lv, J.; Xu, J.; Liu, H.; Wang, S.; Zhu, D., A Colorimetric and Fluorometric Dual-Modal Assay for Mercury Ion by a Molecule. *Org. Lett.* **2007,** *9*, 2313-2316.

51. Peng, X.; Du, J.; Fan, J.; Wang, J.; Wu, Y.; Zhao, J.; Sun, S.; Xu, T., A Selective Fluorescent Sensor for Imaging Cd^{2+} in Living Cells. *J. Am. Chem. Soc.* **2007,** *129*, 1500-1501.

52. Dodani, S. C.; He, Q.; Chang, C. J., A Turn-On Fluorescent Sensor for Detecting Nickel in Living Cells. *J. Am. Chem. Soc.* **2009,** *131*, 18020-18021.

53. Wang, J. B.; Wu, Q. Q.; Min, Y. Z.; Liu, Y. Z.; Song, Q. H., A novel fluorescent probe for Au(III)/Au(I) ions based on an intramolecular hydroamination of a Bodipy derivative and its application to bioimaging. *Chem. Commun.* **2012,** *48*, 744-746.

54. Qi, X.; Jun, E. J.; Xu, L.; Kim, S. J.; Hong, J. S.; Yoon, Y. J.; Yoon, J., New BODIPY derivatives as OFF-ON fluorescent chemosensor and fluorescent chemodosimeter for Cu2+: cooperative selectivity enhancement toward Cu2+. *J. Org. Chem.* **2006,** *71*, 2881-2884.

55. Wang, R.; Yu, F.; Liu, P.; Chen, L., A turn-on fluorescent probe based on hydroxylamine oxidation for detecting ferric ion selectively in living cells. *Chem. Commun.* **2012,** *48*, 5310-5312.

56. Fu, L.; Jiang, F. L.; Fortin, D.; Harvey, P. D.; Liu, Y., A reaction-based chromogenic and fluorescent chemodosimeter for fluoride anions. *Chem. Commun.* **2011,** *47*, 5503-5505.

57. Ekmekci, Z.; Yilmaz, M. D.; Akkaya, E. U., A monostyryl-boradiazaindacene (BODIPY) derivative as colorimetric and fluorescent probe for cyanide ions. *Org. Lett.* **2008,** *10*, 461-464.

58. (a) Guo, H.; Jing, Y.; Yuan, X.; Ji, S.; Zhao, J.; Li, X.; Kan, Y., Highly selective fluorescent OFF-ON thiol probes based on dyads of BODIPY and potent intramolecular electron sink 2,4-dinitrobenzenesulfonyl subunits. *Org. Biomol. Chem.* **2011,** *9*, 3844-3853; (b) Matsumoto, T.; Urano, Y.; Shoda, T.; Kojima, H.; Nagano, T., A thiol-reactive fluorescence probe based on donor-excited photoinduced electron transfer: key role of ortho substitution. *Org. Lett.* **2007,** *9*, 3375-3377.

59. Gabe, Y.; Urano, Y.; Kikuchi, K.; Kojima, H.; Nagano, T., Highly sensitive fluorescence probes for nitric oxide based on boron dipyrromethene chromophore-rational design of potentially useful bioimaging fluorescence probe. *J. Am. Chem. Soc.* **2004,** *126* (10), 3357-3367.

60. (a) Sun, Z. N.; Liu, F. Q.; Chen, Y.; Tam, P. K.; Yang, D., A highly specific BODIPY-based fluorescent probe for the detection of hypochlorous acid. *Org. Lett.* **2008,** *10*, 2171-2174; (b) Kim, T. I.; Park, S.; Choi, Y.; Kim, Y., A BODIPY-based probe for the selective detection of hypochlorous acid in living cells. *Chem Asian J* **2011,** *6* (6), 1358-61.

61. (a) Kim, T. I.; Park, J.; Park, S.; Choi, Y.; Kim, Y., Visualization of tyrosinase activity in melanoma cells by a BODIPY-based fluorescent probe. *Chem. Commun.* **2011,** *47*, 12640-12462; (b) Komatsu, T.; Urano, Y.; Fujikawa, Y.; Kobayashi, T.; Kojima, H.; Terai, T.; Hanaoka, K.; Nagano, T., Development of 2,6-carboxy-substituted boron dipyrromethene (BODIPY) as a novel scaffold of ratiometric fluorescent probes for live cell imaging. *Chem. Commun.* **2009,** *45*, 7015-7017.

62. (a) Boens, N.; Qin, W.; Baruah, M.; De Borggraeve, W. M.; Filarowski, A.; Smisdom, N.; Ameloot, M.; Crovetto, L.; Talavera, E. M.; Alvarez-Pez, J. M., Rational design, synthesis, and spectroscopic and photophysical properties of a visible-light-excitable, ratiometric, fluorescent near-neutral pH indicator based on BODIPY. *Chem. -Eur. J.* **2011,** *17*, 10924-10934; (b) Baruah, M.; Qin, W.; Basaric, N.; De Borggraeve, W. M.; Boens, N., BODIPY-based hydroxyaryl derivatives as fluorescent pH probes. *J. Org. Chem.* **2005,** *70*, 4152-4157; (c) Chen, Y.; Wang, H.; Wan, L.; Bian, Y.; Jiang, J., 8-Hydroxyquinoline-substituted boron-dipyrromethene compounds: synthesis, structure, and OFF-ON-OFF type of pH-sensing properties. *J. Org. Chem.* **2011,** *76*, 3774-3781.

63. Yogo, T.; Urano, Y.; Ishitsuka, Y.; Maniwa, F.; Nagano, T., Highly efficient and photostable photosensitizer based on BODIPY chromophore. *J. Am. Chem. Soc.* **2005,** *127*, 12162-12163.

64. Kuimova, M. K.; Yahioglu, G.; Levitt, J. A.; Suhling, K., Molecular rotor measures viscosity of live cells via fluorescence lifetime imaging. *J. Am. Chem. Soc.* **2008,** *130*, 6672-6673.

Chapter 2 Diversity-Oriented Synthesis of Novel BODIPY Libraries

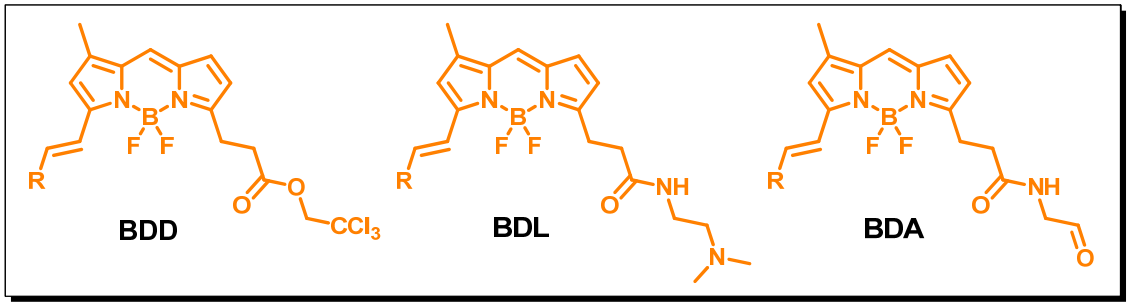

2.1 Introduction

As discussed earlier, BODIPY compounds have found wide applications towards different purposes.[1] However, compared to other fluorophores, construction of diversity-oriented BODIPY libraries is still rarely developed, probably due to the synthetic challenge.[2] The first BODIPY based library was reported by Nagano group in 2007 to study the solvent polarity dependence of their fluorescence and the role of photoinduced electron transfer (PeT).[3] In their strategy, 15 compounds with derivatization at 8-position of the BODIPY core were prepared. However, in this case, the BODIPY compounds in the library were still prepared one-by-one. Parallel synthesis of large numbers of BODIPY dyes was not available until the exploring work by our group. Lee *et al.* prepared a collection of 160 compounds through Knoevenagel condensation reaction on 1,3-dimethyl BODIPY scaffold (**BD**). After *in vitro* screening and cell-based screening, novel sensors for glucagon, dopamine, and bovine serum albumin (BSA) were successfully developed.[4] Although it has been controversial for adapting BODIPY to solid-phase chemistry due to its known acidic and basic sensitivity,[2] our group has successfully constructed a second generation BODIPY library on chlorotrityl resin to minimize the purification steps. Vendrell *et al.* prepared an aminoethyl BODIPY scaffold, attached it to solid-phase, and derivatized at 3-position using Knoevenagel condensation reaction to render 160 BODIPY compounds (BDM). A fluorescent probe for immunoglobulin was successfully discovered after *in vitro* screening.[5]

Encouraged by the successful examples, I prepared our third generation of BODIPY library by introducing an active ester motif to the core structure, and derivatizing it with same Knoevenagel condensation reaction. 160 compounds with good purity and covering broad spectra properties were rendered (**BDD**). This active ester group can be

easily replaced through nucleophilic substitution, and therefore two other functional BODIPY libraries (**BDL** and **BDA**) were further prepared through one step reaction.

2.2 Results and Discussion

2.2.1 Design and Synthesis of an Active Ester BODIPY Library (BDD)

Many commercially available BODIPY probes (e.g., LysoTracker Green DND-26, ALDEFLUOR®, BODIPY® FL C5-ceramide) are prepared from 4,4-difluoro-5,7-dimethyl-4-bora-3a,4a-diaza-s-indacene-3-propionic acid (BODIPY® FL[6]), partially due to its straightforward derivatization. One key intermediate of these probes is the compound **1** (Scheme 2.1), an activated ester of BODIPY® FL.[7] We envisioned that the combinatorial derivatization of **1** may render a suitable toolbox for the discovery of new fluorescent chemosensors, and prepared 160 **BDD** compounds in high purities by Knoevenagel condensation of **1** with structurally diverse aldehydes (Scheme 2.1 and Chart 2.1).

Scheme 2.1 General synthetic scheme of the **BDD** library

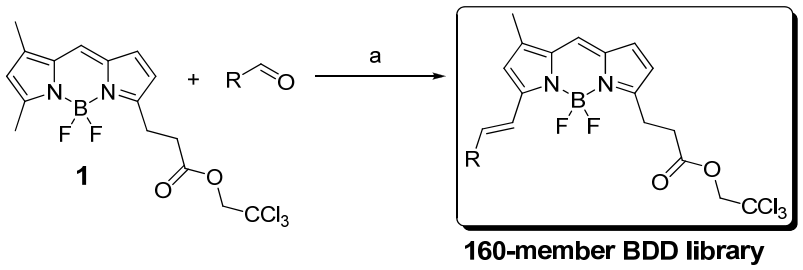

Reagents and conditions: a) pyrrolidine (6 eq.), acetic acid (6 eq.), ACN, 85 ^{o}C, 15 min.

Chart 2.1 A decoding table for **BDD** library

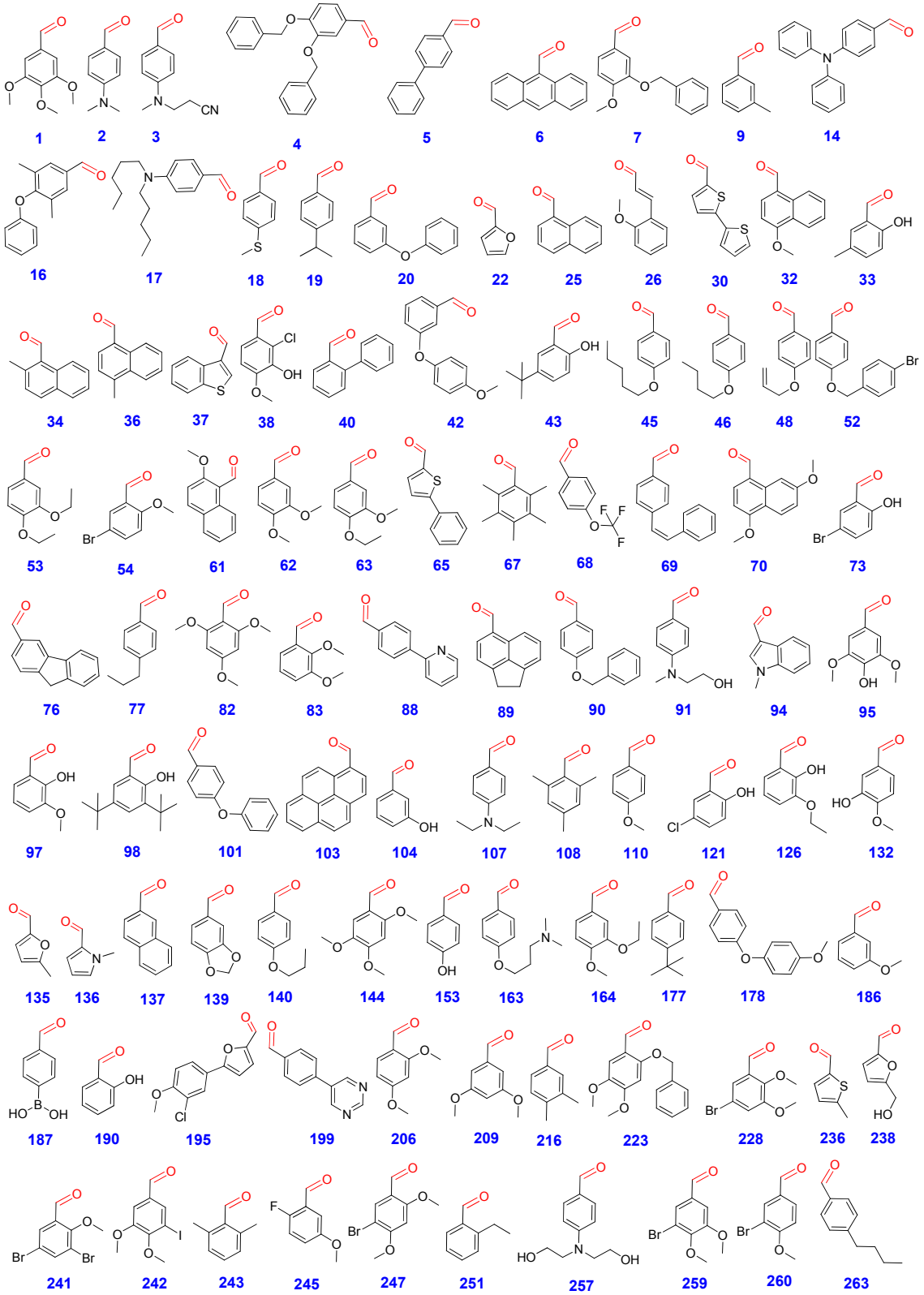

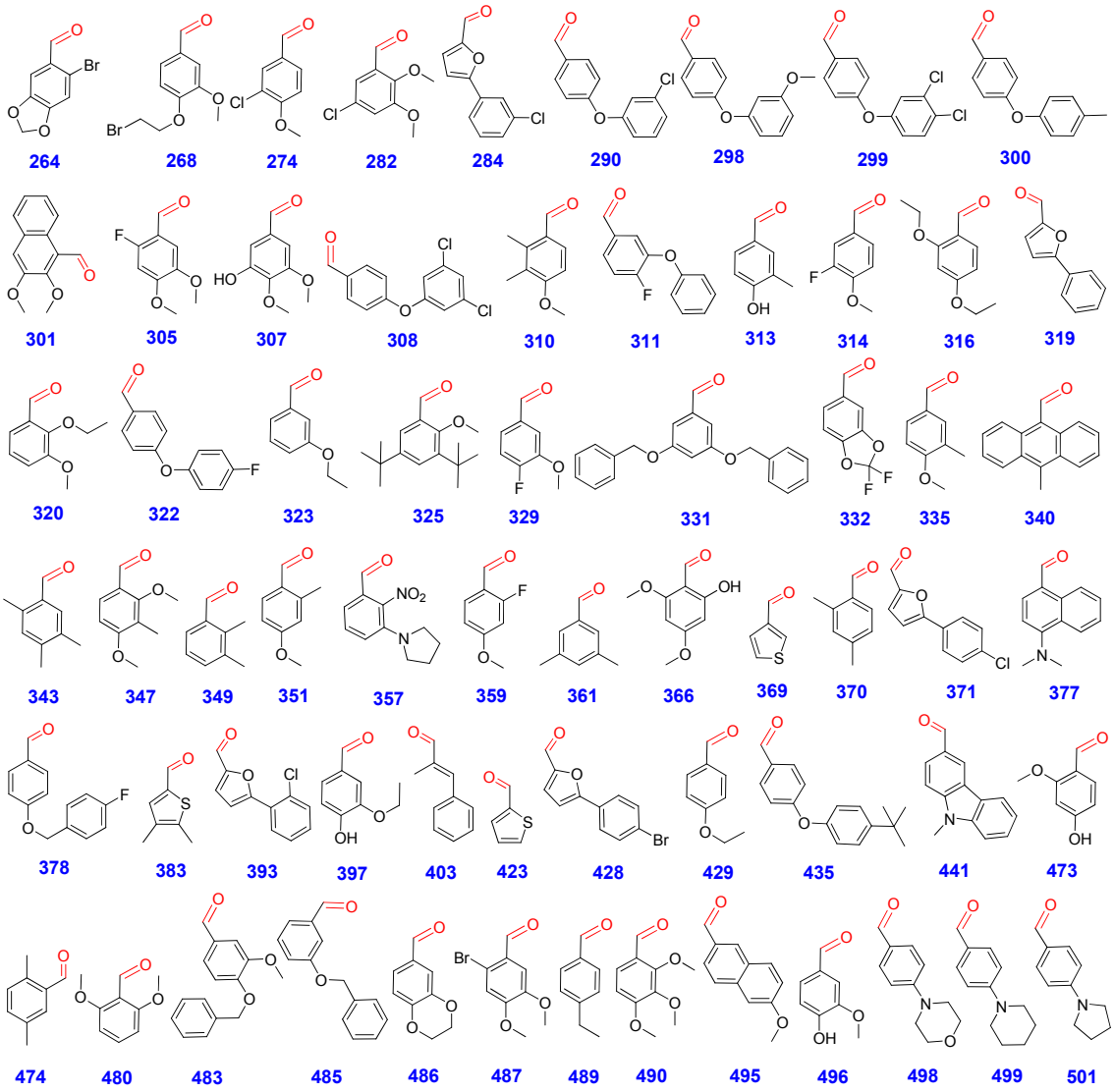
264
268
274
282
284
290
298
299
300
301
305
307
308
310
311
313
314
316
319
320
322
323
325
329
331
332
335
340
343
347
349
351
357
359
361
366
369
370
371
377
378
383
393
397
403
423
428
429
435
441
473
474
480
483
485
486
487
489
490
495
496
498
499
501

2.2.2 Spectroscopic Properties of BDD Library

The condensation reaction led to a red shift in the fluorescence emission properties of **1**, due to the extended π-conjugation system in **BDD** compounds.[8] The broad chemical diversity of the aldehyde building blocks gave rise to very diverse spectral properties for **BDD** derivatives: absorption wavelengths ranged from 540 nm to 627 nm, emission wavelengths from 560 to 795 nm and quantum yields varied from 0.006 to almost 1 (Table 2.1). This wide range of spectroscopic properties asserted the potential of the **BDD** library as a multicolor (from yellow to near infrared) and multi-type (turn-on or quenching) toolbox for the development of new fluorescent probes.

Table 2.1 Spectroscopic properties and purity table for **BDD** library: calculated mass, experimental mass, absorbance maximum (λ_{abs}), fluorescent emission maximum (λ_{em}), extinction coefficient (ε), quantum yield (Φ), and purity.

Code	mass (calc)	m/z (exp)	λ_{abs} (nm)	λ_{em} (nm)	ε ($M^{-1}cm^{-1}$)	Φ	Purity (%)[c]
BDD1	600.1	580.8	574	592	887259	0.56	97
BDD2	553.1	554.1[a]	615	744	2113457	0	95
BDD3	592.1	573.1	608	725	1138519	0.01	98
BDD4	722.1	703.1	579	602	901654	0.69	92
BDD5	586.1	567.1	576	591	722370	0.81	96
BDD6	610.1	591.1	544	560	458025	0.2	99
BDD7	646.1	626.7	579	601	463259	0.57	99
BDD9	524.1	504.8	566	579	2562321	0.27	97
BDD14	677.1	657.8	601	750	719753	0	98
BDD16	644.1	625.1	572	587	719753	0.88	97
BDD17	637.2	638.3	627	766	320617	0	99
BDD18	556.1	536.7	584	599	442321	0.37	98
BDD19	552.1	532.8	569	582	1129358	0.69	99
BDD20	602.1	583.1	567	585	1150296	0.64	98
BDD22	500	480.8	576	592	212000	0.31	98
BDD25	560.1	540.6	577	596	537852	0.78	96
BDD26	566.1	546.7	572	588	1324346	0.76	97
BDD30	598	579	607	649	1046914	0.07	96

BDD32	590.1	570.7	588	629	1294247	0.13	93
BDD33	540.1	520.8	576	593	651704	0.26	94
BDD34	574.1	555.1	559	592	552247	0.76	96
BDD36	574.1	555.1	580	602	341556	0.59	98
BDD37	566	546.5	577	596	647778	0.72	94
BDD38	590	571	577	598	701432	0.03	96
BDD40	586.1	567.1	567	582	526074	0.94	95
BDD42	632.1	612.7	567	579	92914	0.16	91
BDD43	582.1	563.7	576	595	1094025	0.38	94
BDD45	610.2	590.8	577	595	772099	0.79	93
BDD46	582.1	563.1	576	595	477654	0.67	99
BDD48	566.1	547	575	594	558790	0.8	99
BDD52	694	675.1	575	594	1083556	0.94	99
BDD53	598.1	579.1	579	605	862395	0.68	94
BDD54	618	599.6	573	587	1287704	0.61	95
BDD61	590.1	570.7	586	618	993259	0.42	98
BDD62	570.1	551.1	579	604	1015506	0.77	95
BDD63	584.1	565.2	579	604	1036444	0.53	94
BDD65	592.1	573.1	601	626	560099	0.2	97
BDD67	580.1	561.1	550	583	490741	>0.99	99
BDD68	594	593.0[b]	565	577	493358	0.86	94
BDD69	612.1	593.1	587	604	1440815	0.25	89
BDD70	620.1	601.1	592	651	851926	0.07	92
BDD73	604	584.6	574	588	473728	0.49	91
BDD76	598.1	579.1	584	598	189753	0.31	91
BDD77	552.1	533.2	570	583	719753	0.75	92
BDD82	600.1	580.7	589	620	810049	0.51	92
BDD83	570.1	551.1	568	581	357259	0.72	96
BDD88	587.1	588.1[a]	576	589	2529605	0.25	97
BDD89	586.1	567.1	588	616	1463062	0.19	96
BDD90	616.1	597.1	576	593	485506	0.75	92
BDD91	583.1	584.1[a]	619	752	527383	0	96
BDD94	563.1	544.1	584	648	94222	0.02	98
BDD95	586.1	567.1	584	618	477654	0.02	95
BDD97	556.1	537.1	573	588	1961654	0.01	97
BDD98	638.2	618.8	572	587	1427728	0.4	95
BDD101	602.1	593.1	575	588	756395	0.61	99
BDD103	634.1	615.1	605	638	1175160	0.2	89
BDD105	526.1	507.1	568	580	757704	0.78	94
BDD107	581.1	582.7[a]	624	759	582346	0	93

BDD108	552.1	533.1	559	593	959235	0.54	99
BDD110	540.1	521.1	575	594	625531	0.91	98
BDD121	560	541	573	587	243407	0.42	94
BDD126	554.1	535.1	580	605	887259	0.09	94
BDD132	556.1	537.1	573	586	444938	0.02	97
BDD135	514.1	494.7	565	585	369037	0.47	94
BDD136	513.1	514.1[a]	601	646	974938	0.12	95
BDD137	560.1	540.6	576	587	1162074	0.53	95
BDD139	554.1	534.8	576	598	927827	0.97	98
BDD140	568.1	549.1	576	596	1226198	>0.99	96
BDD144	600.1	581.1	590	651	991951	0.01	97
BDD153	526.1	507.1	578	601	1211802	0.65	96
BDD163	611.1	612.1[a]	579	597	81136	0.07	92
BDD164	584.1	565.1	579	604	625531	0.69	98
BDD177	566.1	547.1	569	583	790420	>0.99	97
BDD178	632.1	613.1	573	590	1299481	0.85	99
BDD186	540.1	520.8	567	579	378198	>0.99	92
BDD187	554.1	535.1	570	583	590198	0.94	98
BDD190	526.1	507.1	574	588	299679	0.53	96
BDD195	640	621.1	610	645	243407	0.13	89
BDD199	588.1	589.1[a]	574	587	353333	0.75	97
BDD206	570.1	551.1	583	609	1108420	0.7	99
BDD209	570.1	550.8	567	581	463259	>0.99	93
BDD216	538.1	519.1	570	584	547012	>0.99	94
BDD223	676.1	657.2	590	653	632074	0.02	97
BDD228	648	629.1	568	582	535235	>0.99	99
BDD236	530	511	586	606	1022049	0.61	94
BDD238	530.1	511.1	582	600	231630	0.3	94
BDD241	695.9	676.9	569	583	497284	0.91	88
BDD242	696	677	572	586	481580	>0.99	97
BDD243	538.1	519	554	579	378198	>0.99	99
BDD245	558.1	539.1	570	582	582346	0.75	94
BDD247	648	628.5	582	605	280049	0.62	90
BDD251	538.1	519	566	584	832296	0.83	94
BDD257	613.1	614.1[a]	620	754	375580	0	91
BDD259	648	629	570	585	73284	0.08	96
BDD260	618	598.6	574	589	223778	0.64	97
BDD263	566.1	547.1	570	583	209383	0.66	94
BDD264	632	613	577	597	702741	0.74	95
BDD268	662	643	577	600	230321	0.44	98

BDD274	574	554.7	573	588	294444	>0.99	98
BDD282	604	584.7	568	581	405679	>0.99	98
BDD284	610	591	604	625	218543	0.21	93
BDD290	636.1	617.1	571	586	154420	0.5	97
BDD298	632.1	613.1	568	583	582346	>0.99	91
BDD299	670	650.9	567	579	187136	0.72	90
BDD300	616.1	597.2	573	590	297062	0.82	91
BDD301	620.1	600.7	574	600	391284	0.97	97
BDD305	588.1	568.8	577	597	278741	0.77	90
BDD307	586.1	566.7	574	593	459333	0.26	95
BDD308	670	651.1	567	580	649086	>0.99	92
BDD310	568.1	549.2	577	605	338938	0.88	97
BDD311	620.1	601.1	567	580	113852	0.38	92
BDD313	540.1	521.1	580	606	181901	0.28	93
BDD314	558.1	538.8	565	578	261728	0.91	97
BDD316	598.1	579.2	584	610	409605	0.74	99
BDD319	576.1	557.1[a]	564	581	140025	0.26	91
BDD320	584.1	564.8	568	582	321926	0.89	98
BDD322	620.1	601.1	572	587	227704	0.74	99
BDD323	554.1	535	567	580	125630	0.45	95
BDD325	652.2	633.1	569	585	1080938	0.33	96
BDD329	558.1	538.7	567	580	293136	0.95	96
BDD331	722.1	703.1	568	581	151802	0.58	99
BDD332	590	571	565	580	68049	0.11	99
BDD335	554.1	535.1	577	597	117778	0.32	98
BDD340	624.1	605.2	540	561	654321	0.45	94
BDD343	552.1	533.1	572	592	779951	0.99	99
BDD347	584.1	565.2	578	599	1443432	0.24	93
BDD349	538.1	519.1	566	583	1141136	0.45	96
BDD351	554.1	535.1	577	601	489432	>0.99	94
BDD357	624.1	625.2[a]	595	656	573185	0.01	94
BDD359	558.1	539.1	573	589	463259	>0.99	98
BDD361	538.1	519.1	568	588	830988	0.87	92
BDD366	586.1	567.1	590	622	532617	0.66	95
BDD369	516	497	569	581	557481	>0.99	98
BDD370	538.1	519.1	571	588	634691	>0.99	98
BDD371	610	591.1	606	628	1049531	0.2	93
BDD377	603.1	584.1	583	795	91605	0	97
BDD378	634.1	615.1	575	594	104691	0.34	94
BDD383	544.1	525.1	590	613	588889	0.57	95

BDD393	610	591.1	564	583	129556	0.27	96
BDD397	570.1	550.8	582	618	718444	0.19	91
BDD403	550.1	531.1	575	594	117778	0.33	99
BDD423	516	497.1	580	595	181901	0.43	97
BDD428	654	635	564	585	74593	0.1	96
BDD429	554.1	534.7	576	596	451481	>0.99	95
BDD435	658.2	639.2	567	580	350716	>0.99	99
BDD441	627.1	608	593	648	965778	0.29	99
BDD473	556.1	537.1	587	619	126938	0.18	95
BDD474	538.1	519.1	568	583	434469	>0.99	93
BDD480	570.1	551.1	577	593	359877	0.92	94
BDD483	646.1	627.2	579	602	244716	0.67	98
BDD485	616.1	597.1	567	580	366420	>0.99	94
BDD486	568.1	549.1	576	595	328469	0.94	99
BDD487	647.1	628	577	598	541778	>0.99	95
BDD489	538.1	519.1	569	591	892494	0.82	96
BDD490	600.1	581.2	577	598	319309	>0.99	97
BDD495	590.1	571.1	581	601	427926	>0.99	99
BDD496	556.1	537.1	580	600	64123	0.02	88
BDD498	595.1	596.1[a]	595	734	499901	0	95
BDD499	593.1	594.1[a]	605	750	316691	0	96
BDD501	579.1	580.1[a]	624	772	447556	0	98

All absorbance and fluorescence excitation and emission data were recorded by a Synergy 4, Biotek Inc. fluorescent plate reader (10 μM compounds in DMSO (100 μL) for λ_{abs}, 2 μM compounds in DMSO (100 μL) for λ_{em}) in 96-well polypropylene plates. Mass was calculated as (M+), and found in ESI-MS (M-F), *a:* found mass (M+H), *b*: found mass (M-H) in the negative mode scan, *c:* Purity data was calculated on the basis of the integration in HPLC trace at 254 nm.

2.2.3 Derivatization of BDD Library-LysoTracker Library (BDL)

Lysosomes are the major cellular digestive organelle. The acid hydrolases they contain help to digest and dispose the waste of cells, such as excess organelles, food particles, and bacterias.[9] Lysosomes are also one of the organelles that help to repair damages to the plasma membranes.[10] The disorder of lysosomal storage can cause serious diseases, including Niemann Pick Type C disease,[11] Fabry disease,[12] Parkinson disease,[13] Pompe's disease,[14] and so on.[15] Therefore, understanding biosynthesis and pathogenesis of lysosomes is of critical importance. On the other hand, the interior condition of lysosomes is known to be acidic (i.e., pH around 4.8) compared to cytosol (i.e., pH around 7.2), due to the required condition for the digestive enzymes to work. Therefore, weakly basic amines can selectively accumulate in lysosomes.[16] To date, many fluorescent small molecules containing tertiary amine motifs have been developed for selective staining of lysosomes in cell image. They were covered under the name of "LysoTracker" or "LysoSensor" (Figure 2.1). However, all these sensors are still restricted to only several colours.

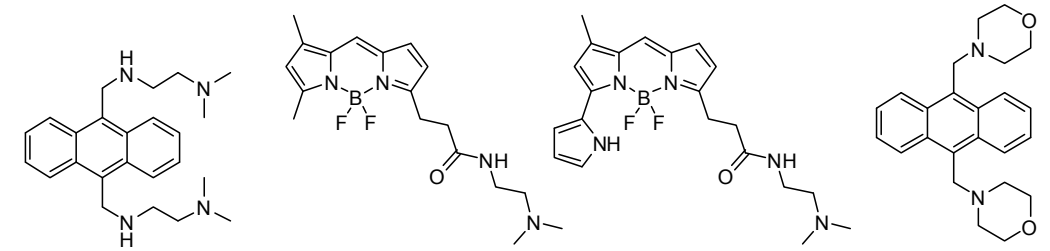

LysoTracker® Blue DND-22 LysoTracker® Green DND-26 LysoTracker® Red DND-99 LysoSensor™ Blue DND-167

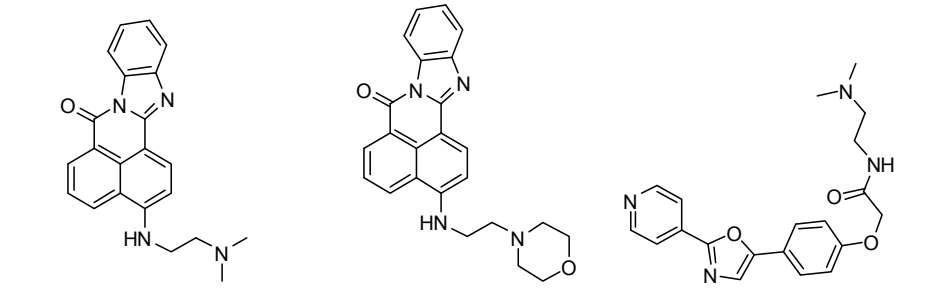

LysoSensor™ Green DND-153 LysoSensor™ Green DND-189 LysoSensor™ Yellow/Blue DND-160

Figure 2.1 Selected representative structures of commercial LysoTracker® or LysoProbe™.

BDD compounds were designed with active ester motifs which can be replaced by nucleophiles, providing the flexibility to further convert **BDD** to other functional libraries. Considering the important role of lysosomes and the limitation of current LysoTracker® or LysoProbe^{TM}, we designed and synthesized a "LysoTracker" library (**BDL**). **BDL** was prepared through replacing the active ester part of **BDD** compounds with N^1,N^1-dimethylethane-1,2-diamine under neat condition (Scheme 2.2 and Chart 2.2), to render 80 compounds with good purity after a simple workup. The diverse structural property of **BDL** library would provide more versatile probes for selective staining of lysosomes.

Scheme 2.2 General synthesis scheme of the **BDL** library.

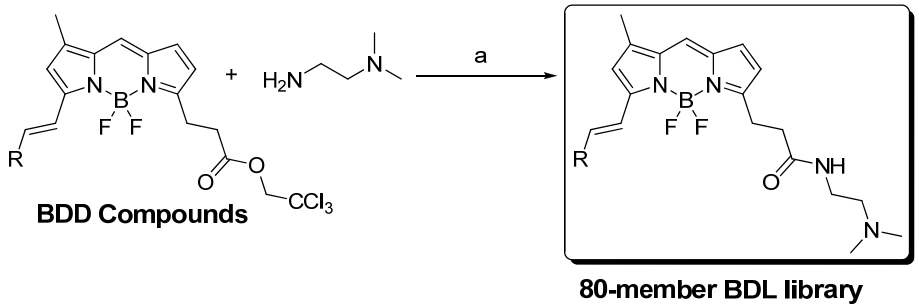

Reaction conditions: a) neat, room temperature, 15 min.

Chart 2.2 A decoding table for **BDL** library

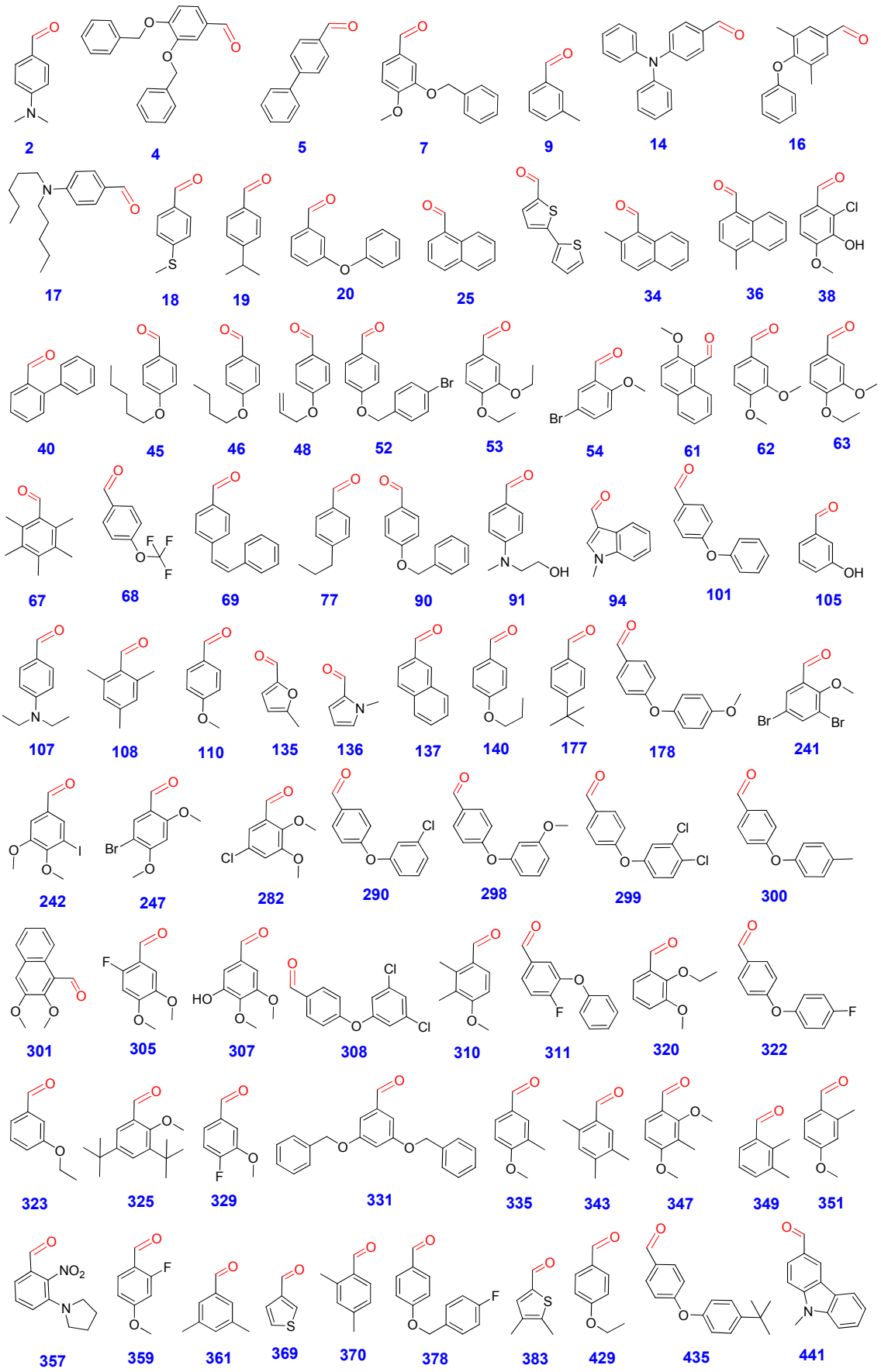

2.2.4 Spectroscopic Properties of BDL Library

The spectroscopic properties of **BDL** compounds are summarized in Table 2.2. **BDL** compounds show similar spectroscopic properties to **BDD** compounds with maximum absorption wavelengths ranging from 551 nm to 628 nm, maximum emission wavelengths from 578 nm to 755 nm, quantum yields varied from 0.003 to almost 1. **BDL** compounds displayed an average quantum yield value of 0.69, which suggest that many of the **BDL** compounds can be used as either fluorescent turn-on or quenching probes.

Table 2.2 Spectroscopic properties and purity table for **BDL** library: calculated mass, experimental mass, absorbance maximum (λ_{abs}), fluorescent emission maximum (λ_{em}), extinction coefficient (ε), quantum yield (Φ), and purity.

Code	mass (calc)	m/z (exp)	λ_{abs} (nm)	λ_{em} (nm)	ε ($M^{-1}cm^{-1}$)	Φ	Purity (%)[a]
BDL2	493.3	494.3	614	745	41235	0.15	90
BDL4	662.3	663.3	580	604	33839	>0.99	92
BDL5	526.3	527.3	578	592	24427	0.62	93
BDL7	586.3	587.3	581	603	17816	0.89	93
BDL9	464.3	465.3	569	581	20057	0.85	92
BDL14	617.3	618.4	602	738	27004	0.003	95
BDL16	584.3	585.4	574	588	18936	0.98	93
BDL17	577.4	578.4	628	750	39442	0.006	96
BDL18	496.2	497.3	581	603	27788	0.85	96
BDL19	492.3	493.3	571	591	38209	0.95	97
BDL20	542.3	543.2	569	581	16471	0.75	93
BDL25	500.3	501.3	579	599	9524	0.42	90
BDL30	538.2	539.2	610	648	12886	0.05	93
BDL34	514.3	515.3	561	595	20393	>0.99	95
BDL36	514.3	515.3	581	603	11093	0.57	92
BDL38	530.2	531.3	576	598	8291	0.06	89
BDL40	526.3	527.3	569	583	20281	>0.99	92
BDL45	550.3	551.4	578	597	17816	0.88	89
BDL46	522.3	523.3	579	595	10084	0.48	90
BDL48	506.3	507.3	577	596	33615	>0.99	97
BDL52	634.2	635.2	577	594	12213	0.88	94

BDL53	538.3	539.3	581	606	20953	0.87	94
BDL54	558.2	559.2	574	587	15687	0.77	92
BDL61	530.3	531.3	587	617	27900	0.84	93
BDL62	510.3	511.3	580	603	23306	>0.99	96
BDL63	524.3	525.3	581	605	20729	0.96	97
BDL67	520.3	521.3	551	582	13894	>0.99	97
BDL68	534.2	535.2	566	578	10420	0.46	94
BDL69	552.3	553.3	574	590	13334	0.79	96
BDL77	492.3	493.3	571	584	12885	0.76	93
BDL90	556.3	557.3	577	596	10757	0.51	92
BDL91	523.3	524.3	621	750	48854	0.006	95
BDL94	503.3	504.3	599	651	7059	0.1	92
BDL101	542.3	543.3	574	589	28909	>0.99	95
BDL105	466.2	467.2	569	582	22186	0.97	98
BDL107	521.3	522.3	624	755	37537	0.05	94
BDL108	492.3	493.3	561	585	23867	>0.99	99
BDL110	480.3	481.2	576	594	14342	0.98	97
BDL135	454.2	455.3	589	611	16359	0.45	90
BDL136	453.3	454.2	604	647	22858	0.25	94
BDL137	500.3	501.2	576	590	26331	>0.99	98
BDL140	508.3	509.3	578	597	30030	>0.99	97
BDL177	506.3	507.3	571	583	10757	0.5	90
BDL178	572.3	573.3	575	590	12998	0.46	89
BDL241	636.1	637.2	572	585	13334	0.39	89
BDL242	636.2	637.2	574	587	10197	0.44	90
BDL247	588.2	588.7	583	606	23979	0.81	88
BDL282	544.2	545.1	570	583	12438	0.54	91
BDL284	550.2	550.6	604	628	14230	0.21	95
BDL290	576.2	577.3	572	587	12550	0.73	96
BDL298	572.3	573.2	570	585	24763	0.99	93
BDL299	610.2	610.6	569	581	23083	>0.99	98
BDL300	556.3	557.3	578	597	25772	>0.99	90
BDL301	560.3	561.3	575	600	28237	>0.99	99
BDL305	528.3	529.2	578	599	35856	>0.99	92
BDL307	526.3	527.3	576	595	25660	0.5	94
BDL308	610.2	611.3	569	581	25660	0.86	93
BDL310	508.3	509.3	579	614	25996	>0.99	99
BDL311	560.3	561.3	568	581	16247	0.68	94
BDL320	524.3	525.2	570	583	23643	>0.99	94
BDL322	560.3	561.3	574	589	16920	0.89	97

BDL323	494.3	495.2	569	581	10869	0.6	93
BDL325	592.4	593.4	570	591	41011	0.89	99
BDL329	498.2	498.9	568	581	18040	0.88	97
BDL331	662.3	663.4	569	582	8416	0.44	98
BDL335	494.3	495.1	577	598	7619	0.3	94
BDL343	492.3	493.2	574	590	22970	>0.99	96
BDL347	524.3	525.2	580	600	12438	0.67	92
BDL349	478.3	479.1	568	594	36977	0.89	97
BDL351	494.3	495.2	579	602	38097	>0.99	98
BDL357	564.3	565.4	596	601	18040	0.07	96
BDL359	498.2	499.1	574	591	20729	>0.99	94
BDL361	478.3	478.8	570	581	12438	0.67	91
BDL369	456.2	457.2	569	583	16696	0.93	91
BDL370	478.3	479.3	572	589	21738	>0.99	94
BDL378	574.3	575.3	577	594	20057	>0.99	94
BDL383	484.2	485.2	592	617	35072	0.68	99
BDL429	494.3	495.1	588	605	14230	0.65	98
BDL435	598.3	599.4	569	581	10757	0.57	96
BDL441	567.3	568.4	594	646	41234	0.5	97

All absorbance and fluorescence excitation and emission data were recorded by a Synergy 4, Biotek Inc. fluorescent plate reader with 40 μM compounds in DMSO (100 μL) in 96-well polypropylene plates. Mass was calculated as (M), and found in ESI-MS m/e, *a:* Purity data was calculated on the basis of the integration in HPLC trace at 254 nm.

2.2.5 Derivatization of BDD Library-ALDEFLUOR Library (BDA)

In recent years, cancer stem cell (CSC) theory has changed the classic view of cancer therapy. CSCs are believed to be a small fraction of cells which initiate tumor.[17] They are capable of self-renewing and differentiating to form tumor bulk.[18] In addition to remove differentiated cancer cells, it is also necessary to eliminate CSCs in order to cure cancer.[19] Therefore, identifying CSC is of critical importance in cancer therapy. Aldehyde dehydragenase (ALDH) has been identified as high expressed in CSC, and related to many biological activities (e.g., cell differentiation, drug resistance and oxidative stress response).[20] ALDH was therefore considered as CSC marker,[21] and probes targeting ALDH were developed in order to identify and separate CSC.[22] One example is the commercial probe ALDEFLUOR (Figure 2.2),[22-23] which can be oxidized to carboxylic acid form by ALDH and accumulate in CSC.[24] ALDEFLUOR was widely used in flow cytometry to isolate CSC. However, the expensive price and single emission colour (green) still restricted its application. On the other hand, the active form of ALDEFLUOR is aldehyde instead of ethyl acetal, which indicates activation procedure (i.e., by HCl solution) is necessary before use. The remaining acetal form of ALDEFLUOR may generate high background due to incompletion of activation.

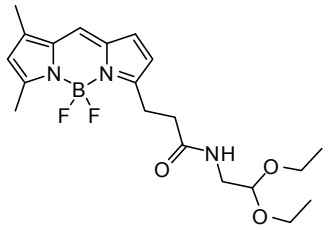

Figure 2.2 Structure of commercial probe ALDEFLUOR

Considering all these factors and utilizing the advantages of the active ester motif of **BDD** library, we designed a library derived from the active form of ALDEFLUOR

(**BDA**), intending to enrich the chemical source for CSC probes and wide their applications. The active ester part of **BDD** compounds were replaced with 2,2-dimethoxyethanamine to give methyl acetal forms of compounds. Methyl acetal has relatively higher reactivity compare to ethyl acetal and can be converted to aldehyde form through a very mild condition by I_2 and acetone.[25] 46 **BDA** compounds with structural diversity from aldehyde building blocks were obtained (Scheme 2.3 and Chart 2.3). They extended the available colour range of CSC probes with lower background.

Scheme 2.3 General synthesis scheme of the **BDA** library.

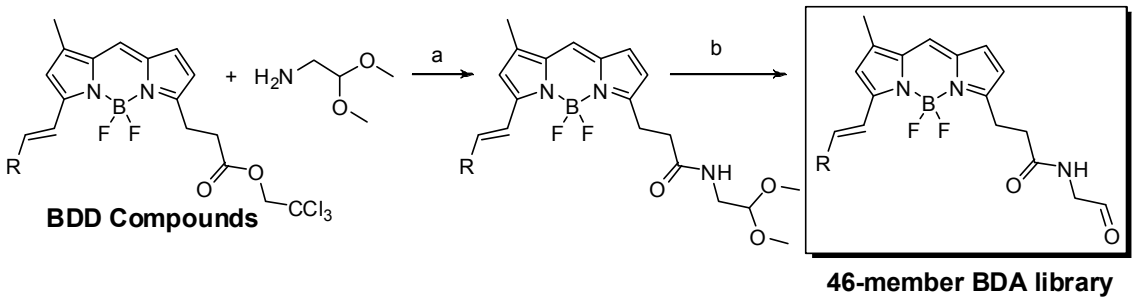

Reaction condition: a) neat, room temperature, 30 min. b) I_2 (0.1 eq.), acetone, room temperature, 1h

Chart 2.3 A decoding table for **BDA** library

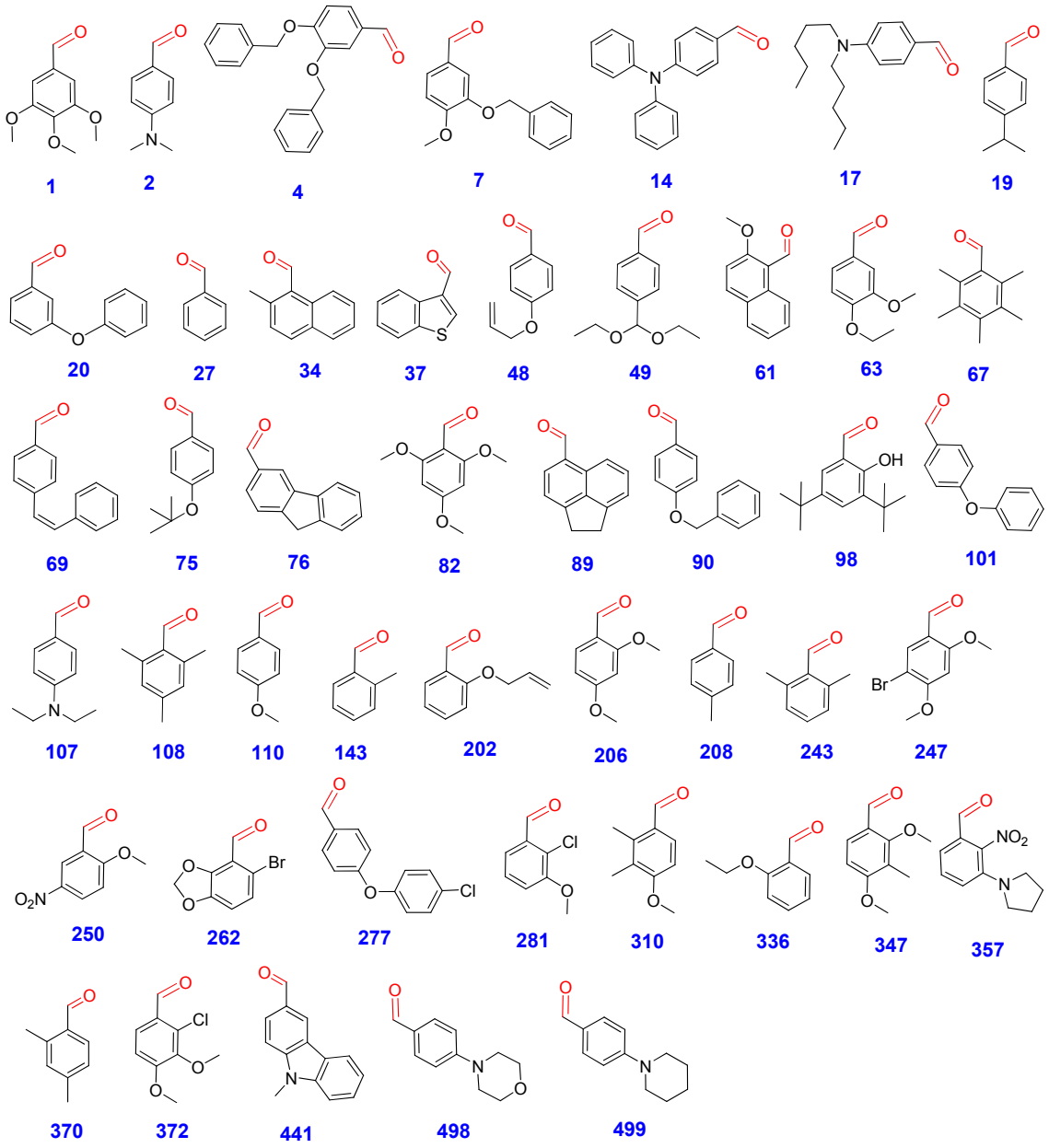

2.2.6 Spectroscopic Properties of BDA Library

The spectroscopic properties of **BDA** compounds are summarized in Table 2.3. **BDA** compounds show similar spectroscopic properties to **BDD** and **BDL** compounds with maximum absorption wavelengths ranging from 552 nm to 627 nm, maximum emission wavelengths from 579 nm to 749 nm, quantum yields varied from 0.002 to 0.56.

Table 2.3 Spectroscopic properties and purity table for **BDA** library: absorbance maximum (λ_{abs}), fluorescent emission maximum (λ_{em}), extinction coefficient (ε), and quantum yield (Φ).

Code	λ_{abs} (nm)	λ_{em} (nm)	ε ($M^{-1}cm^{-1}$)	Φ
BDA1	575	594	57818	0.34
BDA2	616	579	50423	0.01
BDA4	580	602	14791	0.05
BDA7	580	604	17704	0.10
BDA14	602	732	70144	0.002
BDA17	627	748	121015	0.002
BDA19	571	585	45717	0.33
BDA20	568	582	30478	0.25
BDA27	567	581	106672	0.50
BDA34	561	593	28461	0.30
BDA37	578	598	24651	0.19
BDA48	577	597	67455	0.32
BDA49	577	592	95691	0.44
BDA61	587	620	102863	0.22
BDA63	581	605	28013	0.05
BDA67	552	585	99277	0.56
BDA69	588	606	33167	0.19
BDA75	574	594	23307	0.17
BDA76	584	603	17032	0.08
BDA82	590	623	43027	0.15
BDA89	590	622	146114	0.35
BDA90	578	596	17256	0.11
BDA98	574	591	106224	0.43
BDA101	574	589	19721	0.15
BDA107	625	749	56025	0.006

BDA108	561	587	86727	0.46
BDA110	577	597	89416	0.49
BDA143	568	584	49078	0.36
BDA202	574	587	17032	0.11
BDA206	584	611	26444	0.13
BDA208	512	584	22410	0.15
BDA243	555	581	28013	0.28
BDA247	584	610	118774	0.37
BDA250	571	584	16359	0.07
BDA262	573	586	29133	0.20
BDA277	574	588	51543	0.34
BDA281	569	583	24203	0.24
BDA310	579	607	91658	0.39
BDA336	574	589	34960	0.30
BDA347	580	602	64989	0.26
BDA357	596	589	84038	0.02
BDA370	572	589	71264	0.45
BDA372	576	593	21066	0.17
BDA441	595	647	37425	0.10
BDA498	596	590	25996	0.02
BDA499	605	582	38770	0.03

All absorbance and fluorescence excitation and emission data were recorded by a Synergy 4, Biotek Inc. fluorescent plate reader with 20 μM compounds in DMSO (100 μL) in 96-well polypropylene plates.

2.3 Conclusion

In summary, we have designed a novel BODIPY library, **BDD**, by introducing an active ester motif to the scaffold. **BDD** library was prepared through Knoevenagle condensation reaction with commercial aldehyde building blocks with good purity. The active ester motif it contains provided the feasibility to further convert **BDD** to other functional libraries, LysoTracker library (**BDL**) and ALDEFLUOR library (**BDA**). **BDD**, **BDL** and **BDA** cover a broad range of photophysical properties due to the structural diversity of aldehyde building blocks. **BDL** compounds, derived from lysosome probe, provided more colour options for selective staining of lysosomes in the cell, while **BDA** compounds, derived from CSC probes, enlarged the available chemical source for identifying and isolating CSCs with lower background.

2.4 Experimental Section

Materials and Methods

All the chemicals (aldehyde building blocks and others) and solvents were purchased from Sigma-Aldrich, Alfa Aesar, Fluka, Merck or Acros, and used without further purification. Normal phase purifications were carried our using Merck Silica Gel 60 (particle size: 0,040-0.063 mm, 230-400 mesh). Analytical characterization was performed on a HPLC-MS (Agilent-1200 series) with a DAD detector and a single quadrupole mass spectrometer (6130 series) with an ESI probe. Analytical method, unless indicated: eluents: A: H_2O (0.1% HCOOH), B: ACN (0.1% HCOOH), gradient from 30 to 100% B in 5 min; C18 (2) Luna column (4.6 x 50 mm^2, 5 µm particle size). Normal phase purification of BDD compounds were performed using column chromatography, and eluting with Hexane-Ethyl Acetate (ranging from 10:1 to 3:1). Spectroscopic and quantum yield data were measured on a fluorometer and UV/VIS

instrument, Synergy 4 of Bioteck Company. The slit width was 1 nm for both excitation and emission, and the data analysis was performed using Microsoft Excel 2007.

2.4.1 General Procedure for Synthesis of BDD Library

1 (20 mg, 47 μmol) and aldehyde (94 μmol, 2 equiv) were dissolved in acetonitrile (3 mL), with 6 equiv of pyrrolidine (23.5μL, 282 μmol) and 6 equiv of AcOH (16.1 μL, 282 μmol). The condensation reaction was performed by heating to 85 ^{o}C. After every step, the reaction mixture was cooled down to room temperature and then monitored by TLC. The reactions were completed between 5 to 20 min. The resulting crude mixtures were concentrated under vacuum, and purified by short silica column. The characterization of the whole library was performed.

2.4.2 General Procedure for Synthesis of BDL Library

BDD compounds (1 μmol) and N^1,N^1-dimethylethane-1,2-diamine (10 μL, large excess) were stirred at room temperature for 15 mins. The reaction mixture were diluted with DCM and washed with 1 ml $NaHCO_3$ aqueous solution for 3 times. The organic layer was then separated, dried over Na_2SO_4, filtered and concentrated. The characterization of the whole library was performed.

2.4.3 General Procedure for Synthesis of BDA Library

BDD compounds (2 μmol) and 2,2-dimethoxyethanamine (10 μL, large excess) were stirred at room temperature for 30 mins. The reaction mixture were diluted with DCM and washed with 1 ml 0.5N HCl aqueous solution for 3 times. The organic layer was then separated, dried over Na_2SO_4, filtered and concentrated.

A mixture of the resulting compound (2 μmol) and iodine (0.2 μmol) in acetone (1 mL) was stirred at room temperature for 60 min. The acetone was then removed under vacuum, and the residue was diluted with DCM (1 mL). The mixture was washed with 5% aqueous $Na_2S_2O_3$ (1 mL), H_2O (1 mL), and brine (1 mL). The organic layer was

separated, dried over Na_2SO_4, filtered and concentrated. The characterization of the whole library was performed.

2.4.4 Quantum Yield Measurements

Quantum yields were calculated by measuring the integrated emission area of the fluorescent Spectrum and comparing that value to the area measured for Rhodamine B in DMSO when excited at 500 nm ($\Phi_{rho\text{-}B} = 0.49$). Quantum yields for the **BDD**, **BDL** and **BDA** library were then calculated using equation (1), where *F* represents the area of fluorescent emission, *n* is reflective index of the solvent, and Abs is absorbance at excitation wavelength selected for standards and samples. Emission was integrated between 560 to 700 nm.

$$\Phi_{flu}^{sample} = \Phi_{fl}^{reference}\left(\frac{F^{sample}}{F^{reference}}\right)\left(\frac{\eta^{sample}}{\eta^{reference}}\right)\left(\frac{Abs^{reference}}{Abs^{sample}}\right) \quad (1)$$

References

1. Loudet, A.; Burgess, K., BODIPY Dyes and Their Derivatives: Syntheses and Spectroscopic Properties. *Chem. Rev.* **2007,** *107*, 4891-4932.

2. Lavis, L. D.; Raines, R. T., Bright ideas for chemical biology. *ACS Chem. Biol.* **2008,** *3*, 142-155.

3. Sunahara, H.; Urano, Y.; Kojima, H.; Nagano, T., Design and synthesis of a library of BODIPY-based environmental polarity sensors utilizing photoinduced electron-transfer-controlled fluorescence ON/OFF switching. *J. Am. Chem. Soc.* **2007,** *129*, 5597-5604.

4. (a) Lee, J. S.; Kang, N. Y.; Kim, Y. K.; Samanta, A.; Feng, S.; Kim, H. K.; Vendrell, M.; Park, J. H.; Chang, Y. T., Synthesis of a BODIPY library and its application to the development of live cell glucagon imaging probe. *J. Am. Chem. Soc.* **2009,** *131*, 10077-10082; (b) Lee, J. S.; Kim, H. K.; Feng, S.; Vendrell, M.; Chang, Y. T., Accelerating fluorescent sensor discovery: unbiased screening of a diversity-oriented BODIPY library. *Chem. Commun.* **2011,** *47*, 2339-2341.

5. Vendrell, M.; Krishna, G. G.; Ghosh, K. K.; Zhai, D.; Lee, J. S.; Zhu, Q.; Yau, Y. H.; Shochat, S. G.; Kim, H.; Chung, J.; Chang, Y. T., Solid-phase synthesis of BODIPY dyes and development of an immunoglobulin fluorescent sensor. *Chem. Commun.* **2011,** *47*, 8424.

6. Johnson, I., Fluorescent probes for living cells. *Histochem J.* **1998,** *30*, 123-140.

7. Malan, S. F.; van Marle, A.; Menge, W. M.; Zuliana, V.; Hoffman, M.; Timmerman, H.; Leurs, R., Fluorescent ligands for the histamine H2 receptor: synthesis and preliminary characterization. *Bioorg. Med. Chem.* **2004,** *12*, 6495-6503.

8. (a) Atilgan, S.; Ozdemir, T.; Akkaya, E. U., A sensitive and selective ratiometric near IR fluorescent probe for zinc ions based on the distyryl-bodipy fluorophore. *Org. Lett.* **2008,** *10*, 4065-4067; (b) Baruah, M.; Qin, W.; Flors, C.; Hofkens, J.; Vallee, R. A.; Beljonne, D.; Van der Auweraer, M.; De Borggraeve, W. M.; Boens, N., Solvent and pH dependent fluorescent properties of a dimethylaminostyryl borondipyrromethene dye in solution. *J. Phys. Chem. A* **2006,** *110*, 5998-6009.

9. (a) Mindell, J. A., Lysosomal acidification mechanisms. *Annu. Rev. Physiol.* **2012,** *74*, 69-86; (b) Saftig, P., Physiology of the lysosome. **2006**.

10. Han, R.; Campbell, K. P., Dysferlin and muscle membrane repair. *Curr. Opin. Cell. Biol.* **2007,** *19*, 409-416.

11. Wijburg, F. A.; Sedel, F.; Pineda, M.; Hendriksz, C. J.; Fahey, M.; Walterfang, M.; Patterson, M. C.; Wraith, J. E.; Kolb, S. A., Development of a Suspicion Index to aid diagnosis of Niemann-Pick disease type C. *Neurology* **2012,** *78*, 1560-1567.

12. Thurberg, B. L.; Politei, J. M., Histologic abnormalities of placental tissues in Fabry disease: a case report and review of the literature. *Hum Pathol* **2012,** *43* (4), 610-4.

13. Ebrahimi-Fakhari, D.; McLean, P. J.; Unni, V. K., Alpha-synuclein's degradation in vivo: opening a new (cranial) window on the roles of degradation pathways in Parkinson disease. *Autophagy* **2012,** *8*, 281-283.

14. Angelini, C.; Semplicini, C., Enzyme replacement therapy for Pompe disease. *Curr. Neurol. Neurosci. Rep.* **2012,** *12*, 70-75.

15. Cox, T. M.; Cachon-Gonzalez, M. B., The cellular pathology of lysosomal diseases. *J. Pathol.* **2012,** *226*, 241-254.

16. (a) Goldman, S. D.; Funk, R. S.; Rajewski, R. A.; Krise, J. P., Mechanisms of amine accumulation in, and egress from, lysosomes. *Bioanalysis* **2009,** *1*, 1445-1459; (b) Kaufmann, A. M.; Krise, J. P., Lysosomal sequestration of amine-containing drugs: analysis and therapeutic implications. *J. Pharm. Sci.* **2007,** *96*, 729-746.

17. (a) La Porta, C. A., Thoughts about cancer stem cells in solid tumors. *World J. Stem Cells* **2012,** *4*, 17-20; (b) Yu, Y.; Ramena, G.; Elble, R. C., The role of cancer stem cells in relapse of solid tumors. *Front Biosci.* **2012,** *4*, 1528-1541.

18. (a) Prud'homme, G. J., Cancer stem cells and novel targets for antitumor strategies. *Curr. Pharm. Des.* **2012,** *18*, 2838-2849; (b) Li, Y.; Laterra, J., Cancer stem cells: distinct entities or dynamically regulated phenotypes? *Cancer Res.* **2012,** *72*, 576-580; (c) Martin-Belmonte, F.; Perez-Moreno, M., Epithelial cell polarity, stem cells and cancer. *Nat. Rev. Cancer* **2012,** *12*, 23-38.

19. Vaiopoulos, A. G.; Kostakis, I. D.; Koutsilieris, M.; Papavassiliou, A. G., Colorectal cancer stem cells. *Stem Cells* **2012,** *30*, 363-371.

20. Moreb, J. S., Aldehyde dehydrogenase as a marker for stem cells. *Curr. Stem Cell Res. Ther.* **2008,** *3*, 237-246.

21. Ma, I.; Allan, A. L., The role of human aldehyde dehydrogenase in normal and cancer stem cells. *Stem Cell Rev.* **2011,** *7*, 292-306.

22. Alison, M. R.; Guppy, N. J.; Lim, S. M.; Nicholson, L. J., Finding cancer stem cells: are aldehyde dehydrogenases fit for purpose? *J. Pathol.* **2010,** *222*, 335-344.

23. Christ, O.; Lucke, K.; Imren, S.; Leung, K.; Hamilton, M.; Eaves, A.; Smith, C.; Eaves, C., Improved purification of hematopoietic stem cells based on their elevated aldehyde dehydrogenase activity. *Haematologica* **2007,** *92*, 1165-1172.

24. Crabb, D. W.; Matsumoto, M.; Chang, D.; You, M., Overview of the role of alcohol dehydrogenase and aldehyde dehydrogenase and their variants in the genesis of alcohol-related pathology. *Proc. Nutr. Soc.* **2004,** *63*, 49-63.

25. Sun, J.; Dong, Y.; Cao, L.; Wang, X.; Wang, S.; Hu, Y., Highly efficient chemoselective deprotection of O,O-acetals and O,O-ketals catalyzed by molecular iodine in acetone. *J. Org. Chem.* **2004,** *69*, 8932-8934.

Chapter 3 Fluorescence Emission Response Profiling for Sensor Discovery

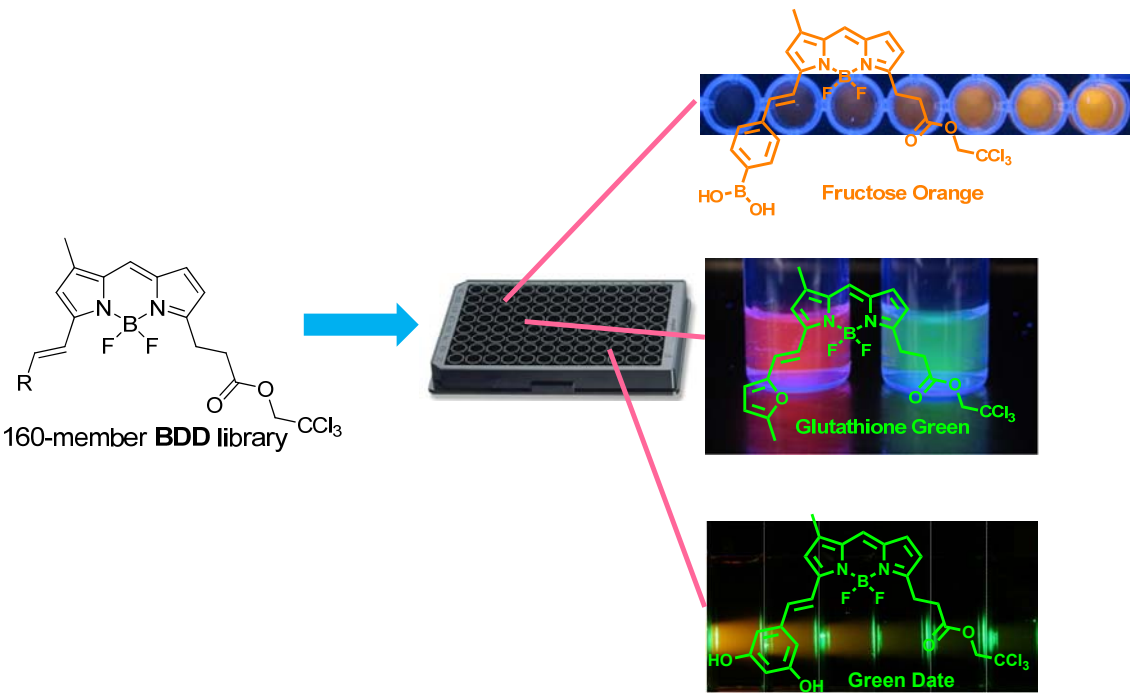

3.1 Introduction

The conventional screening platform for sensor development is to assess the spectral properties of sensor candidates in the presence of different analytes. Recent technical advances in parallel library synthesis and high-throughput screening greatly improved the screening efficiency. Unbiased fluorescence screenings, which can cover diverse biological problems, are powerful approach now in sensor discovery, especially for proteins and metabolites, by profiling the response of diversity-oriented fluorescent libraries.[1]

There are several criteria should be considered when designing such unbiased screening format. First, in order to enhance the successful rate, broad biological events or targets should be covered. In the meantime, the selectivity of sensor candidates could also be evaluated through parallel comparison against similar analytes. Second, the concentration of analytes set in the screening should match with the real situation. Because after sensors were discovered from primary screening, they are valuable only after they can be validated using real samples. In other words, the concentration of analytes should be within the detection range of sensors. Usually, series of concentration should be included in the screening platform. Third, screening should be carried out in similar environmental condition to real biological events. For example, if we intend to detect the analytes inside cells, buffer which can mimic intracellular condition (e.g., HEPES buffer) should be used as screening medium. Last, hit compounds indentified from the screening system should be further confirmed and evaluated with real samples. Because, in addition to the detection limit, other factors, such as viscosity and pH, may also affect the behaviour of sensors.

3.2 Results and Discussion

3.2.1 Unbiased High-throughput Fluorescence Screenings

In order to discover novel sensors from **BDD**, **BDL** and **BDA** libraries, we designed the unbiased high-throughput fluorescence screening system by examining the fluorescent properties of the three library compounds after incubation with 52 analytes. The analytes covered a broad range of biological activities and can be classified into seven different categories: (1) pH standard solutions, (2) viscous buffer solutions, (3) nucleotides and nucleosides, (4) nucleic acids, (5) proteins, (6) oxidation-reduction related molecules, and (7) miscellaneous analytes (Table 3.1). Four different concentrations of analytes were used to study the dose-dependence of the fluorescence emission.

Table 3.1 List of biomolecule selected for unbiased screening

Analyte class	Individual analyte molecules	Concentrations
Control	HEPES	20 mM (pH=7.4)
Viscosity	Glycerol	volume : 40 %, 20 %, 10 %, 5 %
	DMSO	volume : 50 %, 25 %, 12.5 %, 6.25 %
pH	pH 2, 3, 4, 5, 6, 7, 8, 9, 10, 11	
Nucleotides and Nucleosides	Adenosin, AMP, ADP, ATP, Guanosine, GTP, cyclic AMP, cyclic GMP	2 mM, 1 mM, 0.5 mM, 0.25 mM
Genetic Macromolecules	double strand DNA (dsDNA) total RNA	1 mg/ml, 0.5 mg/ml, 0.25 mg/ml, 0.125 mg/ml
Proteins	Human Immunoglobulin G (human IgG) Human serum albumin (HSA) Human serum albumin lipid free Bovine serum albumin (BSA)	1 mg/ml, 0.5 mg/ml, 0.25 mg/ml, 0.125 mg/ml

	Insulin Hemoglobin Cytochrome C Lysozyme	
Oxido-reduction related molecules	L-Glutathione reduced form (GSH) L-Glutathione oxidized form (GSSG) Nicotinamide adenine dinucleotide (NAD) Nicotinamide adenine dinucleotide, reduced disodium salt, trihydrate (NADH) Nicotinamide adenine dinucleotide 2'-phosphate reduced tetrasodium salt (NADPH) Hydrogen peroxide (H_2O_2) NaClO	5 mM, 2.5 mM, 1.25 mM, 0.625 mM
Miscellaneous molecules	Histamine, Dopamine Serotonin Gamma-aminobutyric acid (GABA) γ-Butyrolactone (GHB) Monosodium glutamate (MSG) L-Glutamine Acetylcholine	5 mM, 2.5 mM, 1.25 mM, 0.625 mM
	Heparin Chontroitin Glycogen Inositol	1 mg/ml, 0.5 mg/ml, 0.25 mg/ml, 0.125 mg/ml
	Caffeine	2 mM, 1 mM, 0.5 mM, 0.25 mM
	Glucose, Fructose, Sucrose,	10 mM, 5 mM, 2.5 mM, 1.25 mM
	Malachite green	1 ug/ml, 0.5 ug/ml, 0.25 ug/ml, 0.125 ug/ml

3.2.2 Development of a Fructose Sensor-Fructose Orange

3.2.2.1 Fructose

Fructose is one of the most common sugars which can be found in our daily food. In nature, fructose exists in many trees, fruits, flowers, honey and most root vegetables. Due to its low cost and highest sweetness among natural carbohydrates, fructose is commercially used in foods and beverages. The major commercial forms of fructose include crystalline fructose (high purity) and high-fructose corn syrup (HFCS, mixture of fructose and glucose), while HFCS is an ingredient in almost all soft drinks.[2] Similar to glucose and galactose, fructose can be absorbed directly into the bloodstream during digestion.[3] However, after absorption, fructose is directed towards the liver compared to glucose, which can be used as an energy source or stored as glycogen under the influence of insulin.[4] Studies showed that excess consumption of fructose can cause serious health problem, such as weight gaining,[5] metabolic syndrome,[6] type II diabetes,[7] and non-alcoholic fatty liver disease.[8] Therefore, it is important to know the fructose level in our daily food. Since the discovery of the interaction between boronic acid and diol of saccharides,[9] the design of fructose sensors has become easier, however, their selectivity to fructose against other saccharides (e.g., glucose, galactose and sucrose) remains challenging.[10]

3.2.2.2 Discovery of Fructose Orange

This high-throughput screening and fluorescence response profiling system resulted in the identification of a turn-on sensor with high response and selectivity for fructose, and we named it **Fructose Orange** (Figure 3.1b). **Fructose Orange** contained a boronic acid motif, which is a well-known sugar binding group.[11] Although several boronic acid-based sensors for saccharides have been reported,[12] highly selective fluorescent fructose sensors are limited. The most selective sensor for fructose reported to date was a

tetrathiafulvaleneanthracene boronic acid, which showed a 5-fold fluorescence increase upon fructose recognition.[13] **Fructose Orange** exhibited a remarkable 24-fold fluorescence enhancement (i.e., its quantum yield changed from 0.01 in the absence of fructose to 0.27 in the presence of 200 mM fructose) (Figure 3.1) with a dissociation constant (K_d) of 30 mM and an excellent selectivity among a large collection of 24 saccharides (Figure 3.2).

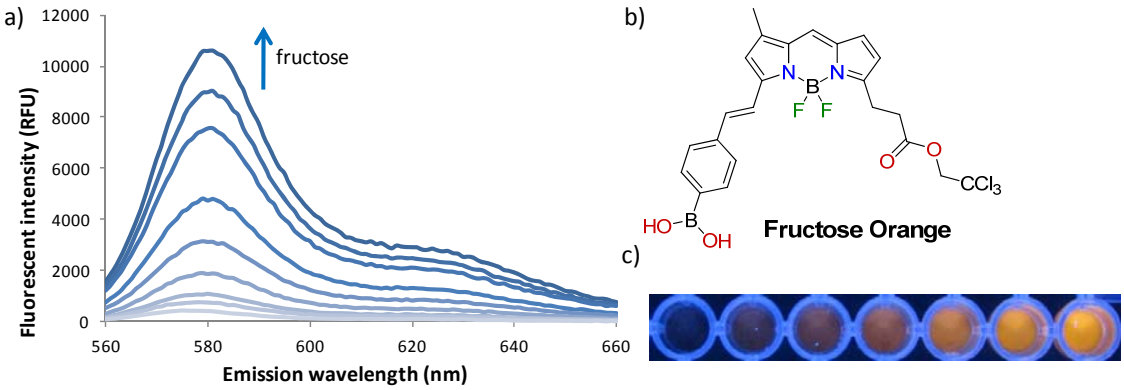

Figure 3.1 (a) Fluorescent spectra of **Fructose Orange** (10 μM) after incubation with fructose (0, 1, 2, 5, 10, 20, 50, 100 and 200 mM) in HEPES buffer (20 mM, pH=7.4) under excitation at 530 nm. (b) Structure of **Fructose Orange**. (c) Pictures of **Fructose Orange** (10 μM) solutions containing fructose (from left to right: 0, 5, 10, 20, 50, 100 and 200 mM) under irradiation with a hand-held 365-nm lamp.

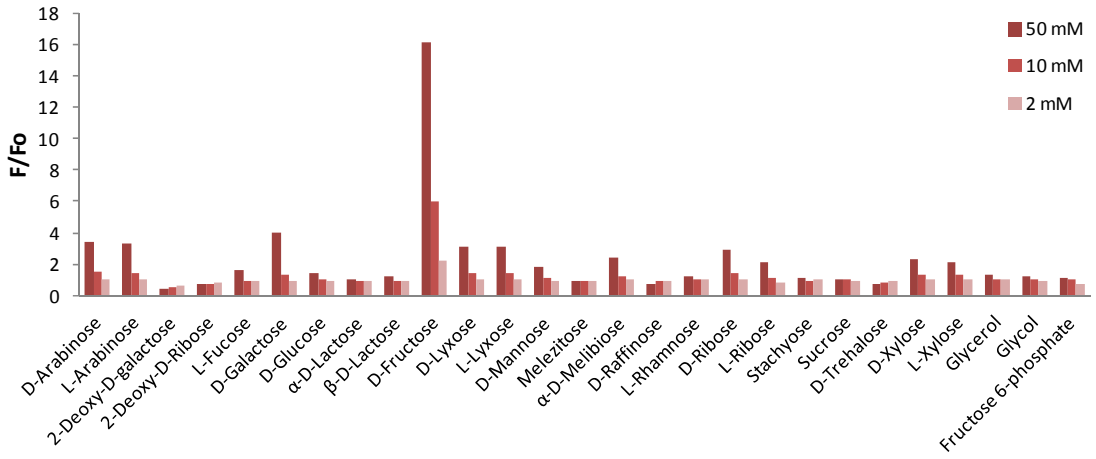

Figure 3.2 Selectivity of **Fructose Orange** (10 μM) against 24 different sugars, glycerol, glycol and fructose 6-phosphate at 3 different concentrations in HEPES buffer (20 mM, pH=7.4). Excitation wavelength: 530 nm.

3.2.2.3 Solubility and pH-Dependence of Fructose Orange

To figure out the possible application condition for **Fructose Orange**, next we evaluated its solubility and pH-dependence. Spectral measurements confirmed that the dye is soluble in HEPES buffer (20 mM, pH=7.4) with 1% DMSO in a broad concentration range (i.e., 1 to 100 μM) (Figure 3.3), and that a consistent fluorescent response to fructose was observed within a pH range from 6 to 9 (Figure 3.4).

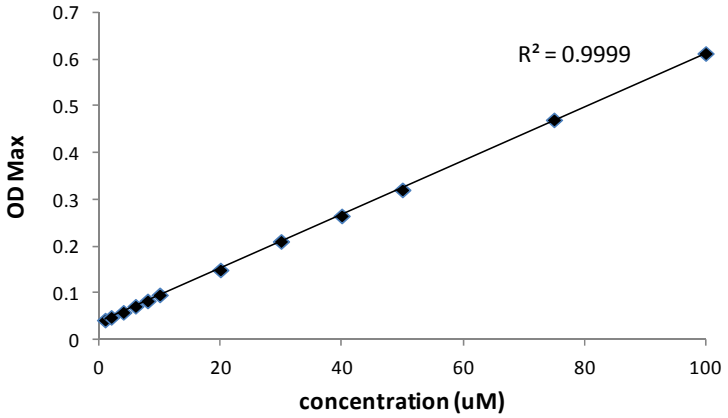

Figure 3.3 Absorbance of **Fructose Orange** dissolving at different concentrations (1, 2, 4, 6, 8, 10, 20, 30, 40, 50, 75 and 100 uM) in HEPES buffer (20 mM, pH=7.4) with 1% DMSO.

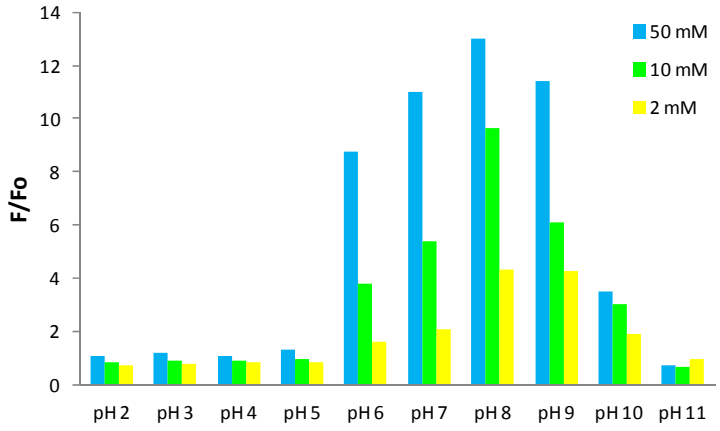

Figure 3.4 Fold change of **Fructose Orange** (10 uM) mixing with different concentrations of fructose at different pH.

3.2.2.4 Structure-Fluorescence Relationship Study

In order to determine structure-fluorescence relationships, we compared the fluorescence response of **Fructose Orange** to **BD-187**, a BODIPY derivative containing a phenylboronic acid but without the trichloroethyl ester moiety.[1b] As depicted in Figure 3.5, **BD-187** only showed a 2.5-fold fluorescence increase to fructose, which proved that the selectivity of **Fructose Orange** toward the saccharide was due to both the boronic acid and the ester groups. We further prepared six new derivatives (**FO1-6**) in which we functionalized the alkyl moiety with different esters and amides. While all **FO1-6** showed a dose-dependent fluorescent enhancement upon incubation with fructose, **Fructose Orange** displayed the highest fold change(Figure 3.6), indicating the importance of the trichloroethyl ester for the molecular recognition. **FO2** exhibited a better selectivity profile than **BD-187** (Figure 3.7), which corroborated the implication of the ethyl ester group in the binding process.

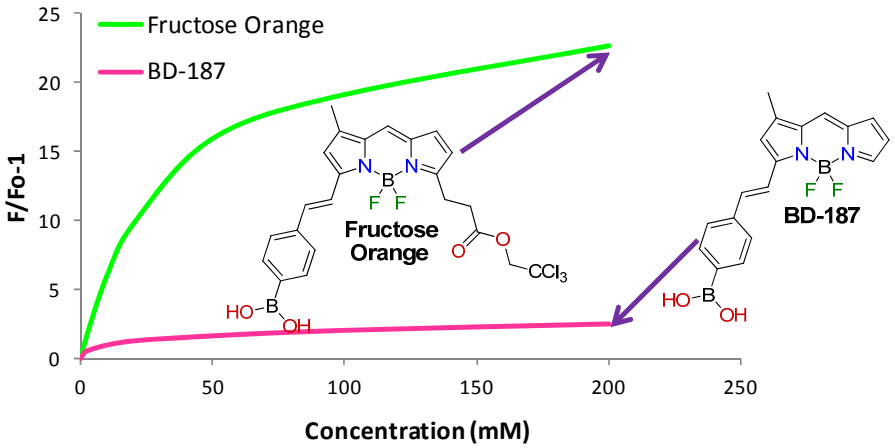

Figure 3.5 Chemical structures and fluorescence responses of **Fructose Orange** and **BD-187** (10 μM) after incubation with fructose (from 0 to 200 mM).

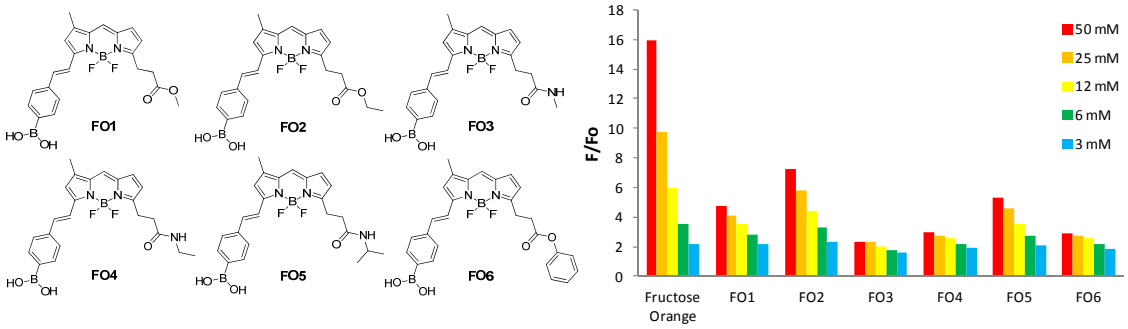

Figure 3.6 Structures of **FO1-6** and fluorescent response of **Fructose Orange** and **FO1-6** (10 μM) towards fructose in HEPES buffer (20 mM, pH=7.4).

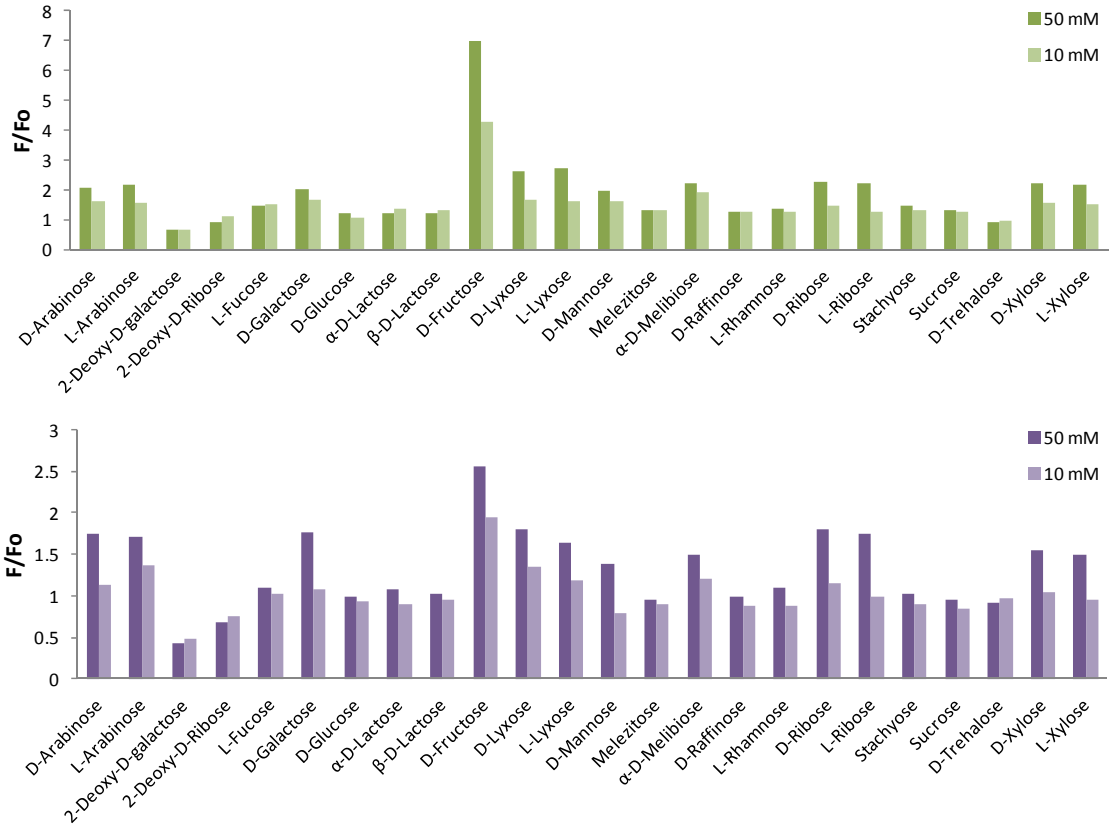

Figure 3.7 Selectivity of **FO 2** (green) and **BD-187** (purple) against 24 different sugars at 2 different concentrations in HEPES (20 mM, pH=7.4).

3.2.2.5 Bing-Site Study

Eggert and co-workers reported spectroscopic evidence of the complexes formed by fructose and *p*-tolylboronic acid using ^{13}C NMR to determine the $^{1}J_{CC}$ coupling constants.[14] To investigate the binding mode of **Fructose Orange**, we performed a similar analysis using ^{13}C-fructose. In DMSO-d_6, fructose presents three major (i.e. β-fructofuranose, β-fructopyranose and α-fructofuranose) and two minor isomeric forms (i.e. α-fructopyranose and fructoketose).[15] The signals of these five isomers and the C-Ccoupling constant were detected by ^{13}C-NMR and assigned according to the literature (Table 3.2 and 3.3).[14-15] After mixing fructose with **Fructose Orange** in a 1:1 ratio, five different complexes (**1-5**, Figure 3.8) were formed. The most abundant complex was **1**, as proven by the 2D-COSY spectra and the decrease on the signal corresponding to the C-2 hydroxyl group.

Table 3.2 ^{13}C Chemical shifts (ppm) for the fructose part of complexes and free fructose isomers.

Compound	C-1	C-2	C-3	C-4	C-5	C-6
β-fructofuranose	62.8	101.9	75.2[a]	75.6[a]	81.8	62.8
α-fructofuranose	63.6	104.0	82.8	75.7	80.8	61.0
β-fructopyranose	64.3	97.9	67.7	69.8[a]	69.0[a]	62.9
α-fructopyranose	63.7	97.1	68.0	71.4	62.9	58.7
Fructoketose	66.2	213.5	75.4	72.3[a]	70.5[a]	63.7
2	63.0	115.2	87.7[a]	76.4	88.0[a]	61.5
3	64.0	99.7	82.3	78.0	85.0	62.1
4	64.1	105.0	72.1[a]	71.9[a]	71.4[a]	61.1
5	73.0	107.8	69.6[a]	69.1[a]	68.8[a]	65.6
6	[b]	92.6	[b]	67.3	[b]	59.7

[a] Assignment can be interchanged. [b] Assignment cannot be done because of overlapping signals.

Table 3.3 $^{1}J_{CC}$ coupling constant (in Hz) for the fructose part of complexes and free fructose isomers[a]

Compound	$J_{1,2}$	$J_{2,3}$	$J_{3,4}$	$J_{4,5}$	$J_{5,6}$
β-fructofuranose	50.0	50.0		42.5	42.6
α-fructofuranose	51.0	46.6	42.4	42.1	42.4
β-fructopyranose	49.8	47.5	37.6	37.1	35.2
α-fructopyranose	53.0	46.8	38.0	38.4	40.0
Fructoketose	41.1	43.0	40.0	42.9	43.0
2	54.0	36.5	40.9	38.9	46.4
3	47.3	44.6	42.1	36.5	43.8
4					37.4
5	42.1				37.4
6	47.1	44.0	40.8	36.9	

[a]the absence of an entry indicates that the value cannot be calculated either due to overlapping signals or too strong coupled nuclei.

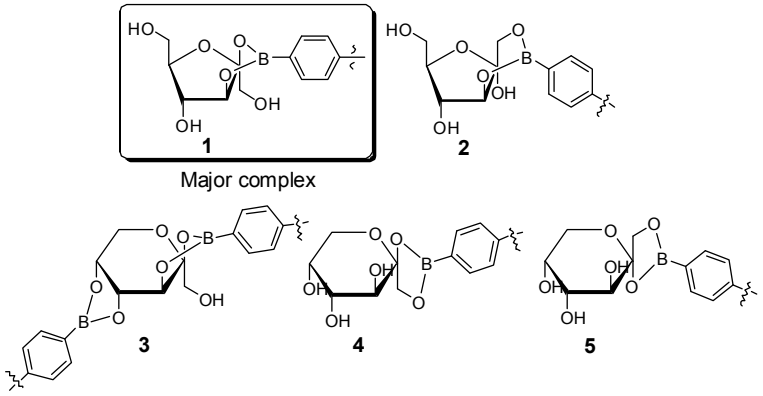

Figure 3.8 Structures of the complexes detected in DMSO-d_6 upon interaction of **Fructose Orange** and fructose.

3.2.2.6 Application of Fructose Orange

In view of the sensitivity and selectivity of **Fructose Orange**, we examined its potential for the quantification of fructose in real samples. First, we observed that the fluorescent intensity of **Fructose Orange** showed a good linear correlation with the concentration of fructose up to 10 mM in both HEPES and 1% fructose-free Coca Cola solutions (Figure 3.9a). These results confirmed that the matrix of soft drinks did not interfere in the fluorescence response of **Fructose Orange**. Secondly, we applied our sensor to determine the concentration of fructose in regular Coca Cola and compared our results to a conventional method. The concentration of fructose in regular Coca Cola determined by **Fructose Orange** was 272 mM, which matched well with the results obtained by HPLC quantification (i.e. 245 mM) (Figure 3.9b). With this data, we validated the use of **Fructose Orange** to quantify the levels of fructose in real samples.

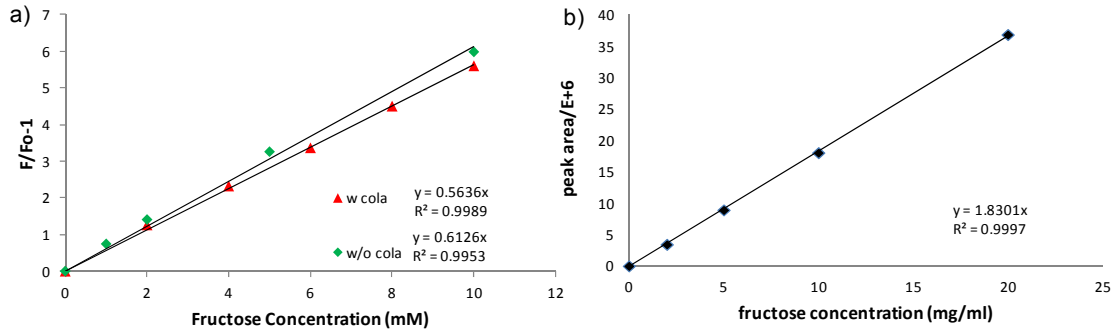

Figure 3.9 (a) Application of **Fructose Orange** in real samples. A series of fructose solutions were mixed without and with 1% fructose-free Coca Cola in HEPES buffer (20 mM, pH 7.4). Emission intensity values of **Fructose Orange** at 580 nm were plotted against the total concentration of fructose. Excitation wavelength: 530 nm. (b) Quantification of fructose in Coca Cola by HPLC. Values of the standard curve are represented as means of 3 different experiments. The area of a 5-fold diluted Coca Cola sample corresponded to 16.12 E+6, and the total concentration of fructose was determined as 44.0 mg/ml (245 mM).

3.2.3 Development of a Ratiometric Glutathione Sensor-Glutathione Green

3.2.3.1 Glutathione

Glutathione (GSH) is of crucial importance in cellular process, especially preventing the damage to cellular component caused by reactive oxygen species.[16] This is controlled by the equilibrium between GSSG and GSH.[17] The GSH level in cell and organism is closely related to many diseases, such as cancer, HIV, cystic fibrosis (CF), neurodegenerative diseases and aging.[18] Hence, it is important to monitor the GSH level in biosystem. So far, a variety of fluorescent probes for biothiol based on different fluorophores, such as rodamine, fluoroscein, coumarin and so on, have been developed.[19] Most of these probes were made by designed approach, utilizing either the 1,4-addition of thiols to α,β-unsaturated ketones, or the attacking of thiols to double sulphur bond. These reactions not only enable the attack of thiols but also other nucleophiles in the biosystem. Therefore, discovering novel glutathione probes especially with new specific binding site is of great importance.

3.2.3.2 Discovery of Glutathione Green

One compound, **BDD-135**, was found to show red-to-green fluorescence change in response to GSH after the unbiased fluorescence screening of **BDD** library (Figure 3.10). **BDD-135** has a furan ring conjugated to BODIPY core. Another 8 compounds from **BDD** library, which also contain furan ring in their structures, were explored for their response to GSH, too. All these 9 compounds showed similar red-to-green fluorescent response upon binding to GSH (Figure 3.11), which reveals that furan ring conjugated to BODIPY is a novel binging site towards thiol group. Among them, **BDD-135** showed highest response, and was therefore selected for further study and named as **Glutathione Green**.

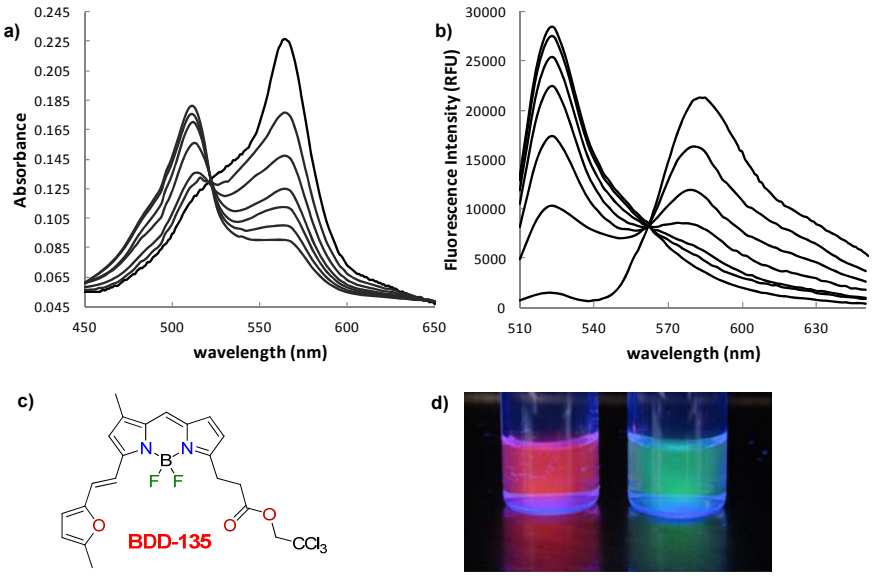

Figure 3.10 Time dependent absorbance (a) and fluorescence (b) spectra of **Glutathione Green** (10 μM) with GSH (5 mM) in DMSO/HEPES buffer (1:4, v/v, 20 mM, pH=7.4). (c)Structure of **Glutathione Green.** (d) A picture of **Glutathione Green** (10 μM) solution with (right) and without (left) 5 mM GSH under irradiation with a hand-held 365-nm lamp.

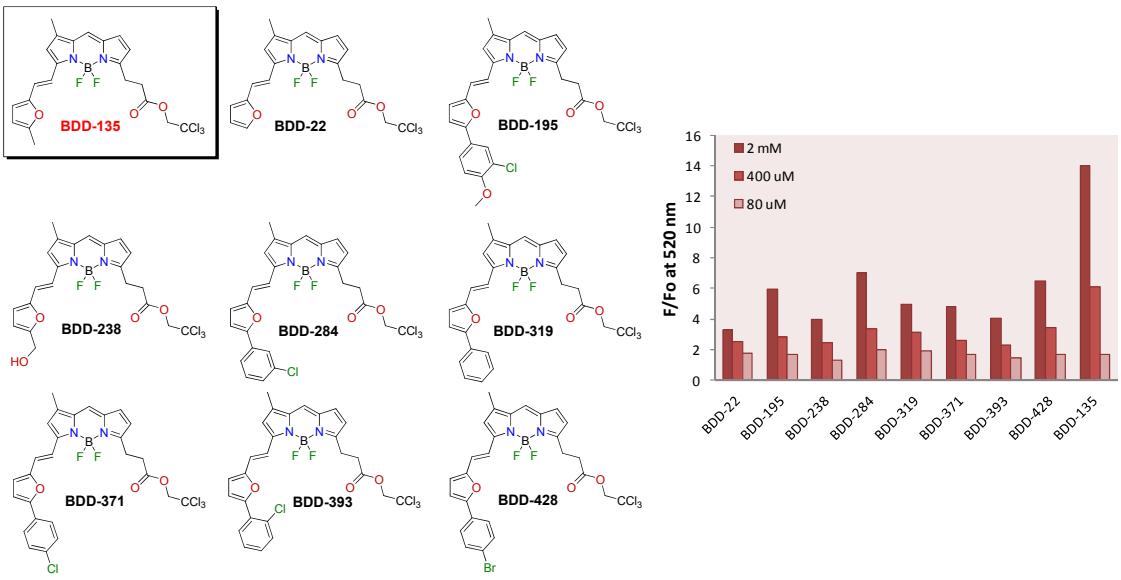

Figure 3.11 Structure of 9 GSH probes and fluorescent response of these 9 probes at 520 nm after incubation with GSH for 30 min in HEPES buffer (20 mM, pH=7.4) under excitation at 470 nm.

3.2.3.3 Spectroscopic Property of Glutathione Green

Glutathione Green exhibits absorption maxima (λ_{abs}) at 565 nm (ε=369 000 $M^{-1}cm^{-1}$) and fluorescence maxima (λ_{flu}) at 585 nm with quantum yield of 0.47 in DMSO (Figure 3.12). When bind to GSH, the fluorescence spectra (as well as absorbance) of **Glutathione Green** exhibited a profound ratiometric change, undergoing a significant hypsochromic shift to 522 nm (512 nm for absorbance) with an apparent isosbestic point at 562 nm (522 nm for absorbance) in 20% DMSO/HEPES buffer solution (Figure 3.10).

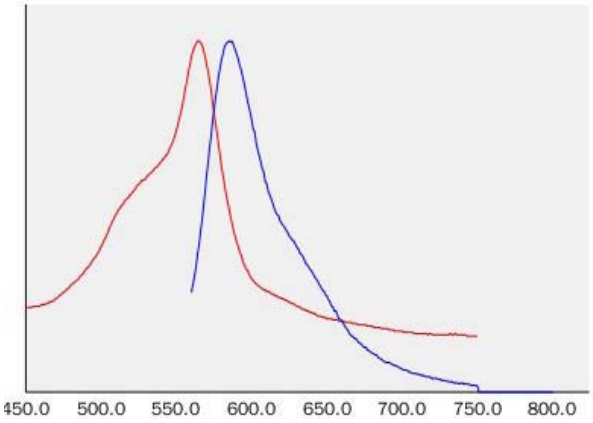

Figure 3.12 Normalized spectrum of the absorbance (red line) and fluorescence (blue line) of **Glutathone Green**.

3.2.3.4 Selectivity and Kinetic Study of Glutathione Green

Glutathione Green showed very good selectivity over other class of analytes, with respect to the response at 522 nm. Even for other biothiol compound, such as cysteine, it also showed good selectivity considering their actual concentration in biosystems (Figure 3.13). The process between **Glutathione Green** and GSH followed *pseudo*-first order kinetics with large excess amount of GSH (2.5 mM), and the *pseudo*-first order reaction constant k'=0.0412 min^{-1} (Figure 3.14a). The plot of k' versus concentration of GSH was a straight line through the origin, indicating the reaction is second-order overall, first-order with respect to **Glutathione Green** and first-order with respect to

GSH, with k=0.28 $M^{-1}s^{-1}$ (Figure 3.14b). This reaction is faster than other reported thiol attack reactions.[19a, 19f]

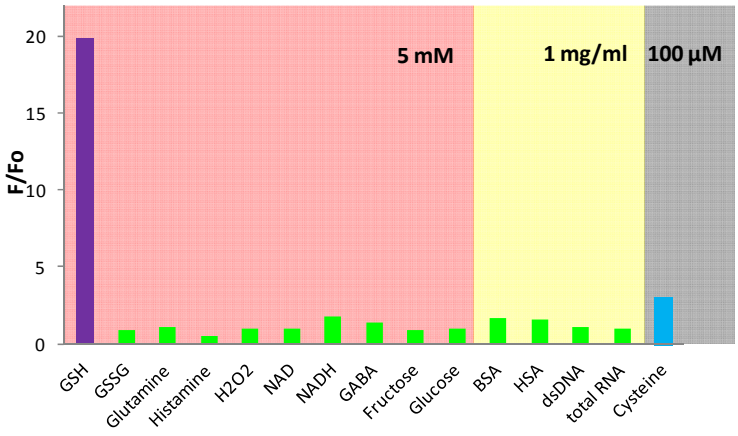

Figure 3.13 Fluorescence responses of **Glutathione Green** (10 µM) toward different analytes at 522 nm.

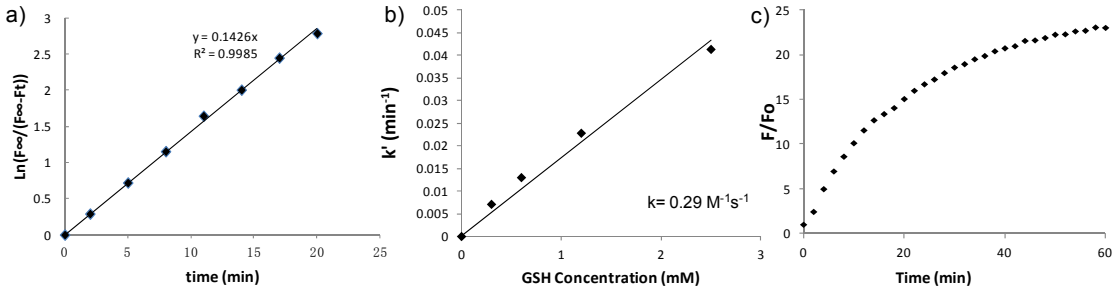

Figure 3.14 (a) Kinetic measurement by fluorescence of **Glutathione Green** (10 µM) incubated with GSH (2.5 mM). P*seudo*-first order reaction constant to **Glutathione Green** is 0.0412 min^{-1}. (b) Plot of k' versus concentration of GSH. (c) Time dependent fluorescent response of **Glutathione Green** (10 µM) to GSH (2.5 mM) in HEPES buffer (20 mM, pH=7.4).

3.2.3.5 Application of Glutathione Green

The good sensitivity, selectivity, fast reaction speed and ratiometric response of **Glutathione Green** allow both quantitative measurement of GSH amount in cell extracts and direct visualization of GSH level in live cells. α-lipoic acid (LPA)[20] and NMM (N-methylmaleimide)[21] are known to be capable of inducing the synthesis of

GSH and block thiol group inside a variety of cells, respectively. Therefore, 3T3 cells were selected to be pre-treated with α-lipoic acid for 48 h and NMM for 30 min, and the cell extracts were analyzed by **Glutathione Green**, as well as a commercial GSH fluorimetric kit. The results from both the methods correlated very well with each other, indicating that **Glutathione Green** is able to be used for GSH quantification *in vitro* (Figure 3.15a and 3.15b). **Glutathione Green** was also tested to monitor the intracellular GSH concentration. The experiment was also conducted with 3T3 cells. The image intensity of the 3T3 cells labelled with **Glutathione Green** collected from two emission windows (green: FITC; red: texas red) gave an average ratio of F_{green}/F_{red}=1.52. More importantly, **Glutathione Green** also response to the change of GSH concentration in cellular environment: the F_{green}/F_{red} increased to 2.47 when the cells were pre-incubated with α-lipoic acid for 48 h, and decreased to 0.21 upon treatment to the cells with NMM for 30 min (Figure 3.15c and 3.15d). These observations demonstrate that **Glutathione Green** is capable of detecting GSH level in live cells.

3.2.3.6 Solvent Effect and Binding Site Study

Structures of the 9 GSH probes show obvious similarity, which directs the reaction position of **GSH Green** with GSH to be the furan ring. Furthermore, the reaction between **GSH Green** and GSH did not occur in pure organic solvent, including acetonitrile, methanol, dichloromethane, DMSO and DMF (data not shown). Water is necessary for the reaction to proceed. On the other hand, the reaction speed becomes slower with increasing percentage of DMSO (Figure 3.16a). These indicate that water molecule participated in the reaction between **Glutahione Green** and GSH. In low DMSO solution, the reaction was fast enough to enable us to observe the red-to-green colour change directly. However, when DMSO percentage increased to 50%, it was

obvious that the colour changed from red-to-orange-to-green with much longer time (Figure 3.16b). LCMS data also confirmed the formation of the orange colour intermediate (experimental section). On the other hand, it is known that furan ring is easy to open under certain conditions.[22] Based on all these information, we speculated that the reaction occurred as shown in Figure 3.17. However, due to the poor stability in organic solvent, the intermediate could not be separated.

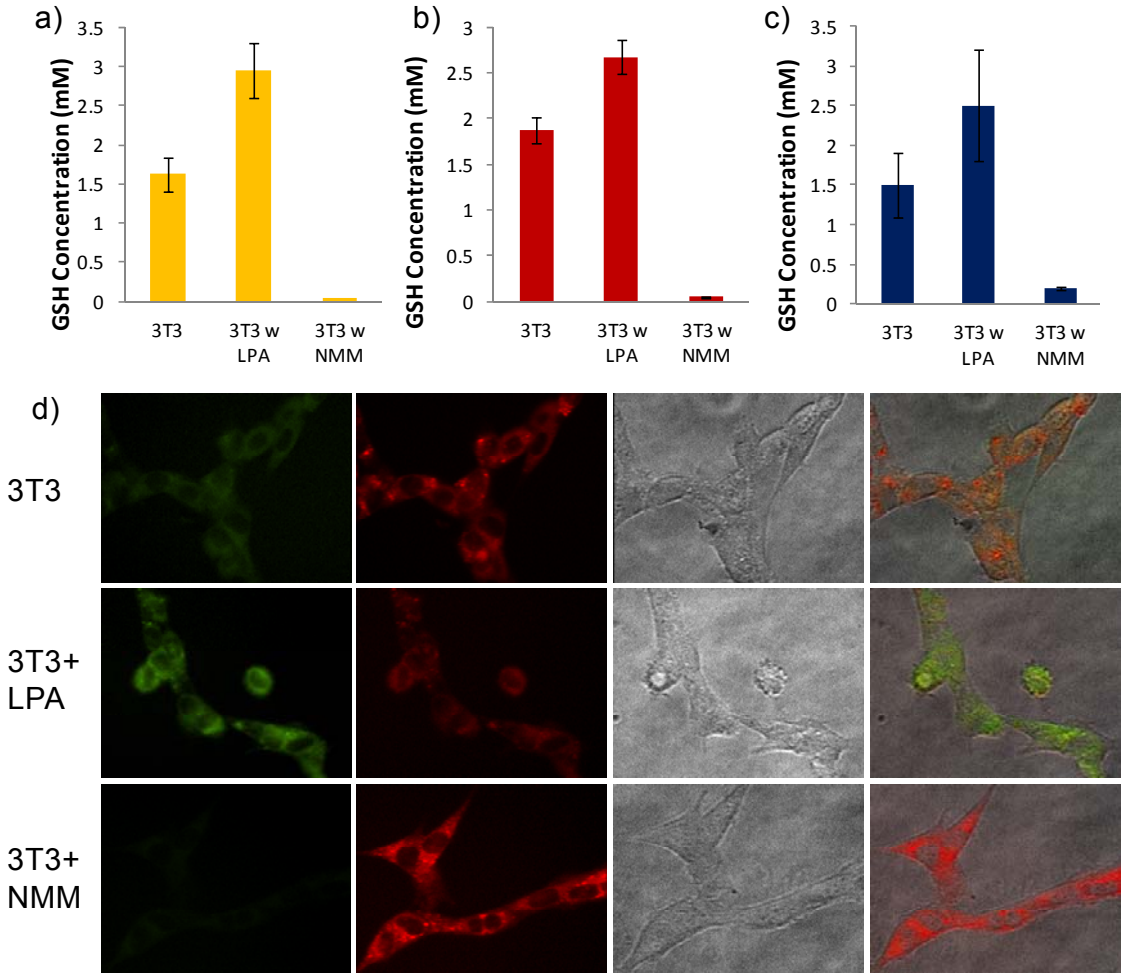

Figure 3.15 (a) GSH concentration in cell extract calculated by using commercial GSH fluorimetric kit. (b) GSH concentration in cell extract calculated by using **Glutahione Green**. (c) Average image intensity ratio (F_{green}/F_{red}) collected from two emission window, FITC (green) and Texas Red (red) channel. (d) Fluorescent microscopic image of live 3T3 cells stained with 2 µM **GSH Green** upon pre-incubate of NMM (1 mM) for 30 min (top), LPA (250 µM) for 48 h (middle), and control (down).

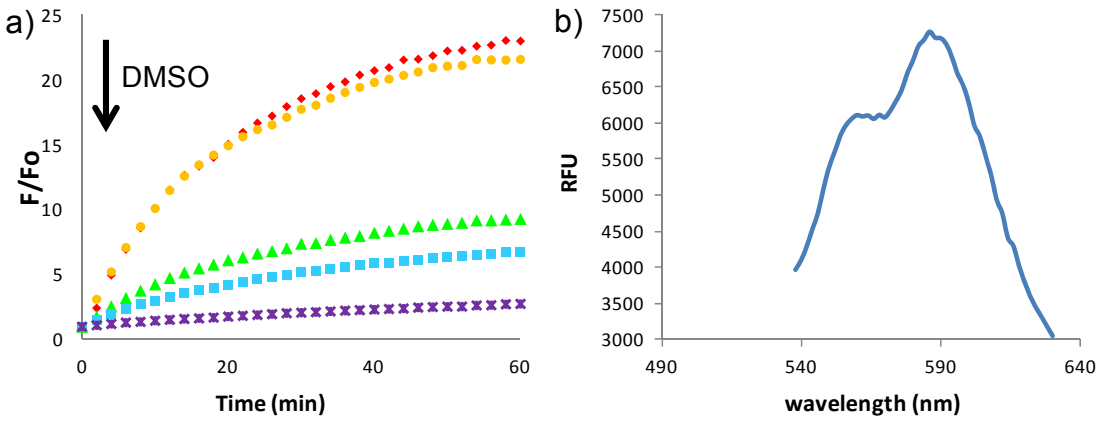

Figure 3.16 (a) Time dependent fluorescent response of **Glutathione Green** (10 μM) to GSH (2 mM) in HEPES buffer (20 mM, pH=7.4) with different percentage of DMSO (1%, 5%, 10%, 25% and 50%). (b) Fluorescence spectrum of **Glutathione Green** (10 μM) incubated with GSH (2 mM) after 30 min in HEPES buffer (20 mM, pH=7.4) with 50% DMSO.

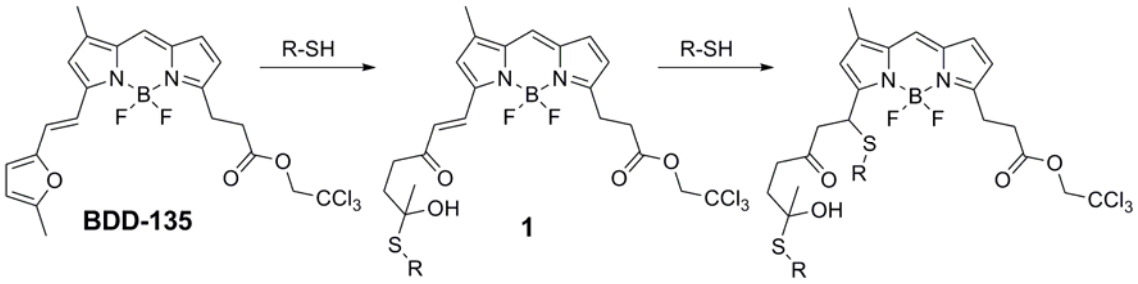

Figure 3.17 Proposed reaction scheme of **Glutathione Green** with thiol.

3.2.4 Development of Fluorescent Sensor for Illicit Date-Rape Drug-GBL

3.2.4.1 Drug-Facilitated Sexual Assault and Gamma-Butyrolactone

Drug-facilitated sexual assault (DFSA) is a crime act defined as the "voluntary or involuntary ingestion of a drug by a victim that results in an act of sexual activity without consent".[23] In addition to alcohol, the drugs most often used in the commission of DFSA include gamma-hydroxybutyric acid (GHB), gamma-butyrolactone (GBL), Rohypnol, ketamine, and Soma.[24] These drugs, which are covered under the name of "date-rape drug", can lead to a person losing the ability to make decisions and even unconscious within a short period.[25] DFSA is a dangerous social problem, as date-rape drugs are typically distributed in parties, clubs and bars, and even increasingly sold in schools and on college campuses. Hence, it desperately needs a solution.

GHB is a powerful depressant for central nervous system and used illicitly for its sedative and euphoric effects.[26] It was classified as Schedule I drug under the Controlled Substances Act in 2000. As a result of the more stringent regulations to purchase GHB, consumers began to turn to its pro-drug, GBL, as a substitute to circumvent the law.[27] GBL itself is pharmacologically inactive, however, it is easily metabolised to GHB in the presence of peripheral lactonases *in vivo*.[28] Therefore, GHB and GBL have similar psychopharmacological effects after ingestion. GBL is a common industrial solvent widely used in paint stripper, nail polishers and stain removals. Although GBL was later classified as Schedule I drug, too, its usage in the legitimate chemical industry is still approved, which makes the availability of GBL even spread over the internet.[29] Both GHB and GBL are notorious date-rape drugs due to their speedy elimination after ingestion, colourless property and high solubility in aqueous solutions.[30] Compared with alcohol, the withdrawal effect of GHB and GBL are much more rapid, commonly felt within 1–6 hours of the last dose.[31] In contrast to GHB, GBL

is more lipophilic and can be absorbed upon oral administration more rapidly, leading to its higher bioavailability.[32] There is an increase shift of users from GHB to GBL, arising from its less harsh legal status, inexpensiveness, and easier availability.[33] Overdose of GBL may lead to dangerously low respiratory rates, unconsciousness, seizures, bradycardia and even death.[34] Therefore, development of real time detection method for GBL would have great contribution on solving the DFSA problem.

Efforts have been made over years to develop detection kits for these date-rape drugs. Several test kits have been introduced to detect GHB in drinks, including "DrinkSafe^{TM}" cards, "DrinkSafe^{TM}" coasters, and "Drink Detective^{TM}".[35] However, these kits fail to detect drugs in wine-based drinks, beverages containing dairy products, fat liquors, tonic water, or acidic beverages. Another latest development in such kits is "drug detection straw", developed by Tel Aviv University in 2011.[36] However, this kit is only practical on the detection of GHB and ketamine. No on-site detection method has been reported for GBL.

3.2.4.2 Discovery of GBL Sensor-Green Date

Based on the purpose to develop novel fluorescent GBL sensor, we designed a screening platform towards GBL using in-house diversity-oriented fluorescent libraries. The frequent recreational dosage of GHB is between 2.5 and 4 g,[37] which is also around the detection limit of "DrinkSafe^{TM}" cards (0.012 g/ml, assuming volume of drink is 200 ml). 2.1 g of high purity (99%) GBL provides consumers similar effect to consumption of 2.5g of GHB. Therefore, the screening concentration of GBL was set as 0.010 g/ml in water. 64 diversity-oriented fluorescent libraries (5,120 dyes) based on different fluorescent scaffolds were screened using 384-well black plate, and 83 compounds (data not shown) were selected as primary hits due to their more than 2-fold fluorescence enhancement upon the addition of GBL. Secondary screening was then

carried out with a wide range of concentrations of GBL (i.e., 0.003, 0.005, 0.010, 0.020, 0.040 g/ml) to eliminate the false positive results using 96-well black plate. Finally, 5 best responsive and reproducible hit compounds (Figure 3.18) were rendered.

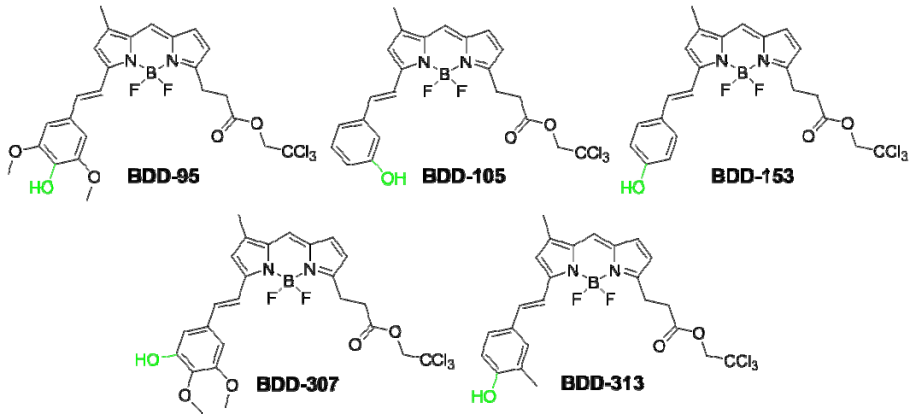

Figure 3.18 Structures of the 5 hit compounds for GBL from **BDD** library

These 5 hits are all from **BDD** library, and their structures showed similarity with a hydroxyl group at either para- or meta-position of the phenyl ring. Postulating that hydroxyl group may play a prominent role in the interaction with GBL, we further synthesized 2 derivatives (**6** and **7**) with di-hydroxyl group (Scheme 3.1). Interestingly, Compound **6** showed even better response to GBL than the 5 hit compounds, while compound **7** exhibited poor stability in aqueous solution. Hence, compound **6** was selected as the final GBL fluorescent sensor, and named as **Green Date**.

Scheme 3.1 Synthetic scheme of derivative **6** and **7**.

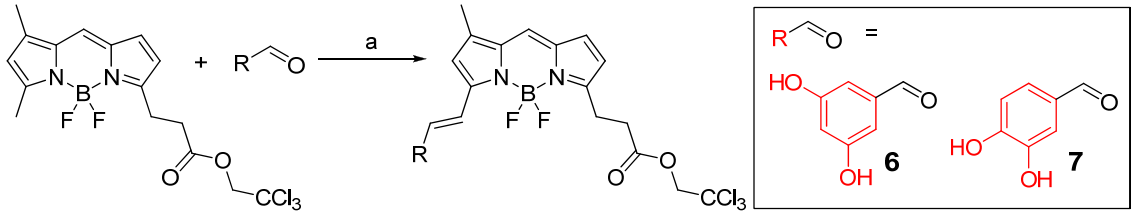

Reagents and conditions: a) pyrrolidine, acetic acid, acetonitrile, 85 ^{o}C, 5 min.

3.2.4.3 Validation of Green Date

Green Date has absorption and emission maximum at 569 and 582 nm, respectively, with quantum yield of 0.05 in water. It exhibited more than 2-fold fluorescent increase with 0.010 g/ml GBL in water, and has a detection limit of 0.003 g/ml (Figure 3.19a). The fluorescence intensity of **Green Date** showed linear increase to the concentration of GBL within 0 to 0.100 g/ml range, as well as obvious colour change excited by green light (Figure 3.19b). As GBL is usually dosed in drinks, especially alcohols, next we evaluated the pH-dependence and ethanol-effect of **Green Date**. A consistent fluorescent response to GBL was observed within a pH range from 2 to 11 (Figure 3.20a), indicating that **Green Date** can be used in both acidic and basic conditions. Low percentage of ethanol (i.e., up to 10%) did not significantly affect the linear fluorescent enhancement of **Green Date** to GBL (Figure 3.20b), showing that it can also detect GBL in alcoholic drinks.

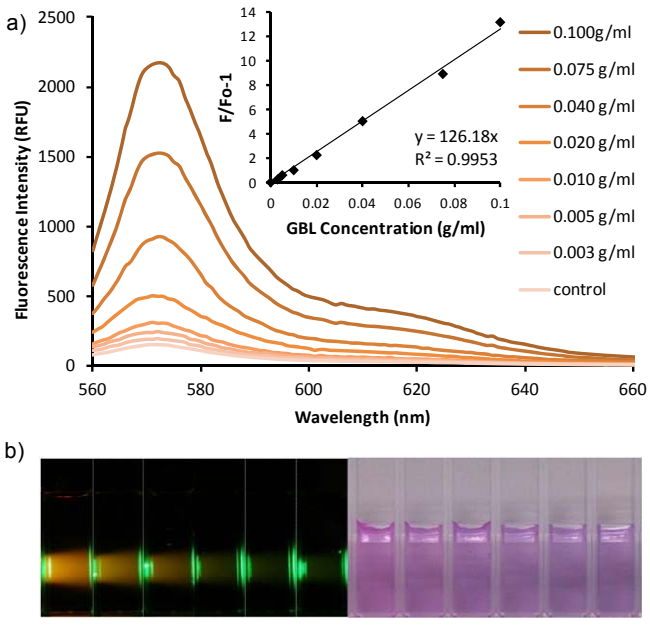

Figure 3.19 (a) Fluorescent spectra of **Green Date** (10 μM) after incubation with different concentration of GBL. (inner) Linear correlation of fold increase of fluorescence versus concentration of GBL. (b) Pictures of **Green Date** (10 μM) solution containing GBL (from left to right: 0.100, 0.075, 0.040, 0.020, 0.010 and 0 g/ml) under irradiation of green light (left) and white light (right).

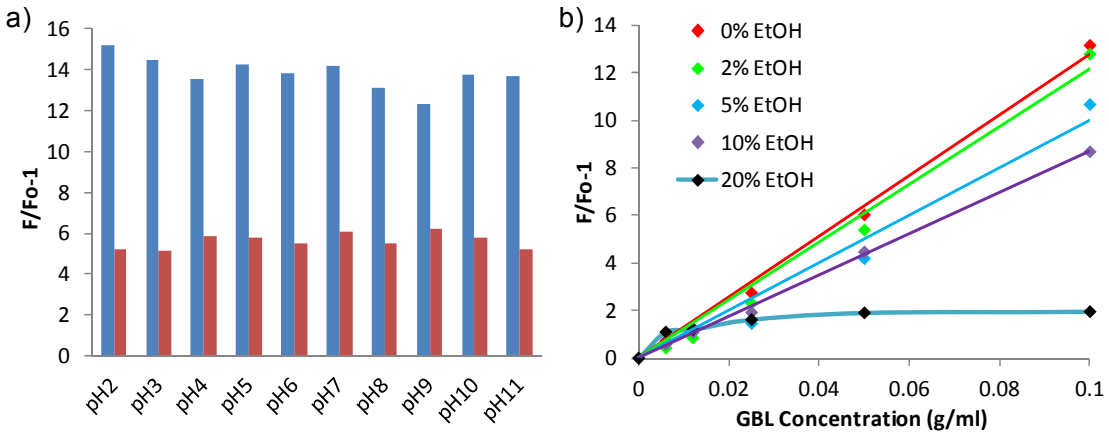

Figure 3.20 (a) Fluorescent response of **Green Date** (10 µM) to GBL (blue bar: 0.100 g/ml; red bar: 0.050 g/ml) under different pH conditions. (b) Linear correlation of fluorescence enhancement of **Green Date** (10 µM) versus concentrations of GBL with different percentage of EtOH.

3.2.4.4 Application of Green Date

Next we examined the potential of **Green Date** to detect GBL dosed in real drink samples. Several beverages representing alcoholic, non-alcoholic, coloured and colourless drinks were selected. We aimed to develop a convenient way (e.g., direct visualization using a green laser pointer) to check whether a drink is safe or not. An extraction method was designed to eliminate the ethanol and coloured components effects, as well as to pre-concentrate GBL. 5 ml of drink samples were extracted with 1 ml chloroform. The organic layer was then separated, air-dried, and re-suspended in 100 µl water containing 10 µM **Green Date** (Figure 3.21). GBL could be pre-concentrated to about 10 times of its original concentration using this method. It showed that other components in the drinks (e.g., ethanol, coloured materials) either was not extract by chloroform or have no response with **Green Date**. It was also clear that **Green Date** showed very different fluorescence intensity to the drinks with and without GBL. These results illustrated that **Green Date** is able to detect GBL in various drinks after a simple extraction method.

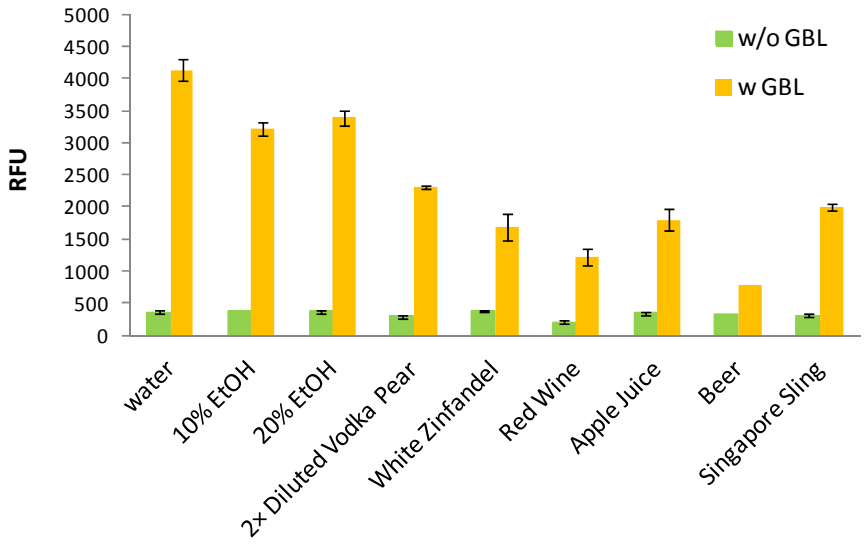

Figure 3.21 Fluorescent response of **Green Date** (10 μM) to different drink samples after extraction method. (Each experiment was repeated 3 to 5 times; GBL concentration: 0.050 g/ml).

3.3 Conclusion

After 3 novel diversity-oriented BODIPY libraries were constructed, they were applied to fluorescence emission response profiling system in order to discover useful sensors. After the high-throughput screening towards a collection of various analytes, two novel sensors, **Fructose Orange** and **Glutathione Green**, were discovered. **Fructose Orange** showed a 24-fold fluorescence increase upon recognition of fructose and an outstanding selectivity among 24 different saccharides. NMR studies confirmed that five different binding interactions were formed between the sensor and fructose. Furthermore, **Fructose Orange** was applied to the quantification of fructose in soft drinks, being the most selective fluorescent sensor for fructose reported to date. **Glutahione Green** showed high response and outstanding selectivity over other analytes. Further experiment showed that **Glutahione Green** is capable of GSH quantification in cell extract, as well as responding to the GSH concentration change in cellular environment.

In order to explore useful sensors for illicit date-rape drug-GBL, high-throughput screening was performed on 5,120 in-house fluorescent compounds, identifying **Green Date** as the final GBL sensor. **Green Date** showed high fluorescence response to GBL in various pH conditions and up to 10% EtOH. Furthermore, **Green Date** is able to detect the existence of GBL in different kinds of drinks samples after a simple extraction method. This discovery will help to secure the safety of our drinks in public place and solve the DFSA problems.

3.4 Experimental Section

Materials and Methods

All the chemicals and solvents were purchased from commercial source and used without further purification. Analytical characterization was performed on a HPLC-MS (Agilent-1200 series) with a DAD detector and a single quadrupole mass spectrometer (6130 series) with an ESI probe. ^{1}H-NMR and ^{13}C-NMR spectra were recorded on Bruker Avance 300 NMR and 500 NMR spectrometers, and chemical shifts are expressed in parts per million (ppm) and coupling constants are reported as a *J* value in Hertz (Hz). High resolution mass spectrometry (HRMS) data was recorded on a Micromass VG 7035 (Mass Spectrometry Laboratory at National University of Singapore (NUS)). Spectroscopic and quantum yield data were measured on spectroscopic measurements, performed on a fluorometer and UV/VIS instrument, Synergy 4 of Bioteck Company. The slit width was 1 nm for both excitation and emission, and the data analysis was performed using GraphPrism 5.0. The concentration measurement for fructose in cola was performed on HPLC (Waters 515) with a Refractive Index Detector (Waters 2414) and a plus Autosampler (Waters 717). Analytical method: eluents: H_2O 0.5 ml/min; Waters Sugar-Pak column (6.5 x 300 mm).

3.4.1 Characterization of Fructose Orange

^{1}H NMR (300 MHz, DMSO-d_6): 2.32 (s, 3H), 2.96 (t, J=7.5 Hz, 2H), 3.24 (t, J=7.5 Hz, 2H), 4.94 (s, 2H), 6.48 (d, J=3.9 Hz, 1H), 7.10 (s, 1H), 7.13 (d, J=3.9 Hz, 1H), 7.47 (d, J=16.2 Hz, 1H), 7.58 (d, J=8.1 Hz, 2H), 7.70 (d, J=16.2 Hz, 1H), 7.71 (s, 1H), 7.87 (d, J=8.1 Hz, 2H), 8.16 (s, 2H).

^{13}C NMR (75.5 MHz, DMSO-d_6): 11.3, 23.4, 31.8, 73.8, 95.3, 117.1, 124.2, 126.3, 128.3, 128.7, 133.7, 134.5, 134.9, 136.1, 137.1, 137.2, 139.0, 143.6, 155.8, 156.1, 170.7.

ESI-MS m/z ($C_{23}H_{21}B_2Cl_3F_2N_2O_4$) calculated: 554.1 found: 555.1 (M+H), 535.1 (M-F).

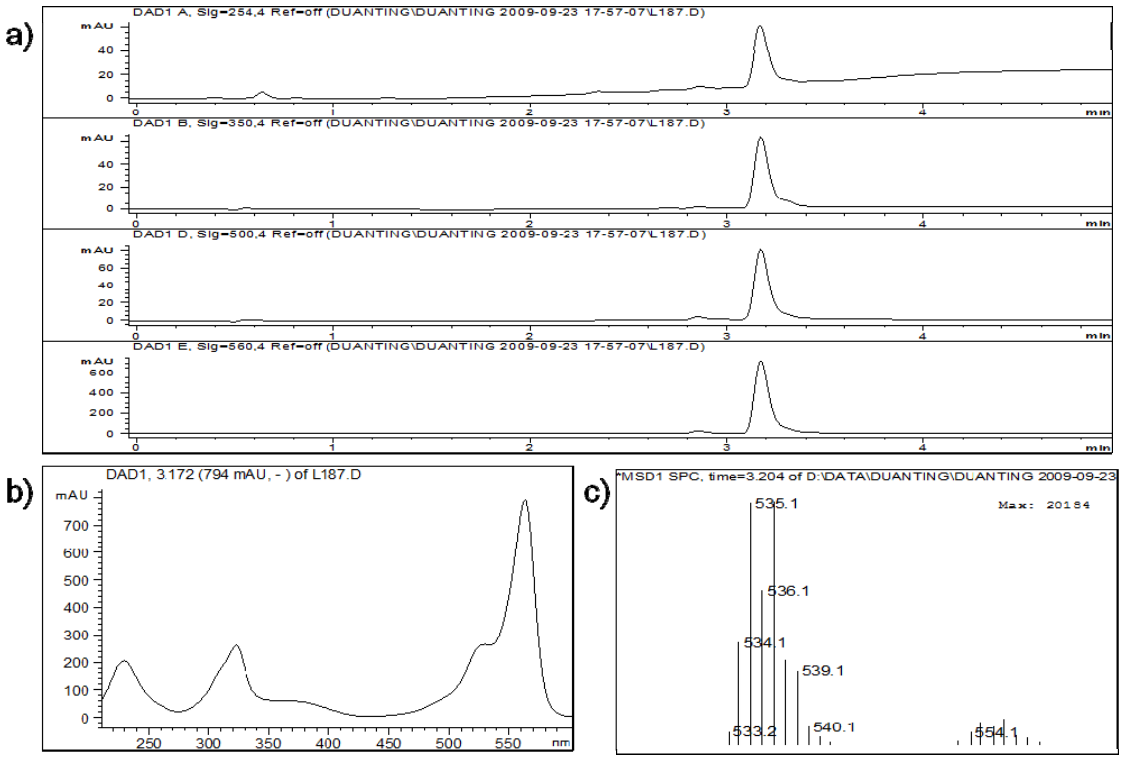

HPLC-MS characterization of **Fructose Orange**. (a) chromatograms (*descending order*) at 254 nm, 350 nm, 500 nm and 560 nm; (b) spectra profile (200-600 nm); (c) ESI-MS positive spectra. HPLC conditions: A: H_2O-HCOOH: 99.9:0.1. B: CH_3CN-HCOOH: 99.9:0.1; gradient 30% B to 100% B (5 min), isocratic 100% B (2.5 min). Reversephase Phenomenex C_{18} Luna column (4.6 x 50 mm^2) 3.5 µm, flow rate: 1.2 mL/min.

3.4.2 Characterization of FO1-6

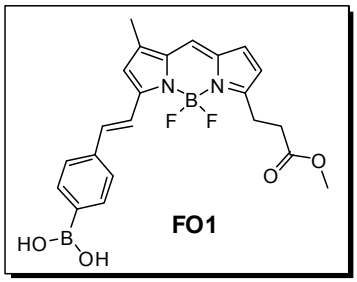

^{1}H NMR (300 MHz, $CDCl_3$+MeOD): 2.29 (s, 3H), 2.79 (t, *J*=7.5 Hz, 2H), 3.35 (t, *J*=7.5 Hz, 2H), 3.71 (s, 3H), 6.31 (d, *J*=3.9 Hz, 1H), 6.73 (s, 1H), 6.90 (d, *J*=3.9 Hz, 1H), 7.09 (s, 1H), 7.29 (d, *J*=8.1 Hz, 2H), 7.32 (d, *J*=16.2 Hz, 1H), 7.59 (d, *J*=8.1 Hz, 2H), 7.65 (d, *J*=16.2 Hz, 1H).

HRMS *m/z* ($C_{22}H_{22}B_2F_2N_2O_4$) calculated: 438.1734 found: 437.1667 (M-H).

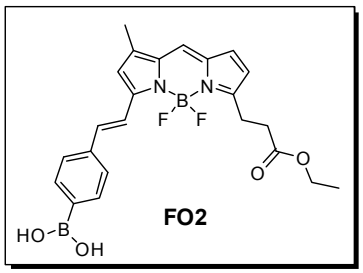

^{1}H NMR (300 MHz, $CDCl_3$+MeOD): 1.25 (t, *J*=7.2 Hz, 3H), 2.28 (s, 3H), 2.77 (t, *J*=7.5 Hz, 2H), 3.32 (t, *J*=7.5 Hz, 2H), 4.15 (q, J=7.2 Hz, 2H), 6.29 (d, *J*=3.9 Hz, 1H), 6.71 (s, 1H), 6.89 (d, *J*=3.9 Hz, 1H), 7.07 (s, 1H), 7.27 (d, *J*=8.1 Hz, 2H), 7.30 (d, *J*=16.2 Hz, 1H), 7.57 (d, *J*=8.1 Hz, 2H), 7.63 (d, *J*=16.2 Hz, 1H).

HRMS *m/z* ($C_{23}H_{24}B_2F_2N_2O_4$) calculated: 452.1890 found: 451.1822 (M-H).

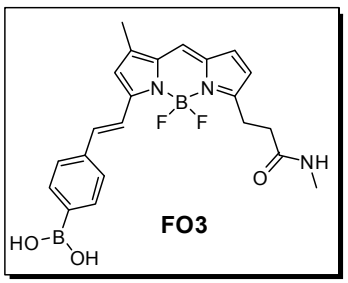

^{1}H NMR (300 MHz, $CDCl_3$+MeOD): 2.29 (s, 3H), 2.63 (t, *J*=7.5 Hz, 2H), 3.28 (t, *J*=7.5 Hz, 2H), 3.62 (s, 3H), 6.31 (d, *J*=3.9 Hz, 1H), 6.73 (s, 1H), 6.89 (d, *J*=3.9 Hz, 1H), 7.07 (s, 1H), 7.26 (d, *J*=8.1 Hz, 2H), 7.32 (d, *J*=16.2 Hz, 1H), 7.57 (d, *J*=8.1 Hz, 2H), 7.61 (d, *J*=16.2 Hz, 1H).

HRMS *m/z* ($C_{22}H_{23}B_2F_2N_3O_3$) calculated: 437.1894 found: 436.1818 (M-H).

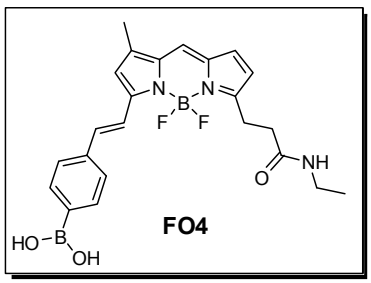

^{1}H NMR (300 MHz, $CDCl_3$+MeOD): 1.03 (t, *J*=7.2 Hz, 3H), 2.27 (s, 3H), 2.62 (t, *J*=7.5 Hz, 2H), 3.19 (q, J=7.2 Hz, 2H), 3.26 (t, *J*=7.5 Hz, 2H), 6.30 (d, *J*=3.9 Hz, 1H), 6.72 (s, 1H), 6.88 (d, *J*=3.9 Hz, 1H), 7.07 (s, 1H), 7.28 (d, *J*=8.1 Hz, 2H), 7.31 (d, *J*=16.2 Hz, 1H), 7.58 (d, *J*=8.1 Hz, 2H), 7.64 (d, *J*=16.2 Hz, 1H).

HRMS *m/z* ($C_{23}H_{25}B_2F_2N_3O_3$) calculated: 451.2050 found: 450.1983 (M-H).

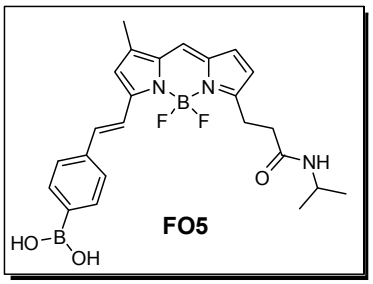

^{1}H NMR (300 MHz, $CDCl_3$+MeOD): 1.03 (d, *J*=6.6 Hz, 6H), 2.27 (s, 3H), 2.61 (t, *J*=7.5 Hz, 2H), 3.25 (t, *J*=7.5 Hz, 2H), 3.95 (m, 1H), 6.29 (d, *J*=3.9 Hz, 1H), 6.72 (s, 1H), 6.88 (d, *J*=3.9 Hz, 1H), 7.07 (s, 1H), 7.28 (d, *J*=8.1 Hz, 2H), 7.31 (d, *J*=16.2 Hz, 1H), 7.58 (d, *J*=8.1 Hz, 2H), 7.64 (d, *J*=16.2 Hz, 1H).

HRMS *m/z* ($C_{24}H_{27}B_2F_2N_3O_3$) calculated: 465.2207 found: 464.2160 (M-H).

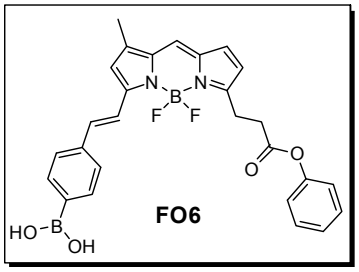

^{1}H NMR (300 MHz, $CDCl_3$+MeOD): 2.28 (s, 3H), 2.78 (t, *J*=7.5 Hz, 2H), 3.34 (t, *J*=7.5 Hz, 2H), 6.29 (d, *J*=3.9 Hz, 1H), 6.72 (s, 1H), 6.89 (d, *J*=3.9 Hz, 1H), 7.08 (s, 1H), 7.27 (d, *J*=8.1 Hz, 2H), 7.30 (d, *J*=16.2 Hz, 1H), 7.35 (s, 5H), 7.58 (d, *J*=8.1 Hz, 2H), 7.63 (d, *J*=16.2 Hz, 1H).

HRMS *m/z* ($C_{27}H_{24}B_2F_2N_2O_4$) calculated: 500.1890 found: 499.1808 (M-H).

3.4.3 Characterization of Glutathione Green

^{1}H NMR (300 MHz, $CDCl_3$): 7.40 (d, *J*=16.2 Hz, 1H), , 7.04 (d, *J*=16.2 Hz, 1H), 7.01 (s, 1H), 6.84 (d, *J*=3.9 Hz, 1H), 6.64 (s, 1H), 6.51 (d, *J*=3.3 Hz, 1H), 6.29 (d, *J*=3.9 Hz, 1H), 6.10 (d, *J*=3.3 Hz, 1H), 4.78 (s, 2H), 3.40 (t, *J*=7.5 Hz, 2H), 2.96 (t, *J*=7.5 Hz, 2H), 2.40 (s, 3H), 2.27 (s, 3H).

^{13}C NMR (75.5 MHz, $CDCl_3$): 11.3, 22.7, 23.8, 31.9, 74.1, 93.9, 109.2, 110.4, 114.9, 115.5, 116.2, 116.7, 121.2, 124.2, 125.6, 126.5, 129.5, 137.2, 144.6, 151.1, 155.9, 171.1.

ESI-MS *m/z* ($C_{22}H_{20}BCl_3F_2N_2O_3$) calculated: 514.1 found: 515.0 (M+H), 495.0 (M-F).

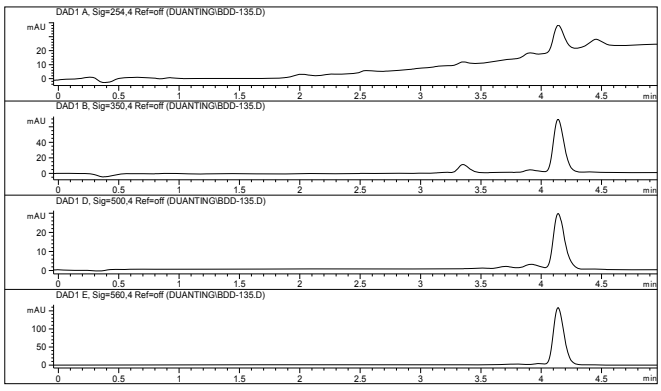

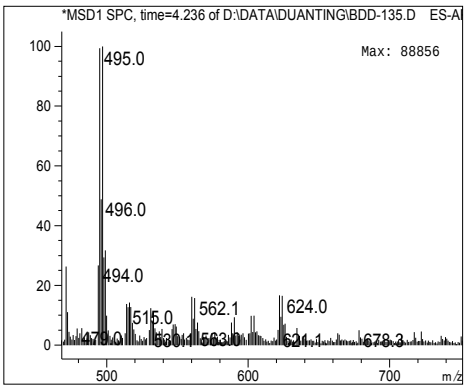

HPLC-MS characterization of **Glutahone Green**. (left) chromatograms (*descending order*) at 254 nm, 350 nm, 500 nm and 560 nm; (right) ESI-MS positive spectra. HPLC conditions: A: H_2O-HCOOH: 99.9:0.1. B: CH_3CN-HCOOH: 99.9:0.1; gradient 30% B to 100% B (5 min), isocratic 100% B (2.5 min). Reversephase Phenomenex C_{18} Luna column (4.6 x 50 mm^2) 3.5 µm, flow rate: 1.2 mL/min.

3.4.4 LCMS Characterization of Glutathione Green Incubated with GSH

(a) HPLC-MS characterization of **Glutathione Green**

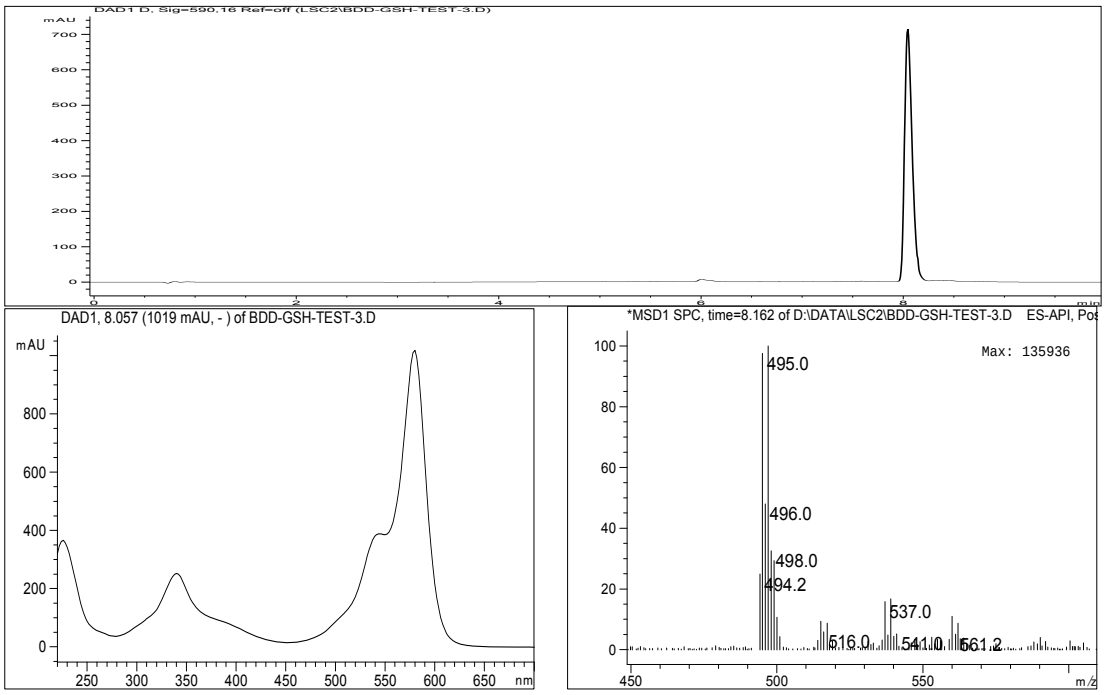

(b) HPLC-MS characterization of **Glutathione Green** with GSH in 50% DMSO 10 min.

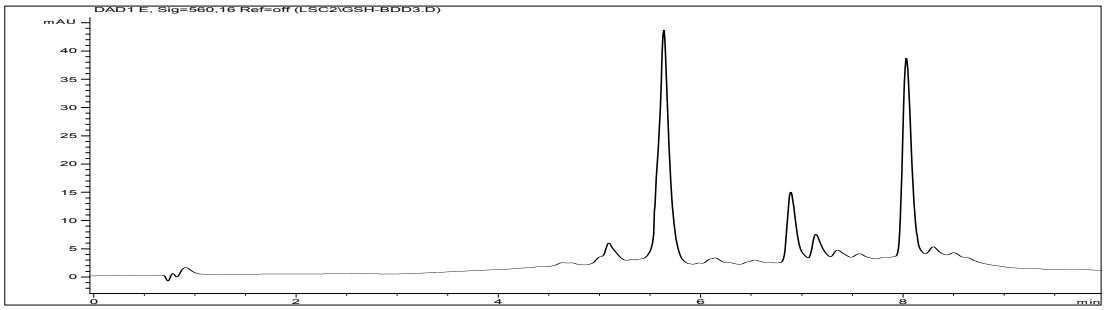

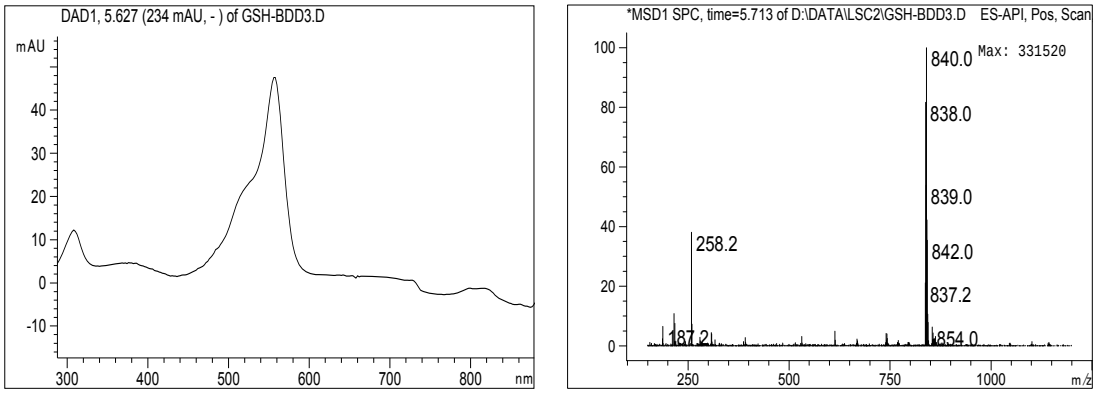

(c) HPLC-MS characterization of **Glutathione Green** with GSH in 50% DMSO for 2h.

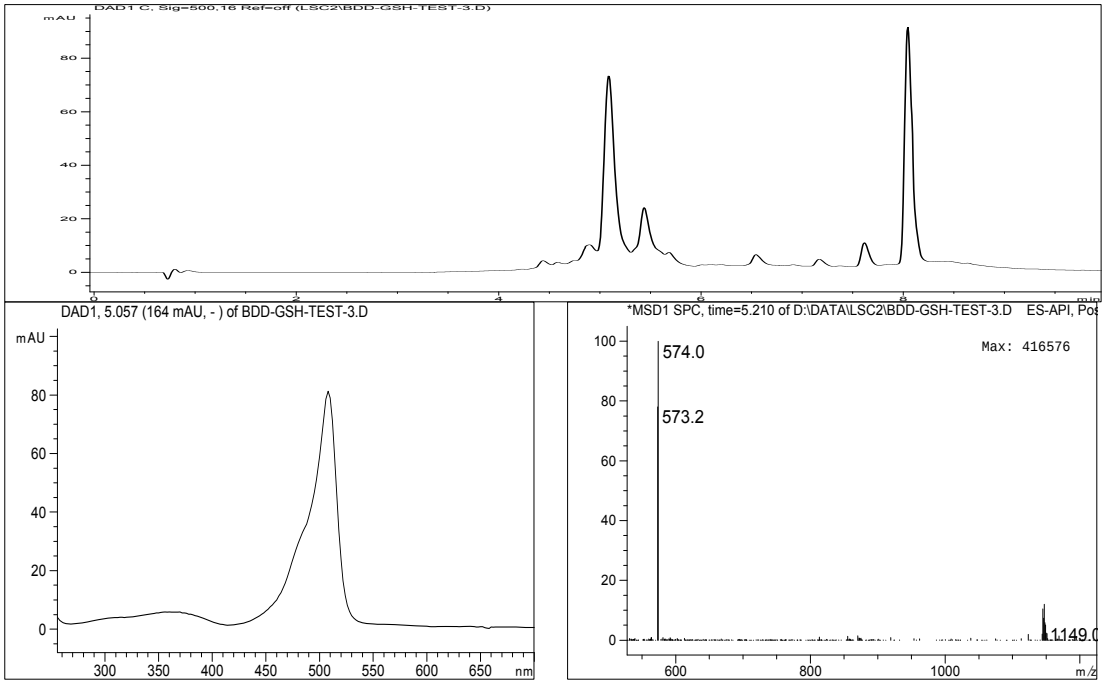

Glutathione Green (10 μM) incubated with GSH (5 mM) in 20 mM HEPES (pH= 7.4) with 50% DMSO. The resulting new peaks have a mass of 838.0 [M+H] (mono-substitution), 1145.0 [M+H] (di-substitution), 573.2 [(M+2H)/2] (di-substitution).

3.4.5 Cell Culture and Imaging Experiments

(1) Cell Culture:

3T3 fibroblast cells were grown on cell culture Petri dished in Dulbecco's Modified Eagle Medium (Sigma) with 10 % newborn calf serum and 5 mM L-glutamine and 5 mg/mL gentamicin. Cell cultures were maintained in an incubator at 37 ^{o}C with 5% CO_2.

Cells were cultured in glass bottom, 96-well black plates for imaging experiment, 24-36 hour prior to conduction of experiments.

(2) Imaging Experiments.

Cells were subjected for imaging with ImageXpress automated acquisition (Molecular Devices). FITC Long Pass (ex 450-490nm, em 515 nm) and Texas Red filters were used for fluorescence imaging applications. **GSH Green** stock solution in DMSO was added directly to the cell culture wells to reach the desired concentration. Total DMSO was lower than 1%. After incubation time, cells were imaged at ambient temperature in the medium without washing steps.

3.4.6 Characterization of Green Date

^{1}H NMR (300 MHz, $CDCl_3$+MeOD): 2.15 (s, 3H), 2.80 (t, *J*=7.5 Hz, 2H), 3.19 (t, *J*=7.5 Hz, 2H), 4.64 (s, 2H), 6.17 (d, *J*=3.9 Hz, 1H), 6.19 (t, *J*=2.1 Hz, 1H), 6.47 (d, *J*=2.1 Hz, 2H), 6.60 (s, 1H), 6.76 (d, *J*=3.9 Hz, 1H), 6.99 (s, 1H), 7.09 (d, *J*=16.2 Hz, 1H), 7.35 (d, *J*=16.2 Hz, 1H).

^{13}C NMR (75.5 MHz, $CDCl_3$+MeOD): 10.9, 23.4, 31.6, 73.6, 94.6, 104.2, 106.1, 107.9, 108.9, 116.3, 116.6, 118.1, 122.2, 127.2, 130.8, 137.7, 139.1, 155.2, 158.0, 158.5, 171.0

ESI-MS *m/z* ($C_{23}H_{20}BCl_3F_2N_2O_4$) calculated: 542.1 found: 523.1 (M-F).

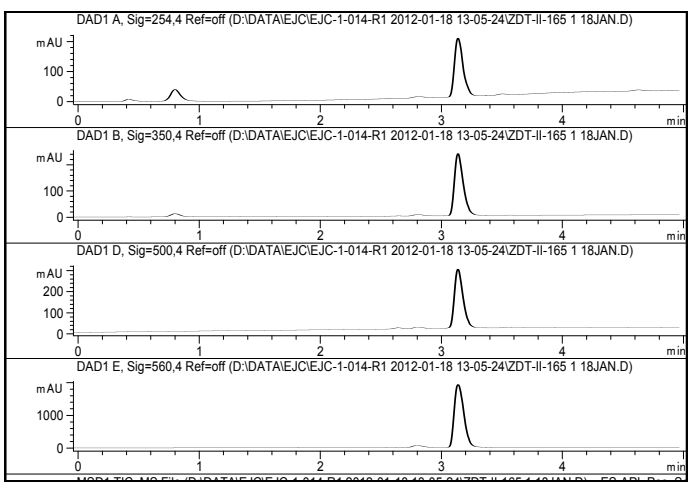

HPLC-MS characterization of **Green Date**. (left) chromatograms (*descending order*) at 254 nm, 350 nm, 500 nm and 560 nm; (right) ESI-MS positive spectra. HPLC conditions: A: H_2O-HCOOH: 99.9:0.1. B: CH_3CN-HCOOH: 99.9:0.1; gradient 30% B to 100% B (5 min), isocratic 100% B (2.5 min). Reversephase Phenomenex C_{18} Luna column (4.6 x 50 mm^2) 3.5 µm, flow rate: 1.2 mL/min.

3.4.7 Characterization of 5 Hit Compounds for GBL

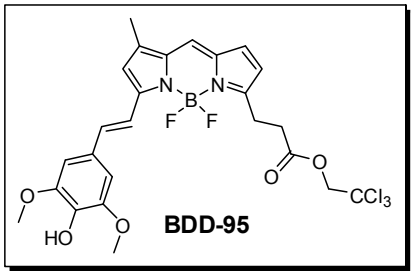

^{1}H NMR (300 MHz, $CDCl_3$): 2.29 (s, 3H), 2.96 (t, *J*=7.5 Hz, 2H), 3.40 (t, *J*=7.5 Hz, 2H), 3.97 (s, 6H), 4.78 (s, 2H), 6.30 (d, *J*=3.9 Hz, 1H), 6.70 (s, 1H), 6.83 (s, 2H), 6.86 (d, *J*=3.9 Hz, 1H), 7.04 (s, 1H), 7.26 (d, *J*=16.2 Hz, 1H), 7.44 (d, *J*=16.2 Hz, 1H).

ESI-MS *m/z* ($C_{25}H_{24}BCl_3F_2N_2O_5$) calculated: 586.1 found: 567.1 (M-F).

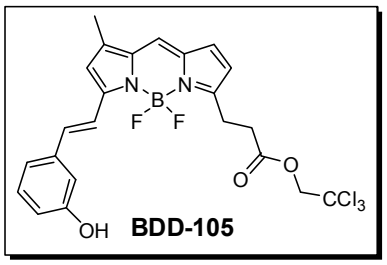

^{1}H NMR (300 MHz, $CDCl_3$+MeOD): 2.23 (s, 3H), 2.89 (t, *J*=7.5 Hz, 2H), 3.30 (t, *J*=7.5 Hz, 2H), 4.71 (s, 2H), 6.25 (d, *J*=3.9 Hz, 1H), 6.67 (s, 1H), 6.77 (d, *J*=7.8 Hz, 1H), 6.83 (d, *J*=3.9 Hz, 1H), 7.00 (d, J=7.8 Hz, 1H), 7.03 (s, 2H), 7.16 (dd, *J*=7.8 Hz, 7.8 Hz, 1H), 7.23 (d, *J*=16.2 Hz, 1H), 7.48 (d, *J*=16.2 Hz, 1H).

ESI-MS *m/z* ($C_{25}H_{24}BCl_3F_2N_2O_5$) calculated: 526.1 found: 507.0 (M-F).

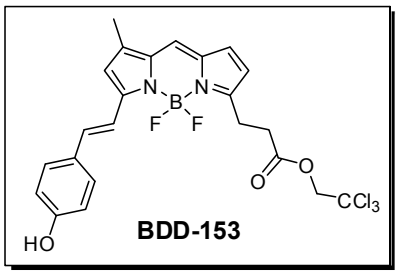

^{1}H NMR (300 MHz, $CDCl_3$): 2.29 (s, 3H), 2.97 (t, *J*=7.5 Hz, 2H), 3.40 (t, *J*=7.5 Hz, 2H), 4.78 (s, 2H), 6.30 (d, *J*=3.9 Hz, 1H), 6.70 (s, 1H), 6.84 (d, *J*=8.7 Hz, 2H), 6.86 (d, *J*=3.9 Hz, 1H), 7.04 (s, 1H), 7.28 (d, *J*=16.2 Hz, 1H), 7.47 (d, *J*=16.2 Hz, 1H) 7.48 (d, *J*=8.7 Hz, 2H).

ESI-MS *m/z* ($C_{25}H_{24}BCl_3F_2N_2O_5$) calculated: 526.1 found: 507.0 (M-F).

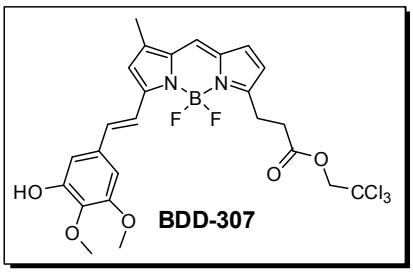

^{1}H NMR (300 MHz, $CDCl_3$): 2.28 (s, 3H), 2.97 (t, *J*=7.5 Hz, 2H), 3.40 (t, *J*=7.5 Hz, 2H), 3.93 (s, 3H), 3.94 (s, 3H), 4.78 (s, 2H), 6.31 (d, *J*=3.9 Hz, 1H), 6.70 (s, 1H), 6.72 (d, *J*=2.1 Hz, 1H), 6.86 (d, *J*=2.1 Hz, 1H), 6.87 (d, *J*=3.9 Hz, 1H), 7.05 (s, 1H), 7.20 (d, *J*=16.2 Hz, 1H), 7.48 (d, *J*=16.2 Hz, 1H).

ESI-MS *m/z* ($C_{25}H_{24}BCl_3F_2N_2O_5$) calculated: 586.1 found: 567.0 (M-F).

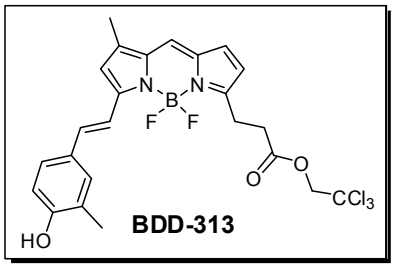

^{1}H NMR (300 MHz, $CDCl_3$+MeOD): 2.16 (s, 3H), 2.18 (s, 3H), 2.87 (t, *J*=7.5 Hz, 2H), 3.28 (t, *J*=7.5 Hz, 2H), 4.69 (s, 2H), 6.19 (d, *J*=3.9 Hz, 1H), 6.62 (s, 1H), 6.69 (d, *J*=8.4 Hz, 1H), 6.74 (d, *J*=3.9 Hz, 1H), 6.94 (s, 1H), 7.20 (d, *J*=16.2 Hz, 1H), 7.23 (d, *J*=8.4 Hz, 1H), 7.29 (s, 1H), 7.34 (d, *J*=16.2 Hz, 1H).

ESI-MS *m/z* ($C_{24}H_{22}BCl_3F_2N_2O_3$) calculated: 540.1 found: 521.1 (M-F).

3.4.8 Detailes of Real Beverages Used in Experiment for Green Date

1. Absolute Vodka Pear; Anus Sweeden
    - 20% Alcohol/vol (Diluted 1:1 with water)
    - Ingredients: Vodka, Pear Flavour
2. Arbor Mist Strawberry White Zinfandel; New York
    - 6% Alcohol/ Vol
    - Ingredients: White Zinfandel, water, high fructose corn syrup, natural flavours, carbon dioxide, citric acid, potassium sorbate, potassium bonzoate, potassium metabisulfite
3. Red wine First Cavicchioli 1928 Lambrusco; Umberto Cavicchioli & Figli
    - 7.5% Alcohol/ Vol
    - Ingredients: Grapes from Emilia area

4. Guinness Foreign Extra; St James' gate Dublin
    - 6.8% Alcohol/ Vol
    - Ingredients: Water, malt, barley, hops.
5. F&N Fruit Tree Fresh Apple Juice ; Singapore
    - Ingredients: Apple juice Concentrate, Pear juice concentrate, Aloe Vera juice, flavouring, Malic acid, Vitamin C, Permitted colouring, Preservatives.
6. Cocktail Singapore Sling; Singapore
    - 6.8% Alcohol/ Vol
    - Ingredients: Pomegaranate Fruit Juice, Pineapple Juice, Gin, Grenadine, Cherry Brandy, Cointreau, Benedictine, Angosutra Bitters.

3.4.9 NMR Spectrum

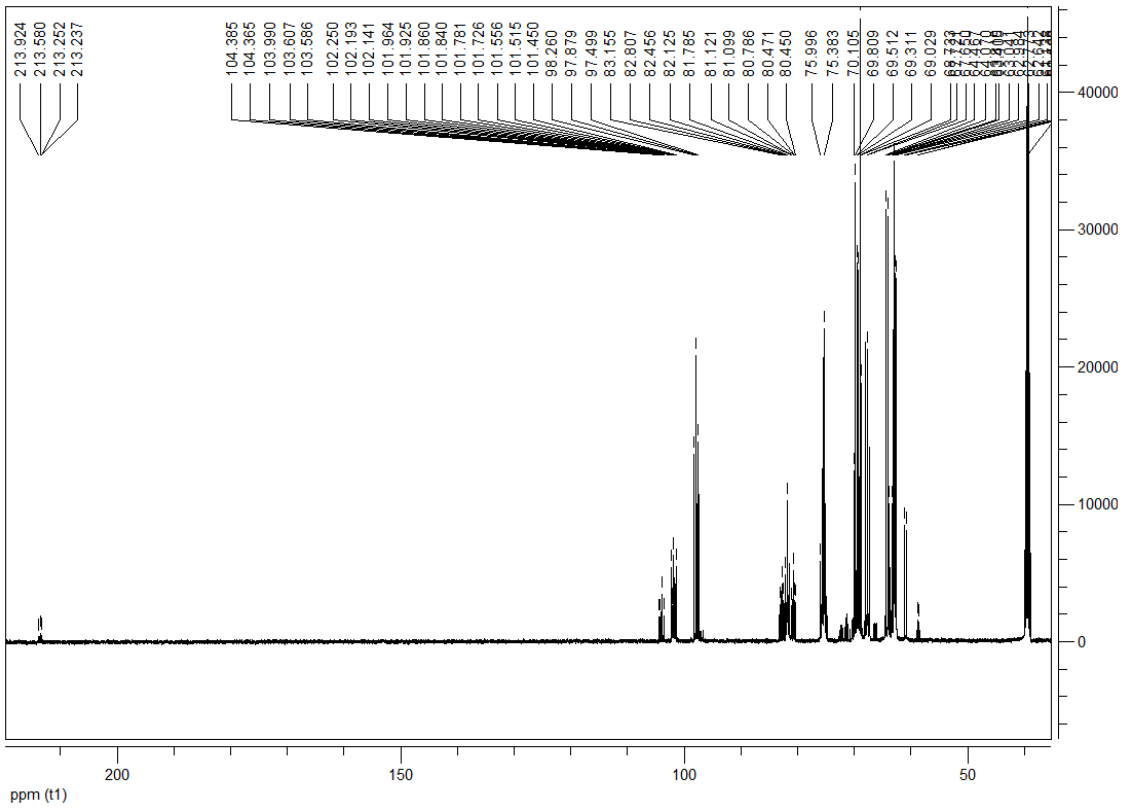

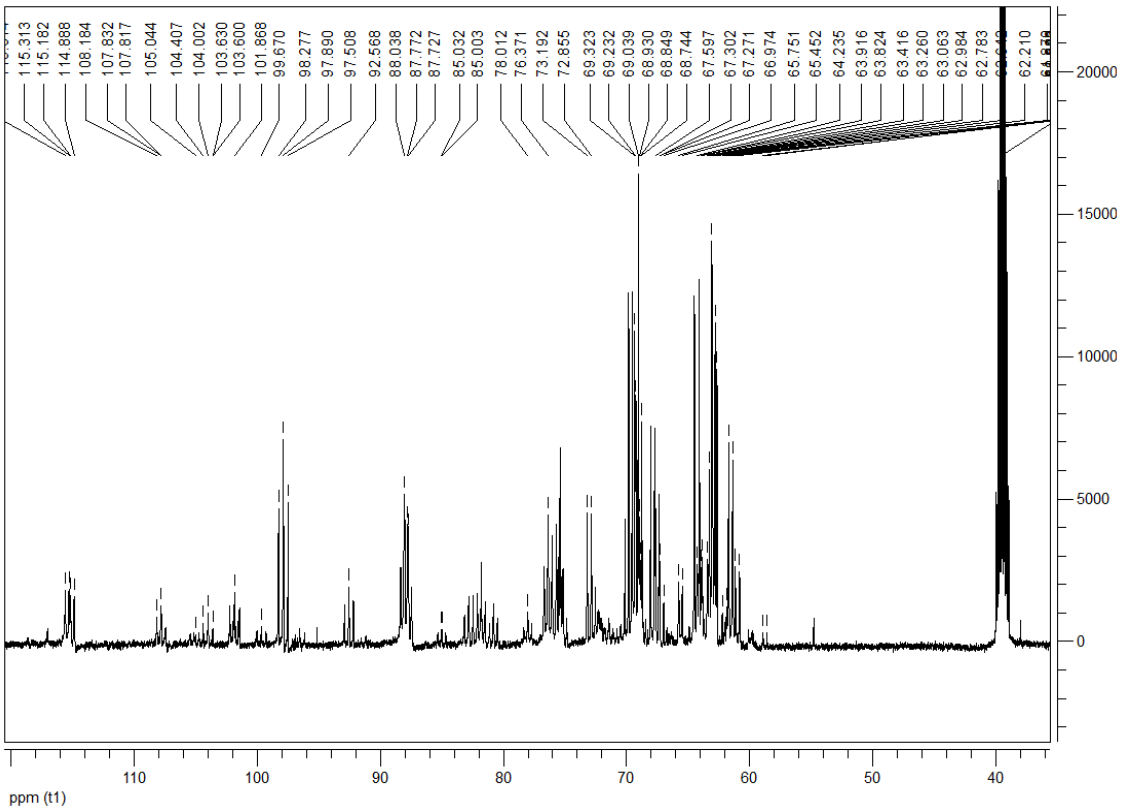

^{13}C NMR spectrum of (up) Fructose-$^{13}C_6$ (30 mM) in DMSO-d_6, and (down) Fructose-$^{13}C_6$ (30 mM) mixed with **Fructose Orange** (30 mM) in DMSO-d_6.

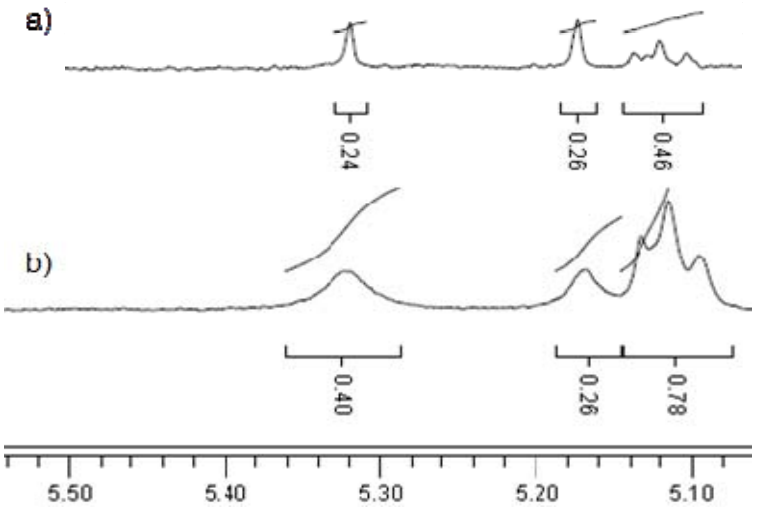

Expansion of the ^1H NMR spectra of solutions of (a) a mixture of **Fructose Orange** and fructose with 1:1 ratio (DMSO-$d_6$with 1% D_2O) and (b) fructose (DMSO-$d_6$with 1% D_2O). The assignments are δ (ppm): 5.32 (C2-OH, α-fructofuranose), 5.17 (C2-OH, β-fructopyranose), 5.11 (C3-OH, β-fructofuranose).

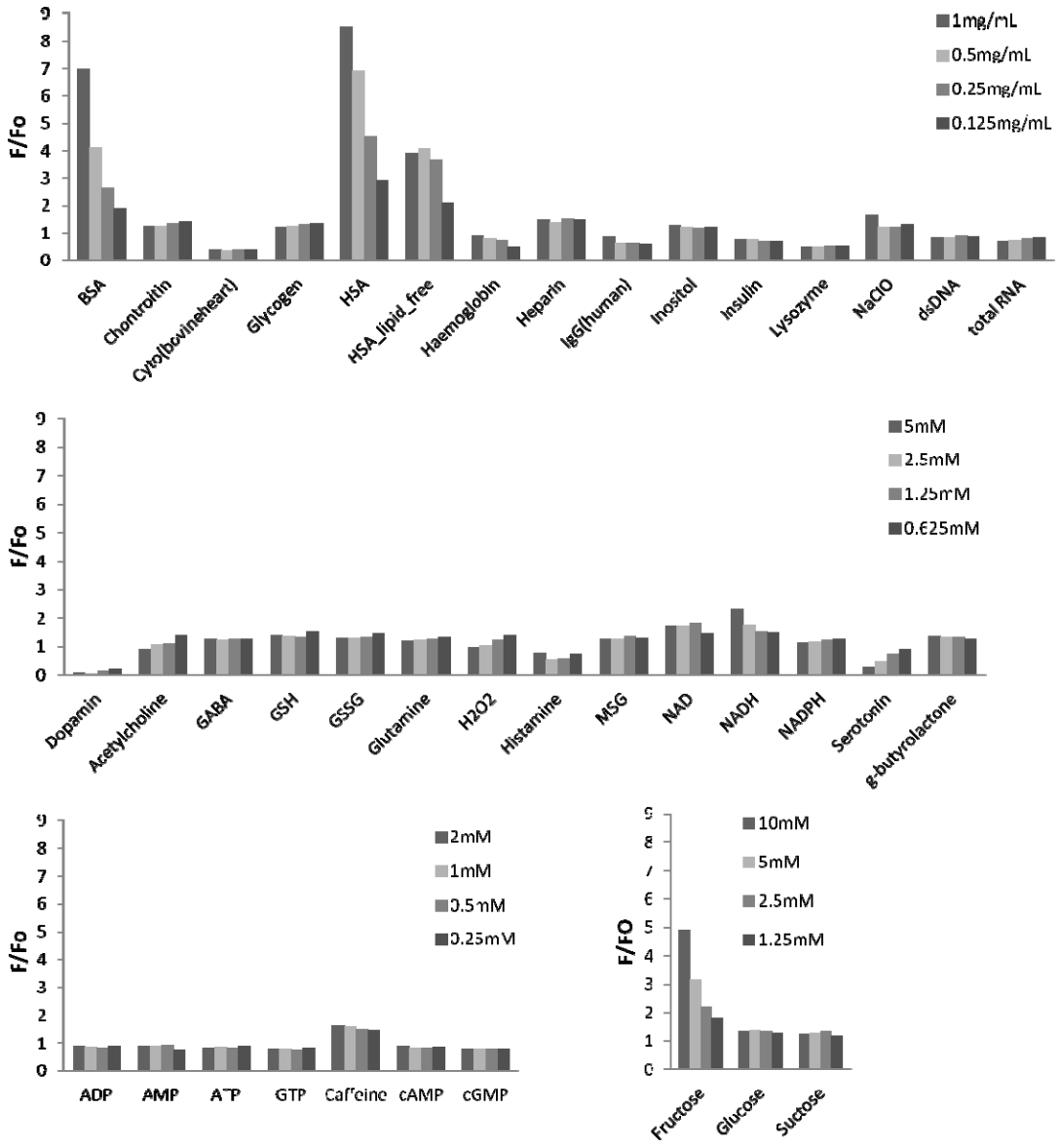

Fluorescence Response of **Fructose Orange** to Different Analytes

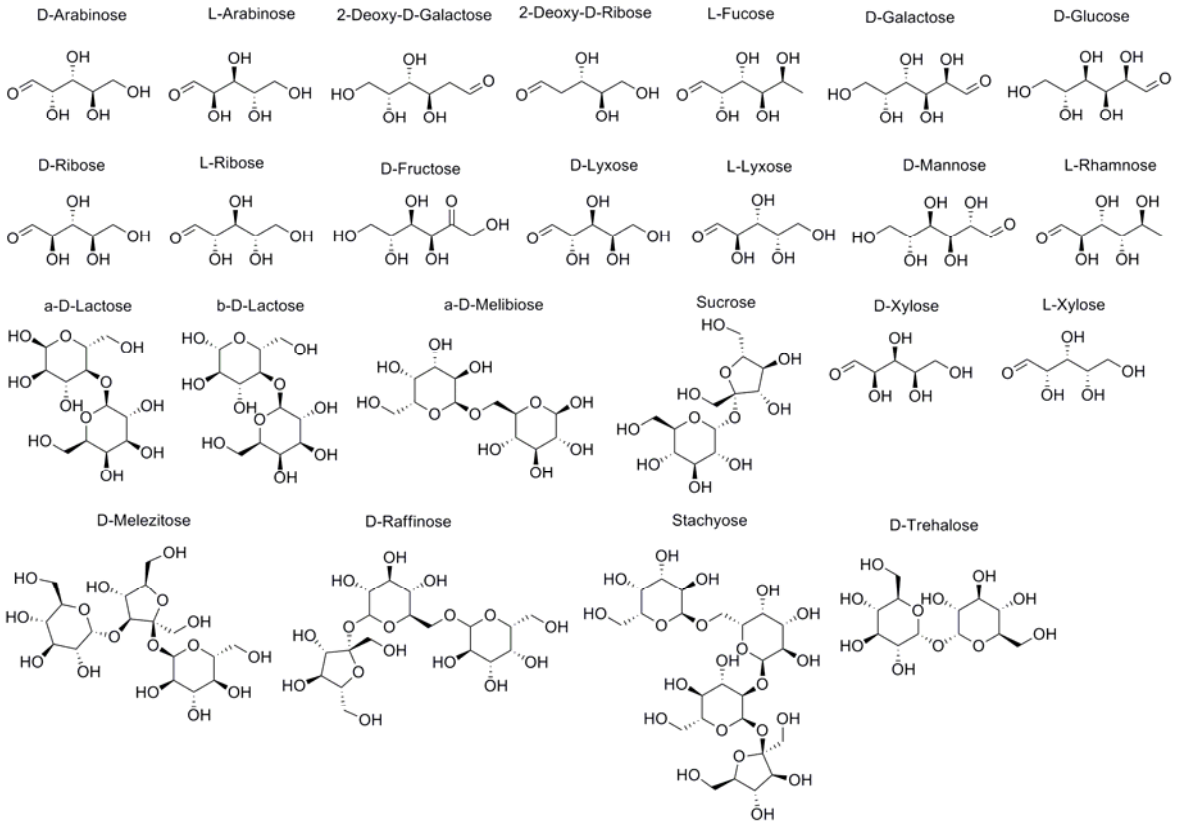

Chemical structures of 24 selected sugars

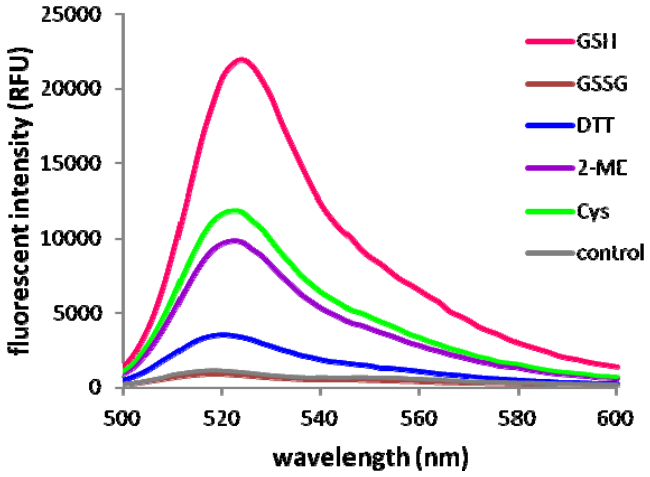

Fluorescence response of **GSH Green** (10 μM) incubated with different thiol compounds (5 mM) after 30 min in HEPES buffer (20 mM, pH=7.4) under excitation at 470 nm.

References

1. (a) Lee, J. S.; Baldridge, A.; Feng, S.; SiQiang, Y.; Kim, Y. K.; Tolbert, L. M.; Chang, Y. T., Fluorescence response profiling for small molecule sensors utilizing the green fluorescent protein chromophore and its derivatives. *ACS Comb. Sci.* **2011,** *13*, 32-38; (b) Lee, J. S.; Kim, H. K.; Feng, S.; Vendrell, M.; Chang, Y. T., Accelerating fluorescent sensor discovery: unbiased screening of a diversity-oriented BODIPY library. *Chem. Commun.* **2011,** *47*, 2339-2341.

2. Latulippe, M. E.; Skoog, S. M., Fructose malabsorption and intolerance: effects of fructose with and without simultaneous glucose ingestion. *Crit. Rev. Food Sci. Nutr.* **2011,** *51*, 583-592.

3. (a) Soleimani, M., Dietary fructose, salt absorption and hypertension in metabolic syndrome: towards a new paradigm. *Acta Physiol (Oxf)* **2011,** *201* (1), 55-62; (b) Levin, R. J., Digestion and absorption of carbohydrates--from molecules and membranes to humans. *Am. J. Clin. Nutr.* **1994,** *59*, 690S-698S.

4. Nuttall, F. Q.; Gannon, M. C., Plasma glucose and insulin response to macronutrients in nondiabetic and NIDDM subjects. *Diabetes Care* **1991,** *14*, 824-838.

5. Sievenpiper, J. L.; de Souza, R. J.; Mirrahimi, A.; Yu, M. E.; Carleton, A. J.; Beyene, J.; Chiavaroli, L.; Di Buono, M.; Jenkins, A. L.; Leiter, L. A.; Wolever, T. M.; Kendall, C. W.; Jenkins, D. J., Effect of fructose on body weight in controlled feeding trials: a systematic review and meta-analysis. *Ann Intern Med* **2012,** *156* (4), 291-304.

6. Soleimani, M., Dietary fructose, salt absorption and hypertension in metabolic syndrome: towards a new paradigm. *Acta Physiol.* **2011,** *201*, 55-62.

7. Samuel, V. T., Fructose induced lipogenesis: from sugar to fat to insulin resistance. *Trends Endocrinol. Metab.* **2011,** *22*, 60-65.

8. Yilmaz, Y., Review article: fructose in non-alcoholic fatty liver disease. *Aliment. Pharmacol. Ther.* **2012,** *35*, 1135-1144.

9. (a) Wulff, G., Selective Binding to Polymers Via Covalent Bonds. The Construction of Chiral Cavities as Specific Receptor Sites. *Pure Appl. Chem.* **1982,** *54*, 2093-2102; (b) James, T. D.; Samankumara Sandanayake, K. R. A.; Shinkai, S., Saccharide sensing with molecular receptors based on boronic acid. *Angew. Chem., Int. Ed.* **1996,** *35*, 1910-1922.

10. James, T. D.; Philips, M. D.; Shinkai, S., *Boronic Acids in Saccharide Recognition*. RSC Publishing: Cambridge, UK, 2006.

11. (a) Striegler, S., Selective carbohydrate recognition by synthetic receptors in aqueous solution. *Curr. Org. Chem.* **2003,** *7*, 81-102; (b) Wang, W.; Gao, X. M.; Wang, B. H., Boronic acid-based sensors. *Curr. Org. Chem.* **2002,** *6*, 1285-1317.

12. (a) Liu, Y.; Deng, C. M.; Tang, L.; Qin, A. J.; Hu, R. R.; Sun, J. Z.; Tang, B. Z., Specific Detection of D-Glucose by a Tetraphenylethene-Based Fluorescent Sensor. *J. Am.*

Chem. Soc. **2011,** *133*, 660-663; (b) Gao, X. M.; Zhang, Y. L.; Wang, B. H., New boronic acid fluorescent reporter compounds. 2. A naphthalene-based on-off sensor functional at physiological pH. *Org. Lett.* **2003,** *5*, 4615-4618; (c) Jiang, S.; Escobedo, J. O.; Kim, K. K.; Alpturk, O.; Samoei, G. K.; Fakayode, S. O.; Warner, I. M.; Rusin, O.; Strongin, R. M., Stereochemical and regiochemical trends in the selective detection of saccharides. *J. Am. Chem. Soc.* **2006,** *128*, 12221-12228.

13. Wang, Z.; Zhang, D. Q.; Zhu, D. B., A new saccharide sensor based on a tetrathiafulvalene-anthracene dyad with a boronic acid group. *J. Org. Chem.* **2005,** *70*, 5729-5732.

14. Norrild, J. C.; Eggert, H., Boronic acids as fructose sensors. Structure determination of the complexes involved using (1)J(CC) coupling constants. *J. Chem. Soc., Perkin Trans.* **1996,** *12*, 2583-2588.

15. Jaseja, M.; Perlin, A. S.; Dais, P., 2-Dimensional NMR spectral study of the tautomeric equilibria of D-fructose and related-compounds. *Magn. Reson. Chem.* **1990,** *28*, 283-289.

16. Wood, Z. A.; Schroder, E.; Robin Harris, J.; Poole, L. B., Structure, mechanism and regulation of peroxiredoxins. *Trends Biochem. Sci.* **2003,** *28*, 32-40.

17. Kizek, R.; Vacek, J.; Trnkova, L.; Jelen, F., Cyclic voltammetric study of the redox system of glutathione using the disulfide bond reductant tris(2-carboxyethyl)phosphine. *Bioelectrochemistry* **2004,** *63*, 19-24.

18. Townsend, D. M.; Tew, K. D.; Tapiero, H., The importance of glutathione in human disease. *Biomed. Pharmacother.* **2003,** *57*, 145-155.

19. (a) Kim, G.-J.; Lee, K.; Kwon, H.; Kim, H.-J., Ratiometric Fluorescence Imaging of Cellular Glutathione. *Org. Lett.* **2011,** *13*, 2799-2801; (b) Sreejith, S.; Divya, K. P.; Ajayaghosh, A., A Near-Infrared Squaraine Dye as a Latent Ratiometric Fluorophore for the Detection of Aminothiol Content in Blood Plasma. *Angew. Chem., Int. Ed.* **2008,** *47*, 7883-7887; (c) Long, L.; Lin, W.; Chen, B.; Gao, W.; Yuan, L., Construction of a FRET-based ratiometric fluorescent thiol probe. *Chem. Commun.* **2011,** *47*, 893; (d) Chen, X.; Ko, S.-K.; Kim, M. J.; Shin, I.; Yoon, J., A thiol-specific fluorescent probe and its application for bioimaging. *Chem. Commun.* **2010,** *46*, 2751; (e) Lin, W.; Yuan, L.; Cao, Z.; Feng, Y.; Long, L., A Sensitive and Selective Fluorescent Thiol Probe in Water Based on the Conjugate 1,4-Addition of Thiols to α,β-Unsaturated Ketones. *Chem. -Eur. J.* **2009,** *15*, 5096-5103; (f) Lim, C. S.; Masanta, G.; Kim, H. J.; Han, J. H.; Kim, H. M.; Cho, B. R., Ratiometric Detection of Mitochondrial Thiols with a Two-Photon Fluorescent Probe. *J. Am. Chem. Soc* **2011,** *133*, 11132-11135.

20. Hultberg, B.; Andersson, A.; Isaksson, A., Lipoic acid increases glutathione production and enhances the effect of mercury in human cell lines. *Toxicology* **2002,** *175*, 103-110.

21. Yellaturu, C. R.; Bhanoori, M.; Neeli, I.; Rao, G. N., N-Ethylmaleimide inhibits platelet-derived growth factor BB-stimulated Akt phosphorylation via activation of protein phosphatase 2A. *J. Biol. Chem.* **2002,** *277*, 40148-40155.

22. (a) Mel'chin, V. V.; Butin, A. V., Furan ring opening-furan ring closure: cascade rearrangement of novel 4-acetoxy-9-furylnaphtho[2,3-b]furans. *Tetrahedron Lett.* **2006,** *47*, 4117-4120; (b) Butin, A. V.; Smirnov, S. K.; Stroganova, T. A., Furan ring opening-indole ring closure: Synthesis of furo[2 ',3 ': 3,4]cyclohepta[1,2-b]indolium chlorides. *J. Heterocyclic Chem.* **2006,** *43*, 623-628; (c) Abaev, V. T.; Dmitriev, A. S.; Gutnov, A. V.; Podelyakin, S. A.; Butin, A. V., Furan ring opening - Isocoumarine ring closure: A recyclization reaction of 2-carboxyaryldifurylmethanes. *J. Heterocyclic Chem.* **2006,** *43*, 1195-1204; (d) Butin, A. V.; Stroganova, T. A.; Lodina, I. V.; Krapivin, G. D., Furyl(aryl)methanes and their derivatives, part 22. Furan ring opening-indole ring closure: a new modification of the Reissert reaction for indole synthesis. *Tetrahedron Lett.* **2001,** *42*, 2031-2033; (e) Eftax, D. S. P.; Dunlop, A. P., Hydrolysis of Simple Furans . Products of Secondary Condensation. *J. Org. Chem.* **1965,** *30*, 1317; (f) Butin, A. V.; Smirnov, S. K., Furan ring opening - indole ring closure: pseudooxidative furan ring opening in the synthesis of indoles. *Tetrahedron Lett.* **2005,** *46*, 8443-8445; (g) Butin, A. V.; Abaev, V. T.; Mel'chin, V. V.; Dmitriev, A. S., Furan ring opening-isochromene ring closure: a new approach to isochromene ring synthesis. *Tetrahedron Lett.* **2005,** *46*, 8439-8441.

23. Bishop, S. C.; Lerch, M.; McCord, B. R., Micellar electrokinetic chromatographic screening method for common sexual assault drugs administered in beverages. *Forensic. Sci. Int.* **2004,** *141*, 7-15.

24. Schwartz, R. H.; Milteer, R.; LeBeau, M. A., Drug-facilitated sexual assault ('date rape'). *South Med. J.* **2000,** *93*, 558-561.

25. Jansen, K. L.; Theron, L., Ecstasy (MDMA), methamphetamine, and date rape (drug-facilitated sexual assault): a consideration of the issues. *J. Psychoactive Drugs* **2006,** *38*, 1-12.

26. Nicholson, K. L.; Balster, R. L., GHB: a new and novel drug of abuse. *Drug Alcohol Depend.* **2001,** *63*, 1-22.

27. Mason, P. E.; Kerns, W. P., 2nd, Gamma hydroxybutyric acid (GHB) intoxication. *Acad. Emerg. Med.* **2002,** *9*, 730-739.

28. Lettieri, J.; Fung, H. L., Improved pharmacological activity via pro-drug modification: comparative pharmacokinetics of sodium gamma-hydroxybutyrate and gamma-butyrolactone. *Res. Commun. Chem. Pathol. Pharmacol.* **1978,** *22*, 107-118.

29. Shannon, M.; Quang, L. S., Gamma-hydroxybutyrate, gamma-butyrolactone, and 1,4-butanediol: a case report and review of the literature. *Pediatr. Emerg. Care* **2000,** *16*, 435-440.

30. Brailsford, A. D.; Cowan, D. A.; Kicman, A. T., Pharmacokinetic properties of gamma-hydroxybutyrate (GHB) in whole blood, serum, and urine. *J. Anal. Toxicol.* **2012,** *36*, 88-95.

31. Miotto, K.; Darakjian, J.; Basch, J.; Murray, S.; Zogg, J.; Rawson, R., Gamma-hydroxybutyric acid: patterns of use, effects and withdrawal. *Am. J. Addict.* **2001,** *10*, 232-241.

32. Palatini, P.; Tedeschi, L.; Frison, G.; Padrini, R.; Zordan, R.; Orlando, R.; Gallimberti, L.; Gessa, G. L.; Ferrara, S. D., Dose-dependent absorption and elimination of gamma-hydroxybutyric acid in healthy volunteers. *Eur. J. Clin. Pharmacol.* **1993,** *45*, 353-356.

33. Palmer, R. B., Gamma-butyrolactone and 1,4-butanediol: abused analogues of gamma-hydroxybutyrate. *Toxicol. Rev.* **2004,** *23*, 21-31.

34. (a) Roberts, D. M.; Smith, M. W.; Gopalakrishnan, M.; Whittaker, G.; Day, R. O., Extreme gamma-butyrolactone overdose with severe metabolic acidosis requiring hemodialysis. *Ann. Emerg. Med.* **2011,** *58*, 83-85; (b) Liechti, M. E.; Kunz, I.; Greminger, P.; Speich, R.; Kupferschmidt, H., Clinical features of gamma-hydroxybutyrate and gamma-butyrolactone toxicity and concomitant drug and alcohol use. *Drug Alcohol Depend.* **2006,** *81*, 323-326.

35. Meyers, J. E.; Almirall, J. R., A study of the effectiveness of commercially available drink test coasters for the detection of "date rape" drugs in beverages. *J. Anal. Toxicol.* **2004,** *28*, 685-688.

36. Bradley, M.; Lewis, A. Drug Detection Straw. Feb.17,2011, 2011.

37. Lesar, C. T.; Decatur, J.; Lukasiewicz, E.; Champeil, E., Report on the analysis of common beverages spiked with gamma-hydroxybutyric acid (GHB) and gamma-butyrolactone (GBL) using NMR and the PURGE solvent-suppression technique. *Forensic Sci. Int.* **2011,** *212*, e40-5.

Chapter 4 Discovery of a Neural Stem Cell Probe from Cell-Based Screening

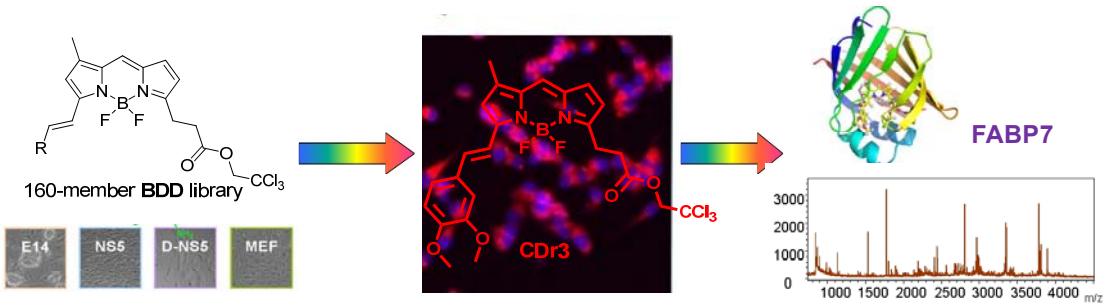

4.1 Introduction

The development of high-throughput imaging technique and analysis software in the past few years has significantly accelerated the discovery of fluorescent probes from cell-based screening.[1] Cell-based screening, originally mainly used to validate sensors developed from in vitro screening,[2] has now become a versatile tools to study signaling pathways, proteins' functions and cellular phenotypes.[3] Compared to in vitro screening, cell-based screening is more complicated and difficult to predict due to many unknown factors. This is one of the major obstacles to develop specific probes in rational design. On the other hand, the chance of probe discovery can be enhanced due to the unique characteristics of each specific cell type generated from combination of many in vivo factors. From this point of view, diversity-oriented fluorescent libraries contribute an excellent toolbox to discover cell-specific probe because screening is performed directly on the cells with diverse structural compounds.[4]

Development of cell-specific probes is of critical importance because the identification and separation of some interesting cell lines (e.g., stem cells) is still restricted to antibody, which may render the cells unsuitable for further applications. The screening assays performed on this purpose usually involve two or more cell lines which are in close proximity within a tissue or functionally related to each other. One of the examples is the development of α-cell probe reported by our group. 160 BODIPY compounds were screened on three cell lines (αTC1 and βTC6 cells, which secrete glucagon and insulin, respectively, and HeLa as a control cell line), and one compound (**BD-105**) was identified to show high fluorescence intensity only to αTC1 cells. **BD-105** was further confirmed to selectively respond to glucagon.[5] Stem cells have received much attention in the past decades due to their therapeutic importance. The lack of tool for their isolation drove our group to find specific stem cell probes. Screening was

performed on mouse embryonic stem cells (mESC) and mouse embryonic fibroblasts (MEF, generally used as feeder cells), and two compounds (CDy1 and CDb8) were identified as mESC-selective probes from a Rosamine library and a xanthone library, respectively.[6]

4.2 Results and Discussion

4.2.1 Neural Stem Cell

Neural stem cells (NSCs) generate the nervous system, promote neuronal plasticity and repair damage throughout life by self-renewing and differentiating into neurons and glia.[7] NSCs derived from pluripotent stem cells or isolated directly from brain tissue have great potential for therapeutic use in patients suffering from various neurological diseases[8] and also as a research tool for drug development[9]. The conventional method for the detection and characterization of NSCs depends on their behaviour in a defined culture medium such as neurosphere formation and immunodetection of marker molecules. These methods, however, are time-consuming and involve the use of xenogenic antibodies, which is limited to the expression of cell surface molecules and may render the cells unsuitable for further experimental and therapeutic applications. Therefore, there is a significant unmet need for more convenient and safer methods that detect living NSCs.

4.2.2 Discovery of a Neural Stem Cell Probe-CDr3

In order to discover neural stem cell probes, **BDD**, **BDL** and **BDA** compounds were screened in a set of cells at different stages of development into neural cells, including E14 mESC, E14-derived NSC (NS5), differentiated NS5 into astrocyte (D-NS5)[10] and MEF. Based on fluorescence intensity analyzed using image analysis software and visual confirmation, 3 **BDD** compounds (**BDD-36**, **BDD-62**, **BDD-359**) that stained NS5 more brightly than the other cell types were selected for further validation. These

primary hits were tested for different incubation times ranging from 1 hour to 48 hours and then validated by flow cytometry to identify **BDD-62** as the final hit that stains NS5 most selectively and brightly, and dubbed as CDr3 (compound of designation red 3; $\lambda_{ex}/\lambda_{em}$ = 579/604 nm; extinction coefficient = 1.02 × 10^6 M^{-1} cm^{-1}; quantum yield = 0.77, Chapter 2) (Figure 4.1). The half maximal staining intensity measured after 1 h incubation with NS5 was obtained at 0.39 μM (Figure 4.2). We further assessed the specificity of CDr3 in mixed brain cell cultures prepared from postnatal mouse brains. With the appearance of numerous morphologically distinct populations of cells after 2 weeks *in vitro* culture, they were stained with CDr3 and Hoechst33342. While the NS5 treated with the same procedure in parallel were brightly stained by CDr3, the various

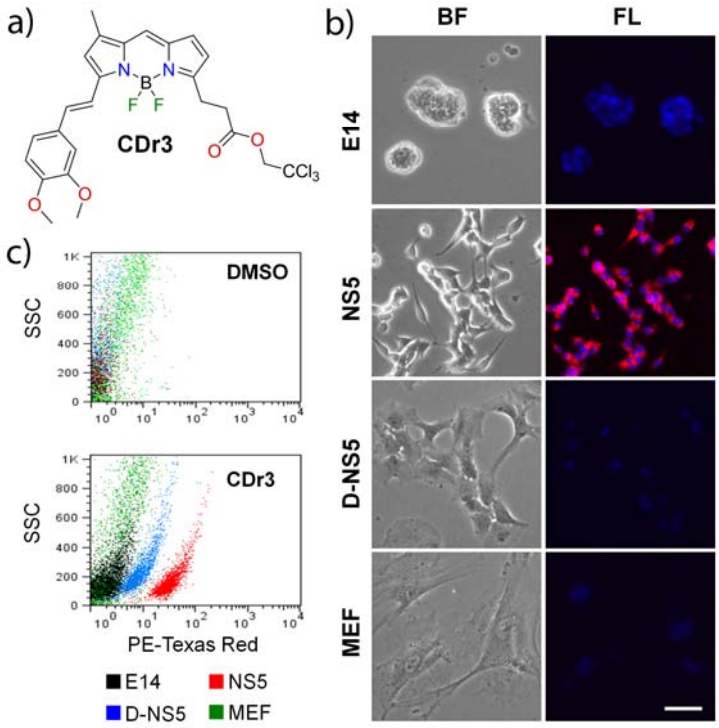

Figure 4.1 Selective Staining of NS5 by CDr3. (a) Chemical structure of CDr3. (b) Nuclei of E14, NS5, D-NS5 and MEF were visualized by Hoechst 33342; but only NS5 was selectively stained by CDr3. (left) phase contrast bright-field (BF) images; (right) fluorescent (FL) images obtained with DAPI and Texas Red filter set. Scale bar, 50 μm. (c) Flow cytometry dot plot images of E14, NS5, D-NS5 and MEF incubated with CDr3. DMSO was added for unstained control cells. The images of each type of cells were overlaid.

types of primary cells were not stained. The primary cells thereafter were immunostained to demonstrate the presence of neurons, astrocytes and other types of cells (Figure 4.3).

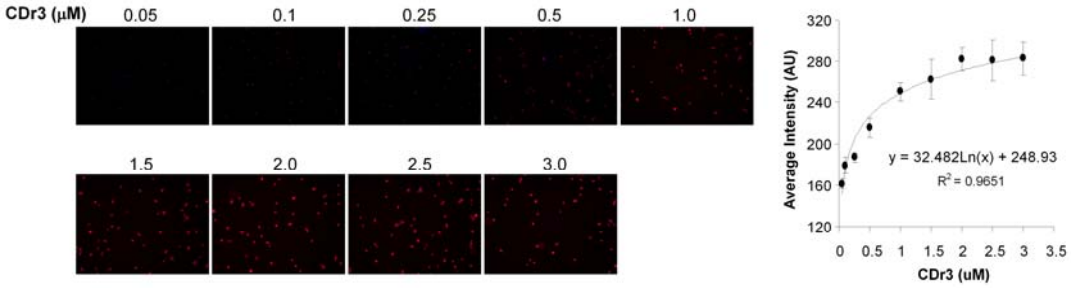

Figure 4.2 Image-based CDr3 Titration for Neural Stem Cell Staining. NS5 cells were incubated with different concentrations of CDr3 for 1 hour and washed out with fresh medium for 1 hour. The cell images (12 images for each concentration) were acquired using ImageXpress Micro™and the fluorescence intensity of the stained cells was analyzed using MetaXpress® image processing software. Mean ± SD values of the average intensity were used to draw the graph with a trend line added. The half maximal staining intensity was obtained at 0.39 μM.

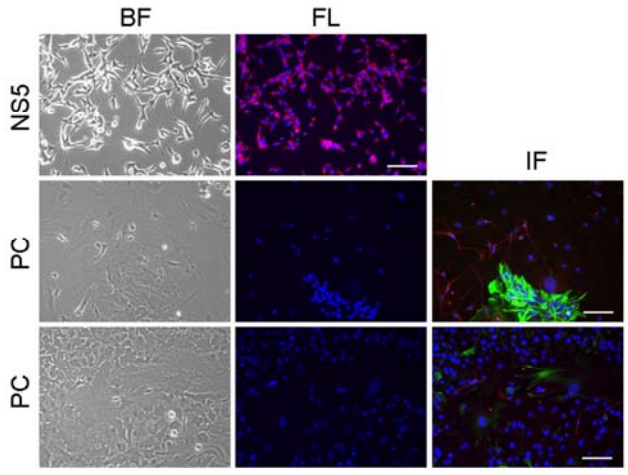

Figure 4.3 Differentiated primary neural cell staining: Mixed primary mouse brain cells (PC) cultured for 2 weeks *in vitro* were incubated with CDr3 and Hoechst33342. The images of live cells are shown in phase contrast bright-field (BF) and fluorescence (FL) panels. The images of the same cells were acquired after immunofluorescence staining (IF) with antibodies to neuron-specific class III β-tubulin (Tuj1, red) and astrocyte-specific glial fibrillary acidic protein (GFAP, green). Scale bar, 100 μm.

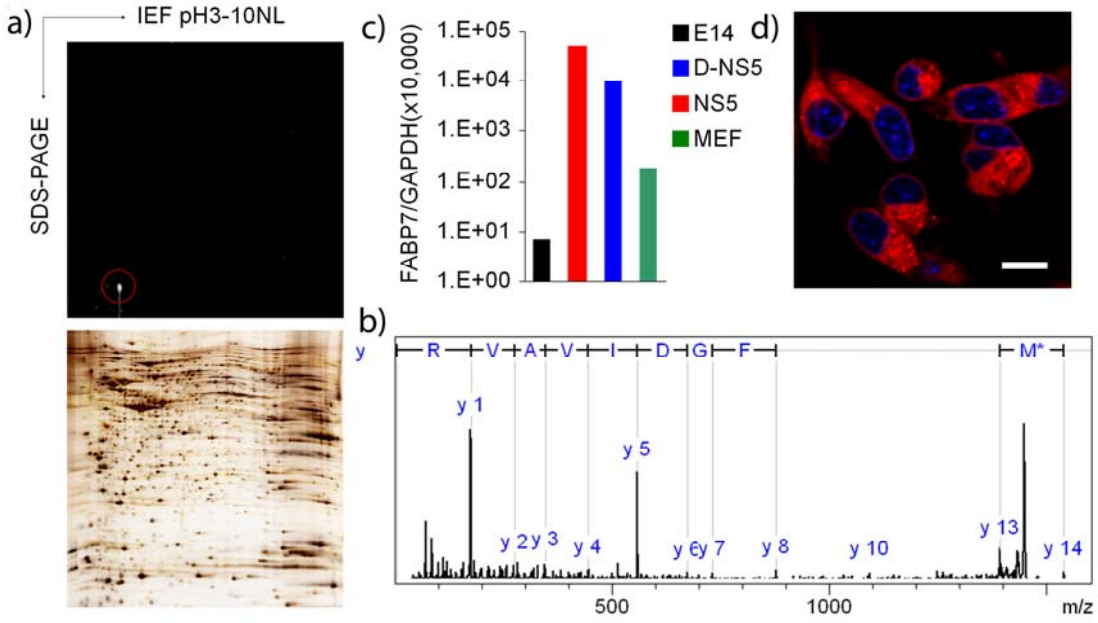

Figure 4.4 Identification of CDr3 Binding Protein. (a) Protein lysate of CDr3-stained NS5 was separated by 2DE. The major fluorescent spot was marked with a red circle (Upper). Many silver-stained protein spots were detected in a duplicate gel (Lower). (b) MS/MS fragment ion analysis of tryptic peptide (MVVTLTFGDIVAVR) indicated FABP7 as a binding target of CDr3. Only the main y-series of ion fragmentation was labelled in the spectrum. M* indicates oxidation at methionine residue. (c) Quantitative real time RT-PCR analysis of FABP7 mRNA in E14, NS5, D-NS5 and MEF. Relative expression level of FABP7 to GAPDH is depicted. (d) The confocal fluorescence image acquired on a Nikon A1R microscope using a 100× objective lens shows cytoplasmic localization of CDr3. Nuclei were stained with Hoechst 33342. Scale bar, 10 μm.

4.2.3 Target of CDr3-FABP7

When we subjected CDr3-stained NS5 cell lysate to 2-dimensional SDS-PAGE for a fluorescence scan, a major spot of around15 kDa was detected (Figure 4.4). MALDI-TOF/TOF MS and MS/MS analysis allowed us to identify the stained protein as fatty acid binding protein 7 (FABP7) (Figure 4.4b). NS5 used in the current study as a NSC is known to express FABP7.[10] We examined the mRNA expression level of FABP7 by real time RT-PCR and observed that its level in NS5 is 282-fold and 7,220-fold higher than in MEF and E14, respectively, and decreases five-fold upon 3 days differentiation

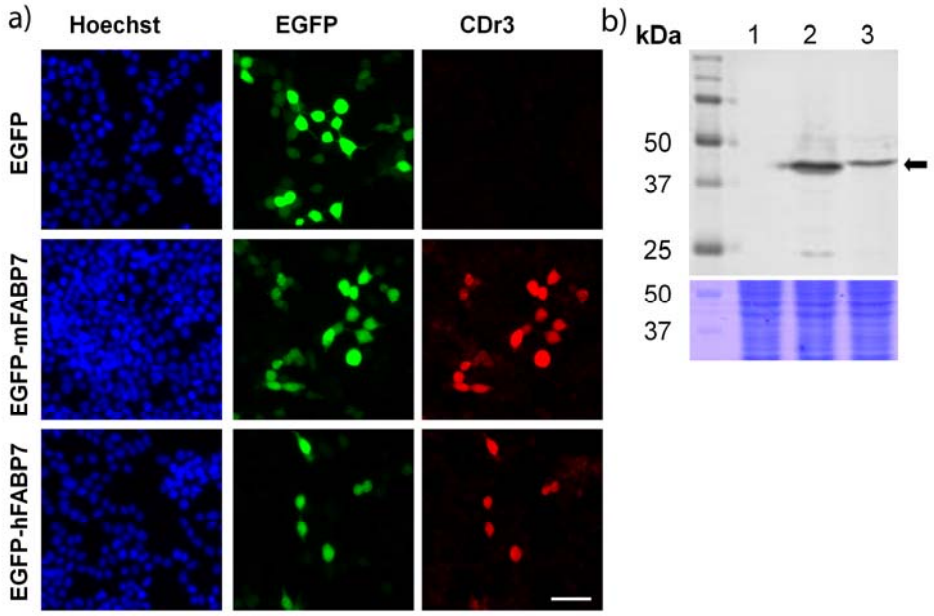

Figure 4.5 CDr3 Binding to Recombinant FABP7. (a) Fluorescence signals from EGFP and CDr3 overlap only in the cells expressing either mouse FABP7 or human FABP7 fused to EGFP. The fluorescence images were acquired on a Nikon Ti microscope using DAPI, FITC and Texas Red filter sets. Scale bar, 50 μm. (b) Western Blot Detection of FABP7 in Transfected HEK293 Cell Lysates. The EGFP (27 kDa) + FABP7 (14 kDa) fusion protein of 41 kDa was detected by an anti-mouse FABP7 antibody, which cross reacts to human protein. Lane1, pEGFP-N1 vector only; lane2, pEGFP-mouse FABP7; lane3, pEGFP-human FABP7. A duplicate gel was stained with Coomassie blue (Lower).

into astrocyte (Figure 4.4c). High magnification confocal microscopy showed that CDr3 stains the cytoplasm of NS5 where the majority of FABP7 localizes (Figure 4.4d). To confirm that FABP7 is the specific binding target of CDr3, we cloned both human and mouse FABP7 genes and fused them to EGFP constructs for expression in HEK293 cells. It was observed that the signals of EGFP and CDr3 overlap in the cells that express either human or mouse FABP7 fused to EGFP (Figure 4.5a). Transient expression of the transfected FABP7 genes was verified by the detection of FABP7 by Western blotting (Figure 4.5b). Then we subcloned the human FABP7 gene into a bacterial expression vector with His-tag to facilitate purification of recombinant FABP7

for in vitro binding assays. The interaction between CDr3 and FABP7 in vitro was demonstrated by FABP7 concentration-dependent increase of CDr3 fluorescence with a dissociation constant of 9.6 μM (Figure 4.6a). Job plot analysis showed a symmetrical shape of fluorescence increase with a maximum at a CDr3 ratio of 0.5 implying that the binding stoichiometry between CDr3 and FABP7 is 1:1 (Figure 4.6b).

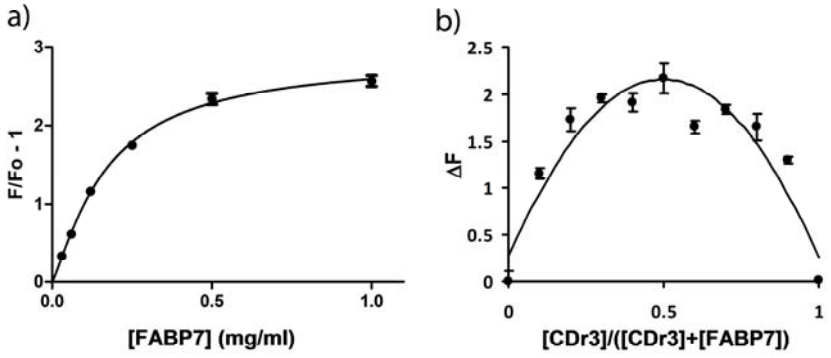

Figure 4.6 Binding Kinetics. (a) The best fitting curve was obtained by plotting CDr3 fluorescence fold increase (F/F_0-1) against various concentrations of human FABP7. The data are presented as mean ± SD of 3 independent experiments. (B) Job plot for the complexation of CDr3 with human FABP7. ΔF [fluorescence fold increase × CDr3 ratio] was plotted against CDr3 ratio in a total concentration of 20 μM.

4.2.4 Validation of CDr3

4.2.4.1 CDr3 Does Not Affect Normal Proliferation of NSCs

We determined whether CDr3 affects NSC proliferation by culturing NS5 and mouse neurospheres in the presence of CDr3. Total numbers of NS5 cells grown for 6 h and 48 h and the percentage of BrdU positive cells pulse-labeled in the CDr3-containing medium were not different from those of cells grown in DMSO-only containing medium which was used as a vehicle control (Figure 4.7a and b). In accordance with the result of experiment with NS5 cells, the number and size of neurospheres generated in the presence of CDr3 were not different from control (Figure 4.7c).

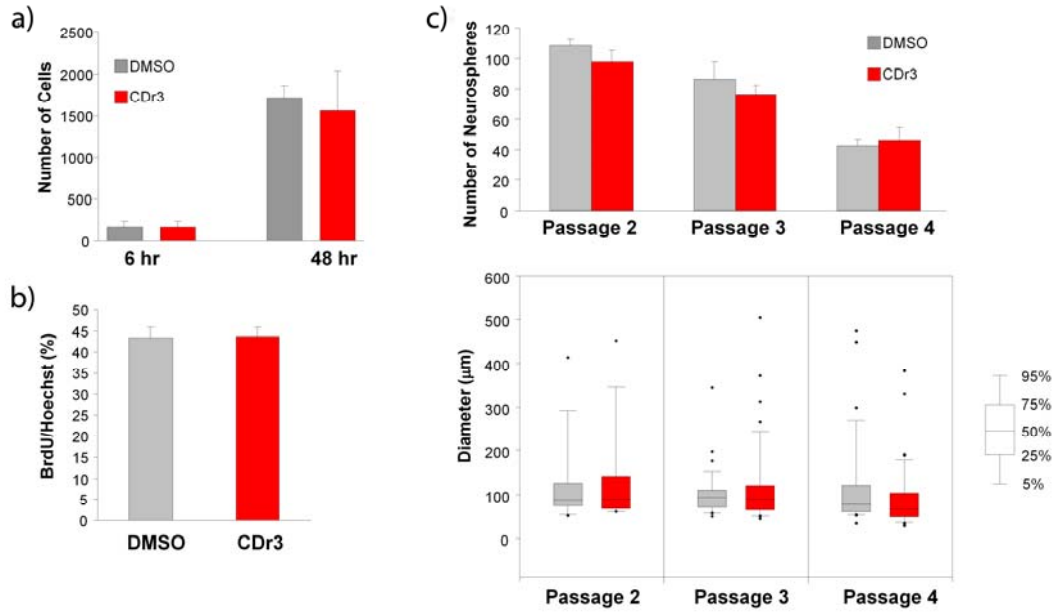

Figure 4.7 Cell Proliferation Assay. (a) NS5 cells were cultured in the presence of 1 μM CDr3 or 0.1% DMSO for 6 h and 48 h. Nuclei were stained with Hoechst33342 for image acquisition and cell counting using MetaXpress® image processing software (n = 32). (b) NS5 cells pulse-labeled with BrdU for 6 h were visualized using FITC-conjugated anti-BrdU antibody. The percentage of BrdU-positive cells was determined by counting both Hoechst33342 stained nuclei and BrdU positive nuclei in the same images (n = 8). (C) Same numbers of neurosphere cells were serially plated and cultured in six well plates with 1 μM CDr3 or 0.1% DMSO. The numbers (Upper) and sizes (Lower) of neurospheres were determined every 6 d (n = 3).

4.2.4.2 CDr3 Identifies Both Mouse and Human NSCs

Having found that CDr3 stains not only mouse FABP7 expressing HEK293 cells, but also human FABP7 expressing cells, we attempted to test CDr3 on ReNcell VM human NSC line (Millipore) derived from the ventral mesencephalon region of human fetal brain tissue. This cell line, immortalized by retroviral transduction with the v-myc gene, is karyotypically normal, expresses high level of NSC marker nestin and can differentiate into neuron, astrocyte and oligodendrocyte.[11] However, it has not previously been known to express FABP7. We first examined the expression level of FABP7 by real time RT-PCR and found a 540-fold higher level of FABP7 mRNA in

ReNcell VM than in H1 human ESC. This expression was dramatically (20-fold) down-regulated upon differentiation into neurons (Figure 4.8a).Western blot analysis demonstrated a similar observation in protein expression levels with a strong FABP7 band at 14 kDa detected in ReNcell VM lysate while no FABP7 was detected in the lysates of H1 and ReNcell VM-derived neurons (Figure 4.8b). In accordance with the Western blot data, ReNcell VM were strongly stained by FABP7 antibody while H1 and ReNcell VM-derived neurons were not stained (Figure 4.8c). We then incubated the 3 types of cells with CDr3 to determine whether live ReNcell VM could be distinguished by the compound among others. As expected from the FABP7 expression analysis data, CDr3 selectively stained ReNcell VM in live cell cultures (Figure 4.8d).

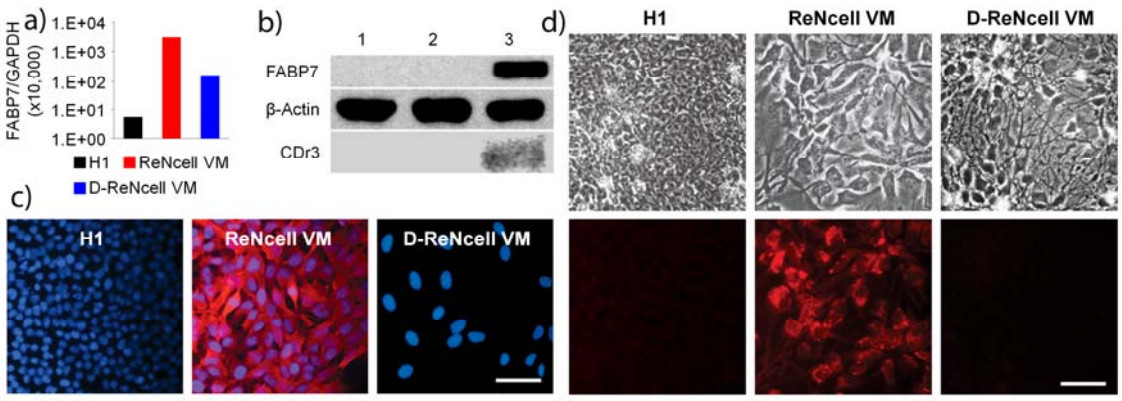

Figure 4.8 Selective Staining of Human NSC ReNcell VM by CDr3. (a) Real-time PCR analysis of FABP7 expression in H1, ReNcell VM and ReNcell VM-differentiated neurons. Relative expression level of FABP7 to GAPDH is depicted. (b) Strong signal of FABP7 protein (14 kDa) was detected by Western blotting in ReNcell VM (lane 3) lysate, while it was not detectable in the lysates of H1 (lane 1) and ReNcell VM-differentiated neurons (lane 2). β-Actin (42 kDa) staining demonstrates consistent loading across sample lanes. Fluorescence scan showed CDr3-labelled FABP7 in the lysate of ReNcell VM (lane 3) incubated with CDr3. (c) Immunocytochemistry of FABP7 in H1, ReNcell VM and ReNcell VM-differentiated neurons (D-ReNcell VM). Only ReNcell VM was brightly stained by FABP7 antibody. Scale bar, 50 μm. (d) H1, ReNcell VM and ReNcell VM-differentiated neurons were incubated with CDr3. Fluorescence signal was detected only in ReNcell VM. Upper: phase contrast bright field image; Lower: fluorescence image. Scale bar, 50 μm.

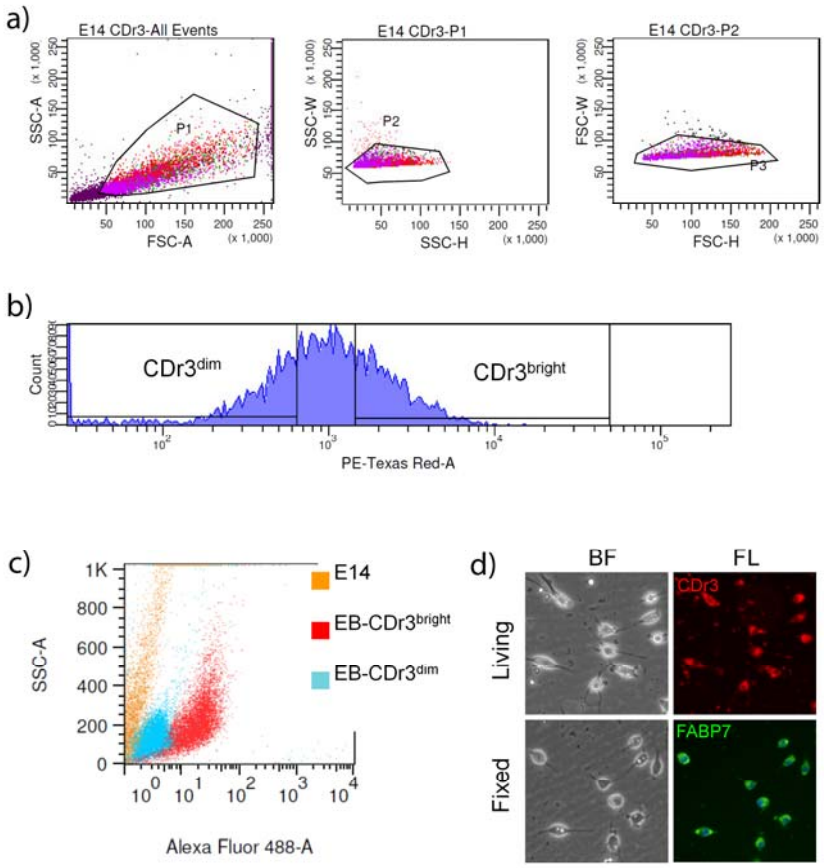

Figure 4.9 Differentiated mESC FACS Using CDr3. (a) The CDr3-stained embryoid body cells were gated by forward and side scattering to remove cell debris. (b) The gated cells were separated into CDr3^{bright} and CDr3^{dim} populations. (c) The expression of FABP7 in CDr3^{bright} and CDr3^{dim} cells was determined by immunocytochemistry followed by flow cytometry. (d) CDr3^{bright} cells were cultured and stained by CDr3. Subsequent fixation and immunofluorescence staining with anti-FABP7 antibody showed the expression of FABP7 in the CDr3^{bright} cells. Scale bar, 50 μm.

4.2.5 Application of CDr3

Next, we were interested to test whether CDr3 can be used for the isolation of living NSCs from heterogeneous population of cells generated by a random differentiation of ESCs. We induced differentiation of mESC to embryoid bodies using retinoic acid.[12] CDr3^{bright} and CDr3^{dim} cells were separately collected by FACS from embryoid body cells stained with CDr3 (Figure 4.9a and b). Each cell population was stained with FABP7 antibody and analyzed by flow cytometry. The overlay plot showed two well-

separated clusters, which can be interpreted as the cells isolated by CDr3 from the heterogeneous embryoid body cells were FABP7 expressing cells (Figure 4.9c). The expression of FABP7 in cultured CDr3^{bright} cells was confirmed by immunocytochemistry (Figure 4.9d).

4.3 Conclusion

Identification of specific types of living cells mostly depends on cell surface marker detection using antibodies. However, certain types of cells can be distinguished more specifically by intracellular markers which can be detected by small molecules but not by antibodies. The binding target of CDr3, FABP7, is a well-known intracellular marker of NSC. Among the currently known nine mammalian FABPs that play pivotal roles in transporting and trafficking of lipids in various tissues, FABP7 is particularly expressed in the central nervous system.[13] Its expression is pronounced during the fetal period contributing to the normal development of neuroepithelial cells and knocking down the gene's expression causes premature differentiation of neuroepithelial cells to neurons.[14] The FABP7 knockout mouse exhibits enhanced anxiety, reduced prepulse inhibition and shorter startle latency. A dramatic decrease in the number of neural stem cells is also observed in the hippocampal dentate gyrus of the mouse.[15] The neuroepithelial cells differentiate into radial glial cells which further differentiate to neurons and glias in the developing and also adult brains.[16] During in vitro neural differentiation of ESC, FABP7 expressing radial glial cells are the common NSCs which intermediate between ESC and fully differentiated neurons and glias.[17] In the presence of CDr3 in the medium, the ESC, differentiated NSC and primary brain cells are stained, but not as bright as NS5 or ReNcell VM. By rinsing, CDr3 is rapidly washed out from these cells, while NS5 and ReNcell remain brightly stained. These observations imply that CDr3

passively diffuses into the cell to be retained by binding to FABP7 rendering CDr3 specific for FABP7-expressing NSCs.

Even though the majority of the drugs on the market that promote or inhibit specific biological processes are small molecules, the application of fluorescent small molecules in biomedical science has been restricted to the production of fluorescently labelled biomolecules and cell type-independent organelle staining dyes. By generating DOFL and screening them in different types of cells including NSC, we developed a NSC-specific fluorescent chemical compound CDr3. DOFL approach has many advantages for developing cell type specific imaging probes and identifying their binding targets. Our data presented here successfully exemplifies the practical use of DOFL in the development of cell type specific small molecular weight imaging probes and identification of their cellular binding targets. As the first NSC-specific fluorescent chemical compound that binds specifically to an intracellular NSC marker FABP7, CDr3 will be a valuable tool in the study and applications of NSCs.

4.4 Experimental Section

4.4.1 DOFL High Throughput/Content Screening

DOFL compounds were diluted from 1mM DMSO stock solutions with the culture medium to make final concentration of 0.5 μM or 1.0 μM. The four different types of cells plated side by side on 384-well plates were incubated with the compounds overnight at 37 °C. The nuclei were stained with Hoechst33342 the next day before image acquisition. The fluorescence cell images of two regions per well were acquired using ImageXpress Micro™ cellular imaging system (Molecular Device) with 10× objective lens and the intensity was analyzed by MetaXpress® image processing software (Molecular Device). The hit compounds which stained NS5 more brightly than

other cells were selected based on the intensity data and manual screening of the raw images.

4.4.2 Characterization of CDr3

^{1}H NMR (300 MHz, $CDCl_3$): 2.28 (s, 3H), 2.96 (t, *J*=7.5 Hz, 2H), 3.40 (t, *J*=7.5 Hz, 2H), 3.92 (s, 3H), 3.97 (s, 3H), 4.78 (s, 2H), 6.30 (d, *J*=3.9 Hz, 1H), 6.71 (s, 1H), 6.85 (d, *J*=3.9 Hz, 1H), 6.86 (d, *J*=8.1 Hz, 1H), 7.03 (s, 1H), 7.12 (d, *J*=1.8 Hz, 1H), 7.16 (dd, *J*=1.8, 8.4 Hz, 1H), 7.29 (d, *J*=16.2 Hz, 1H), 7.48 (d, *J*=16.2 Hz, 1H).

^{13}C NMR (75.5 MHz, $CDCl_3$): 11.3, 23.7, 29.6, 33.0, 55.9, 56.0, 56.1, 74.0, 94.9, 109.6, 110.4, 111.1, 116.2, 116.6, 121.6, 122.1, 122.2, 126.7, 129.2, 133.6, 139.1, 143.0, 149.3, 150.8, 171.0.

ESI-MS *m/z*($C_{25}H_{24}BCl_3F_2N_2O_4$) calculated: 571.1 $(M+H)^+$, found: 551.1 (M-F).

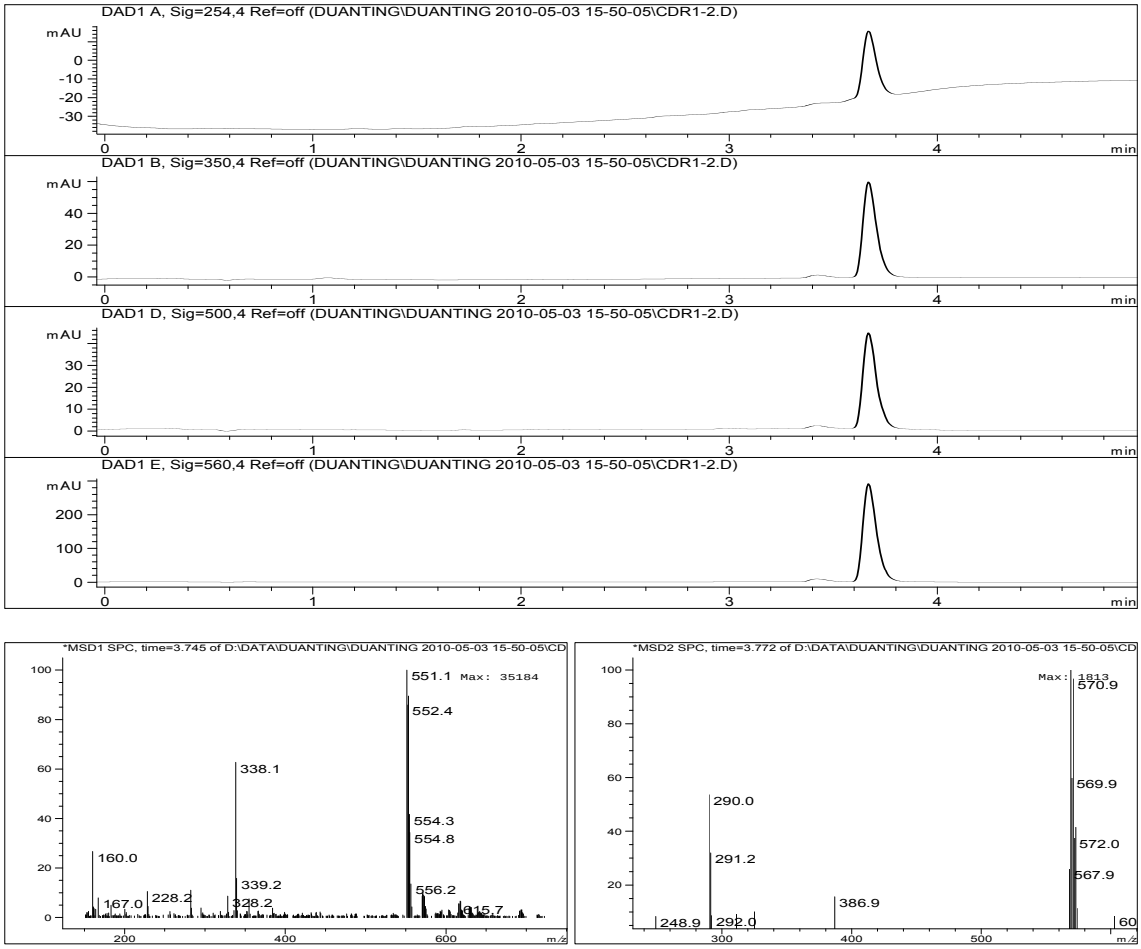

HPLC-MS characterization of CDr3. (Upper) HPLC chromatogram: (descending order)

at 254, 350, 500 and 560 nm. HPLC conditions: A: H2O-HCOOH: 99.9:0.1. B: ACN-HCOOH: 99.9:0.1; gradient 30% B to 100% B (5 min), isocratic 100% B (2.5 min). Reverse-phase Agilent C18 Zorbax column (2.1 × 30 mm^2) 3.5 µm, flow rate: 1 ml⁄min; (Lower) ESI-MS spectra: (left) ESI-positive, (right) ESI-negative spectra.

4.4.3 Living Cell Staining

The cells were incubated with 0.5 µM CDr3 in Opti-MEM GlutaMAXTM for 1 h and, if necessary, subsequently with 2 µM of Hoechst 33342 for 15 min at 37 °C. Then the cells were rinsed in maintenance medium for 1 h and the medium was replaced again with fresh medium before image acquisition. The bright field and fluorescence images were acquired on ECLIPSE Ti microscope (Nikon Instruments Inc.) or A1R confocal microscope (Nikon Instruments Inc.) using NIS Elements 3.10 software or on Axio Observer D1 using AxioVision v 4.8 software (Carl Zeiss Inc.).

4.4.4 MALDI-TOF/TOF MS and MS/MS Analyses

Tryptic peptide of 0.6 µl was spotted onto Prespotted AnchorChip target plate (Bruker Daltonics Inc.) according to manufacturer's protocol. The peptide mass fingerprint and selected peptide MS/MS fragment ion analysis were carried out on UltraFlex III TOF-TOF (Bruker Daltonics Inc.) with the compass 1.2 software package including FlexControl 3.0 and FlexAnalysis 3.0 with PAC peptide calibration standards. The peak lists of MS and MS/MS were submitted to in-house Mascot server (http://phenyx.bii.a-star.edu.sg/search_form_select.html) through BioTools 3.2 with the database of SwissProt 57.8 (509,019 sequences) allowing peptide mass tolerance of 100 ppm and 0.5 Da with maximum one missed cleavage and considering variable modifications of carbamidomethyl at cysteine (C) and oxidation at methionine (M).

4.4.5 Cell Culture and Differentiation

E14 was maintained on gelatin-coated dishes in high-glucose DMEM supplemented with 10% FBS, 2 mM L-glutamine, 100 U⁄ml penicillin, 100 μg⁄ml streptomycin, 0.1 mM nonessential amino acids, 0.1% β-mercaptoethanol and 100 U⁄ml leukemia inhibitory factor (LIF, Chemicon). For differentiation, the cells were detached from their culture plates using 0.25% trypsin with 1 mM EDTA solution (Invitrogen) and subcultured in nonadherent bacteria culture dishes in the E14 media but without LIF. Subsequently, 90% of the media was changed on a daily basis for a total of 4 d and then retinoic acid (Sigma) was added to the final concentration of 1 μM. On day six, the embryoid bodies were harvested and dissociated in 0.05% trypsin with 0.2 mM EDTA solution for 3 min at 37 °C to obtain a single cell suspension. NS5 was maintained in Euromed-N medium supplemented with 100 μg⁄ml Apo-transferin (Sigma), 5.2 ng⁄ml Sodium Selenite (Sigma), 19.8 ng⁄ml progesterone (Sigma), 16 μg⁄ml Putrescine (Sigma), 25 μg⁄ml insulin (Sigma), 50.25 μg⁄ml BSA (Gibco), 10 ng⁄ml bFGF (Gibco), 10 ng⁄ml EGF (Gibco), 100 U⁄ml penicillin (Gibco), 100 μg⁄ml streptomycin (Gibco) and 2 mM L-glutamine (Gibco). For differentiation of NS5 into astrocyte, the medium was changed to NS5 maintenance medium containing 5% FBS but without bFGF and EGF. MEF was maintained in the same media as used for E14 but without LIF. H1 was maintained in a feeder-free condition on matrigel-coated dishes in MEFconditioned medium containing Knockout DMEM/10% serum replacement (Gibco), 0.1 mM MEM nonessential amino acids (Gibco), 1 mM L-glutamine (Gibco), 0.1 mM β-mercaptoethanol (Gibco), 8% plasmanate (NUH pharmacy), 12 ng⁄ml LIF, and 10 ng⁄ml (bFGF; Gibco). ReNcell VM (Millipore #SCC008) was maintained on laminin-coated dishes in ReNcell NSC Maintenance Medium (Millipore #SCM005) containing 20 ng⁄ml bFGF and 20 ng⁄ml EGF. For neural differentiation, ReNcell VM were seeded on

PLO/Laminin-coated plates and cultured for up to 3 wks in media comprising a 1:1 mix of N2-DMEM/F12 and B27-Neurobasal media supplemented with 0.1mMMEM nonessential amino acids and 1 mM L-glutamine, all obtained from Gibco/Invitrogen. For mixed primary brain cell culture, the brains of neonatal mouse pups were cut into small pieces and digested in 0.25% trypsin with 1 mMEDTA solution (Invitrogen) for 30 min at 37 °C before neutralization with FBS. After washing with PBS by centrifugation and resuspension, the tissues were triturated using a 10-ml pipette fitted with 1-ml tip and the suspension was filtered through a strainer with 40 μm nylon mesh. The obtained single cells were plated on 35 mm cell culture dishes in OptiMEM- Gluta-MAX™containing 10% FBS. Unattached cells and cell debris were removed the next day by replacing the medium. One half of the medium was replaced twice a week thereafter.

4.4.6 Flow Cytometry and FACS

The cells incubated with CDr3 were harvested by trypsin treatment, washed and resuspended in PBS. The fluorescence intensity of the cells was measured on a flow cytometry (BD™ LSR II) or collected using FACS Aria™ (BD). The data were analyzed and processed using FlowJo 7 software.

4.4.7 Neurosphere Preparation and Assay

E14.5 fetal mouse brains were trypsinized in 0.25% trypsin with 1 mM EDTA solution (Invitrogen) for 30 mins at 37 °C before neutralization with FBS. The tissues were triturated sequentially with a 10-ml pipette followed by a 1-ml blue tip and a 0.2-ml yellow tip attached to the 10-ml pipette until the cell suspension flows through smoothly. The tissue suspension was washed three times with PBS by repeated resuspension and centrifugation and filtered through a 40-μm strainer. The obtained single cells were plated in a DMEM/F12 medium containing 10 ng⁄ml bFGF, 20 ng⁄ml

EGF and B27 without vitamin A (Invitrogen) to grow forming spheres. For cytotoxicity assay, dissociated neurosphere cells were plated in triplicate in six well culture plates at a density of 3,000 cells per well and cultured in the presence of 1 μM CDr3 or 0.1% DMSO for 6 d. After 6 d, the number of neurospheres was counted manually and the images were taken using a microscope (Eclipse Ti, Nikon) for measuring the sizes neurospheres. For serial assay, the neurospheres were further passaged in the same condition as they were generated in. All animal experiment procedures were performed in accordance with a protocol approved by the Institutional Animal Care and Use Committee.

4.4.8 Cell Proliferation Assay

NS5 were seeded into 96 well plates (Greiner) at a density of 1000 cells⁄well. The next day, DMSO and 1 mM DMSO stock of CDr3 was added into 32 wells for each to be diluted to 0.1% and 1 uM, respectively. At 6 h and 48 h time points, 1 ug⁄ml of Hoechst 33342 was added and incubated for 15 min for image acquisition using an ImageXpress Micro™ and MetaXpress Imaging system (Molecular Devices). Hoeschst33342 and CDr3 signals were detected via DAPI and Texas red filters, respectively, and the images of a total of four areas were captured per well. Multi wavelength scoring analysis was then run to quantify the number of cells based on Hoechst33342-stained nuclei image. Due to the uneven distribution of the cells in wells, the highest and lowest values from the obtained four values from a well were excluded for statistical analysis using ANOVA. For the quantification of pulse-labeled cells with BrdU, the cells were stained using FITC conjugated anti-BrdU antibody (BD Pharmingen™) according to the manufacturer's instruction. Total numbers of Hoechst 33342-stained and BrdU-labeled nuclei were counted by image based analysis using ImageJ-ITCN software.

4.4.9 Two-Dimensional Gel Electrophoresis

CDr3-stained NS5 pellet was lysed in a lysis buffer (40mMTrizma, 7MUrea, 2Mthiourea and 4% CHAPS) premixed with 10 μl/ml Protease Inhibitor Cocktail (EDTA free, GE healthcare), 50 μg/ml DNase I and 50 μg/ml RNase A (Roche). The cell extract was homogenized by vortexing followed by ultrasonication on ice for 10 s, and incubated for 30 min at room temperature. The supernatant was collected after centrifugation at 20,000 × g for 45 min at 10 °C and protein concentration was determined by Bradford protein assay reagent (Bio-Rad). Isoelectric focusing (IEF) was performed using PROTEAN IEF Cell (Bio-Rad) with an 18 = −cm ReadyStrip pH 3–10 NL (Bio-Rad). The sample of 1 mg protein was diluted into 340 μl of rehydration buffer (7 M urea, 2 M thiourea, 4% CHAPS, 20 mM DTT, 0.5% IPG buffer pH 3–10 NL (GE healthcare), and loaded to each IPG strip with passive rehydration and focused for 60,000 Vhrs at 20 °C. The IEF strips were reduced in equilibration buffer I (50 mM Tris-HCl, pH 8.8, 6 M urea, 30% glycerol, 2% SDS, 2% DTT) at room temperature for 10 min and alkylated with SDS-PAGE Equilibration Buffer II (50 mM Tris-HCl, pH 8.8, 6 M urea, 30% glycerol, 2% SDS, 2.5% iodoacetamide, and a trace of bromophenol blue) at room temperature for an additional 10 min. The equilibrated IEF strips were embedded in 0.5% low melting temperature agarose in 1× Tris-glycine-SDS buffer on top of a second dimension SDS-PAGE (12%) gel. After electrophoresis for 5 h at 30 mA, the 2D fluorescence image of gels was acquired using a Typhoon 9400 scanner (GE healthcares) at excitation/emission wavelengths of 532 nm⁄610 nm with PMT at 500 v and a duplicate gel was stained using PlusOne™ Silver Staining Kit (GE healthcare) according to the manufacturer's protocol. The fluorescent labelled protein spots were directly excised from the gel for in-gel trypsin digestion and peptide extraction as described previously.[18]

4.4.10 Immunostaining

The primary and secondary antibodies used for Western blotting and immuocytochemistry in this study are as follows: anti- beta-Actin (1:2;000, Santa Cruz), beta-Tubulin III (1:500, Sigma), B-FABP (1:1;000, Santa Cruz), BLBP (1:1;000, abcam), GFAP (1:1;000 DAKO), mouse IgG-Alexa Fluor 488 (1:300, Invitrogen), mouse IgG-HRP (1:4;000, Santa Cruz), rabbit IgG-Cy3 (1:300, Zymed) and rabbit IgG-HRP (1:4;000, Santa Cruz).

4.4.11 Real Time RT-PCR

Total RNA was extracted from the cells using RNeasy Mini Kit (QIAGEN Inc.) according to the manufacturer's instruction. For the RNA samples isolated from E14, NS5, D-NS5 and MEF, the reverse transcription and amplification were carried out using Power SYBR® Green RNA-to-CT™ 1-Step Kit (Applied Biosystem) on a StepOne™ Real-Time PCR System (Applied Biosystem). For the RNA samples from H1, ReNcell VM and ReNcell-differentiated neurons, cDNA was synthesized from the total RNA using the High Capacity Cdna Archive kit (Applied Biosystems) according to the manufacturer's instructions. PCR reaction was conducted using Power SYBR ® Green PCR Master Mix (Applied Biosystems) on an ABI Prism 7900 machine. The relative mRNA levels of the genes of interest were normalized and compared to that of GAPDH using Q-gene relative expression software tool. The primer sequences (5′ to 3′) used in this study are as follow:

Mouse FABP7	Forward	ccagctgggagaagagtttg
Mouse FABP7	Reverse	tttctttgccatcccacttc
Mouse GAPDH	Forward	aagggctcatgaccacagtc
Mouse GAPDH	Reverse	ggatgcagggatgatgttct
Human FABP7	Forward	acagaaatgggatggcaaag
Human FABP7	Reverse	ctcatagtggcgaacagcaa
Human GAPDH	Forward	cagcctcaagatcatcagca
Human GAPDH	Reverse	tgtggtcatgagtccttcca

4.4.12 Mouse and Human FABP7 Gene Cloning

cDNAs of mouse and human FABP7 genes were synthesized by RT-PCR from the total RNAs extracted from NS5 and U251 human neuroblastoma cell line, respectively. The primer sequences (5′ to 3′) for FABP7 ORF cloning are as follows:

Mouse FABP7	Forward	cccagatctccaccatggtagatgctttctgcgcaacct
Mouse FABP7	Reverse	cccaagctttgccttttcataacagcgaacagca
Human FABP7	Forward	cccagatctccaccatggtggaggctttctgtgctacct
Human FABP7	Reverse	cccaagctttgccttctcatagtggcgaacagcaa

BglII/HindIII restriction enzyme sites underlined were incorporated. Acquired PCR products were digested with BglII/HindIII and inserted into the pEGFP-N1 vector (Clontech). For bacterial expression of FABP7, ORF of human FABP7 was amplified by PCR, digested with SalI/HindIII and inserted into pQE31 vector (Qiagen). The primer sequences (5′ to 3′) for the subcloning are as follows:

Human FABP7	Forward	cccgtcgacatggtggaggctttctgtgctagc
Human FABP7	Reverse	cccaagctttgccttctcatagtggcgaacagcaa

SalI/HindIII restriction enzyme sites underlined were incorporated.

4.4.13 Transformation and Transfection

The constructs were transformed into E. coli DH5α for amplification and verified by sequencing. The transfection of 293HEK cells with the plasmid constructs were carried out using Lipofectamine 2000 (Invitrogen) according to the manufacturer's instructions.

4.4.14 Recombinant Protein Expression and Purification

pQE31-hFABP7 plasmid was transformed into an E. Coli strain SG13009(Qiagen), which allows stringent control of IPTG inducible promoter. Transformed SG13009 was cultured in SOB medium and the recombinant hFABP7 was induced by 0.5mMIPTG for 8 h at 30 °C. Bacterial pellet was harvested by centrifugation and the Histagged hFABP7 was purified using a Ni-NTA column of QiaExpress expression kit (Qiagen)

according to the manufacturer's instruction. The protein was delipidated by incubation with an equal volume of Lipidex-1000 at 37 °C for 10 min and elution. The buffer was exchanged to 10 mM potassium phosphate buffer (pH = 7.4) by five times repeated concentration and dilution using Amicon-Ultra 3K (Millipore) and the protein was finally concentrated to the concentration of 1.05 mg⁄ml.

4.4.15 *In Vitro* Binding Assay

To determine dissociation constant CDr3 (10 μM) was incubated with different concentrations of FABP7 (0–1 mg⁄ml) in 10 mM potassium phosphate buffer (pH = 7.4) at 37 °C for 10 min and the fluorescence intensities were recorded on a SpectraMax M2 plate reader (excitation: 530 nm; emission: 590 nm). The dissociation constant was obtained from a fitting curve using GraphPad Prism 5.0 software. For stoichiometry determination of CDr3-FABP7 complex, a total concentration of CDr3 (final concentrations: 0, 2, 4, 6, 8, 10, 12, 14, 16, 18, 20 μM) and FABP7 (final concentrations: 20, 18, 16, 14, 12, 10, 8, 6, 4, 2, 0 μM) mixtures were incubated in 10 mM potassium phosphate buffer (pH = 7.4) containing 1% DMSO at 37 °C for 10 min, and the fluorescence intensities of each mixture were recorded on a SpectraMax M2 plate reader (excitation: 530 nm; emission: 590 nm) for Job plot analysis.

References

1. Carpenter, A. E., Image-based chemical screening. *Nat. Chem. Biol.* **2007,** *3*, 461-465.

2. (a) Ahn, Y. H.; Lee, J. S.; Chang, Y. T., Combinatorial rosamine library and application to in vivo glutathione probe. *J. Am. Chem. Soc.* **2007,** *129*, 4510-4511; (b) Feng, S.; Kim, Y. K.; Yang, S.; Chang, Y. T., Discovery of a green DNA probe for live-cell imaging. *Chem. Commun.* **2010,** *46*, 436-438.

3. Inglese, J.; Johnson, R. L.; Simeonov, A.; Xia, M.; Zheng, W.; Austin, C. P.; Auld, D. S., High-throughput screening assays for the identification of chemical probes. *Nat. Chem. Biol.* **2007,** *3*, 466-479.

4. Vendrell, M.; Lee, J. S.; Chang, Y. T., Diversity-oriented fluorescence library approaches for probe discovery and development. *Curr. Opin. Chem. Biol.* **2010,** *14*, 383-389.

5. Lee, J. S.; Kang, N. Y.; Kim, Y. K.; Samanta, A.; Feng, S.; Kim, H. K.; Vendrell, M.; Park, J. H.; Chang, Y. T., Synthesis of a BODIPY library and its application to the development of live cell glucagon imaging probe. *J. Am. Chem. Soc.* **2009,** *131*, 10077-10082.

6. (a) Im, C. N.; Kang, N. Y.; Ha, H. H.; Bi, X.; Lee, J. J.; Park, S. J.; Lee, S. Y.; Vendrell, M.; Kim, Y. K.; Lee, J. S.; Li, J.; Ahn, Y. H.; Feng, B.; Ng, H. H.; Yun, S. W.; Chang, Y. T., A fluorescent rosamine compound selectively stains pluripotent stem cells. *Angew. Chem., Int. Ed.* **2010,** *49*, 7497-7500; (b) Ghosh, K. K.; Ha, H. H.; Kang, N. Y.; Chandran, Y.; Chang, Y. T., Solid phase combinatorial synthesis of a xanthone library using click chemistry and its application to an embryonic stem cell probe. *Chem. Commun.* **2011,** *47*, 7488-90.

7. (a) Falk, S.; Sommer, L., Stage- and area-specific control of stem cells in the developing nervous system. *Curr. Opin. Genet. Dev.* **2009,** *19*, 454-460; (b) Kaneko, N.; Sawamoto, K., Adult neurogenesis and its alteration under pathological conditions. *Neurosci. Res.* **2009,** *63*, 155-164.

8. Lindvall, O.; Kokaia, Z., Stem cells for the treatment of neurological disorders. *Nature* **2006,** *441*, 1094-1096.

9. Schule, B.; Pera, R. A.; Langston, J. W., Can cellular models revolutionize drug discovery in Parkinson's disease? *Biochim. Biophys. Acta* **2009,** *1792*, 1043-1051.

10. Conti, L.; Pollard, S. M.; Gorba, T.; Reitano, E.; Toselli, M.; Biella, G.; Sun, Y.; Sanzone, S.; Ying, Q. L.; Cattaneo, E.; Smith, A., Niche-independent symmetrical self-renewal of a mammalian tissue stem cell. *PLoS Biol* **2005,** *3*, e283.

11. Donato, R.; Miljan, E. A.; Hines, S. J.; Aouabdi, S.; Pollock, K.; Patel, S.; Edwards, F. A.; Sinden, J. D., Differential development of neuronal physiological responsiveness in two human neural stem cell lines. *BMC Neurosci.* **2007,** *8*, 36.

12. (a) Liour, S. S.; Yu, R. K., Differentiation of radial glia-like cells from embryonic stem cells. *Glia* **2003,** *42*, 109-117; (b) Bibel, M.; Richter, J.; Schrenk, K.; Tucker, K. L.; Staiger, V.;

Korte, M.; Goetz, M.; Barde, Y. A., Differentiation of mouse embryonic stem cells into a defined neuronal lineage. *Nat. Neurosci.* **2004,** *7*, 1003-1009.

13. Storch, J.; Corsico, B., The emerging functions and mechanisms of mammalian fatty acid-binding proteins. *Annu. Rev. Nutr.* **2008,** *28*, 73-95.

14. (a) Shimizu, F.; Watanabe, T. K.; Shinomiya, H.; Nakamura, Y.; Fujiwara, T., Isolation and expression of a cDNA for human brain fatty acid-binding protein (B-FABP). *Biochim. Biophys. Acta* **1997,** *1354*, 24-28; (b) Feng, L.; Hatten, M. E.; Heintz, N., Brain lipid-binding protein (BLBP): a novel signaling system in the developing mammalian CNS. *Neuron* **1994,** *12*, 895-908; (c) Arai, Y.; Funatsu, N.; Numayama-Tsuruta, K.; Nomura, T.; Nakamura, S.; Osumi, N., Role of Fabp7, a downstream gene of Pax6, in the maintenance of neuroepithelial cells during early embryonic development of the rat cortex. *J. Neurosci.* **2005,** *25*, 9752-9761.

15. (a) Owada, Y.; Abdelwahab, S. A.; Kitanaka, N.; Sakagami, H.; Takano, H.; Sugitani, Y.; Sugawara, M.; Kawashima, H.; Kiso, Y.; Mobarakeh, J. I.; Yanai, K.; Kaneko, K.; Sasaki, H.; Kato, H.; Saino-Saito, S.; Matsumoto, N.; Akaike, N.; Noda, T.; Kondo, H., Altered emotional behavioral responses in mice lacking brain-type fatty acid-binding protein gene. *Eur. J. Neurosci.* **2006,** *24*, 175-187; (b) Watanabe, A.; Toyota, T.; Owada, Y.; Hayashi, T.; Iwayama, Y.; Matsumata, M.; Ishitsuka, Y.; Nakaya, A.; Maekawa, M.; Ohnishi, T.; Arai, R.; Sakurai, K.; Yamada, K.; Kondo, H.; Hashimoto, K.; Osumi, N.; Yoshikawa, T., Fabp7 maps to a quantitative trait locus for a schizophrenia endophenotype. *PLoS Biol* **2007,** *5*, e297.

16. (a) Gotz, M.; Huttner, W. B., The cell biology of neurogenesis. *Nat. Rev. Mol. Cell Biol.* **2005,** *6*, 777-788; (b) Malatesta, P.; Hartfuss, E.; Gotz, M., Isolation of radial glial cells by fluorescent-activated cell sorting reveals a neuronal lineage. *Development* **2000,** *127*, 5253-5263; (c) Merkle, F. T.; Tramontin, A. D.; Garcia-Verdugo, J. M.; Alvarez-Buylla, A., Radial glia give rise to adult neural stem cells in the subventricular zone. *Proc. Natl. Acad. Sci. USA* **2004,** *101*, 17528-17532.

17. (a) Pankratz, M. T.; Li, X. J.; Lavaute, T. M.; Lyons, E. A.; Chen, X.; Zhang, S. C., Directed neural differentiation of human embryonic stem cells via an obligated primitive anterior stage. *Stem Cells* **2007,** *25*, 1511-1520; (b) Liour, S. S.; Kraemer, S. A.; Dinkins, M. B.; Su, C. Y.; Yanagisawa, M.; Yu, R. K., Further characterization of embryonic stem cell-derived radial glial cells. *Glia* **2006,** *53*, 43-56; (c) Nat, R.; Nilbratt, M.; Narkilahti, S.; Winblad, B.; Hovatta, O.; Nordberg, A., Neurogenic neuroepithelial and radial glial cells generated from six human embryonic stem cell lines in serum-free suspension and adherent cultures. *Glia* **2007,** *55*, 385-399.

18. Bi, X.; Lin, Q.; Foo, T. W.; Joshi, S.; You, T.; Shen, H. M.; Ong, C. N.; Cheah, P. Y.; Eu, K. W.; Hew, C. L., Proteomic analysis of colorectal cancer reveals alterations in metabolic pathways: mechanism of tumorigenesis. *Mol. Cell Proteomics* **2006,** *5*, 1119-1130.

Chapter 5 Diversity-Oriented BODIPY Library for "Taming"

BODIPY Compound

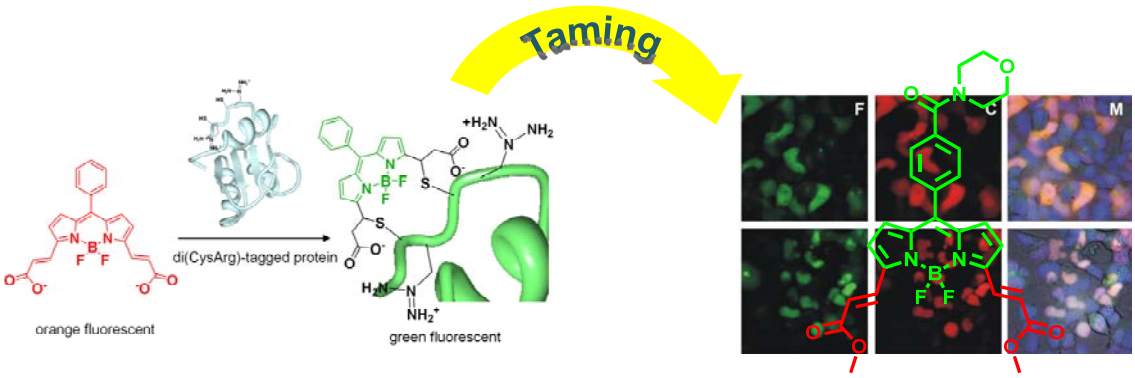

5.1 Introduction

Diversity-oriented fluorescent libraries (DOFL), in combining with high-throughput screening, have successfully proved their ability in sensor development.[1] However, their potential was not restricted to such an aspect. With the advances of screening technique and analysis software,[2] the images acquired from DOFL compounds could be more informatics and aim at specific applications. From this respect, preliminary researches have been done to study the structure-localization[3] or cell retention[4] relationship of fluorescent dyes. To expand the knowledge of cellular localization-specific groups (e.g., tertiary amines selectively localize in lysosome[5] and positive charged molecules prefer to go to mitochondria[6]), Shedden and Rosania performed high-throughput screening of a fluorescent styryl library. After analyzing the image, they successfully correlated the staining pattern with contribution of building blocks and concluded that charge migration and distribution played an important role in determining the localization of styryl compounds.[3] To study the non-stickiness property of fluorescent dyes, which is important to imaging intracellular receptors, Nath *et al.* designed a screening platform with three genetic-different mammalian cell lines using Rosamine compounds. After quantifying the cellular temporal uptake and retention of each compound, they found the relationship between non-stickiness property and structural similarity of Rosamine compounds.[4]

These researches provided generally useful information of fluorescent dyes' behavior, however, limited to certain scope. Styryl and Rosamine compounds are both positive charged molecules, which may induce background effect of the behavior of compounds. On the other hand, localization-specificity and non-stickiness are important issues but not the only ones. With these concerns, we aim to perform a study to obtain more comprehensive information about fluorescent compounds' behavior, in order to

further “tame” them in later sensor development. A fluorescent library was designed based on BODIPY scaffold, which is a special neutral structure and would induce minimal perturbation to its conjugated functional groups. After screening them to different cell lines, we found the general structure-cellular behavior relationship of BODIPY compounds, and successfully applied it to “tame” the probe and solve the background problem in later developing a protein tag system.

5.2 Results and Discussion

5.2.1 Construction of a BODIPY Library with Diverse Physical Properties

BODIPY was selected as the fluorescent scaffold, due to its superior photophysical properties, flexibility in chemical modification, and electrically neutral property. 3 different colors (Chart 5.1 and Scheme 5.1), from green to NIR were considered in order to obtain diverse spectral property of the library. 30 amines with very diverse physical properties, covering hydrophobic (e.g., **25**, **26**), hydrophilic (e.g., **1**, **3**), positive charged (e.g. **30**), negative charged (e.g., **23**, **24**), neutral (e.g., **16**, **22**) and other functional groups, were incorporated as building blocks (Chart 5.1). Two different positions of BODIPY core (5- and 8-) were modified to study the position effect. 120 compounds were rendered through acid-amine coupling reaction with good purity (Scheme 5.2) and named as “Taming” library, as the aim of constructing this library was to get general information for “taming” fluorescent dye in probe development.

Chart 5.1 A decoding table for Taming library.

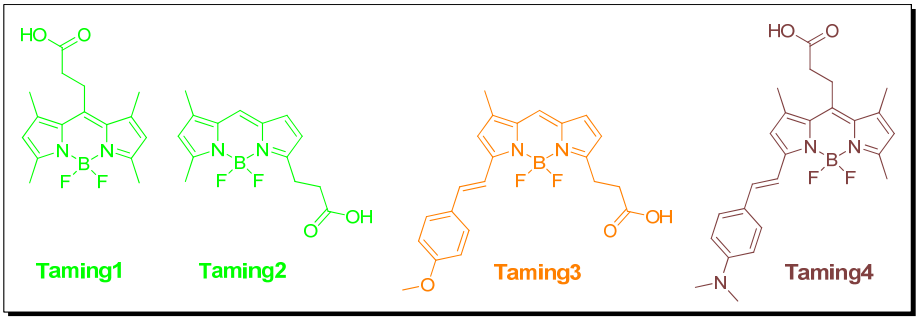

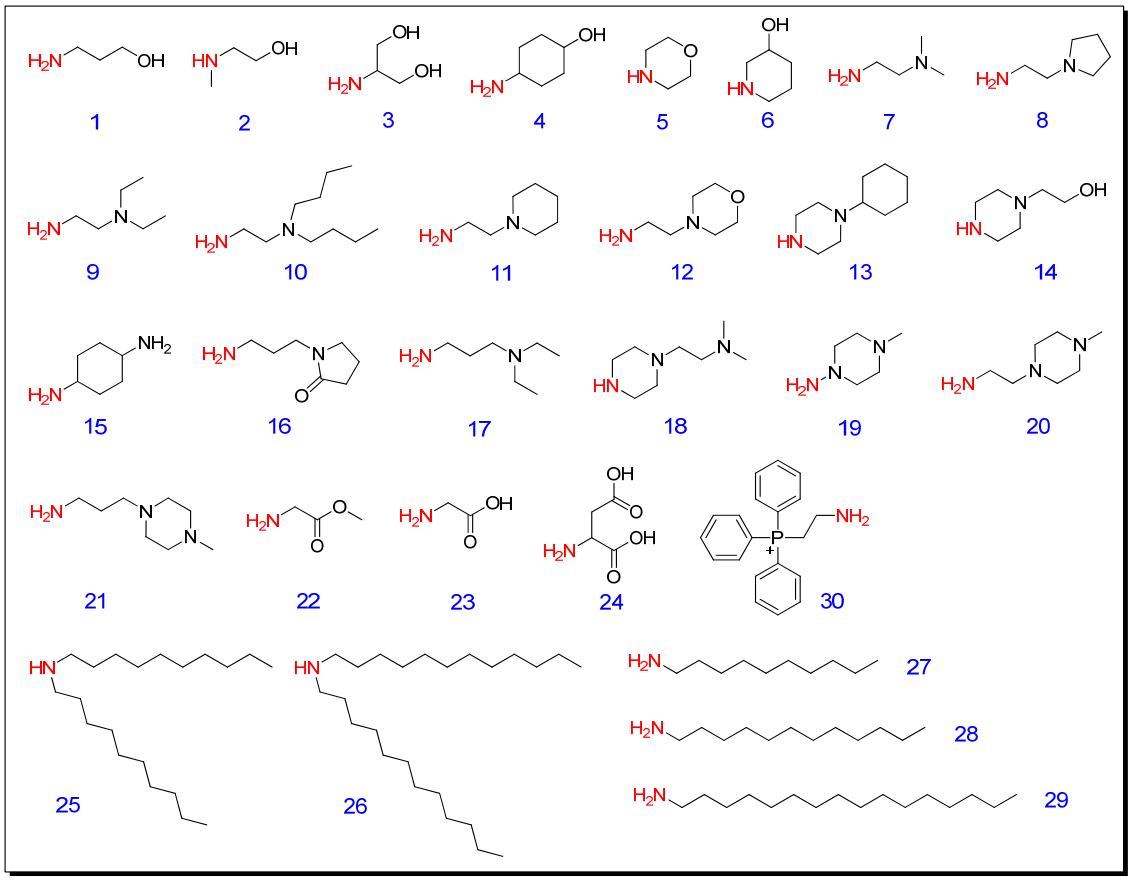

(upper) Structures of BODIPY cores; (lower) Structures of amine building blocks.

Scheme 5.1 Synthetic scheme of the starting materials of Taming1-4

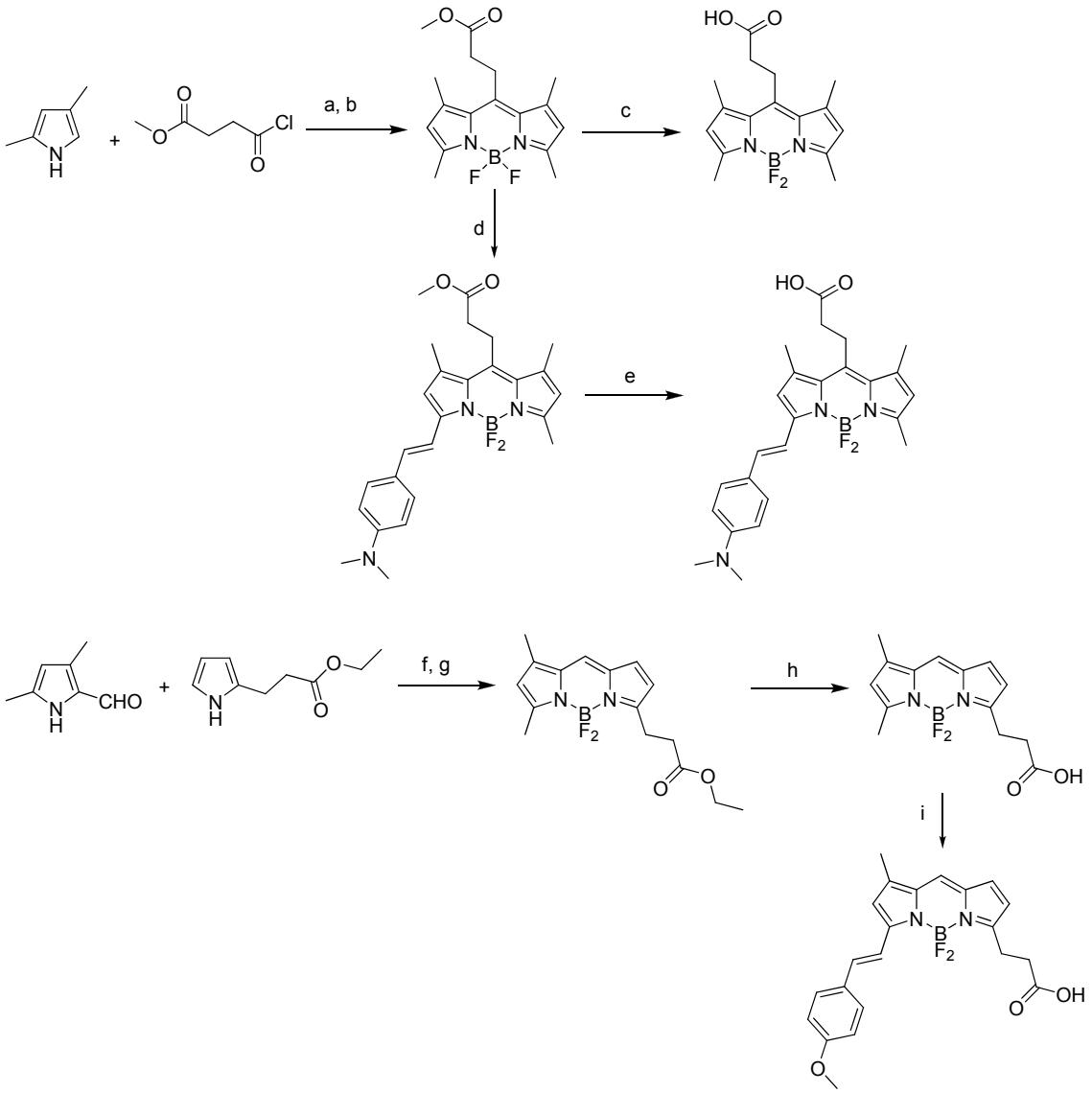

Reagents and conditions: a) DCM, reflux, 4h; b) DIEA (4 eq.), BF_3OEt_2 (4 eq.), DCM, r.t., overnight; c) KOH, MeOH/H_2O, r.t., overnight; d) 4-dimethylaminobenzaldehyde, pyrrolidine (6 eq.), acetic acid (6 eq.), ACN, 85 ^oC, 15 min; e) KOH, MeOH/H_2O, r.t., overnight; f) $POCl_3$, DCM, r.t., 4h; g) DIEA (4 eq.), BF_3OEt_2 (4 eq.), DCM, r.t., overnight; h) HCl, THF/H_2O, reflux, overnight; i) 4-methoxybenzaldehyde, pyrrolidine (6 eq.), acetic acid (6 eq.), ACN, 85 ^oC, 15 min.

Scheme 5.2 General synthetic scheme of Taming library

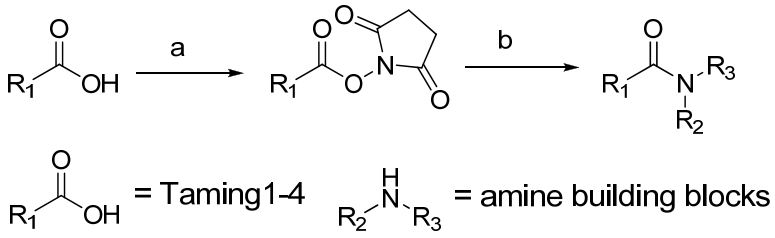

Reagents and conditions: a) N-hydroxylsuccinimide, DCC, DMAP, THF, r.t., overnight; b) amine building blocks, THF, r.t., 6 h.

5.2.2 Spectroscopic Properties of Taming Library

The coupling reaction does not change the conjugation system of each BODIPY core. Therefore, Taming compounds from each set has similar absorbance and emission wavelengths. However, their quantum yields vary from 0.001 to almost 1 with different amine structures (Table 5.1).

Table 5.1 Spectroscopic properties and purity table for Taming library: calculated mass, experimental mass, absorbance maximum (λ_{abs}), fluorescent emission maximum (λ_{em}), extinction coefficient (ε), quantum yield (Φ), and purity.

Code	mass (calc)	m/z (exp)	λ_{abs} (nm)	λ_{em} (nm)	ε ($M^{-1}cm^{-1}$)	Φ	Purity (%)[d]
Taming1-1	377.2	376.1[a]	498	514	209383	0.98	91
Taming1-2	377.2	376.1[a]	497	513	410914	0.97	99
Taming1-3	393.2	392.2[a]	498	514	222469	0.97	98
Taming1-4	417.3	416.2[a]	498	514	655630	0.98	99
Taming1-5	389.2	388.1[a]	498	513	437086	0.34	99
Taming1-6	403.3	402.2[a]	498	513	217235	0.94	98
Taming1-7	390.3	389.2[a]	499	514	82444	0.13	98
Taming1-8	416.3	415.2[a]	499	514	132173	0.56	97
Taming1-9	418.3	417.1[a]	499	514	179284	0.44	96
Taming1-10	488.5	487.2[a]	499	514	126938	0.66	98
Taming1-11	430.3	429.1[a]	498	514	342864	0.82	98
Taming1-12	432.3	431.3[a]	499	515	159654	0.91	99
Taming1-13	470.4	469.2[a]	498	514	163580	>0.99	99

Taming1-14	432.3	431.1[a]	498	514	145259	0.97	98
Taming1-15	416.3	415.2[a]	499	513	155728	0.95	95
Taming1-16	444.3	443.1[a]	498	514	995877	0.75	98
Taming1-17	432.4	431.3[a]	498	514	261728	0.61	95
Taming1-18	459.4	440.4	499	514	104691	0.40	92
Taming1-19	417.3	416.2[a]	499	515	307531	0.87	95
Taming1-20	445.4	444.1[a]	498	514	134790	0.84	97
Taming1-21	459.4	458.3[a]	497	514	75901	0.42	96
Taming1-22	391.2	390.1[a]	499	513	176667	0.69	97
Taming1-23	377.2	376.2[a]	401	515	68049	0.22	97
Taming1-24	435.2	434.1[a]	499	514	225086	0.84	93
Taming1-25	599.7	598.3[a]	498	515	311457	0.68	96
Taming1-26	655.8	654.4[a]	498	515	248642	0.68	97
Taming1-27	459.4	458.2[a]	498	514	666099	0.87	97
Taming1-28	487.5	486.2[a]	498	514	694889	>0.99	97
Taming1-29	543.6	542.3[a]	498	514	519531	0.97	90
Taming1-30	608.5	608.2[b]	499	515	392593	0.90	89
Taming2-1	349.2	330.1	507	521	136099	0.81	93
Taming2-2	349.2	330.1	507	521	283975	0.95	95
Taming2-3	365.2	346.1	506	519	1264148	0.94	95
Taming2-4	389.2	370.1	506	519	757704	>0.99	95
Taming2-5	361.2	341.1	506	521	198914	>0.99	98
Taming2-6	375.2	356.0	507	520	384741	0.88	93
Taming2-7	362.2	343.1	506	519	153111	0.86	99
Taming2-8	388.3	369.2	507	522	1124123	0.38	97
Taming2-9	390.3	371.2	506	520	244716	>0.99	91
Taming2-10	460.5	441.3	506	519	338938	0.95	92
Taming2-11	402.3	383.2	507	520	266963	0.71	98
Taming2-12	404.3	385.2	507	520	261728	0.78	97
Taming2-13	442.4	423.2	506	520	82444	0.44	90
Taming2-14	404.3	385.2	507	521	366420	0.90	94
Taming2-15	388.3	369.2	508	522	670025	0.66	98
Taming2-16	416.3	397.2	506	519	300988	0.95	90
Taming2-17	404.3	385.2	506	520	416148	0.96	92
Taming2-18	431.3	412.2	508	520	345481	0.72	91
Taming2-19	389.3	370.2	507	519	208074	0.63	95
Taming2-20	417.3	398.1	508	520	787802	0.20	98
Taming2-21	431.3	412.2	508	519	473728	0.24	90
Taming2-22	363.2	344.1	506	519	575802	0.99	98
Taming2-23	349.1	330.0	507	519	2691877	0.20	92

Taming2-24	407.2	388.1	506	519	1290321	0.82	99
Taming2-25	571.6	552.3	506	519	120395	>0.99	92
Taming2-26	627.7	608.4	506	520	163580	>0.99	94
Taming2-27	431.4	412.2	506	520	140025	>0.99	94
Taming2-28	459.4	440.2	506	520	198914	>0.99	98
Taming2-29	515.5	496.2	506	519	176667	0.96	98
Taming2-30	580.4	580.2[b]	506	519	217235	>0.99	98
Taming3-1	467.3	448.1	577	595	527383	0.37	97
Taming3-2	467.3	448.1	577	594	367728	0.30	93
Taming3-3	483.3	464.1	577	594	200222	0.21	99
Taming3-4	507.4	488.2	577	596	249951	0.27	92
Taming3-5	479.3	460.1	577	596	177975	0.22	98
Taming3-6	493.4	474.2	577	596	184519	0.21	95
Taming3-7	480.4	461.2	577	594	281358	0.24	96
Taming3-8	506.4	487.2	577	595	294444	0.23	95
Taming3-9	508.4	489.2	576	595	954000	0.31	97
Taming3-10	578.6	559.3	576	596	1358370	0.35	99
Taming3-11	520.4	501.2	577	595	1198716	0.38	96
Taming3-12	522.4	503.2	577	595	1065235	0.45	94
Taming3-13	560.5	541.3	577	595	422691	0.29	94
Taming3-14	522.4	503.2	577	596	961852	0.41	94
Taming3-15	506.4	487.2	577	596	455407	0.58	94
Taming3-16	534.4	515.2	577	595	1245827	0.47	94
Taming3-17	522.4	503.2	577	595	312765	0.22	98
Taming3-18	549.5	530.2	577	594	509062	0.27	98
Taming3-19	507.4	488.2	577	594	231630	0.21	92
Taming3-20	535.4	516.2	577	594	395210	0.29	92
Taming3-21	549.5	530.2	577	595	744617	0.39	94
Taming3-22	481.3	462.1	577	596	2104296	0.52	95
Taming3-23	467.3	448.1	577	594	366420	0.32	99
Taming3-24	525.3	506.1	577	594	141333	0.17	95
Taming3-25	689.8	670.4	577	595	989333	0.45	94
Taming3-26	745.9	726.5	577	596	957926	0.44	98
Taming3-27	549.5	530.2	577	596	1537654	0.52	94
Taming3-28	577.6	558.3	577	596	1125432	0.46	93
Taming3-29	633.7	614.4	577	595	1211802	0.49	94
Taming3-30	698.6	698.5[b]	577	595	787802	0.44	95
Taming4-1	508.4	509.2[b]	602	740	634691	0.008	90
Taming4-2	508.4	509.2[b]	602	733	408296	0.008	90
Taming4-3	524.4	525.3[b]	603	741	654321	0.009	99

Taming4-4	548.5	549.3[b]	603	738	859778	0.008	99
Taming4-5	520.4	521.3[b]	601	743	231630	0.007	98
Taming4-6	534.4	535.3[b]	602	730	138716	0.005	98
Taming4-7	521.5	522.3[b]	606	756	177975	0.004	90
Taming4-8	547.5	548.4[b]	605	735	359877	0.005	92
Taming4-9	549.5	550.4[b]	605	731	316691	0.005	93
Taming4-10	619.6	620.4[b]	603	693	181901	0.004	94
Taming4-11	561.5	562.4[b]	605	728	274815	0.004	95
Taming4-12	563.5	564.4[b]	606	739	321926	0.005	98
Taming4-13	601.6	602.4[b]	605	732	393901	0.005	97
Taming4-14	563.5	564.3[b]	605	743	421383	0.007	98
Taming4-15	547.5	546.1[a]	603	744	383432	0.009	89
Taming4-16	575.5	598.3[c]	602	737	163580	0.006	97
Taming4-17	563.5	564.3[b]	607	742	257802	0.005	93
Taming4-18	590.6	591.4[b]	604	738	236864	0.007	98
Taming4-19	548.5	529.3	605	733	889877	0.006	98
Taming4-20	576.5	577.4[b]	606	755	352025	0.005	96
Taming4-21	590.6	591.4[b]	607	746	1205259	0.004	92
Taming4-22	522.4	523.3[b]	605	745	308840	0.007	96
Taming4-23	508.4	509.3[b]	604	741	951383	0.006	98
Taming4-24	566.4	565.1[a]	603	731	594123	0.007	95
Taming4-25	730.9	731.5[b]	600	759	90296	0.001	90
Taming4-26	787.0	767.5	599	732	98148	0.003	89
Taming4-27	590.6	591.4[b]	604	748	290519	0.008	93
Taming4-28	618.7	619.5[b]	603	742	506444	0.008	91
Taming4-29	674.8	675.1[b]	605	750	188444	0.006	92
Taming4-30	739.7	740.4[b]	604	686	327160	0.008	98

All absorbance and fluorescence excitation and emission data were recorded by a Synergy 4, Biotek Inc. fluorescent plate reader with 20 μM compounds in DMSO (100 μL) in 96-well polypropylene plates. Mass was calculated as (M+), and found in ESI-MS (M-F), *a:* found mass (M-H) in the negative mode scan, *b*: found mass (M+H), *c:* found mass (M+Na), *d:* Purity data was calculated on the basis of the integration in HPLC trace at 254 nm.

5.2.3 Cell-Based Screening for Taming Compounds

5.2.3.1 Localization Specificity Study

Taming library compounds were incubated with live A549 cells growing on glass bottom of 384-well plates to check their cellular localizations. To facilitate data acquisition and analysis, Hoechst33342 was used to label the nucleus of cells. Images of two regions per well were acquired using ImageXpress Micro™ cellular imaging system (Molecular Device) with 40× objective lens, and DAPI (for Hoechst33342), FITC (for Taming1 and 2), Texas Red (for Taming3) and Cy5 (for Taming4) filter sets. It was found that Taming1 and 2 compounds localized to specific sub-cellular compartments (e.g., mitochondria, vesicles, cytoplasma). Furthermore, Taming1 and 2 with same class of functional groups showed similar staining pattern inside the cells. Compounds with hydroxyl or alkoxy groups stained whole cytoplasm of cells with high background, while compounds with carboxylic acid group are not cell permeable. It is already known that tertiary amine and triphenylphophonium compounds specifically go to lysosome and mitochondria in the cell, respectively. Our experiment further confirmed that BODIPY cores of Taming1 and 2 did not affect their conjugates' behaviour. Furthermore, substituted position difference on BODIPY core did not affect the cellular behaviour of compounds, either (Figure 5.1). Taming3 compounds showed similar staining pattern with same anime structures as Taming1 and 2. However, most Taming4 compounds selectively localized in mitochondrial due to the conjugated 4-dimethylamino styryl motif, which easily gets positively charged under physiological conditions (Figure 5.2). It is known that positively charged molecules can accumulate in the mitochondrial of the cell due to the membrane potential. On the other hand, this also proved that neutral BODIPY structures can induce minimum perturbation to the function of their conjugates compared to other charged fluorophores.

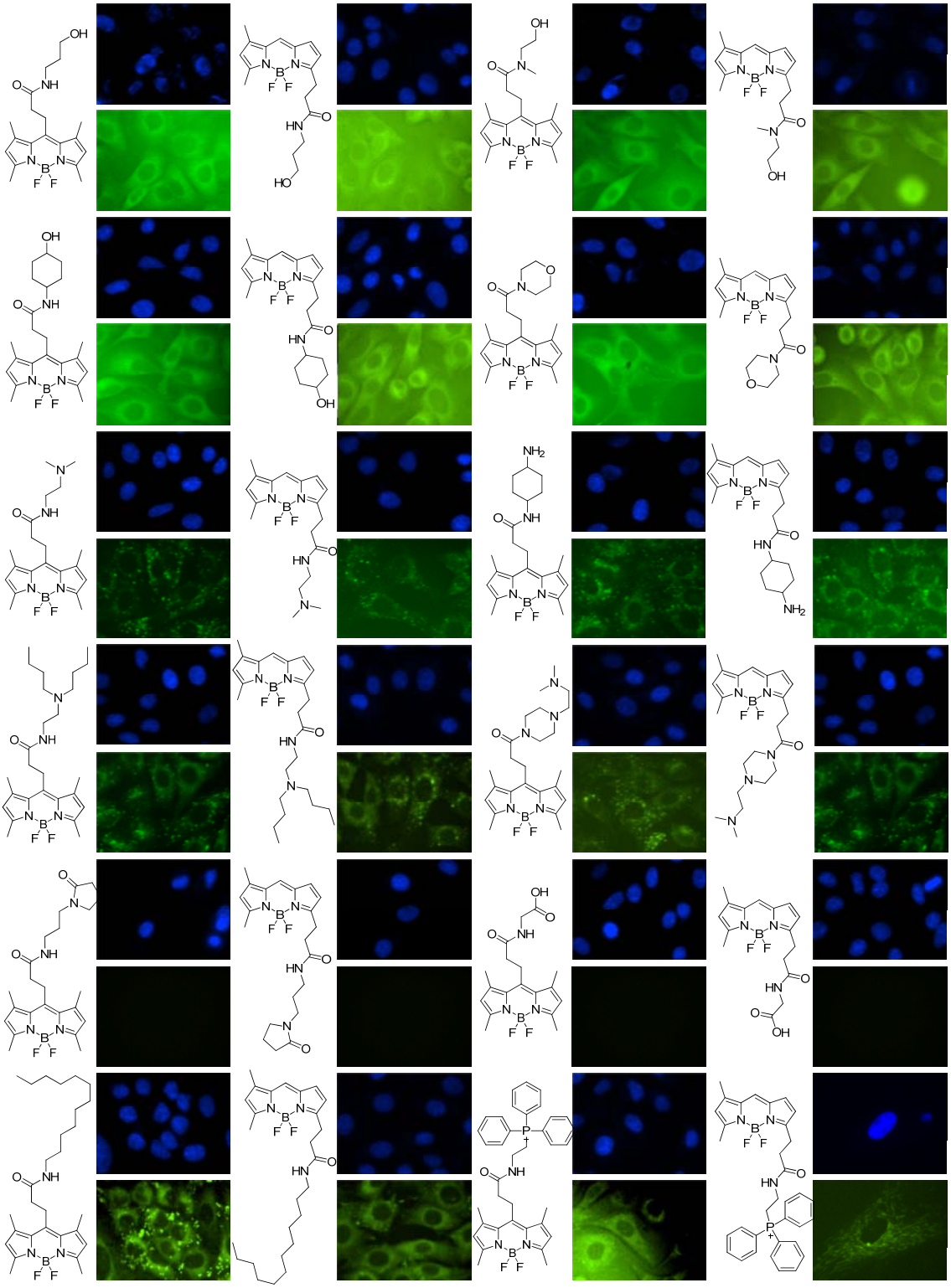

Figure 5.1 Structures and images acquired from Hoechst33342, and Taming1 and 2 compounds. Cells were stained with Hoechst33342 at 2 μM for 10 min (blue images from DAPI channel) and the compound at 2 μM for 30 min (green images from FITC channel).

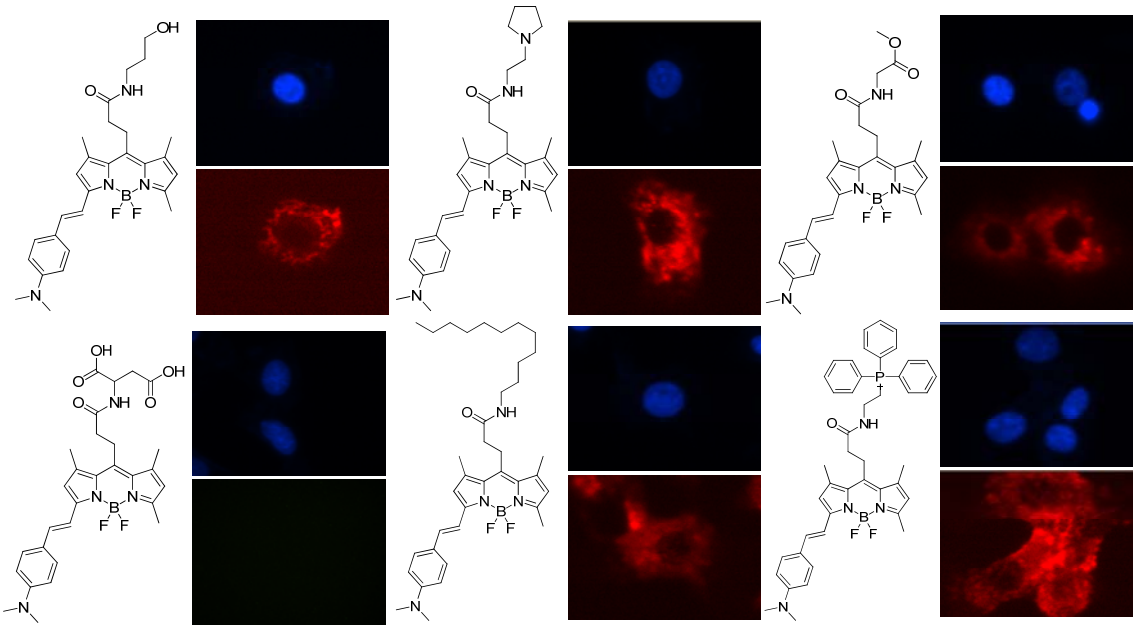

Figure 5.2 Structures and images acquired from Hoechst33342, and Taming4 compounds. Cells were stained with Hoechst33342 at 2 μM for 10 min (blue images from DAPI channel) and the compounds at 2 μM for 30 min (red images from Cy5 channel).

5.2.3.2 Cell Retention Study

Next we studied the structure-cell retention relationship of Taming compounds. Taming4 compounds were excluded in this study due to the big effect of 4-dimethylamino styryl motif on their cellular behaviour. Taming1, 2 and 3 compounds were incubated with live COS7, CHO, and HeLa cells growing on glass bottom of 96-well plates, and the images were acquired from 0 to 60 min with 10 min interval. Then the compounds were washed out at 60 min time point, and images were taken every 10 min to another 60 min. To facilitate data acquisition and analysis, Hoechst33342 was used to label the nucleus of cells. Images of two regions per well were acquired using ImageXpress Micro™ cellular imaging system (Molecular Device) with 10× objective lens, and DAPI (for Hoechst33342), FITC (for Taming1 and 2), Texas Red (for Taming3) filter sets. It was found that Taming compounds with hydroxyl or ether functional groups (i.e., Taming1-1 to 6, Taming2-1 to 6 and Taming 3-1 to 6) can be

taken up and washed out from the cells very fast, and after washing, the compounds leave no background in the cells. Taming compounds with amine groups (i.e., Taming1-7 to 21, Taming2-7 to 21, and Taming3-7 to 21) can also be taken up and washed out from the cells quickly, however, after washing, small percentage of compounds remained in the cells. Taming compounds with long carbon chains (i.e., Taming1-25 to 29, Taming2-25 to 29, and Taming3-25 to 29) were much stickier compared to the former two classes of compounds as they can be taken up by the cells slowly, and leave high background after washing (Figure 5.3). Besides, all these compounds showed similar cell retention pattern among 3 different cell lines.

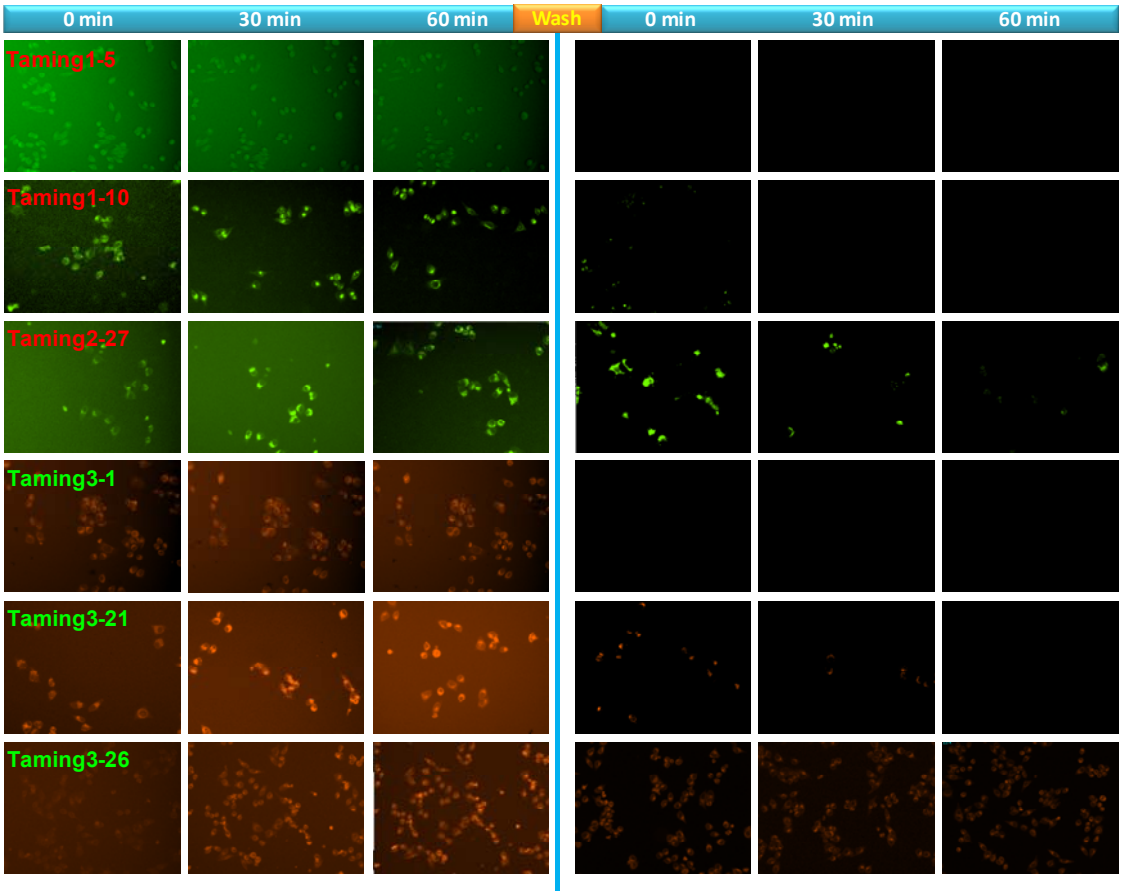

Figure 5.3 Representative images acquired from Taming1, 2 and 3 compounds in HeLa cells. Cells were stained with compound at 2 μM, and images were taken from 0 to 60 min. Then the compounds were washed out at 60 min time point, after washing images were taken from 0 to another 60 min. (green images from FITC channel and orange images from Texas Red channel)

5.2.4 Application of Taming Compounds-Case Study: BODIPY-Diacrylate Imaging Probes for Targeted Proteins inside Live Cells

Taming compounds have been screened in cells based on different platforms. Their cellular behaviour can be successfully correlated to the contribution from different classes of functional groups. These results are quite informative in developing specific probes based on BODIPY structure, which can help us to find the general guides (e.g., organelle-specific probes and low-background probes after washing). Here, we introduce one example of developing image probes for targeted proteins inside live cells, in which the information from cell-based screening of Taming compounds helped to solve the background issue of free molecules.

5.2.4.1 Background

Site-specific labelling of target proteins with fluorescent reporter probes allows numerous *in vivo* studies of protein functions.[7] Although genetic fusion of the fluorescent proteins (FPs) provides critical advantages, its adverse properties, such as large size (27 kDa) or aggregation, often limit the application.[8] Alternatively, a small peptide tag and its binding probe would provide a less invasive way of protein labelling.[9] A pioneering example utilizing the high affinity between a tetracysteine tag and a fluorescent biarsenical probe (FlAsH)[10] has been used in a number of applications inside live cells with step-wise improvements.[11] Development of other peptide tags have been followed, mostly, in two perspectives: first, by exploiting the intrinsic affinity between a probe and a peptide tag, such as the D4 tag/Zn-probe[12] or IQ-tag[13]; and second, by conjugating a probe to a peptide tag with an assistance of trans-acting enzymes as shown by the AviTag[14], LAP-tag[15], or ACP/PCP tag[16]. However, application of the above systems, except the FlAsH, is limited to the extracellular domain of membrane proteins because of the cell-impermeability of labelling reagents,

including the modifying enzymes. Although a recent report by Uttamapinant *et al.* suggests a clever strategy to label peptide tags inside cells,[17] co-expression of the modifying enzyme might affect the simplicity of experimental protocol and deprive the transcription/translational machinery in cells. Therefore, notwithstanding the toxicity of arsenical probes, FlAsH is still the most representative peptide-based method applicable inside cells and thus, new peptide-based labelling systems with safer probes need to be developed. We designed a fluorescent probe based on BODIPY structure which exhibits a large spectral emission shift upon covalent coupling to a designed peptide and demonstrated the successful optical imaging of a target protein labelled by this affinity pair (probe and tag) inside cells.

5.2.4.2 Design and Synthesis of BODIPY-Diacrylate Probes

We designed a fluorescent probe based on BODIPY structure, due to the relatively facile modification on its structure with predictable alteration on the excitation/emission wavelengths.[18] We envisioned that attachment of the Michael acceptor to the BODIPY core will shift the excitation and emission significantly to longer wavelengths, while 1,4-addition of thiols to the Michael acceptor will break the conjugation, shifting the fluorescence back to the green colour of BODIPY.[18-19] Therefore, we incorporated two acrylic acid groups to the BODIPY core and two reactive cysteines to the peptide tag, while the distance between two acrylic groups was similar to the two cysteines (Figure 5.4). Previously, similar design has been reported by Girouard *et al.* through binding a fluorogenic dimaleimide-fluorophore to the dicysteine peptide.[19-20] However, labelling on intracellular proteins is not yet demonstrated.

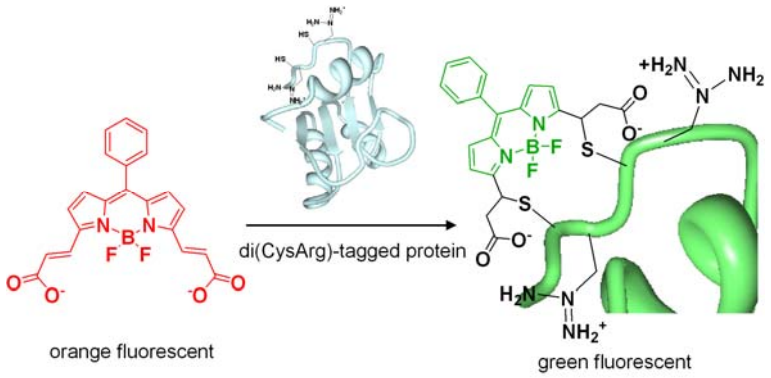

Figure 5.4 Design of a BODIPY fluorophore that exhibits a large spectral change upon covalent conjugation to a tag for potential application to the site-specific labelLing of proteins inside live cells.

Scheme 5.3 Synthetic scheme of BODIPY diacrylates

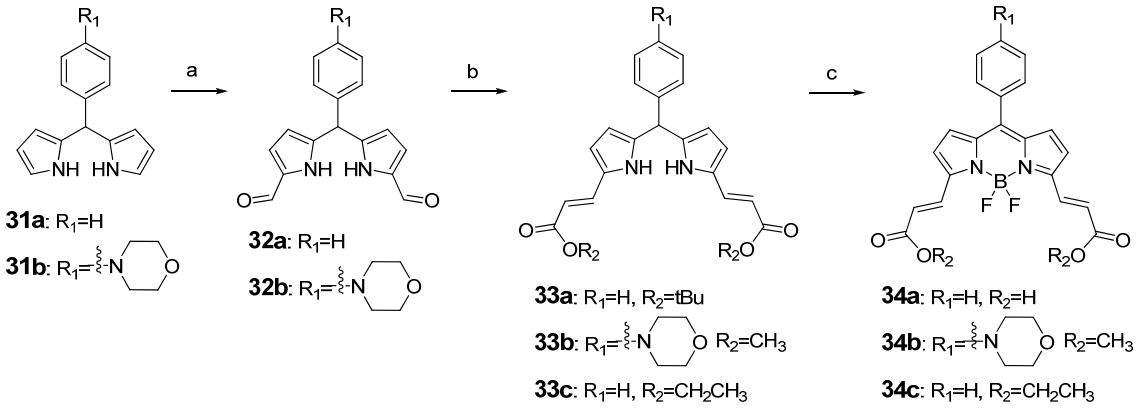

Reagents and conditions: a) $POCl_3$, DMF, 0 ^oC, 1.5 h, then NH_4OAc (aq.), r.t., overnight; b) PPh_3=C(O)OR_2, DCM, overnight; c) DDQ, DCM, r.t., 15 min, then DIEA, BF_3OEt_2 DCM, 3h.

The synthesis of BODIPY-diacrylate derivatives is outlined in Scheme 5.3. Dialdehydes were prepared by Vilsmeier formylation of 5-phenyldipyrromethanes. The Wittig reaction of dipyrromethanes with a triphenylphosphorane reagent afforded the diacrylate compounds, which were characterized as a symmetrical E isomer (J = 16.0 Hz) by ^{1}H-NMR. Phenyldipyrromethane acrylates were oxidized by DDQ and subsequently complexed with BF_3OEt_2, giving a deep purple solid of BODIPY diacrylates.

5.2.4.3 Validation of BODIPY-Diacrylate Probes

Initially, **34a** was evaluated for a spectral change with model peptides *in vitro*. The model peptide P1, based on previous literature, has two cysteines at the i and i+4 positions (Figure 5.5a) and was proven to form an a-helix by CD spectroscopy (Figure 5.5b). Additionally, an Arg was paired with each Cys, which would lower the pKa of thiols and increase the nucleophilicity in physiological pH. Two control peptides are P2, with one pair of Arg-Cys, and P3, having no Arg-cys pairs. Compound **34a** in a buffered condition (50 mM HEPES, pH 7.4) has an absorption maximum at 582 nm and emission at 600 nm with an orange colour fluorescence. Addition of P1 (10 mM) induced an immediate spectral change (reaction rate constant, k=0.1484 s^{-1}, Figure 5.6), resulting in a large blue shift of emission to green fluorescence (530 nm, Figure 5.7a), and the Arg residues appear to contribute to the rapid reaction since control peptide without them induced a slower reaction (k = 0.0882 s^{-1}, Figure 5.6). By contrast, P2 gave a slight spectral change with a new emission peak at 565 nm, possibly due to the single conjugation with Arg-Cys, and P3 showed none. Notably, 10-fold excess of N-acetylcysteine (NAC) induced a small peak at 565 nm. Another control experiment with high concentration of glutathione (up to 5 mM), mimicking the intracellular environment of live cells, induced the orange peak (565 nm) as the major emission and a small green peak (530 nm) as the minor emission. These results might imply the potential background signal when the labelling is performed inside live cells (Figure 5.8). In time-dependent monitoring of fluorescence emission at 530 nm with excitation at 480 nm, only P1 displayed an exclusive increase of emission (Figure 5.9), and therefore, P1 only would enable a selective imaging at this wavelength channel of fluorescence microscope. This selectivity was further validated by checking fluorescence colours under UV irradiation with a hand-held UV lamp (excitation at 365

nm) (Figure 5.7b), and these different colours lasted even after 24 h (data not shown). After we confirmed the conjugation product of P1 and **34a** through the MALDI-TOF/MS and LC/MS analysis, we designated amino acid sequences of the model peptide P1 as the ‘‘RC’’ tag.

a)

P1	AcEAAAREARCRERCARA
P2	AcEAAARAAARERCARA
P3	AcEAAARAAAREAAARA

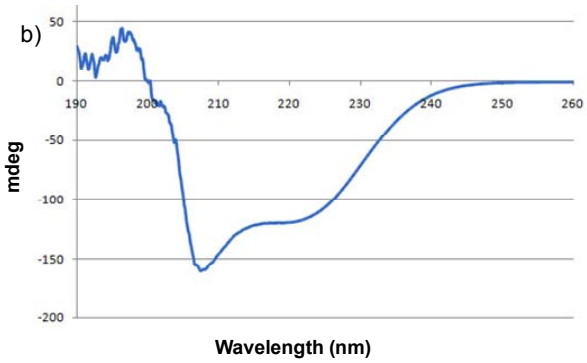

Figure 5.5 (a) Peptide sequences of P1, P2, and P3. (b) Circular dichroism (CD) spectrum of P1; CD was determined with 1 mM of P1 in 10 mM PBS buffer solution. Buffer reading value was subtracted. Typical helix 209, 220 nm excitations were observed.

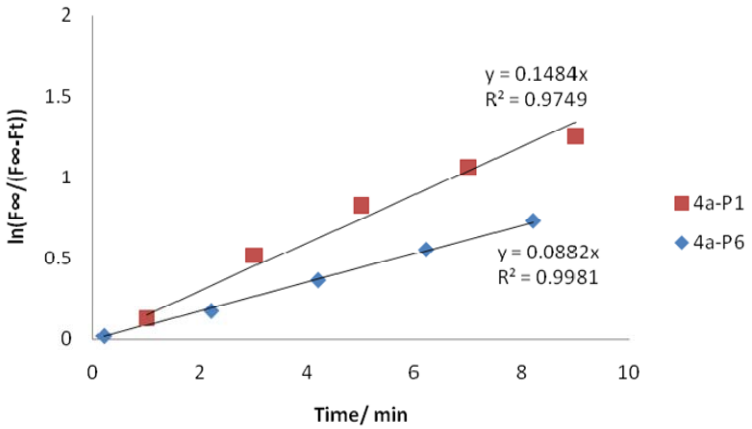

Figure 5.6 Kinetic study to determine the reaction rate constant between dye and peptide. 10 µM of **34a** and 200 µM of peptide (P1 or P6*) of 20 mM HEPES buffer solution, containing 1 % DMSO, was placed in a 96-well plate. Fluorescent intensity at 530 nm, with an excitation at 480 nm, was recorded every 2 min until saturated. (Control peptide without Arg. **P6***: AcGGGGGGGG**C**GGG**C**GGG-NH2)

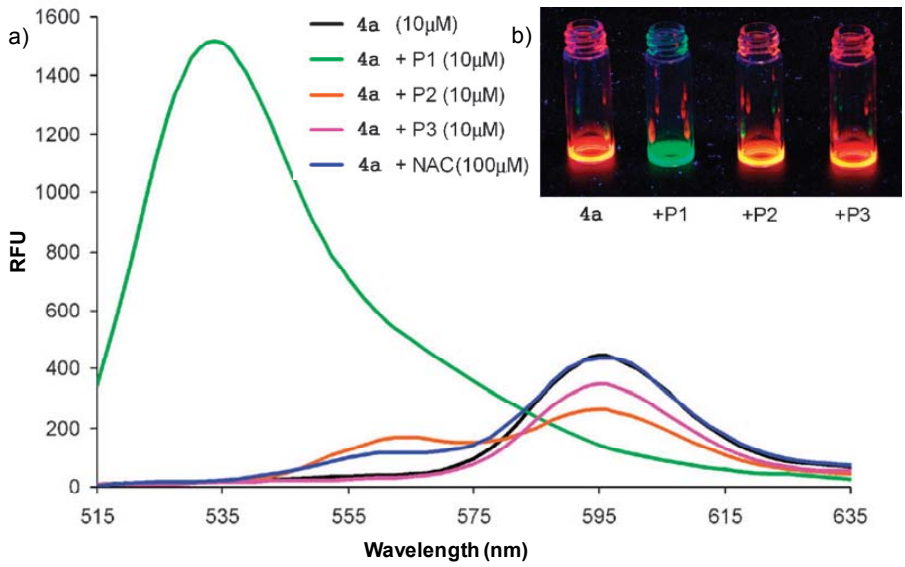

Figure 5.7 Fluorescence responses of **34a** incubated with P1, P2, P3 or NAC in 50 mM HEPES (pH 7.4) with excitation at 480 nm. (a) Emission spectra after incubation for 40 min at RT. (b) A picture of **34a** solutions containing the model peptides under irradiation with a handheld UV lamp (ex = 365 nm).

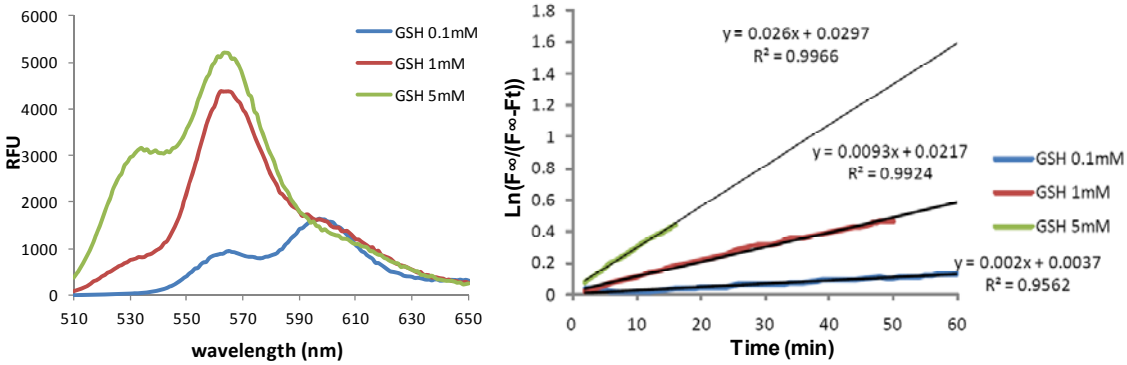

Figure 5.8 Fluorescence responses of **34a** incubated with various concnetration of glutathione. (a) Glutathione was reacted with **34a** (10 μM) in 50 mM HEPES (pH 7.4) with an excitation at 480 nm and the emission spectra are acquired after 40 min incubation at room temperature. (c) Calculation of rate constant; As GSH is large excess, the concentration of GSH was considered to be constant during the reaction with **34a**. The reaction between dye and GSH was considered as *pseudo*-first order reaction.

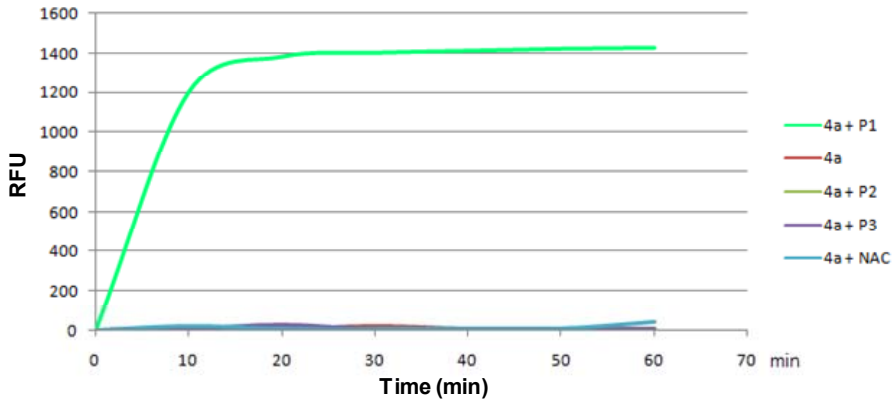

Figure 5.9 Time-dependent fluorescence responses of **34a** incubated with model peptides: **34a** (10 μM) was mixed with P1, P2, P3 (10 μM) or NAC (100 μM) in 50mM HEPES (pH 7.4) and the fluorescence emissions were measured at 530 nm with an excitation at 480 nm.

5.2.4.4 "Tame" 34a for Good Cell Permeability and Low Background

To evaluate the labelling efficacy of the RC tag for intracellular proteins, we further modified the non-cell permeable compound **34a**. By changing the acids into ethyl esters, compounds **34c** were synthesized with good cell permeability. However, further study showed that **34c** were very sticky when treated to the cells, left high background of free compounds even after washed out (data not shown). From our previous screening of Taming compounds, we have discovered that BODIPY compounds with hydroxyl or morpholine groups could be easily washed out from the cells leaving no background. Therefore, to solve the stickiness issue, **34a** were further modified at the para-position of the phenyl ring by introducing morpholine group due to the synthetic simplicity. Furthermore, ethyl ester was changed to methyl ester to further reduce the cell retention property, yielding compound **34b** as the optimum probe (Figure 5.10a).

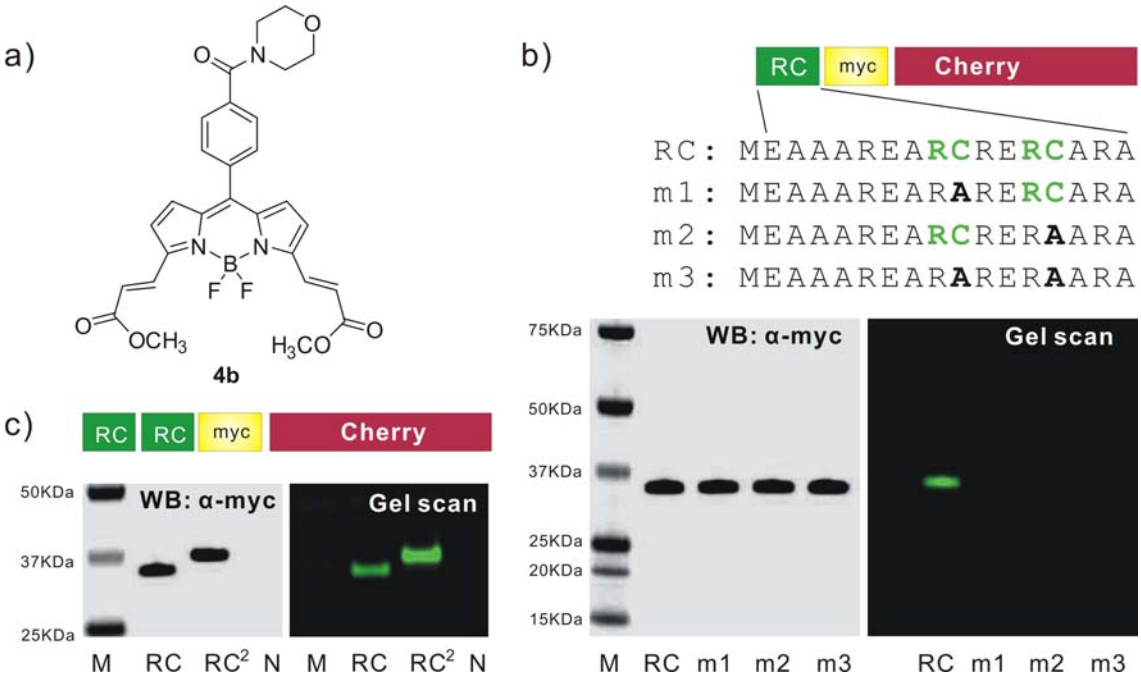

Figure 5.10 (a) Structure of **34b**. (b) RC tagged Cherry and three alanine mutants. Protein extract from the cells, transfected with the vectors and stained with **34b**, were analyzed in the SDS-PAGE and a-myc western blotting confirmed the expression of tagged proteins. M: protein size marker. N: no transfection. (c) Conjugation of **34b** to RC^2 tagged Cherry by SDS-PAGE and western blotting. (Gel scan Ex/Em=488/SP 526 nm).

5.2.4.5 Development of RC tag

First, we fused the RC tag to a model protein (monomeric Cherry, a red fluorescent protein) and analyzed the conjugation of **34b** to the RC-tagged Cherry in gel electrophoresis (SDS-PAGE). Protein extract of the transfected cells showed an apparent green fluorescence band resulted from the covalent binding of **34b** to RC-tagged Cherry at the expected molecular weight (34 kDa). Moreover, we confirmed this spectral change is achieved only when two cysteine residues are faithfully provided, since mutations on either one or two cysteines in the RC tag completely disable the spectral change (Figure 5.10b and Figure 5.11). However, when the RC-tagged Cherry was expressed in cells, the green fluorescent signal provided by the staining with **34b** was marginally strong to be used for clear optical imaging (Figure 5.12). In order to

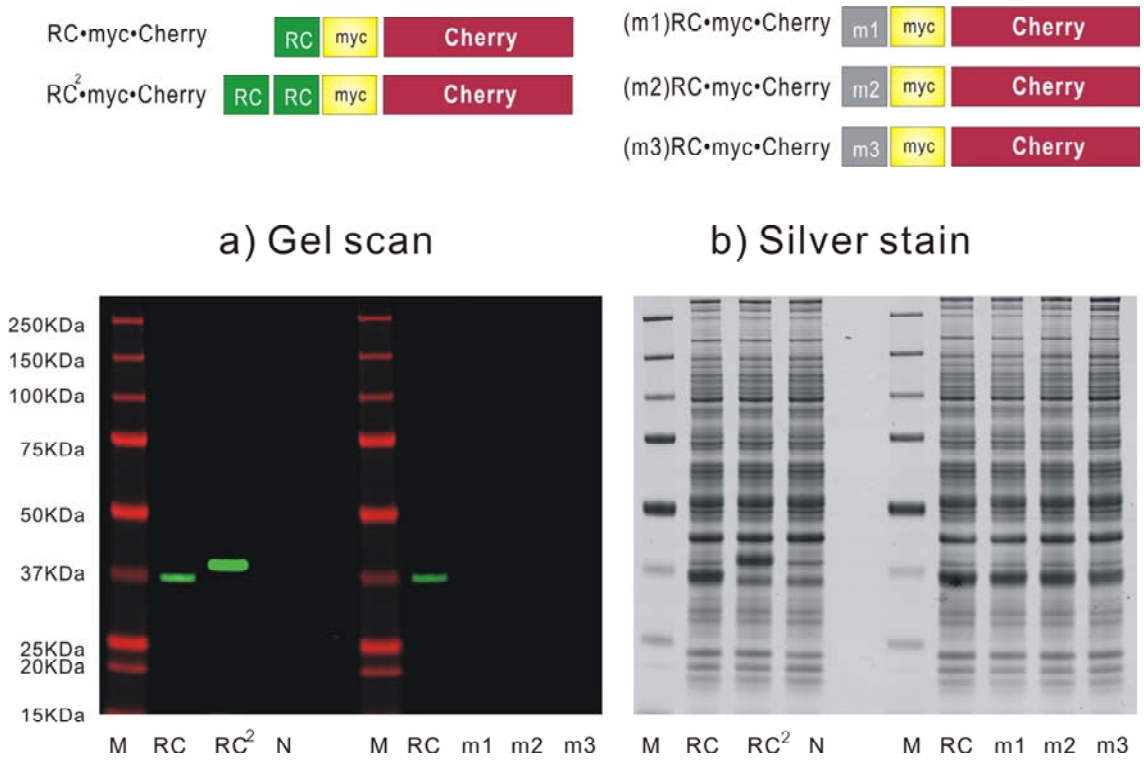

Figure 5.11 Specific-conjugation of **34b** to RC^2 tagged target proteins in the total proteome. HEK293 cells, transfected with the **RC**·myc·Cherry and **RC**2·myc·Cherry or the alanine mutation clones, were stained with **34b** (1 μM, 30 min, 37 ºC) and the total lysates were analyzed on SDS-PAGE. After fluorescence gel scanning (a), the gel was subjected to silver staining (b) to reveal the total proteome resolved on gel.

enhance the labelling efficiency, we dimerized the RC tag and doubled the binding motif (–RCXXRC–) in the tag (RC^2) (see the experimental section for the amino acids sequences of RC^2). As expected the RC^2 tag produced a stronger fluorescent band in gel (Figure 5.10c) than RC and thus, we focused on this RC^2 tag for further live cell imaging. Combining **34b** with the RC^2 tag, cell images showed much stronger green fluorescence than with the RC tag by the expected spectral change and the green fluorescence overlapped clearly with the red signal from Cherry inside cells (Figure 5.13a and 5.14). Green fluorescence intensity reached saturation within 15min and washing/further incubation for 30min to 1 h in fresh medium significantly helped the removal of background signal of **34b**. In addition, when we confined the expression of

RC^2 tagged Cherry to the nucleus, by introducing a nuclear localization signal (NLS) to the expression cassette, the green signal from compound **34b** also was strictly localized to the nucleus in transfected cells in accordance with the red fluorescence of Cherry (Figure 5.14).

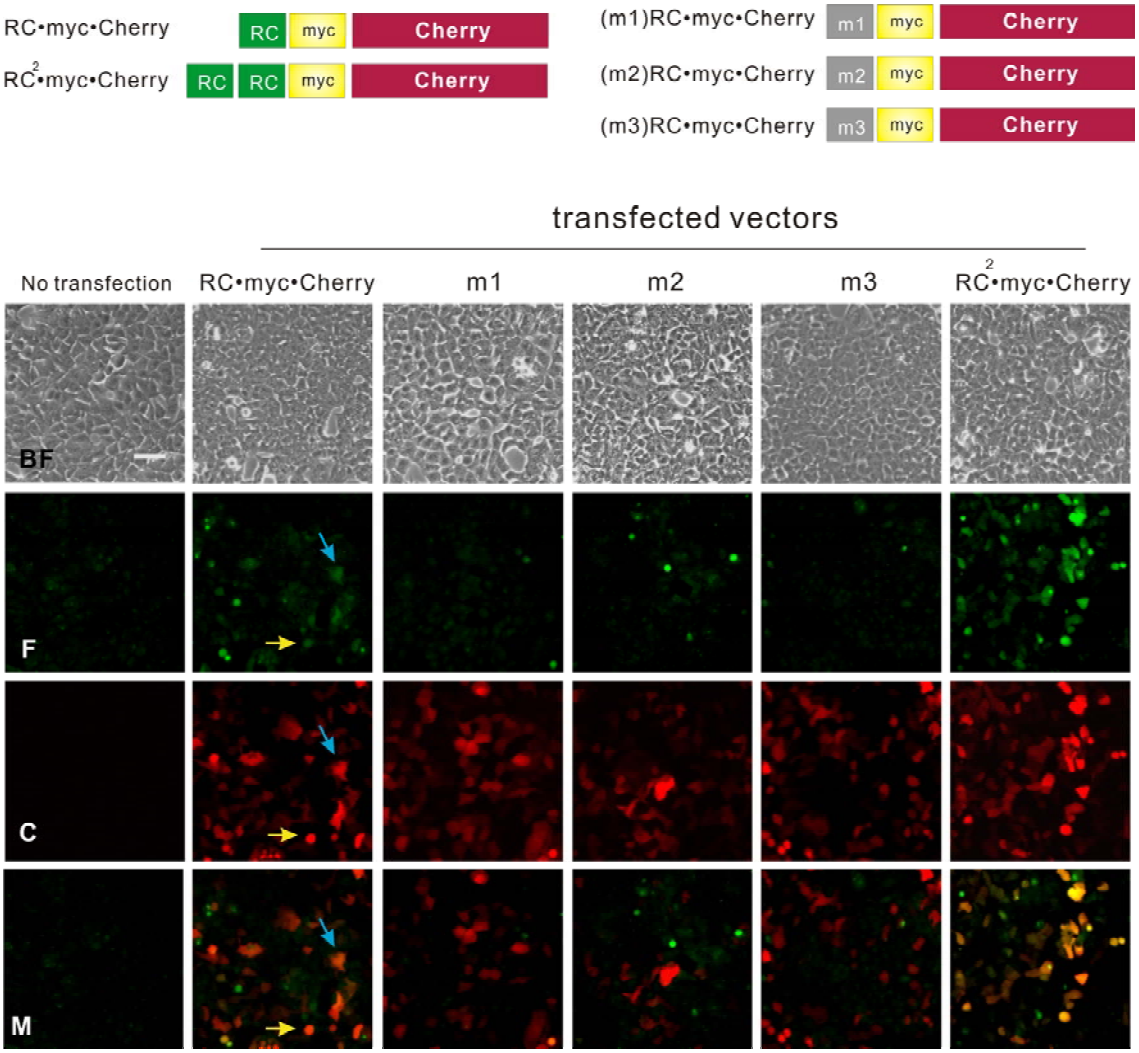

Figure 5.12 Dimerization of RC tag enables an effective labelling of target protein by **34b** in live cells. HEK 293 cells were transfected with the expression vectors encoding Cherry that is tagged with **RC**, **RC**2 or the alanine mutants of RC (m1, m2, m3) and stained with **34b**. Fluorescence microscopic images taken by FITC filter (F) show the green fluorescence resulting from the spectral change of compound and images taken by Cy5 filter (C) prove the expression of tagged protein (Cherry). The yellow and blue arrows in **RC** tagged Cherry (**RC**·myc·Cherry) indicate cells showing overlapping signals (green and red). Noticeably, the green signal from the dimeric RC tagged protein (**RC2**·myc·Cherry) is significantly stronger than the monomeric RC tagged protein (**RC**·myc·Cherry). BF-bright field, F-FITC, C-Cy5, M-merged (F and C). Scale bar 50 µm.

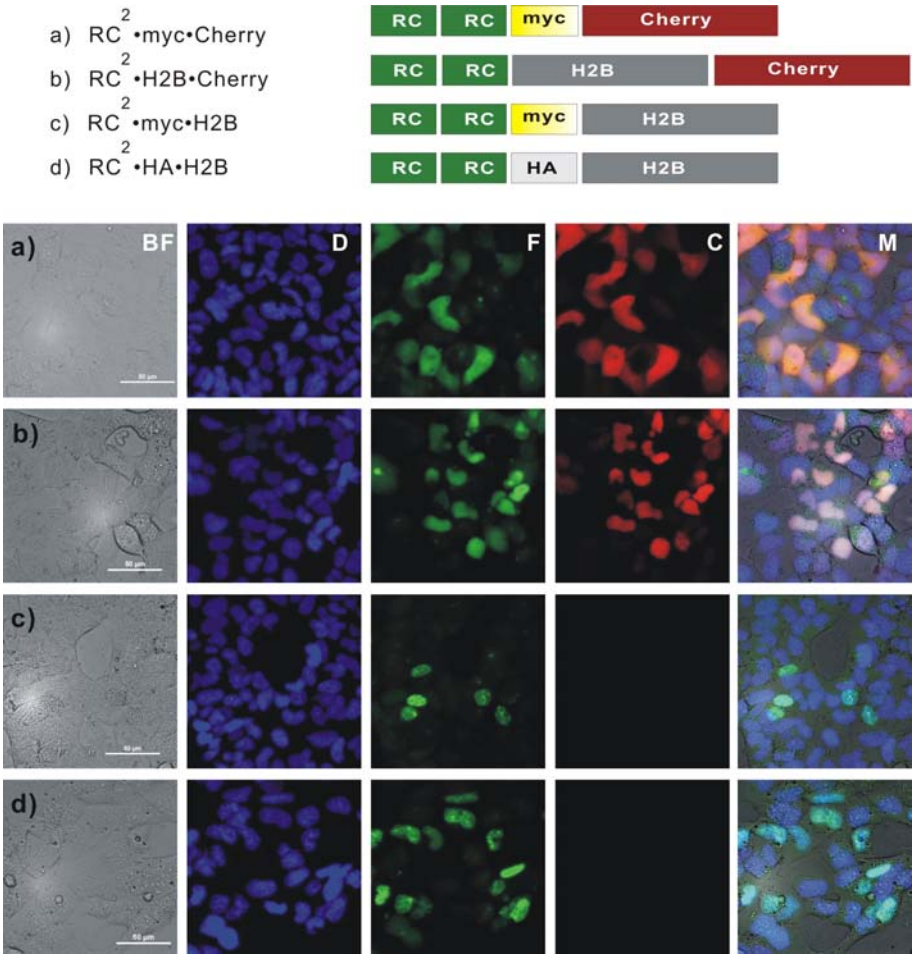

Figure 5.13 Fluorescence microscopic images of **34b** labelling on the RC^2 tagged recombinant proteins expressed in 293A cells. Cells transfected with the respective expression vectors (a–e) were stained with **34b** (1 mM, 15 min, 37 ^oC) and images were taken in live cells. Filters used for fluorescence imaging were BF-bright field, D-DAPI, F-FITC, C-Cy5, M-Merged, scale bars 50 mm, HA-hemmaglutinin tag.

5.2.4.6 Evaluation of RC Tag

Finally, we tested the performance of this labelling system with histone H2B, as a real cellular protein. We linked the ‘‘RC^2_myc’’ casette to the N-terminus of human H2B and fused Cherry to the C-terminus of it as a marker to check the expression. Probe **34b** successfully stained the tagged H2B in live cells demonstrating clear nuclear staining in the transfected cells (Figure 5.13b). In the following experiments of H2B without Cherry, **34b** and the RC^2 tag provided a reliable labelling to the tagged H2B,

which is specific enough to be recognized without the aid of the tracking marker (Cherry) (Figure 5.13c). Additionally, the RC^2 tag was compatible with other peptide tags; combination with other small peptide tags such as the HA tag, myc tag, or hexa-histidine tag, barely affected the labelling efficiency (Figure 5.13d) and the C-terminal tagging was also available (Figure 5.15 lane 4).

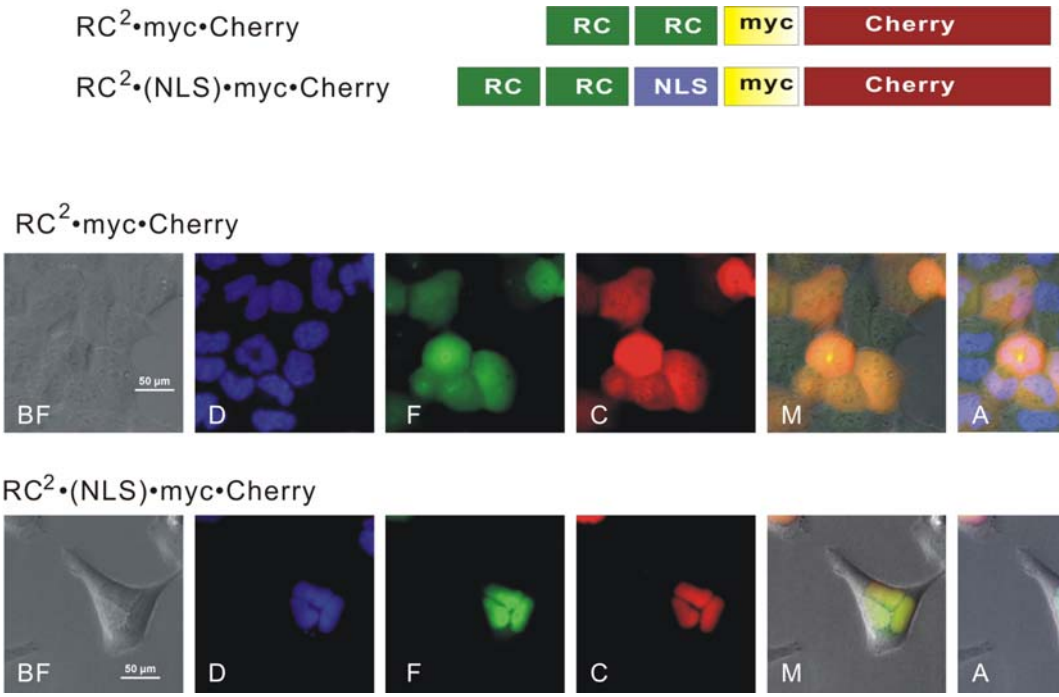

Figure 5.14 Fluorescence microscopic images of RC2 tagged nuclear protein labeled by **34b** in HEK293 cells. Cells transfected with the pc-**RC2**·myc·Cherry or pc-**RC2**·(NLS)·myc·Cherry and were stained with **34b** (1 μM, 15 min, 37 ºC) and followed by the Hoechst staining (10 μM, 30 min, 37 ºC). Images were taken in live cells. Filters used for fluorescence imaging were BF-bright field, D-DAPI, F-FITC, C-Cy5, M-Merged., A-images of all filters are merged (BF+D+F+C). Scale bars 50 μm.

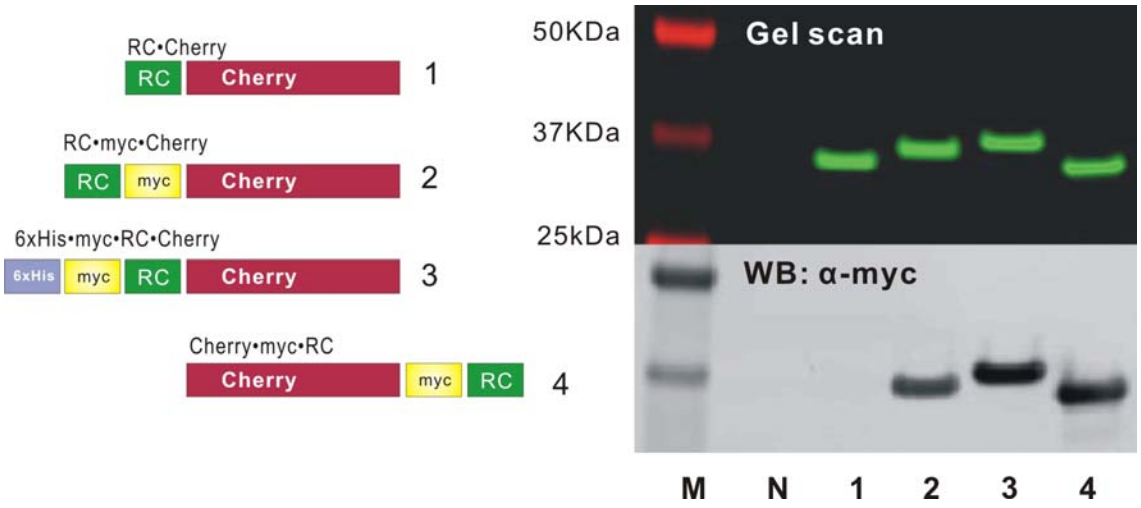

Figure 5.15 Labelling of target protein by **RC** tag in various locations. Plasmid vectors were prepared to express the monomeric Cherry with an **RC** tag placed in diverse position in combination with other small peptide tags. HEK293 cells transfected with the expression vectors were stained with **34b** (1 μM, 30 min, 37 ºC) and the total lysates were analyzed on SDS-PAGE. After fluorescence scanning of the gel, protein was transferred to PVDF membrane and was subjected to western blotting (α-myc) for the confirmation exogenous protein expression. M-protein size marker, N-no transfection.

5.3 Conclusion

DOFL compounds not only can be used to develop novel fluorescent sensors, but also could be more informatics and aim at specific applications. We constructed a Taming fluorescent library with very diverse physical properties and different colours based on BODIPY structures. After applying to cell-based screening system, cellular localization and retention of compounds were successfully correlated to the structures of substitutions of BODIPY dyes. Using the information, cell-permeability and background issues were successfully overcome in developing a protein tag system based on BODIPY diacrylate structure.

This novel peptide-based protein labelling system by utilizing a fluorescent BODIPY compound preferably changed the spectral property when it encounters a designed peptide containing two pairs of Arg-Cys. Dimeric peptide tag RC^2 and its

partner compound **34b** would benefit the current protein labelling methods, especially the optical imaging of specific target protein inside living cells as demonstrated. This system would provide a promising tool for optical imaging of specific protein due to the following advantageous properties: the small size of the tag (less than 5 kDa, composed of 34 amino acids encoded by RC2), independence from other enzymes or cofactors, applicability to intracellular proteins through the cell-permeability of probe, optical confirmation of proper conjugation from the apparent spectral change, stable binding be analyzed in SDS-PAGE, and negligible toxicity to the users when using the BODIPY-based reagent.

5.4 Experimental Section

Materials and Methods

All reactions were performed in oven-dried glassware under a positive pressure of nitrogen. Unless otherwise noted, starting materials and solvents were purchased from Aldrich, Alfa Aesar, Fluka, Merck or Acros organics and used without further purification. Amino acids, Rink amide MBHA resin, and coupling reagents for preparation of peptides were purchased from peptide international, Inc. Analytical TLC was carried out on Merck 60 F254 silica gel plate (0.25 mm layer thickness) and visualization was done with UV light. Column chromatography was performed on Merck 60 silica gel (230-400 mesh). NMR spectra were recorded on a Bruker Avance 400 NMR spectrometer. Chemical shifts are reported as δ in units of parts per million (ppm) and coupling constants are reported as a *J* value in Hertz (Hz). Mass of all the compounds was determined by LC-MS of Agilent Technologies with an electrospray ionization source. High resolution mass was recorded on a Bruker MicroTOFQ-II. CD spectra of peptide were measured by Jasco J-810 spectropolarimeter. All fluorescence

assays were performed with a Gemini XS fluorescence plate reader. Spectroscopic measurements were performed on a fluorometer and UV/Vis instrument, Synergy 4 of bioteck company. The slit width was 1 nm for both excitation and emission.

5.4.1 Synthesis of BODIPY Diacrylates

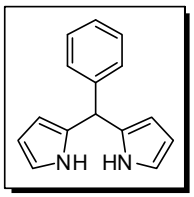

5-Phenyldipyrromethane (31a): 31a was synthesized according to the previous literature. The analytical properties are identical. ^{1}H-NMR (300 MHz. $CDCl_3$): 7.87 (bs, 2H), 7.25 (m, 5H), 6.67 (dd, *J* =2.4, 4.0, 2H), 6.15 (dd, *J*=2.8, 6.0, 2H), 5.90 (bs, 2H), 5.45 (s, 1H). ^{13}C-NMR ($CDCl_3$): 142.1, 132.5, 128.7, 128.4, 127.0, 117.2, 108.5, 107.3, 44.0. ESI-MS *m/z* ($C_{15}H_{14}N_2$): calculated 223.1 (M+H), found 223.1 (M+H).

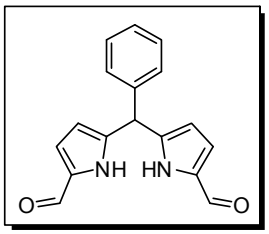

1,9-Diformyl-5-phenyldipyrromethane (32a): To DMF (10 mL) was added $POCl_3$ (1.5 mL, 16.4 mmol) slowly, and the mixture was stirred for 5 min at 0 ^{o}C. This Vilsmeir reagent (7.5 mL, 10.7 mmol) was added slowly to a solution of **31a** (1.0 g, 4.5 mmol) in DMF (15 mL), and stirred for 1.5 h at 0 ^{o}C. The saturated sodium acetate solution (50 mL) was added and stirred at r.t. overnight. After the reaction completion monitored by TLC, the reaction mixture was diluted with EtOAc, and washed with water and brine. The organic layer was dried over sodium sulfate. The filtrate was concentrated and purified by silica gel column chromatography (DCM:EtOAc=9:1) to give the greenish yellow solid (1.07 g, 85%). ^{1}H-NMR (300 MHz, $CDCl_3$): 10.59 (bs, 2H), 9.20 (s, 2H), 7.31 (m, 5H), 6.86 (dd, *J*=2.4, 4.0, 2H), 6.06 (dd, *J*=2.4, 3.2, 2H), 5.59 (s, 1H). ^{13}C-NMR ($CDCl_3$): 179.0, 141.6, 139.2, 132.7, 129.0, 128.5, 127.7, 122.3, 111.6, 44.5. ESI-MS *m/z* ($C_{17}H_{14}N_2O_2$): calculated 279.1 (M+H), found 279.1 (M+H).

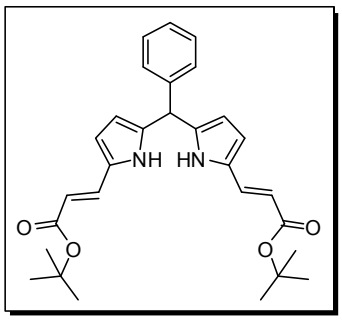

1,9-bis(*tert*-butoxycarbonylethenyl)-5 Phenyldipyrromethane (33a): To a solution of **32a** (500 mg, 1.80 mmol) in DCM (20 mL) was added (*tert*-butoxycarbonylmethylene)triphenylphosphorane (2.03 g, 5.40 mmol) at 0 ^{o}C, and the mixture was stirred at r.t. overnight. The reaction mixture was diluted with DCM and washed with brine. The organic layer was dried over sodium sulfate, filtered, concentrated, and purified by silica gel column chromatography (EtOAc:DCM=1:40) to give a greenish yellow solid **33a** (375 mg, 44 %). ^{1}H-NMR (400 MHz, $CDCl_3$): 8.37 (bs, 2H), 7.32 (d, *J*=16.0), 7.26 (m, 5H), 6.42 (app t, *J*=2.8, 2H), 5.94 (app t, *J*=2.8, 2H), 5.77 (d, *J*=16.0, 2H), 5.45 (s, 1H). ^{13}C-NMR ($CDCl_3$): 166.9, 140.2, 136.4, 133.0, 129.0, 128.5, 128.3, 127.6, 114.7, 113.0, 110.4, 80.1, 44.3, 28.3. ESI-MS *m/z* ($C_{29}H_{32}N_2O_4$): calculated 475.2 (M+H), found 475.2 (M+H).

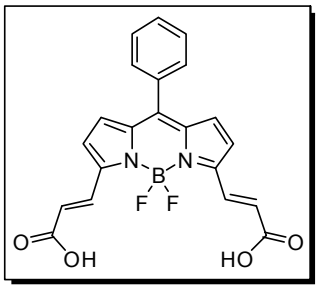

Bodipy diacrylate (34a): To a solution of **33a** (200 mg, 0.421 mmol) in DCM (35 mL) was added DDQ (144 mg, 0.636 mmol). After stirring for 15 min at r.t., the mixture was cooled to 0 ^{o}C. To this mixture, DIEA (2 mL, 11.6 mmol) and BF_3OEt_2 (1.4 mL, 11.1 mmol) were added and slowly warmed up to r.t. while stirring for 2 hrs. The reaction mixture was diluted with DCM, and washed with aq. $NaHCO_3$ and brine. The organic layer was dried over sodium sulfate and the filtrate was concentrated and purified by silica gel chromatography. To hydrolyze the tert-butyl ester, BF_3OEt_2 (0.3 mL) was added at 0 ^{o}C to the solution of ester in DCM (70 mL). After stirring for 1h, the reaction mixture was diluted with DCM and acidified to pH 3 with aq. HCl solution. The aqueous layer was extracted with 5% *i*PrOH/DCM five times. The organic layer was dried over sodium sulfate. The filtrate was concentrate and

purified by silica gel chromatography (MeOH:DCM:H2O=10:50:1) to give **34a** (60 mg, 80%). ^{1}H NMR (400 MHz, $CDCl_3$+ CD_3OD): 8.11 (d, *J*=16.0, 2H), 7.58 (m, 5H), 7.04 (d, *J*=4.0, 2H), 6.96 (d, *J*=4.0, 2H), 6.66 (d, *J*=16.0, 2H). ^{13}C NMR ($CDCl_3$+CD_3OD): 167.9, 132.0, 131.6, 131.4, 130.8, 130.2, 128.5, 128.3, 128.1, 127.4, 126.0, 125.4 ; ESI-HRMS *m/z* ($C_{21}H_{15}BF_2N_2O_4$): calculated 431.0985 (M+Na), found 431.0990 (M+Na).

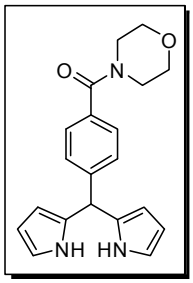

(4-(di(1H-pyrrol-2-yl)methyl)phenyl)(morpholino)methanone (31b): To a solution of 4-(morpholine-4-carbonyl)benzaldehyde (220 mg, 1.0 mmol) in DCM (10 ml), pyrrole (2.2 mmol) was added. The mixture was blown under nitrogen for 10 min. TFA (0.1 mmol) was added. The reaction mixture was stirred at room temperature for 4 h. The reaction was quenched with 0.2 *N* NaOH aqueous solution (20 ml) and extracted with EtOAc. The organic layer was washed with brine and dried over sodium sulfate. The filtrate was concentrated and purified by silica gel chromatography (DCM:EtOAc=8:1) to give **31b** (108 mg, 32%). ^{1}H NMR (300 MHz, $CDCl_3$): 8.06 (bs, 2H), 7.35 (d, *J*=8.4, 2H), 7.26 (d, *J*=8.4, 2H), 6.70 (dd, *J*=1.8, 4.2, 2H), 6.16 (dd, *J*=3.0, 6.0, 2H), 5.90 (bs, 2H), 5.49 (s, 1H), 3.71 (bt, 8H). ^{13}C NMR ($CDCl_3$): 170.2, 144.20, 131.70, 128.53, 127.63, 127.41, 117.42, 108.44, 107.32, 66.83, 43.78, 38.66. ESI-MS *m/z* ($C_{20}H_{21}N_3O_2$): calculated 336.2 (M+H), found 336.1 (M+H).

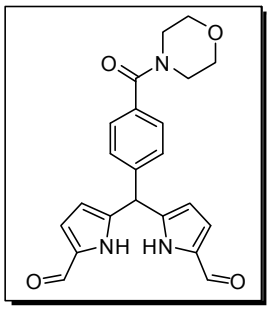

5,5'-((4-(morpholine-4-carbonyl)phenyl)methylene)bis(1H-pyrrole-2-carbaldehyde) (32b): To DMF (1 mL) was added $POCl_3$ (150 μL, 1.60 mmol) slowly, and the mixture was stirred for 5 min at 0 ^{o}C. This Vilsmeier reagent (750 mL, 1.10 mmol) was added slowly to a solution of **31b** (150 mg, 0.45 mmol) in DMF (1.50 mL), and stirred for 1.5 h at 0 ^{o}C. The saturated sodium acetate solution (5 mL) was added and stirred at r.t. overnight. After the reaction completion monitored by

TLC, the reaction mixture was diluted with EtOAc, and washed with water and brine. The organic layer was dried over sodium sulfate. The filtrate was concentrated and purified by silica gel column chromatography (DCM:EtOAc=5:1) to give the greenish yellow solid (142 g, 81%). ^{1}H NMR (500 MHz, $CDCl_3$): 10.67 (bs, 2H), 9.32 (s, 2H), 7.34 (d, *J*=8.4, 2H), 7.24 (d, *J*=8.4, 2H), 6.90 (dd, *J*=1.8, 4.2, 2H), 6.09 (dd, *J*=2.4, 3.2, 2H), 5.60 (s, 1H), 3.72 (bt, 8H). ^{13}C NMR ($CDCl_3$): 176.1, 163.6, 146.4, 137.7, 131.5, 130.6, 129.2, 128.4, 128.3, 123.1, 111.9, 67.5, 54.1, 39.2. ESI-MS *m/z* ($C_{22}H_{21}N_3O_4$): calculated 391.2 (M+H), found 391.1 (M+H).

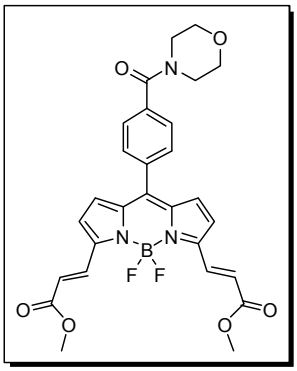

Bodipy diacrylate 34b: To a solution of **32b** (40 mg, 0.10 mmol) in DCM (1 mL) was added methoxycarbonylmethylene triphenylphosphorane (100 mg, 0.30 mmol) at 0 ^{o}C. After stirring at RT overnight, the reaction mixture was diluted with DCM and washed with brine. The organic layer was dried over sodium sulfate. The filtrate was concentrated and purified by silica gel column chromatography (DCM:EtOAc=8:1) to give a greenish yellow solid (36 mg, 71%); This yellow solid (36 mg, 0.07 mmol) was dissolved in DCM (7 mL). To this solution was added DDQ (24 mg, 0.11 mmol). After stirring for 15 min at r.t., the reaction mixture was cooled to 0 ^{o}C. To this solution, DIEA (295 uL, 1.75 mmol) and BF_3OEt_2 (225 μL, 1.75 mmol) were added and slowly warmed up to r.t. while stirring for 2 h. The reaction mixture was diluted with DCM, and washed with saturated $NaHCO_3$ and brine. The organic layer was dried over sodium sulfate. The filtrate was concentrated and purified by silica gel chromatography (DCM:EtOAc=10:1) to give **34b** (24 mg, 62%). ^{1}H NMR (500 MHz, $CDCl_3$): 8.14 (d, =15.9, 2H), 7.55 (m, 4H), 6.91 (d, *J*=4.5, 2H), 6.87 (d, *J*=4.5, 2H), 6.60 (d, *J*=15.9, 2H), 3.87 (s, 6H), 3.84 (bt, 4H),

3.80 (bt, 4H). ^{13}C NMR ($CDCl_3$): 169.1, 166.1, 133.0, 132.2, 132.0, 132.0, 131.6, 130.7, 128.6, 128.4, 127.4, 125.5, 66.9, 58.2, 29.7. ESI-HRMS *m/z* ($C_{28}H_{26}BF_2N_3O_6$): calculated 572.1780 (M+Na), found 572.1786 (M+Na).

5.4.2. Peptides (P1-P6) Preparation

Peptides were synthesized on Rink Amide MBHA resin with standard Fmoc-protected amino acids/HBTU coupling steps followed by piperidine deprotection [Coupling step conditions: Resin (100 mg, 0.48 mmol/g), 0.5 M HBTU in DMF (0.6 mL), 0.5 M Fmoc-Amino acid in NMP (0.6 mL) and 2.0 M DIEA in NMP (0.42 mL) for 3.5 h; Deprotection condition: 20% piperidine in NMP (1.5 mL) for 1 h]. The final N-terminal was capped by acetylation (0.3 M of Ac_2O and 0.27 M of HOBt in DCM for 2h). Peptides were deprotected and cleaved from the resin with the reagent K solution (TFA: H2O: thioanisole: phenol: EDT=10 mL: 0.5 mL: 0.5 mL: 0.75 g: 0.25 mL). Each cleavage solution was drained to chilled ether (20 mL) to precipitate the peptide. Peptide solutions were kept at -20 ^oC overnight for the maximal precipitation. The precipitates were filtered and dried. Peptides were purified by reverse phase HPLC on C18 preparative column with a linear gradient from 0~50% acetonitrile in H_2O containing 0.1% TFA. The collected peptide solutions were lyophilized and the peptide solids were kept at -20 ^oC. Purity was determined by LC-MS with condition of two different columns C18 4.6×50 mm and C18 4.6×150 mm with different eluents composition at the wavelength of 214 nm.

5.4.3 Calculation Process to Determine the Reaction Rate Constant between Dye and Peptide or Glutathione.

As peptide is large excess, the concentration of peptide was considered to be constant during the reaction with dye. The reaction between dye and peptide was considered as *pseudo*-first order reaction.

$r = k[dye][peptide] = k'[dye] = -d[dye] / dt$

$d[dye] / [dye] = -k'dt$

$\ln[dye] = -k't + \ln[dye]_0$

$\ln([dye]_0 / [dye]) = k't$

As $[dye]_0 / [dye] = [product]_\infty / ([product]_\infty - [product]) = F_\infty / (F_\infty - F_t)$, so if we plot $\ln(F_\infty / (F_\infty - F_t))$ versus time t, the slope value is k', which is the *pseudo*-first order reaction rate constant.

[dye]: dye concentration as time t

$[dye]_0$: dye initial concentration

[product]: product concentration at time t

$[product]_\infty$: product final concentration

F_∞: fluorescent intensity of product (530 nm) at saturation.

F_t: fluorescent intensity of product (530 nm) at time t

As GSH is large excess, the concentration of GSH was considered to be constant during the reaction with **34a**. The reaction between dye and GSH was considered as *pseudo*-first order reaction.

$r = k[dye][GSH] = k'[dye] = -d[dye] / dt$

$d[dye] / [dye] = -k'dt$

$\ln[dye] = -k't + \ln[dye]_0$

$\ln([dye]_0 / [dye]) = k't$

As $[dye]_0 / [dye] = F_0 / Ft$, so if we plot $\ln(F_0 / Ft)$ versus time t, the slope value is k', which is the *pseudo*-first order reaction rate constant.

[dye]: dye concentration as time t

$[dye]_0$: dye initial concentration

F_0: initial fluorescent intensity of dye (600 nm).

Ft: fluorescent intensity of dye (600 nm) at time t

5.4.4 Construction of the Expression Vectors

pc-**RC**·myc: An oligonucleotide (**RC**·myc) encoding the **RC** tag (P1 peptide, written in green) together with the Myc-tag (blue) was synthesized (GGGGCTAGCCC ACCATGGAAGCTGCCGCACGTGAAGCGAGATGTCGTGAGCGCTGCGCGAGA GAAGCTTGAACAAAAACTCATCTCAGAAGAGGATCTGGGATCCCC, restriction enzyme sites inserted for cloning are underlined). Nucleotides marked in green encode the **RC** tag and in blue encode the Myc tag. Myc tag was inserted to be used as the epitope in the western blotting for the confirmation of recombinant protein expression. Using the "**RC**·myc" as the template, PCR was performed with two short primers (GGGGCTAGCCCACCATGGAA+GGGGGATCCCAGATCCTCTTC). The resulting PCR product was digested with NheI/BamHI and subcloned into the NheI/BamHI sites of pcDNA3.1(+) (Invitrogen). This clone was named as pc-**RC**·myc and was used for further subclonings.

pc-**RC**·myc·Cherry: We amplified the open reading frame (ORF) of a red fluorescent protein (mCherry) using the primers (GCTGGATCCATGGTGAGCAAGG GCGAGGAGGACAACATG+GGGCTCGAGTCACTTGTACAGCTCGTCCATGCC GCCGGTGGA) using the pc-mCherry (Clontech) as the template and inserted into the BamHI/XhoI sites of pc-**RC**·myc. The resulting plasmid (pc-**RC**·myc·Cherry) expresses the monomeric Cherry that is tagged with the P1 peptide and the Myc-tag.

RC tag mutant clones (**m1, m2, m3**): Vectors express mCherry fused to three mutant tags were prepared by sitedirected mutagenesis PCR. Oligonucleotide sets encoding arginine in the place of cysteine are designed as below.

m1_S : GCACGTGAAGCGAGAGCTCGTGAGCGCTGCGCG

m1_AS: CGCGCAGCGCTCACGAGCTCTCGCTTCACGTGC

m2_S : AGATGTCGTGAGCGCGCCGCGAGAGCTAAG

m2_AS: CTTAGCTCTCGCGGCGCGCTCACGACATCT

m3_S : AGAGCTCGTGAGCGCGCCGCGAGAGCTAAG

m3_AS: CTTAGCTCTCGCGGCGCGCTCACGAGCTCT

25 ng of pc-**RC**·myc·Cherry was used as the template for mutations and the PCR-reactions were performed with pfu DNA polymerase with a cycling profile of 95 ºC 30 sec, (95 ºC 30 sec, 55 ºC 60 sec, 68 ºC 10 min)×16 cycles. Reaction product was digested with DpnI for 1 h and transformed to *E. coli* strain DH5. Acquired mutant clones were confirmed by nucleotide sequencing and designated as pc-(**m1**)**RC**·myc·Cherry, pc-(**m2**)**RC**·myc·Cherry, pc-(**m3**)**RC**·myc·Cherry, respectively.

pc-**RC**^{2}·myc·Cherry: Oligonucleotides encoding the RC tag with the Myc tag but without Kozak or initiating methionine codon (ATG) was synthesized (**RC**^{2}·myc:CAAGCTTGAAGCTGCCGCACGTGAAGCGAGATGTCGTGAGCGCTGCGCGAGAGCTGAATTCGCCGATATCGAACAAAAACTCATCTCAGAAGAGGATCTGGGATCCC). Using the "**RC**^{2}·myc" as the PCR template, the "**RC**^{2}·myc" was amplified with primers (CCCAAGCTTGAAGCTGCCGCA+GGGGGATCCCAGATCCTCTTC). The resulting PCR product was digested with HindIII/BamHI and inserted into the HindIII/BamHI sites of the pcpc-**RC**·myc·Cherry. The acquired clone has a dimerized **RC** tag and a myc epitope fused to the Cherry. The amino acid sequence encoded by the resulting **RC**^{2} is shown below.

RC: MEAAAREA**RC**RE**RC**ARA

RC^{2}: MEAAAREA**RC**RE**RC**ARAKLEAAAREA**RC**RE**RC**ARA

pc-**RC**^{2}·(NLS)·myc·Cherry: An oligonucleotide encoding triple copies of nuclear localization signal of the SV40 Large T antigen was synthesized as below. The oligonucleotides were hybridized in the Tris-buffer (100 mM NaCl, 50 mM Tris-HCl,

10 mM $MgCl_2$, 1 mM DTT, pH 7.9) by boiling and slowly cooling-down to the room temperature and digested with EcoRI/EcoRV. The digested double stranded DNA fragment was inserted into the EcoRI/EcoRV sites of pc-**RC**^{2}·myc·Cherry and the resulting clone was named as pc-**RC**^{2}·(NLS)·myc·Cherry.

3×NLS(S): CCCGAATTCGATCCCAAAAAGAAACGCAAGGTGGATGATCCCAAAAAGAAACGCAAGGTGGATGATCCCAAAAAGAAACGCAAGGTGGATATCGGG

3×NLS(AS):CCCGATATCCACCTTGCGTTTCTTTTTGGGATCATCCACCTTGCGTTTCTTTTTGGGATCATCCACCTTGCGTTTCTTTTTGGGATCGAATTCGGG

pc-**RC**^{2}·myc·H2B: ORF of human histone H2B was PCR amplified using the cDNA of normal human fibroblasts. Primers used the amplification were (GGGGGATCCATGCCTGAACCGGCAAAATC+GGGCTCGAGTCACTTGGAGCTGGTGTACT) and the resulting PCR product was digested with BamHI/XhoI and subcloned into the BamHI/XhoI sites of pc-**RC**^{2}·myc·Cherry to exchange the ORF of Cherry with that of H2B.

pc-**RC**^{2}·myc·H2B·Cherry: The ORF of human H2B was PCR-amplified with primers (GGGGAATTCATGCCTGAACCGGGCAAAATC+GGGGATATCCTTGGAGCTGGTGTACTTGG) and the PCR product was digested with EcoRI/EcoRV. Digested DNA was inserted into the EcoRI/EcoRV sites of the pc-**RC**^{2}·(NLS)·myc·Cherry to exchange the NLS with the H2B ORF.

pc-**RC**·Cherry: ORF of Cherry was amplified with primers (GGGAAGCTTATGGTGAGCAAGGGCGAGGAG+GGGCTCGAGCTTGTACAGCTCGTCCATGCCGCCGGTGGA) and the resulting PCR product was digested with HindIII/XhoI and introduced into the HindIII/XhoI sites of pc-**RC**·myc·Cherry to generate the pc-**RC**·Cherry.

pc-6xHis·myc·**RC**·Cherry: Primers GGGCTAGCCACCATGCATCATCATCATC ACCACGAATTCGAACAAAAACTCACTCAGAA+CCCAAGCTTAGCTCTCGCG CAGCGCTCACG)was used to amplify the expression cassette of "6xHis tag and RC tag". The produced PCR product was digested with Nhe1/HindIII and inserted into the NheI/HindIII site of pc-**RC**·myc·Cherry.

pc-Cherry·myc·**RC**: Primers (GGGAATTCGAACAAAAACTCATCTCAGAAGA GGATCTGGATATCGAAGCTGCCGCACGTGAA+CCCCTCGAGTCAAGCTCTCG CGCAGCGCTC)were used to amplify the "myc tag-RC tag" cassette and resulting PCR product was digested with EcoR1/Xho1 and cloned into the pcDNA3.1(+), resulting the pc-myc·**RC**. ORF of Cherry was PCR amplified with (GGGGCTAGCCA CCATGGTGAGCAAGGGCGAGGAG+GGGGAATTCCTTGTACAGCTCTCCATG CCGCCGGTGGA) and the acquired PCR product was cloned into the NheI/EcoRI sites of the pc-myc·**RC** resulting the pc-Cherry·myc·**RC**.

5.4.5 Cell Culture and Transfection

HEK293 cells, an immortalized line of primary human embryonic kidney cells, were purchased from Invitrogen and maintained in the DMEM (10% Fetal Bovine Serum (FBS), 1% antibiotics-antimycotics reagent). Materials used in the cell culture were purchased from Invitrogen. For transient transfection, cells were plated at the density of 2×10^5 cells/well in 12 well plate and 500 ng of plasmid DNA purified by Midi-prep kit (Qiagen) were transfected with Lipofectamine 2000 (Invitrogen). After 2 days incubation, the transfected cells were subjected to the following experiment such as live cell staining or (SDSPAGE/western blotting).

5.4.6 SDS-PAGE, Gel-Scanning, Western Blotting, and Silver Staining

Total protein was extracted by using CelLyticMTM cell lysis solution (Sigma). Generally 10 μg of the protein/well was loaded in SDS-PAGE gel for gel-scanning.

NuPAGE Novex Bis-Tris Gels (Invitrogen) were used for PAGE and the gel was scanned using the Typhoon 9410 Gel Scanner (GE Healthcare). Gel was excited at stained 488nm and was scanned through 526SP emission filter. After gel scanning, proteins were transferred onto the PVDF membrane and subjected to the following western blotting. Western blotting data were generated by fluorescence scanning of the membranes stained with antibodies. A mouse monoclonal α-myc (Santa Cruz, sc-40) antibody and a goat α-mouse IgG tagged with Cy5 (Invitrogen, A10524) were used. Membranes were excited at 633nm and scanned through 670BP emission filter. When the gel was subjected to the silver staining, gel was fixed in fixing solution (50% EtOH, 10% glacial acetic acid) for 10 min. Gel was rinsed with water for 1hr and then, sensitized in 0.02% $Na_2S_2O_3$ for 2 min. After a brief rinsing with water, gel was stained in 0.1% $AgNO_3$ for 30 min. After rinsing with water, gel was developed with 2% Na_2CO_3, 37% (v/v) formaldehyde and the reaction was stopped with 1% CH_3COOH.

5.4.7 Compound Staining and Imaging in the Live Cells

Compounds were reconstituted in DMSO as the 1 mM solution, and stored in -20 ºC. Immediately before staining, medium in the wells were drained and the compound diluted in the pre-warmed growth medium was added directly onto the cells. After incubation (30 min, 37 ºC), cells were washed with growth medium and further incubated in the cell culture incubator for 1 hour. Medium was changed once again, and cells were subjected to the live cell imaging. Bright field images and fluorescence images were acquired by a fluorescent microscope ECLIPSE Ti-E (Nikon Instrument Inc.). Emission filters used are DAPI filter (Ex 340-380 nm, Em 435-485 nm) for Hoechst, FITC filter (Ex 465-495 nm, Em 515-555 nm) for **34b**, and Cy5 filter (Ex 590-650 nm, Em 663-738 nm) for Cherry.

5.4.8 Quantum Yield Measurements

Quantum yields were calculated by measuring the integrated emission area of the fluorescent Spectrum and comparing that value to the area measured for 1, 3, 5, 7-tetramethyl-8-phenyl BODIPY in DMSO. The following equation (1) was used to calculate quantum yield, where *F* represents the area of fluorescent emission, *n* is reflective index of the solvent, and Abs is absorbance at excitation wavelength selected for standards and samples.

$$\Phi_{flu}^{sample} = \Phi_{fl}^{reference}\left(\frac{F^{sample}}{F^{reference}}\right)\left(\frac{\eta^{sample}}{\eta^{reference}}\right)\left(\frac{Abs^{reference}}{Abs^{sample}}\right) \quad (1)$$

5.4.9 LC-MS chromatogram of P1, P2, P3, P6 peptides

P1: AcEAAAREARCRERCARA-NH2

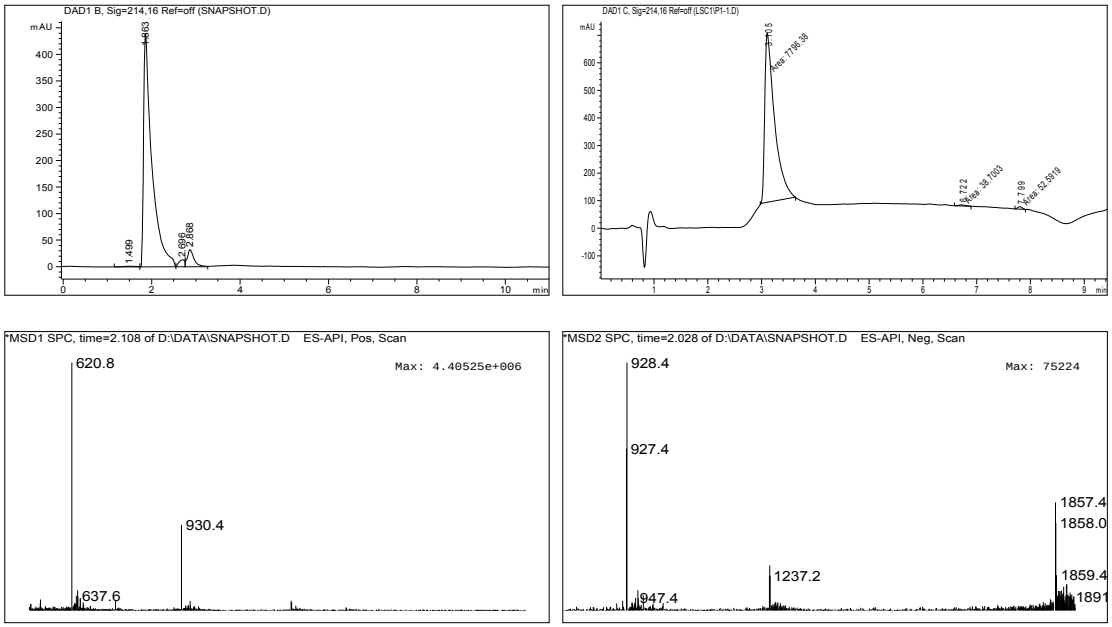

ESI-MS: calculated 1858.9, found 930.4$(M+2H)^{2+}$, 620.8$(M+3H)^{3+}$, 1857.4$(M-H)^{-}$

P2: AcEAAAREAAARERCARA-NH2

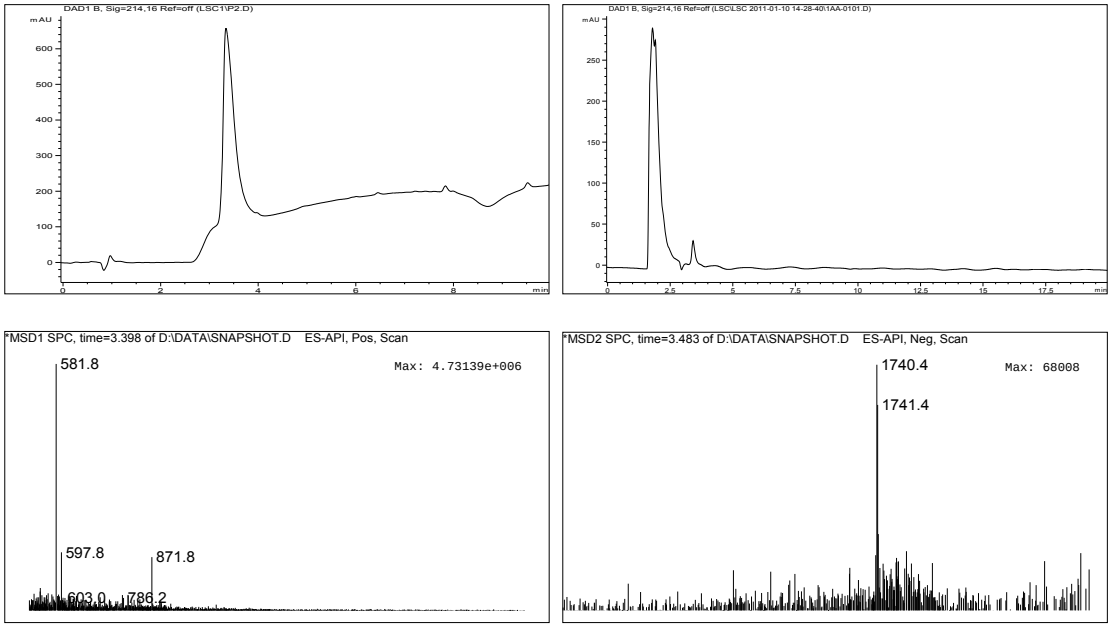

ESI-MS: calculated 1741.9, found 871.8$(M+2H)^{2+}$, 581.8$(M+3H)^{3+}$, 1740.4$(M-H)^{-}$

P3: AcEAAAREAAAREAAARA-NH2

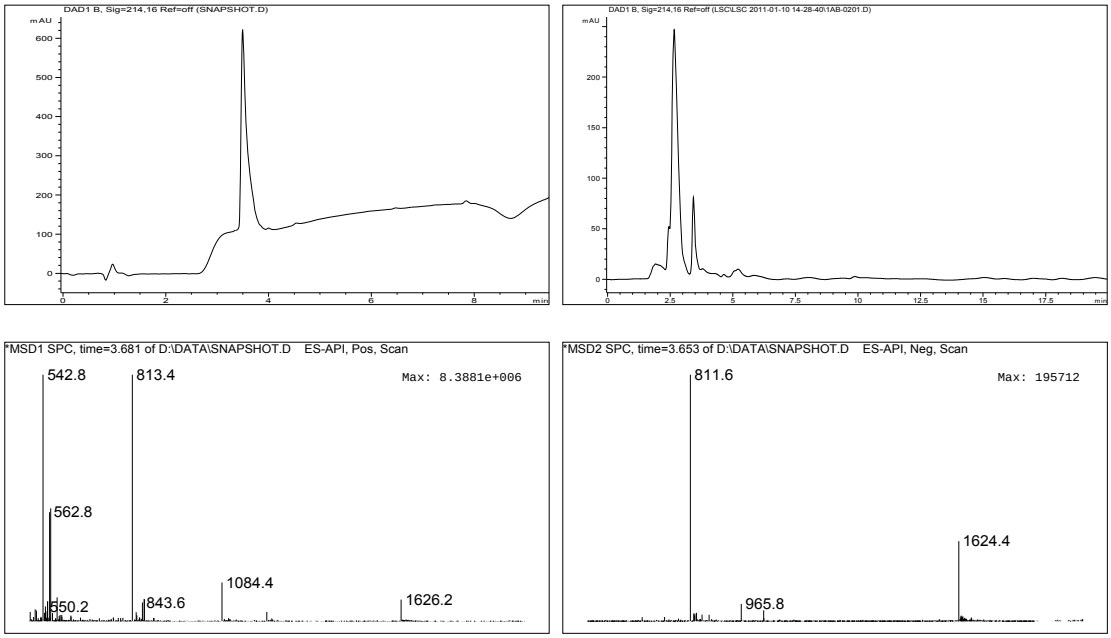

ESI-MS: calculated 1624.8, found 1626.2 $(M+H)^{+}$, 813.4 $(M+2H)^{2+}$, 542.8 $(M+H)^{3+}$, 1624.4 $(M-H)^{-}$

P6: AcGGGGGGGGCGGGCGGG-NH2

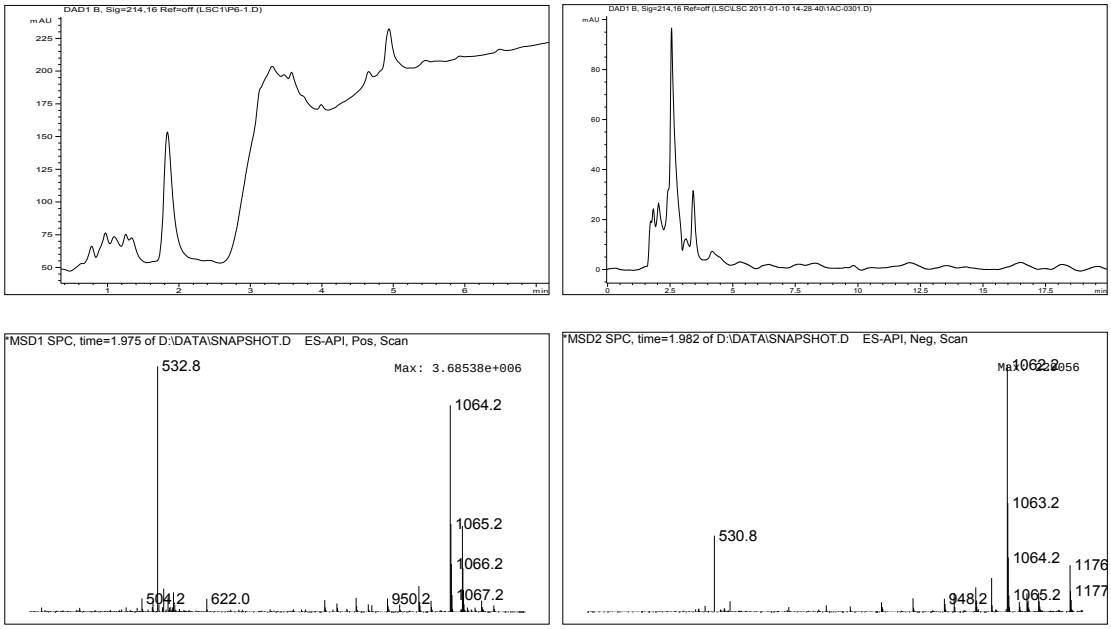

ESI-MS: calculated 1063.4, found 1064.2 $(M+H)^+$, 532.8 $(M+2H)^{2+}$, 1062.3 $(M-H)^-$

LC condition of left: (5% ACN to 100% ACN gradient condition with water, contained 0.1% TFA, run time: 10min, column: C18, 4.6×50 mm, 5 μm, monitored at 214 nm channel); LC condition of right: (15% ACN in water isocratic, contained 0.1% TFA, run time: 20min, column: C18, 4.6×15 mm, 5 μm, monitored at 214 nm channel).

5.4.10 Spectral properties of 34a and 34b

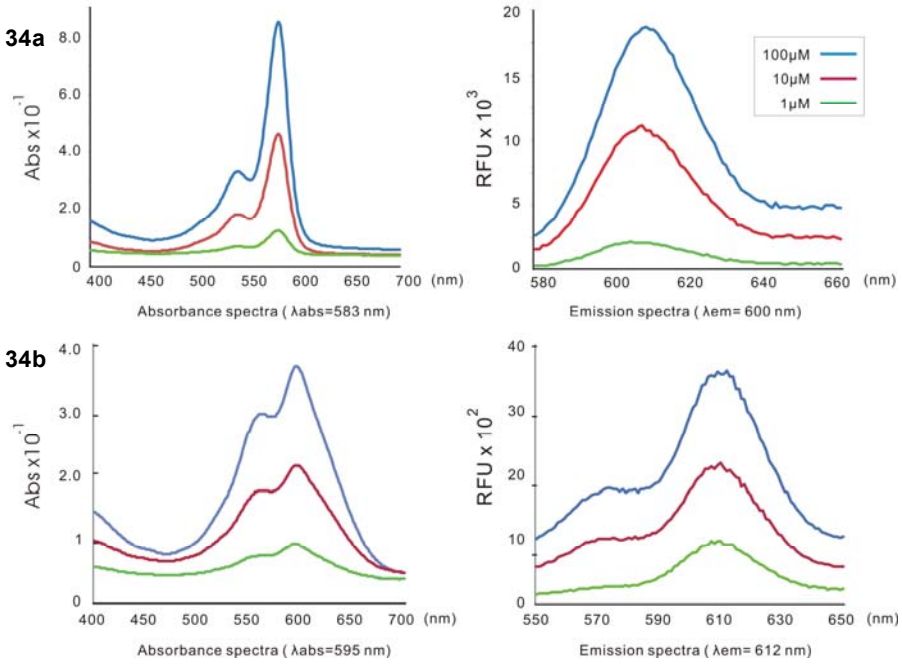

(upper) Absorbance and emission spectra of **34a** in 50 mM HEPES buffer (pH 7.4). Fluorescence spectra were obtained with an excitation at 550 nm (extinction coefficient =66888, quantum yield=0.29). (lower) Absorbance and emission spectra of **34b** in 50 mM HEPES buffer (pH 7.4). Fluorescence spectra were obtained with an excitation at 520 nm (extinction coefficient=55989, quantum yield=0.21).

5.4.11 Conjugation of 34a to Peptide P1

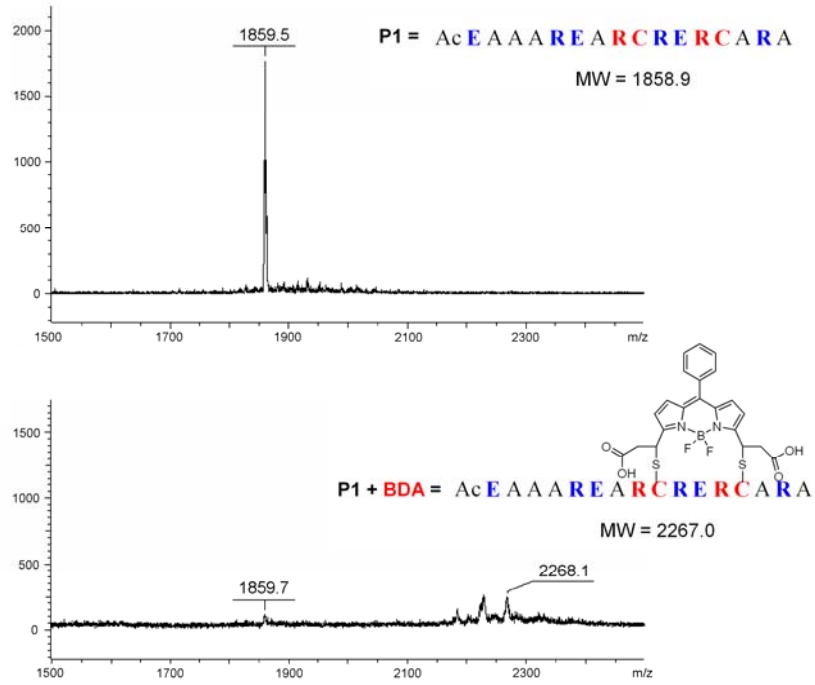

MALDI-TOF spectra of a model peptide P1 after incubation with **34a**: **34a** (10 μM) and P1 (20 μM) were mixed in 50 mM HEPES (pH 7.0), then mixture was analyzed after desalting by C18 ziptip. Mass indicates the presence of the conjugation product of P1-**34a** (2268.1, M+H), with another mass peak at 2228.9 (M-38).

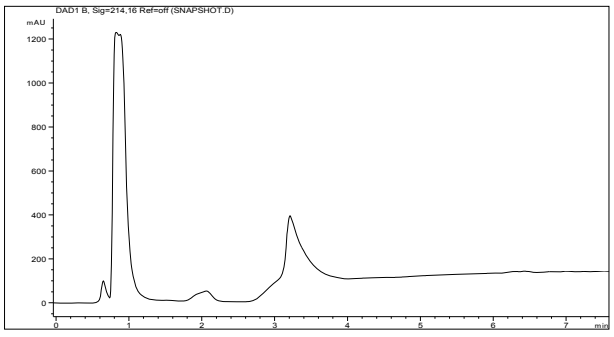

P1 (Rt=3.3 min) LC spectra at 214 nm channel.

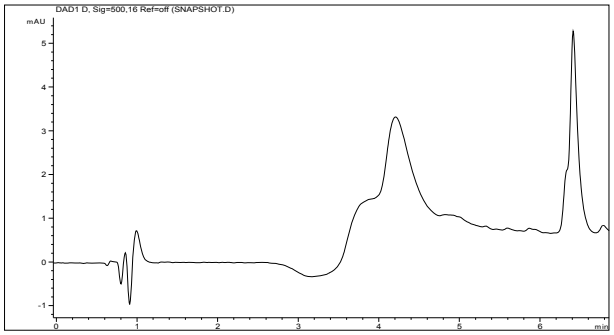

P1+**34a** (Rt=4.3 min) and **34a** (Rt=6.4 min) LC spectra at 500 nm channel.

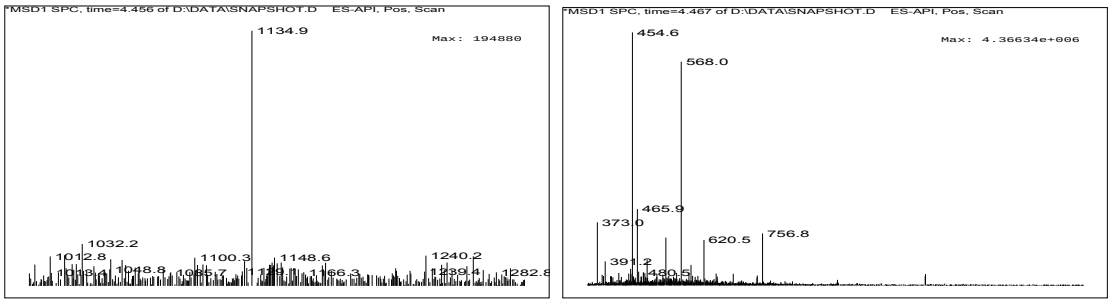

ESI-MS found of **P1**+**34a** conjugation: 1134.9 $[M+2H]^{2+}$, 756.8 $[M+3H]^{3+}$, 568.0 $[M+4H]^{4+}$, 454.6 $[M+5H]^{5+}$.

References

1. (a) Lee, J. S.; Kim, Y. K.; Vendrell, M.; Chang, Y. T., Diversity-oriented fluorescence library approach for the discovery of sensors and probes. *Mol. BioSys.* **2009,** *5*, 411-421; (b) Vendrell, M.; Lee, J. S.; Chang, Y. T., Diversity-oriented fluorescence library approaches for probe discovery and development. *Curr. Opin. Chem. Biol.* **2010,** *14*, 383-389.

2. Carpenter, A. E., Image-based chemical screening. *Nat. Chem. Biol.* **2007,** *3*, 461-465.

3. Shedden, K.; Rosania, G. R., Chemical address tags of fluorescent bioimaging probes. *Cytometry A* **2010,** *77*, 429-438.

4. Nath, S.; Spencer, V. A.; Han, J.; Chang, H.; Zhang, K.; Fontenay, G. V.; Anderson, C.; Hyman, J. M.; Nilsen-Hamilton, M.; Chang, Y.-T.; Parvin, B., Identification of Fluorescent Compounds with Non-Specific Binding Property via High Throughput Live Cell Microscopy. *PLoS One* **2012,** *7*, e28802.

5. (a) Goldman, S. D.; Funk, R. S.; Rajewski, R. A.; Krise, J. P., Mechanisms of amine accumulation in, and egress from, lysosomes. *Bioanalysis* **2009,** *1*, 1445-1459; (b) Kaufmann, A. M.; Krise, J. P., Lysosomal sequestration of amine-containing drugs: analysis and therapeutic implications. *J. Pharm. Sci.* **2007,** *96*, 729-746.

6. Perry, S. W.; Norman, J. P.; Barbieri, J.; Brown, E. B.; Gelbard, H. A., Mitochondrial membrane potential probes and the proton gradient: a practical usage guide. *Biotechniques* **2011,** *50*, 98-115.

7. Zhang, J.; Campbell, R. E.; Ting, A. Y.; Tsien, R. Y., Creating new fluorescent probes for cell biology. *Nat. Rev. Mol. Cell Biol.* **2002,** *3*, 906-918.

8. Wiedenmann, J.; Oswald, F.; Nienhaus, G. U., Fluorescent proteins for live cell imaging: opportunities, limitations, and challenges. *IUBMB Life* **2009,** *61*, 1029-1042.

9. Chen, I.; Ting, A. Y., Site-specific labeling of proteins with small molecules in live cells. *Curr. Opin. Biotechnol.* **2005,** *16*, 35-40.

10. Griffin, B. A.; Adams, S. R.; Tsien, R. Y., Specific covalent labeling of recombinant protein molecules inside live cells. *Science* **1998,** *281*, 269-272.

11. (a) Adams, S. R.; Campbell, R. E.; Gross, L. A.; Martin, B. R.; Walkup, G. K.; Yao, Y.; Llopis, J.; Tsien, R. Y., New biarsenical ligands and tetracysteine motifs for protein labeling in vitro and in vivo: synthesis and biological applications. *J. Am. Chem. Soc.* **2002,** *124*, 6063-6076; (b) Martin, B. R.; Giepmans, B. N.; Adams, S. R.; Tsien, R. Y., Mammalian cell-based optimization of the biarsenical-binding tetracysteine motif for improved fluorescence and affinity. *Nat. Biotechnol.* **2005,** *23*, 1308-1314; (c) Spagnuolo, C. C.; Vermeij, R. J.; Jares-Erijman, E. A., Improved photostable FRET-competent biarsenical-tetracysteine probes based on fluorinated fluoresceins. *J. Am. Chem. Soc.* **2006,** *128*, 12040-12041.

12. Ojida, A.; Honda, K.; Shinmi, D.; Kiyonaka, S.; Mori, Y.; Hamachi, I., Oligo-Asp tag/Zn(II) complex probe as a new pair for labeling and fluorescence imaging of proteins. *J. Am. Chem. Soc.* **2006,** *128*, 10452-10459.

13. Kelly, K. A.; Carson, J.; McCarthy, J. R.; Weissleder, R., Novel peptide sequence ("IQ-tag") with high affinity for NIR fluorochromes allows protein and cell specific labeling for in vivo imaging. *PLoS One* **2007,** *2*, e665.

14. Chen, I.; Howarth, M.; Lin, W.; Ting, A. Y., Site-specific labeling of cell surface proteins with biophysical probes using biotin ligase. *Nat. Methods* **2005,** *2*, 99-104.

15. Fernandez-Suarez, M.; Baruah, H.; Martinez-Hernandez, L.; Xie, K. T.; Baskin, J. M.; Bertozzi, C. R.; Ting, A. Y., Redirecting lipoic acid ligase for cell surface protein labeling with small-molecule probes. *Nat. Biotechnol.* **2007,** *25*, 1483-1487.

16. Zhou, Z.; Cironi, P.; Lin, A. J.; Xu, Y.; Hrvatin, S.; Golan, D. E.; Silver, P. A.; Walsh, C. T.; Yin, J., Genetically encoded short peptide tags for orthogonal protein labeling by Sfp and AcpS phosphopantetheinyl transferases. *ACS Chem. Biol.* **2007,** *2*, 337-346.

17. Uttamapinant, C.; White, K. A.; Baruah, H.; Thompson, S.; Fernandez-Suarez, M.; Puthenveetil, S.; Ting, A. Y., A fluorophore ligase for site-specific protein labeling inside living cells. *Proc. Natl. Acad. Sci. U S A* **2010,** *107*, 10914-10919.

18. Matsumoto, T.; Urano, Y.; Shoda, T.; Kojima, H.; Nagano, T., A thiol-reactive fluorescence probe based on donor-excited photoinduced electron transfer: key role of ortho substitution. *Org. Lett.* **2007,** *9*, 3375-3377.

19. Girouard, S.; Houle, M. H.; Grandbois, A.; Keillor, J. W.; Michnick, S. W., Synthesis and characterization of dimaleimide fluorogens designed for specific labeling of proteins. *J. Am. Chem. Soc.* **2005,** *127*, 559-566.

20. Guy, J.; Caron, K.; Dufresne, S.; Michnick, S. W.; Skene, W. G.; Keillor, J. W., Convergent preparation and photophysical characterization of dimaleimide dansyl fluorogens: elucidation of the maleimide fluorescence quenching mechanism. *J. Am. Chem. Soc.* **2007,** *129*, 11969-11977.

Chapter 6

6.1 Conclusion

Combinatorial approach makes up the shortage of conventional designed approach in sensor development in circumventing the limited knowledge of recognition motifs. Diversity-oriented fluorescent libraries approach, through generating large numbers of fluorescent compounds in a combinatorial way, has become a powerful method to discover novel fluorescent sensors. Among different fluorophores, BODIPY shows unique properties, such as the overall lipophilicity and electrically neutral character. We first designed a novel diversity-oriented BODIPY library by introducing an active ester motif to the core structure (**BDD**). **BDD** library was synthesized through Knoevenagel condensation reaction with aldehyde building blocks to render 160 compounds in high purity. Utilizing the relatively active property of ester motif of **BDD** compounds, they were further reacted with N^1,N^1-dimethylethane-1,2-diamine and 2,2-dimethoxyethanamine to give 80-member **BDL** and 47-member **BDA** libraries, respectively. All these three libraries cover very broad spectral properties, due to the structural diversity of aldehyde building blocks.

The diversity-oriented BODIPY libraries form a good chemical tool box for sensor development, and hence was applied to *in vitro* high-throughput screening. A collection of 52 broad range of biomolecules first served as analytes. Two selective and highly responsive sensors for fructose and glutathione were discovered from the screening, and were named as **Fructose Orange** and **Glutathione Green**, respectively. **Fructose Orange** showed up tp 24-fold fluorescence increase upon recognition of fructose and an outstanding selectivity among 24 different saccharides. NMR studies confirmed the formation of five different binding interactions between the sensor and fructose. Furthermore, **Fructose Orange** was applied to the quantification of fructose in soft

drinks, being the most selective fluorescent sensor for fructose reported to date. **Glutahione Green** showed ratiometric fluorescence response and outstanding selectivity over other analytes. Further experiment showed that **GSH Green** is capable of GSH quantification in cell extract, as well as responding to the GSH concentration change in cellular environment.

In order to explore useful sensors for illicit date-rape drug-GBL, the *in vitro* high-throughput screening was also performed with GBL as analyte, identifying **Green Date** (derivatized from **BDD** library) as a GBL sensor. **Green Date** showed high fluorescence response to GBL in various pH conditions and up to 10% EtOH. Furthermore, **Green Date** is able to detect the existence of GBL in different kinds of drinks samples after a simple extraction method. This discovery will help to secure the safety of drinks in public place and solve the DFSA problems.

Neural stem cells (NSCs) generate the nervous system, promote neuronal plasticity and repair damage throughout life by self-renewing and differentiating into neurons and glia, and hence have great potential for therapeutic use in patients suffering from various neurological diseases and also as a research tool for drug development. In order to develop fluorescent small molecules probe for NSC rather than antibodies, we performed cell-based high throughput screening of in-house generated diversity oriented fluorescence library in stem cells at different developmental stages. One compound from BDD library (CDr3) was identified as a neural stem cell specific probe. This novel compound specifically detects living neural stem cells of both human and mouse origin. Furthermore, we identified its binding target by proteomic analysis as fatty acid binding protein 7 (FABP7) which is highly expressed in neural stem cells and localized in the cytoplasm. CDr3 will be a valuable chemical tool in the study and applications of neural stem cells.

DOFL compounds not only can be used to develop novel fluorescent sensors, but also could be more informatics and aim at specific applications. We constructed a Taming fluorescent library with very diverse physical properties and different colours based on BODIPY structures. After applying to cell-based screening system, cellular localization and retention of compounds were successfully correlated to the structures of substitutions of BODIPY dyes. Using the information, cell-permeability and background issues were successfully overcome in developing a protein tag system based on BODIPY diacrylate structure. This novel peptide-based protein labelling system by utilizing a fluorescent BODIPY compound preferably changed the spectral property when it encounters a designed peptide containing two pairs of Arg-Cys. Dimeric peptide tag RC^2 and its partner compound would benefit the current protein labelling methods, especially the optical imaging of specific target protein inside living cells as demonstrated. This system would provide a promising tool for optical imaging of specific protein due to the following advantageous properties: the small size of tag (less than 5 kDa, composed of 34 amino acids encoded by RC2), independence from other enzymes or cofactors, applicability to intracellular proteins through the cell-permeability of probe, optical confirmation of proper conjugation from the apparent spectral change, stable binding be analyzed in SDS-PAGE, and negligible toxicity to the users when using the BODIPY-based reagent.

6.2 Future Prospective

Development of Tag Systems for Protein Visualization

The information derived from cell-based screening of Taming libraries would have wide application in “Taming” the BODIPY dyes in probe development to overcome the limitations and fulfill the prospects. In the next generation of tag system for protein based on BODIPY structures, we aim to utilize the “easy to wash out and left no

background" properties of some Taming compounds. First, a peptide library will be constructed from yeast express. Taming derivatives with relatively reactive motif and "easy to wash out" property will be optimized and synthesized. The selected fluorescent compounds will then be incubated and washed out from the yeast library to select out the peptide sequence with FACS sorting. After FACS, the bright yeast population would be the one expressing peptide sequence which can selectively bind to Taming derivatives, since the compound should be easy to wash out. The selected peptide sequence will then be fused with a protein of interest and expressed in cells following by the incubation of compounds and washed out to validate the selectively labeling of protein by this tag system.